Numerical Studies of Nonlinear Axisymmetric Waves on Vortex Filaments

Thesis by
Vidyadhar Yogeshwar Mudkavi

In Partial Fulfillment of the Requirements
for the Degree of
Doctor of Philosophy

California Institute of Technology
Pasadena, California

1991

(Submitted May 8, 1991)

Acknowledgements

I would like to thank my advisor, Daniel I. Meiron, for his support and encouragement and, above all, his thorough advice and effort in bringing the thesis to its final shape. I have learned a great deal from his association.

I would like to thank Philip G. Saffman for introducing the problem to me and for his advice during the initial stage of this work and many enlightening discussions at a later stage.

I would like to thank Derek W. Moore for his invaluable discussions on the core waves. I wish to thank Saleh Tanveer for his interest and for his help on the weakly nonlinear analysis. I also wish to thank Robert I. McLachlan for his interest and several discussions and particularly his help in coding the computation of the Padé approximants. I wish to thank Thu Pham for his informal discussions and his friendship.

I wish to thank my wife, Sandhya, for her tremendous help and support. My parents and my sister, K. S. Jalaja, have taught me the value of good education. I have come this far because of their support. I dedicate this thesis to my parents, Dada and Vaini, and to the fond memory of my grandfather, Anna.

While at Caltech, I was supported by institute teaching assistantships and was generously awarded a fellowship during the academic year 1988–89.

Abstract

The equations of Moore & Saffman (1971) are examined and are shown to contain the fast time scale equations governing the core waves on a straight vortex filament. The equations so derived are the same as those reported by Lundgren & Ashurst (1989) except for a correction term that allows for variation of the axial velocity structure within the vortex core. Numerical solutions of the Moore & Saffman equations are presented for various initial conditions consisting of wave-like perturbations on a cylindrical vortex, and they all show development of a jump in the core area. This has been advanced to be a mechanism for vortex breakdown by Lundgren & Ashurst. A comparison of the solutions of the Moore & Saffman equations with the solutions of the Navier-Stokes equations at high Reynolds number is presented for three different cases. In the first case a vortex with a very small perturbation is considered. The Moore & Saffman solution shows steepening of the initial wave resulting in the development of jump in the core area (shock). The Navier-Stokes solution shows bulging of the core. But, there is no indication of formation of a shock. In the second case a vortex with moderate perturbation is considered. The Moore & Saffman solution leads to a shock similar to the weak perturbation case. As before, the Navier-Stokes solution does not develop jump in the core area. However, development of a bubble of reversed flow is seen. In the third case, a jump in the core area in the solutions of the Navier-Stokes equations is seen for a strongly perturbed vortex. But the location and the sense of jump disagrees with jump that develops in the Moore-Saffman solution. Thus, the solutions of the Navier-Stokes equations and the Moore-Saffman equations show qualitative disagreement.

Next, an extension of steady Kelvin waves for two different types of vorticity profiles is considered. In the first case, steady nonlinear waves are constructed via a perturbation method. In this case, the vorticity is nonzero inside the core and sharply drops to zero across the boundary. The shape of the core boundary is determined as part of the problem. The dependence of the Bernoulli function and the circulation

function on the streamfunction are specified. This serves as the additional constraint necessary to determine the solution uniquely. The solutions are free of any vortex sheets. In the second case, nonlinear steady Kelvin waves on smooth vorticity distributions are constructed by means of a direct Newton method and a large order perturbation method. Instead of specifying the dependence of the Bernoulli function and the circulation function on the streamfunction as in the previous case, the solutions are restricted such that they have the same axial mean as the base flow. In both the approaches, regions of reversed flow are observed. This is the structure of bubble type of vortex breakdown.

Next, an analysis of the weakly nonlinear stability of a columnar vortex is presented. It is shown that the amplitude, assumed to vary slowly in time and space, satisfies a cubic-nonlinear Schrödinger equation. Solutions are found to be unstable in the sense that the perturbations grow slowly in time. Solitary wave solutions are possible in this unstable case.

Contents

Part I

CHAPTER 1

Introduction

1.1 General introduction

A vortex filament is a slender tube-like concentration of vorticity. The size of the cross section of a filament is small compared with other length scales in the flow field. The region of fluid containing the vorticity is called the core. Away from the core, the flow is irrotational. Probably the most common example of a vortex filament found in literature is that of aircraft trailing vortices. As a result of variation of the lifting force on the wing of an aircraft, vorticity is shed in to the wake in the form of a vortex sheet. The vortex sheet being highly unstable to infinitesimal disturbances, rolls up immediately into two counter-rotating trailing vortices. The structure of the core immediately after the roll up is that of a tightly wound spiral with several turns. Viscous action smoothes out the velocity across the several layers of the spiral and gives rise to a continuous distribution of the velocity in the core. A mathematical treatment of the roll up of the vortex sheet and the structure of the trailing vortex is found in Moore & Saffman (1973). Trailing vortices associated with a heavy aircraft contain tremendous energy and pose a threat to light airplanes. A great deal of research activity in the 1970's was devoted to the understanding of the motion and decay of a trailing vortex system. A counter-rotating system of vortex filaments also forms due to the roll up of a vortex sheet shed from the leading edge of a delta wing at large angle-of-attack. The leading edge vortices in this case are particularly helpful in increasing the lift on the wing.

The computation of velocity induced by a vortex filament is of utmost practical interest since a general three dimensional flow with a compact distribution of vorticity may be thought of as being composed of a collection of vortex filaments. The

subsequent dynamics of the entire flow field is then represented by the evolution of the filaments moving under the action of the induced velocity. A discussion of this may be found in Leonard (1985). The induced velocity of any vorticity distribution can be computed using the Biot-Savart law. The induced velocity due to a vortex filament can be found approximately by assuming that the vorticity is concentrated on a line passing through the center of the core. When the induced velocity at a point on the filament is needed, the straight forward application of the Biot-Savart law leads to an infinite velocity. The correct induced velocity must be computed by accounting for the core structure exactly. This is often difficult in practice. But simple cut-off methods or a more sophisticated de-singularization of the integral (Rosenhead, 1930) have been used.

A phenomenon most frequently encountered in relation to the dynamics of vortex filaments is vortex breakdown or vortex bursting. Benjamin (1962) states that vortex breakdown or bursting refers to the abrupt and drastic change of structure which sometimes occurs in a swirling flow. Two distinct types of breakdown are observed. They are the bubble type and the spiral type. In the bubble type breakdown, the stream-surface diverges rather drastically to form a bubble like structure that is nearly axisymmetric. This type of breakdown occurs only when an axial component of velocity is present in the core. The overall direction of the axial velocity is reversed in the bubble. In the spiral type breakdown, the axis of the vortex deforms into a spiral with no appreciable growth in the core size. The flow downstream of the breakdown structure in either type is almost always unsteady and turbulent.

In what follows, we first review the various theoretical and experimental work concerning vortex motion and breakdown. We then outline the study undertaken in this thesis and state our objective.

1.2 Theories of vortex motion

The earliest work relating to the motion in a vortex is due to Kelvin (1880). In his paper titled "The vibrations of a columnar vortex," Kelvin considered the effect of

wave-like perturbations on a columnar vortex with no axial velocity. Among the cases considered, he found that axisymmetric linear waves propagate at fixed speed. The speed of propagation depends on the wave-length of the perturbation and is found to satisfy a transcendental dispersion relation involving Bessel functions. These studies were followed by studies of steady motion and vibrations of a hollow vortex ring (Hicks, 1884; Pocklington, 1895). These studies were contributions to the vortex theory of matter which held that atoms consist of vortex rings in an infinite perfect liquid. The rings were either hollow or filled with a rotating liquid.

With the introduction of heavy transport aircraft in the sixties and following the recognition that trailing vortices posed a threat to light aircraft, several researchers focused on the motion, decay and stability aspects of trailing vortices. Crow (1970) analyzed the sinusoidal instability which usually leads to joining of segments of vortex pairs to form an array of vortex rings. The vortices are idealized as interacting lines, thus neglecting the core structure. The singularity in the self induced velocity is removed by cutting off a portion of the vortex around the singularity point. The cut off length is taken to be proportional to the core diameter. The stability was found to depend on the product of the vortex separation, the cut off length and the perturbation wave number.

Widnall, Bliss & Zalay (1971) used the method of matched asymptotic expansions to obtain a general solution for the flow field within and near a curved vortex with an arbitrary distribution of swirl and axial velocities. The inner solution is found by stretching the radial co-ordinate, $\bar{r} = r/\varepsilon$ where ε is the small parameter defined to be the ratio of core size and the local radius of curvature. The local behavior near the axis is assumed to be that of solid body rotation. It was found that the effect of axial velocity was to reduce the angular velocity of the sinusoidal vortex and the speed of the ring. Physically, a larger Kutta lift is needed to sustain the axial component. Working along the same lines, Ting (1971) examined a viscous vortex. He used the same type of stretching for the inner region as Widnall *et al.*, except that the small

parameter was taken to be the inverse square root of the Reynolds number. This gives a way to describe the decay due to viscosity. But it should be noted that the trailing vortices often decay rapidly after a core bursting occurs or rings form after the reconnection with the counter-rotating vortex.

Moore & Saffman (1971; referred to as MS) considered the velocity of a vortex filament of arbitrary shape and arbitrary distribution of swirl and axial velocity distribution in the core. The necessary equation for the evolution of such a vortex is obtained by balancing the forces on an element of the vortex bounded by a curved surface and two plane ends. The solution is constructed accurate to second order in a small parameter defined to be the ratio of the core radius and the local radius of curvature. The procedure is dealt with in more detail in the following chapter. The highlight of the calculation is that the core deformations in the axial direction are systematically incorporated even though they are dropped in the final simplified result.

Adopting an ad-hoc procedure, Lundgren & Ashurst (1989; referred to as LA) also obtained equations describing the motion of a vortex tube. The cross sectional area of the vortex was assumed to be circular but the variation of the core radius along the axis was included. Their procedure was to model the core as a slug of fluid moving along the vortex under the action of external forces. The external forces were found as sums of Kutta lift, vortex tension, etc., the general forms of which were derived by MS and others. Changes in core area were built into the dynamics by adjusting the size of the core according to the stretching of the fluid particles on the vortex axis. Their numerical solutions for a perturbed vortex ring showed the development of a helical wave. The special case of a straight vortex were found to describe vortex breakdown. This case is considered in detail in connection with the equations of MS in the following chapter.

Fukumoto & Miyazaki (1991) rederived the results of MS using the method of matched asymptotic expansions up to the second order in the expansion variable

defined by the ratio of radius of the vortex core and the local radius of curvature. They also used the fact that the changes in the core size along the axis are of higher order. Under the assumption of localized-induction, they were able to reduce the equations governing self induction of a vortex to a nonlinear evolution equation which is integrable. They present some particular solutions of bending waves including soliton solutions.

1.3 Experimental aspects of vortex breakdown

Vortex breakdown was first recognized in the aerodynamic context of flow over a highly swept wing at high angle of attack. Experiments (Elle, 1960; Lambourne & Bryer, 1961; Peckham & Atkinson, 1957, among many others) clearly showed that a vortex core, marked by injection of dye, suffered drastic structural change above the wing surface. Both types of breakdown, bubble and spiral, are observed. In order to exercise some control, subsequent experimental studies of vortex breakdown were conducted in a tube. Harvey (1962) was among the first to investigate breakdown in this configuration. We briefly describe the set up used by Harvey and summarize the observations since they are of importance to our study. The apparatus consists of a long Perspex tube through which air is drawn by means of a fan mounted at the 'down-stream' end or the outlet of the tube. An initial swirl is imparted to the air at the inlet by a set of adjustable vanes. The vortex core develops from the boundary layer shed from a pointed center body located at the inlet. Smoke injection is used to visualize the vortex core. Wall interference could be minimized by controlling the core size via the application of suction on the center body. The swirl angle (defined as the inverse tangent of the ratio of maximum axial velocity to the maximum swirl velocity) could be changed by altering the vane angle. As the swirl angle was slowly increased subsequent to setting up a stable vortex in the tube, a nearly axisymmetric, almost steady bubble formation was observed, the bubble moving upstream with further increase in the vane angle. Unlike the flow over the wing surface, the bubble was quite nearly closed (achieving a slightly elongated spherical shape) with the

flow downstream of it resembling the flow ahead of the bubble. This leads to the conclusion that this type of vortex breakdown is not a result of instability but, rather, a transition between two vortical states. The conclusion is based on the assumption that instability leads to highly unsteady states in fluid flows. By reducing the core size, the bubble size was reduced without any other changes in the flow structure.

In a more elaborate effort, Faler (1976) made detailed velocity measurements of a vortex breakdown. Laser Doppler anemometry was employed (see also Faler & Leibovich, 1977.) Faler used essentially the same type of device as Harvey except that he used water in a slightly diverging tube in order to minimize the influence of the wall boundary layer. Several flow configurations were observed over a range of Reynolds number and swirl. The breakdown structure was found to move slightly and randomly in the axial direction. Often the structure appeared to change its form. Faler recognized seven types of structures. Type 0 (zero) is the so-called axisymmetric mode of vortex breakdown. This is essentially the same form as found by Harvey and was characterized by a stagnation point on the axis. The dye marking the core expanded abruptly to form a bubble with its envelope exhibiting a high degree of axial symmetry. In Faler's experiment, however, the bubble is not closed in the downstream region and is in fact asymmetric. The bubble was observed to move upstream and shrink in size with increasing Reynolds number and/or amount of swirl. Examination of mean streamlines calculated from the time averaged axial velocity reveals a more complex recirculating region. Encapsuled in an enveloping bubble are two distinct recirculating cells. A larger outer cell contains a larger amount of circulation than the inner smaller cell. Dye injected off the axis follows a smooth and regular helical path with no appreciable change. The type 1 structure is "bubble-like" with a rugged asymmetric envelope. Type 2 is the spiral type structure displaying a rapid deceleration of the core fluid followed by a formation of a kink and then by a spiral motion. In the type 6 structure (also reported by Sarpkaya, 1971, 1974) the filament suffered off axis movement and the rest of the observations can be viewed as

some variants of these basic ones.

Garg & Leibovich (1979) made velocity measurements upstream and in the wakes of vortex breakdowns fields of bubble and spiral types. They report that spectral analysis of the data indicates prominent oscillations in the wake of the breakdown structure at less than 10 Hz. The oscillations are found to be more energetic and the vortex core expansions are larger for the bubble mode which, therefore, is inferred to be the stronger form of breakdown. For a more comprehensive review of structure of vortex breakdown and also some reference to the occurrence of the phenomenon in tornados, see Leibovich (1978).

The basic outcome of these experiments is that vortex breakdown is a phenomenon in which a drastic change in the structure occurs as the core flow decelerates to form a stagnation point on the core center. The flow is strictly unsteady in any breakdown configuration. Unsteady behavior in the case of the axisymmetric breakdown is characterized by very slow oscillations. The flow is usually turbulent downstream of the breakdown region. As is demonstrated by Harvey (1962), the breakdown is a transition of one flow state to the other and not a result of onset of instability.

1.4 Theoretical aspects of vortex breakdown

In his review on the theories of vortex breakdown, Stuart (1987) categorizes the ideas into three classes: (i) theories involving considerations of hydrodynamic stability; (ii) theories involving a natural deceleration of the core flow leading to a stagnation on the axis; and (iii) theories involving conjugate states of flow. We evaluate these ideas and review relevant literature.

Stuart observes that the flow instability phenomena encountered in most fluid flows illustrate connection between stable and unstable states depending on parameters such as the Reynolds number. Further, the instability appears to be insensitive to the downstream boundary conditions. This is contrary to the observation in a vortex breakdown which is strongly dependent on the downstream conditions. For example, application of downstream suction results in a vortex flow devoid of any breakdown

structure. Thus flow instability as a mechanism is considered unimportant if not altogether irrelevant.

The theories of stagnation of flow on the axis are based on observational facts mentioned above in the context of experimental work and are related to the natural tendency of rotating flows (dominantly axisymmetric) to decelerate on axis due to axial forces. Consider for example, a nearly cylindrical vortex. The approximate radial momentum equation states that

$$\frac{\partial p}{\partial r} = \frac{v^2}{r}, \tag{1.1}$$

where p is the pressure, v is the swirl velocity and r is the radial co-ordinate. Integrating equation (1.1) and denoting

$$\Omega = vr \tag{1.2}$$

to be the circulation function one obtains

$$\frac{\partial p}{\partial z}(r=0) = \frac{\partial p}{\partial z}(r) - \int_0^r \frac{\partial \Omega^2}{\partial z}\frac{dr}{r^3}, \tag{1.3}$$

where z is the axial co-ordinate. Using the fact that Ω is conserved on a given streamline, one can show that (also see Hall, 1972)

$$\frac{\partial p}{\partial z}(r=0) = \frac{\partial p}{\partial z}(r) + \alpha\Omega^2/r^2, \tag{1.4}$$

where α is related to u/w, u being the radial velocity and w being the axial velocity. Equation (1.4) is regular at $r = 0$ because the circulation behaves like r^2 for a physically meaningful vortex core. The implication of equation (1.4) is that the axial pressure gradient on the axis is higher than at locations off the axis. Thus if at some axial location there is an adverse pressure gradient present in the flow, it is expected to be the largest on the axis. Therefore, there is a great tendency for the flow to decelerate on the axis.

This idea of stagnation is used by Brown & Lopez (1988) to arrive at a criterion for vortex breakdown. They propose that the mechanism for retardation of the flow

occurs through the action of azimuthal vorticity. We describe their considerations here. For the axisymmetric case, the stream-function ψ is defined in terms of radial (u) and axial (w) velocities by

$$u = -\frac{1}{r}\frac{\partial \psi}{\partial z}, \quad w = \frac{1}{r}\frac{\partial \psi}{\partial r}.$$

In a steady flow the Bernoulli function H (or the total head) and Ω are constant on a stream-surface and are expressible as functions of ψ alone. (see Batchelor, 1967.) Denoting the azimuthal vorticity by η, the governing equation of motion can be written

$$\eta = \frac{\Omega}{r}\frac{\mathrm{d}\Omega}{\mathrm{d}\psi} - r\frac{\mathrm{d}H}{\mathrm{d}\psi}. \tag{1.5}$$

This is the so-called Bragg-Hawthorne or the Squire-Long equation, also discussed in part II. Now consider an upstream region of cylindrical (or nearly cylindrical) flow with axial velocity. We can follow a particular streamline in the meridional plane, the plane containing r and z, and ask the question as to under what conditions does it diverge (move away from the axis). Brown & Lopez consider a streamline described by $r = \sigma(z)$ on which (1.5) becomes

$$\eta(z) = \frac{A}{\sigma} - B\sigma, \tag{1.6}$$

where A and B are constants. Suppose that in the upstream region $z = z_0$, and that all the information such as velocity field, value of H etc., is known on the streamline being considered (and denoted by subscript 0). The constants A and B are found at this location and re-inserted into (1.6) to give

$$\frac{\eta}{\eta_0} = \left(\frac{\alpha_0}{\beta_0}\right)\frac{\sigma_0}{\sigma} - \left(\frac{\alpha_0}{\beta_0} - 1\right)\frac{\sigma}{\sigma_0}, \tag{1.7}$$

where α_0 and β_0 are the tangents of the helix angle for the velocity and vorticity respectively. They are defined as

$$\alpha_0 = \frac{v_0}{w_0}, \quad \beta_0 = \frac{\eta_0}{\zeta_0},$$

where ζ_0 is the axial component of vorticity. If the axial flow retardation occurs primarily through the action of azimuthal vorticity, as the theory proposes, then η must become negative at some axial location. Therefore, if η_0 is positive, we must have $\alpha_0/\beta_0 > 1$. Under this condition it is easily seen that as η becomes negative and continues to grow in magnitude, the streamline continues to diverge. Up to this point the theory says nothing about whether the streamline should continue to diverge, or reach another cylindrical flow configuration or even that they should converge. Brown & Lopez argue: "The development of negative η will induce negative axial velocity on the axis which, by continuity, will lead to a further increase in σ and correspondingly, a further increase in negative vorticity, etc. It is this 'positive feedback,' driving a form of instability, which would account for the relatively rapid divergence of stream surfaces in the proximity of 'breakdown'." The proposed positive feedback mechanism clearly fails to explain occurrence of recirculating bubbles. However, the requirement that the ratio of helix angle be greater than unity for the streamlines to diverge is a useful observation.

The theory of conjugate states as an explanation of vortex breakdown is based on the idea of criticality. Parallel situations are encountered in the formation of hydraulic jumps in water channels and shock waves in supersonic flows. This idea forms the core of Benjamin's theory of vortex breakdown (see Benjamin, 1962, 1967). He explains it as an example of a general type of fluid-dynamical mechanism in which the flows occur in conjugate pairs. Specifically, in the case of swirling flows, for a given distribution of total head and circulation over the stream surfaces one possible flow state is 'subcritical' in the sense that infinitesimal axisymmetric standing waves can occur on it, and the conjugate state is 'supercritical.' The two conjugate states form part of the same overall system. He deduces that compared with their conjugates, supercritical flows possess a deficiency of total momentum or the 'flow force' defined as the integral of axial momentum flux plus pressure over a section through the flow. Thus when the flow undergoes a transition from supercritical to subcritical state

spontaneously, it gains flow-force which manifests either as the 'wave resistance' of a stationary wave train in the subcritical flow or it dissipates in a turbulent region. At the end of this process, the flow-forces of both regions of flow are brought to the same value resulting in a steady state. Benjamin shows that if a given primary flow is supercritical then the conjugate flow is necessarily subcritical. A further property possessed by the conjugate flow is that it preserves the same total head and circulation distribution over the stream surfaces as the primary flow.

It is important to note some limitations of this theory. Both primary and conjugate flows are cylindrical. Hence the explanation of a bubble type of breakdown is not addressed. The theory also does not explain the retardation of the axial flow on the axis, and therefore does not predict reversed flow. In fact, in one of the examples of flow in a pipe in which the upstream conditions consist of a uniform axial flow and a swirl with quadratic distribution, the theory gives *acceleration* of the axial component on the axis. Benjamin argues that this is a result due to an unphysical nature of distribution of swirl.

However, success of the theory is demonstrated in a second example. In this example, the primary flow is a 'combined vortex' consisting of a cylindrical core of solid-body rotation immersed in a tube filled with irrotational fluid. In this case the theory predicts a conjugate flow with a swollen core and a slower axial velocity on the axis. Reversed flow in this example is possible if the primary flow is far supercritical.

1.5 Numerical study of vortex breakdown

As regards the numerical study of the vortex breakdown phenomenon, numerous calculations of steady flow developing a bubble are found in the literature. Most of them use the Navier-Stokes equations rather than the Euler equations. The geometry chosen for the computations, compatible with the experiments, usually consists of a vortex in a tube (Harvey, 1962). The controlling parameters are the volumetric flow rate in the tube and the amount of swirl imparted to the vortex. Inflow conditions usually consist of a swirl profile which rises linearly with the radial distance near the

axis and falls off inversely in the far field. Salas and Kuruvila (1989) report existence of several bubbles. In their solutions, with fixed swirl parameter, a single bubble emerges at low Reynolds number, changes its shape and settles down as the Reynolds number increases. Similar behavior is observed with a secondary bubble appearing downstream and so on with a tertiary bubble. Thus they conclude that in the inviscid limit, there will be an array of several bubbles. We note that for some parameters chosen, the bubbles are situated above the symmetry axis. Beran (1989) has computed solutions to Navier-Stokes for the case of an isolated vortex and for the swirling flow through a frictionless pipe. For Reynolds number 200 or higher, Beran finds four vortex states characterized by the swirl parameter. For small swirl parameter the flow is found to be supercritical in the whole entire computational domain. When the swirl parameter is increased, the flow is observed to become critical at some axial location and a transition point forms. The general features of transition are seen to be in agreement with Benjamin's theory. Formation of transition point is associated with the breakdown of quasi-cylindrical equations. Flow reversals are observed only for large swirl parameter.

Hafez, Kuruvila & Salas (1986) and Leibovich & Kribus (1990) have computed solutions to the so called Bragg-Hawthorne (also known as the Squire-Long) equations equivalent to the Euler equations. In this equation the functional form of H and Ω must be stated explicitly. Both the authors arrive at a bubble like structure by continuing from a known linear solution found by solving an eigenvalue problem. Leibovich & Kribus argue that for large amplitudes, steady periodic waves attain characteristics of solitary waves. When a bubble forms, the streamlines inside the bubble need not necessarily be governed by the same dependence of H and Ω on the stream-function as the streamlines outside of the bubble. Both Hafez *et al.* and Leibovich and Kribus assume that the streamlines inside the bubble obey the same dependence of $H(\psi)$ and $\Omega(\psi)$ as the streamlines outside. The role of H and Ω is discussed again in the next section in the context of present study. Hafez *et al.* also

find a second branch of solutions which does not form any bubble for some range of the swirl parameter. They suggest that this branch is not a solution of the inviscid Euler equations for the following reason. When the solution of the Bragg-Hawthorne equations is substituted into the Euler equations, the first branch yields a residual $O(\Delta x^2)$, where Δx is the grid spacing, while the second branch yields a residual of $O(\Delta x)$ over a range of Δx.

1.6 Outline of present study

In this study we are mainly concerned with aspects of wave motion in a vortex with possible connections to vortex breakdown. We restrict ourselves to the axisymmetric flows. The study is divided into two parts. In the first part we consider dynamics of a vortex core and in the second part we consider finite amplitude steady waves. Also included in the second part is an analysis of the weakly nonlinear stability of a columnar vortex.

The physical mechanism that leads to a breakdown is not well understood. It is clear from the experiments that axisymmetric vortex breakdown is associated with rapid divergence of core size. The axial velocity on the axis reduces as the core size increases. Lundgren and Ashurst explain this divergence to be the result of formation of a "shock." The "shock" in this case signifies that the core area experiences a sudden jump at some axial location. The results of LA also show that the axial velocity reduces across the jump. Therefore, the solutions of LA describe most features of a vortex breakdown observed experimentally except the formation of a reversed flow bubble. The most important aspect of this description is that they provide an explanation as to how a breakdown occurs. Besides this, the results of LA show strong similarity with the results of Benjamin's theory. As mentioned before, LA adopt an ad-hoc procedure in deriving the equations governing the core area of a vortex tube. Their approach is to model the vortex core as a slug of fluid moving under the action of various forces. The force terms used by LA were computed by MS correct up to $O(1/\rho^2)$ where ρ is the local radius of curvature of the vortex. To this order, *i.e.*,

$O(1/\rho^2)$, it was shown by MS that the terms describing variation of the core size are unimportant. We re-examine the MS equations for a straight vortex in Chapter 2. We show that the LA equations are contained in the MS equations. We next perform numerical integration of the MS equations for various types of initial conditions. The results indicate that the MS equations lead to shock formation. Motivated by these results, we seek a comparison of the solutions of the MS equations with the solutions of the Navier-Stokes equations at high Reynolds number. The results of the comparison are given in Chapter 4. As our initial conditions for the Navier-Stokes problem, we consider a cylindrical vortex with a sinusoidal perturbation imposed upon it. The initial conditions for the MS problem are derived by averaging the initial conditions of the Navier-Stokes problem. A jump in the core area in the solutions of the MS equations is seen for very small, moderate and strong perturbations. The manner in which the jump in the core area develops can be assessed by computing the maximum value of the magnitude of the slope of the core wave. This shows a monotonic increase of the slope with time. A comparison with the solutions of the Navier-Stokes equations for a small or moderately perturbed vortex shows qualitatively different development of the core wave. The core wave does not appear to steepen and the slope of the core wave oscillates for the Navier-Stokes problem. When compared with a strongly perturbed vortex, the steepening of the core wave is seen to be similar to the MS case. The core does develop a jump. But, both the axial position and the sense of jump are different. The numerical algorithm used to compute the Navier-Stokes solutions is discussed in Chapter 3.

The second part of this thesis deals with the study of axisymmetric waves of permanent form on vortex cores. Inviscid, axisymmetric flows with swirl are characterized by the Bernoulli function, H, and the circulation function, Ω. In a steady flow and on a given streamline in the meridional plane, both H and Ω are constants. Thus they can be expressed as functions of ψ, the stream-function, alone. This dependence, however, can be completely arbitrary. Every solution of the steady Euler

equations is then characterized by specifying the dependence of the H and Ω on the stream-function. Once the functional form is specified, the solution to the Euler equations is uniquely determined. This forms the basis for Chapter 5 wherein we consider nonlinear extension of the Kelvin waves (Kelvin, 1880). The base flow consists of a columnar vortex with a circular core within which the vorticity is uniform and is directed along the axis. Outside the core, the vorticity is zero. For this base flow, the dependence of H and Ω on ψ is easily computed. The linear Kelvin waves are seen to satisfy the same dependence of these functions as the base flow. We assume that the nonlinear solutions are constrained such that $H(\psi)$ and $\Omega(\psi)$ are of the same form as the base flow. The particular choice of H and Ω makes the governing equation linear. Nonlinearity enters into the problem through the continuity conditions across the perturbed boundary of the vortex core. The shape of the vortex core is determined as part of the problem.

There is no meaningful physical reason which demands that a family of waves defined by a parameter, say the wave-height, be connected by the same dependence of H and Ω on ψ. We view the dependence of H and Ω as being the additional constraints necessary to be able to find solutions unambiguously. It is conceivable, therefore, that we can find unique solutions of the Euler equations by specifying conditions other than $H(\psi)$ and $\Omega(\psi)$. This forms the basis for Chapter 6, in which we consider steady periodic waves on a vortex filament with an initially smooth distribution of vorticity. We find a branch of solutions such that every solution on this branch possesses the same axial mean (taken over one period), including the unperturbed cylindrical flow. In this case, the functional dependence of H and Ω varies, in general, from one solution to the other as the parameter characterizing the branch is varied. The form of dependence is easily computed. The solutions are computed using two methods – by using a direct Newton's method and, by using a perturbation approach. The two methods give the same solution. The perturbation co-efficients are uniquely determined. Hence the solution so found is unique. A

parameter β is introduced which controls the base flow vorticity distribution such that when $\beta \rightarrow 0$, the vorticity distribution tends to that of a columnar vortex described in Chapter 5. Since the axial mean for the perturbed solution is the same as that of the unperturbed vortex, it is evident that the solution found here as $\beta \rightarrow 0$ must differ from the solution found in Chapter 5. In particular we show that there must exist a vortex sheet of constant strength bound to the core boundary at the second order perturbation solution.

Both the nonlinear Kelvin waves and the waves on a smooth distribution of vorticity exhibit regions of reversed flow. This is the form of the bubble type of vortex breakdown. Leibovich & Kribus (1990) and Hafez *et al.* (1986) have also found periodic waves with recirculating regions for a vortex in a tube. They compute the solutions for initially smooth distribution of vorticity similar to the solutions found in Chapter 6. The important difference is that they specify the functional dependence of $H(\psi)$ and $\Omega(\psi)$ while we constrain the base flow. When a bubble of reversed flow forms, a set of closed streamlines inside the bubble form as well. When this happens, an important question as to the specification of the flow inside the bubble arises. Since the closed streamlines are isolated from the external streamlines, they need not necessarily be governed by the same dependence of $H(\psi)$ and $\Omega(\psi)$ as the flow outside. In fact, one can recompute the flow inside the bubble by specifying some other dependence of these functions, and, this can be done in infinite ways. The only constraint is that the pressure and the normal velocity across the streamline bounding the bubble (the separating streamline) must be continuous. The Euler equations admit solutions with jump in tangential component of velocity across a streamline. Leibovich & Kribus and Hafez *et al.* argue that the functional dependence of H and Ω inside the bubble is an analytic continuation of the dependence outside the bubble. In the nonlinear Kelvin waves discussed in Chapter 5, the functional dependence is fixed inside the core including the bubble. In the case of waves on a smooth distribution of vorticity discussed in Chapter 6, we compute the dependence of these functions

inside the bubble and show that they are indeed continuous across the separating streamline.

In Chapter 7, we consider the weakly nonlinear stability of a columnar vortex via multi scale analysis. The amplitude of the disturbance is assumed to vary slowly in time and space. We find that the amplitude satisfies a cubic Schrödinger equation. A derivation is presented. The stability is characterized by the sign of the constants in this equations. The constants are evaluated numerically for various columnar vortices. We find that the vortex is unstable for all the cases considered. By instability we mean that a perturbation grows slowly in time. It is only in this unstable case that solitary waves are possible. The amplitude of the solitary wave solutions depends on the ratio of the constants involved in the Schrödinger equation. For various cases tried, we find that this ratio remains independent of the total circulation. In contrast, Leibovich (1970) found that the evolution of a long wave on a vortex constrained in a pipe is governed by the Korteweg-de Vries equation.

CHAPTER 2

Core Waves on a Vortex Filament

2.1 Introduction

In this chapter we consider waves on the core of a vortex filament. The work of Moore and Saffman (1972) forms the starting point for our investigations. Moore and Saffman (MS) considered the motion of a vortex filament with axial flow. In their paper they aimed at the development of equations for the velocity of an arbitrarily shaped vortex tube. Their procedure was to consider an element of the vortex and compute the pressure distribution on the curved surface arising from the motion of the fluid. The pressure was integrated to obtain the forces acting, and, since the surface is material, the balance of forces leads to the desired equations. The various terms arising in the force balance can be traced to different mechanisms that give rise to them. Most important of these are the Kutta lift and vortex tension.

Lundgren & Ashurst (1989; referred to as LA) arrived at evolution equations for a vortex tube by equating the external force terms composed of Kutta lift, etc., as derived by MS to the rate of change of momentum of the fluid inside the element of the vortex. This fluid is modeled as a solid body rotating about its axis and sliding along the vortex tube with local axial velocity. Further, LA retain the variations of core size along the axial direction without justification. Examination of their equations for a straight vortex yields a set of equations that are similar to 1-D gas dynamics equations and to shallow water equations. These equations describe, therefore, transition from one flow state to another – supersonic to subsonic, for example. This is viewed as a mechanism for the vortex breakdown process. The equations allow for the formation of shocks across which the flow quantities jump abruptly. Core area is shown to be one of the quantities which jumps. This provides a good qualitative description of

vortex breakdown.

In what follows, we note that the analysis carried out by MS includes the variations of the core size along the vortex. However, they argue that these variations take place on a time scale much faster than the time scale involved in the motion of the vortex itself. Thus they drop the corresponding terms and simplify the resulting equations. As we are interested in knowing whether the LA equations are derivable directly from the MS analysis, we proceed with the MS analysis by retaining the core size variations. Next we specialize the MS equations to a straight vortex and show that the resulting equations contain the LA equations as a special case. The MS equations are found to be more general in the sense that they allow for variation of velocity structure within the core of the vortex. We include in this chapter numerical solutions of the MS equations for some typical initial conditions consisting of a cylindrical vortex with sinusoidal perturbation. The results show that the core area develops a "shock" which is expected from the equations. These results motivate us to take up numerical simulation of the full Navier-Stokes equations at high Reynolds numbers which is discussed in the following chapter. A description of the algorithm used to compute the numerical solutions of the MS equations is included in this chapter.

2.2 Equations of motion

We now develop the equations giving particular attention to the ones governing the core deformation. Most of the equations given below appear in MS, but we include them for the sake of completeness.

We will suppose that a vortex filament of strength Γ has the parametric equation

$$\mathbf{x} = \mathbf{R}(\xi, t), \tag{2.1}$$

where $\mathbf{x}$ is the position vector with respect to a fixed frame, and ξ is a Lagrangian variable to be defined shortly. The vortex strength Γ is the total circulation of the

filament and is defined by

$$\Gamma = \int_C \mathbf{v} \cdot d\mathbf{l}, \tag{2.2}$$

where C is any closed contour enclosing the vortex core only once, $\mathbf{v}$ is the velocity, and $\mathbf{l}$ is an element of C. Let $s = s(\xi, t)$ denote the arc length and $\mathbf{s}$ denote the unit tangent vector. We then have $\partial s/\partial \xi = |\partial \mathbf{R}/\partial \xi|$ and $\mathbf{s} = (\partial \mathbf{R}/\partial \xi)/(\partial s/\partial \xi)$. The velocity of the vortex is defined to be $\partial \mathbf{R}/\partial \mathrm{t}$. This is arbitrary to the extent of a scalar multiple of $\mathbf{s}$. The vortex moves because of self induced velocity and any external velocity field. Now an element of the vortex with length ds bounded by the curved surface and two plane ends perpendicular to the local tangents at either end of the element is considered. The curved surface constitutes the core and separates two fluid regions; the fluid inside the core is rotational and the fluid outside is irrotational. A force F_E per unit length is exerted on this surface by the fluid outside and a similar force F_I per unit length is exerted by the fluid inside. Since the surface must move with the fluid we require that $F_E + F_I = 0$. We now present the computation of these forces.

2.2.1 Exterior forces

For each point ξ of the filament one can associate an external velocity, denoted by $\mathbf{V}(\xi, t)$, which can be written

$$\mathbf{V} = \mathbf{V}_E(\xi, t) + \mathbf{V}_I(\xi, t), \tag{2.3}$$

where $\mathbf{V}_E$ is the contribution from external sources and $\mathbf{V}_I$ is the contribution from the vortex itself. $\mathbf{V}_I$ is evaluated using the Biot-Savart law at $\mathbf{x} = \mathbf{R}$. The divergent part of the Biot-Savart integral is removed by subtracting off a divergent contribution from an osculating vortex ring of radius ρ at point ξ. The Lagrangian parameter ξ is now specified so that it is constant for a point moving along the vortex with speed $\mathbf{V} \cdot \mathbf{s}$. Thus

$$\partial \mathbf{R}/\partial \mathrm{t} \cdot \mathbf{s} = \mathbf{V} \cdot \mathbf{s}. \tag{2.4}$$

Now a local orthogonal curvilinear coordinate is set up for analyzing the flow in the vicinity of the element. Consider a point $\mathbf{R}(\xi)$ on the filament. There is a plane containing this point, the unit normal vector $\mathbf{n}$ and the unit binormal $\mathbf{b}$. The vectors $\mathbf{n}$ and $\mathbf{b}$ are defined by

$$\frac{\partial \mathbf{R}}{\partial s} = \mathbf{s}, \quad \frac{\partial \mathbf{s}}{\partial s} = \frac{\mathbf{n}}{\rho}, \quad \mathbf{b} = \mathbf{s} \wedge \mathbf{n}, \quad \frac{\partial \mathbf{b}}{\partial s} = -\tau \mathbf{n}, \quad \frac{\partial \mathbf{n}}{\partial s} = -\frac{\mathbf{s}}{\rho} + \tau \mathbf{b}, \tag{2.5}$$

where ρ is the local radius of curvature and τ is the torsion. A point P in the neighborhood of the vortex has the coordinates $\mathbf{x}(\mathrm{P}) = \mathbf{R}(\xi(s)) + x\mathbf{i} + y\mathbf{j}$ where, $\mathbf{i}$ and $\mathbf{j}$ are the unit vectors such that $\mathbf{n}$ makes an angle ψ and $\mathbf{b}$ makes an angle $\pi/2 + \psi$ with $\mathbf{i}$. The velocity potential $\phi(r, s, \theta, t)$ outside the core satisfies Laplace's equation

$$\frac{\partial^2 \phi}{\partial r^2} + \frac{1}{r}\frac{\partial \phi}{\partial r} + \frac{1}{r^2}\frac{\partial^2 \phi}{\partial \theta^2} + \frac{1}{h}\frac{\partial h}{\partial r}\frac{\partial \phi}{\partial r} + \frac{1}{r^2 h}\frac{\partial h}{\partial \theta}\frac{\partial \phi}{\partial \theta} + \frac{1}{h}\frac{\partial}{\partial s}\left(\frac{1}{h}\frac{\partial \phi}{\partial s}\right) = 0. \tag{2.6}$$

Here r and θ are the local polar coordinates defined by

$$x = r\cos\theta, \qquad y = r\sin\theta, \tag{2.7}$$

and $h = 1 - (r/\rho)\cos(\theta - \psi)$ is the metric coefficient along s. To preserve orthogonality, the coordinate system must rotate by an amount $\mathrm{d}\psi/\mathrm{d}s = \tau$. Equation (2.6) is solved by expanding the potential ϕ and the core radius a in a perturbation series

$$\phi = \phi_0 + \phi_1 + \phi_2 + \cdots, \qquad a = a_0 + a_1 + a_2 + \cdots, \tag{2.8}$$

where ϕ_m and a_m are $O(\rho^{-m})$. In addition the derivatives along the filament are assumed to be $O(1/\rho)$ relative to the derivatives in the $r - \theta$ plane. It is easily seen that $\phi_0 = (\Gamma/2\pi)\theta$ for $r \geq a_0(s,t)$ and that ϕ_1 satisfies

$$\frac{\partial^2 \phi_1}{\partial r^2} + \frac{1}{r}\frac{\partial \phi_1}{\partial r} + \frac{1}{r^2}\frac{\partial^2 \phi_1}{\partial \theta^2} = -\frac{\Gamma}{2\pi\rho r}\sin(\theta - \psi). \tag{2.9}$$

This is solved subject to boundary conditions to be satisfied at the core boundary a_0. They are derived by considering a line element $l = r - a$ which must move with the fluid. This gives

$$\left(\frac{\partial}{\partial t} + \left[\nabla\phi - \frac{\partial \mathbf{R}}{\partial t} - \boldsymbol{\Omega} \wedge (\mathbf{x} - \mathbf{R})\right] \cdot \nabla\right)(r - a_0 - a_1 - a_2 - \cdots) = 0$$
$$\text{on} \quad r = a(s, \theta, t). \tag{2.10}$$

Here, $\mathbf{\Omega}$ is the angular velocity of the triad **s**,**i**, **j**.

Now suppose that a portion of the vortex lies in a plain and consider a typical point P on it. The self induced velocity at P is $v_s = O(\Gamma/\rho)$ and the rotation of the triad is associated with the out of the plane motion of the vortex. Thus the angular velocity is $O(v_s/\rho) = O(\Gamma/\rho^2)$. It is argued by MS that the term $\partial a/\partial t$ is also $O(1/\rho^2)$ and is thus dropped. However, we retain this term as well as the terms describing variation of the core size along the axis in the subsequent equations.

We evaluate the boundary condition on ϕ_1

$$\frac{\partial \phi_1}{\partial r} = \frac{\partial \mathbf{R}}{\partial t} \cdot [\mathbf{n}\cos(\theta - \psi) + \mathbf{b}\sin(\theta - \psi)] + \frac{\Gamma}{2\pi a_0^2}\frac{\partial a_1}{\partial \theta} + \frac{\partial a_0}{\partial t} \qquad \text{on} \quad r = a_0. \tag{2.11}$$

The last term is obtained here in addition to MS. This term acts like a source. We can examine the behavior of the contribution of this term by considering an expanding cylinder of radius a. The potential of such a flow is proportional to $\partial a/\partial t\, a \ln r$. Thus we infer that

$$\phi_1 = (\text{MS terms}) + a_0 \ln r \frac{\partial a_0}{\partial t}. \tag{2.12}$$

The pressure on the surface is calculated using the Bernoulli equation

$$p + \frac{1}{2}(\nabla\phi_0)^2 + \nabla\phi_0 \cdot \nabla\phi_1 - \frac{\partial \mathbf{R}}{\partial t} \cdot \nabla\phi_0 = 0. \tag{2.13}$$

The additional term in ϕ_1 does not contribute to pressure as it enters only through the term $\nabla\phi_1$ and the variations in the θ direction drop out. Subscripts may now be dropped and the pressure may be integrated to give us F_E (which is the same as MS)

$$F_E = \Gamma \mathbf{Q} \wedge \mathbf{s} + \frac{\Gamma^2}{4\pi\rho}\left(\ln\frac{8\rho}{a} - \frac{1}{2}\right)\mathbf{n} - \frac{\Gamma^2}{8\pi a^2}\frac{\partial a^2}{\partial s}\mathbf{s} - \frac{\Gamma^2}{8\pi\rho}\mathbf{n}. \tag{2.14}$$

The first term is the familiar Kutta lift. The second term is known as the vortex tension. This force arises due to the curvature. When the fluid particles traverse a curved path within the core, a net centripetal force arises in the direction of the normal. This would have to be compensated by a difference in the forces on the plane ends of the element of the filament. Thus it acts like tension. The third term is a

force which accounts for motion of fluid through the core of variable area. If the core were uniform, this term would be absent. The last term arises due to the swirl in a curved filament. This term, however, cancels with an equal and opposite term in the interior force. We consider the interior forces in the next section.

2.2.2 Interior forces

The interior forces are calculated by integrating the pressure equation and a balance of momentum inside the core. The pressure distribution is assumed to be symmetric to leading order. The final result is

$$F_I = \pi \frac{\partial}{\partial s}\left[\left(\frac{1}{2}a^2\overline{v^2} - a^2\overline{w^2}\right)\mathbf{s} - a^2\overline{w}\frac{\partial \mathbf{R}}{\partial t} - \lambda\frac{\Gamma\overline{w}a^2}{\pi\rho}\mathbf{b}\right] + \frac{\Gamma^2\mathbf{n}}{8\pi\rho} - \pi a^2\overline{w}\frac{\partial \mathbf{s}}{\partial t} - \pi\mathbf{s}\frac{\partial}{\partial t}(a^2\overline{w}) - \pi a^2\overline{w}\mathbf{s}\frac{\partial}{\partial t}\left(\ln\frac{\partial s}{\partial \xi}\right), \tag{2.15}$$

where

$$\lambda = \frac{2\pi}{\Gamma\overline{w}a^2}\int_0^a r^2 v_0 w_0 \mathrm{d}r. \tag{2.16}$$

Here v_0 and w_0 are the undisturbed swirl and axial velocity profiles. An overbar denotes the average of the quantity over the core area defined as

$$\overline{q} = \frac{2}{a^2}\int_0^a rq(r)\mathrm{d}r. \tag{2.17}$$

2.2.3 Area waves

We now derive equations governing the core variations by taking the tangential component of the force balance equation. Force balance simply states that

$$F_I + F_E = 0. \tag{2.18}$$

First, it is convenient to make some simplifications regarding the internal structure of the core. We take the swirl profile to be the same as MS:

$$v_0 = \frac{\Gamma}{2\pi r}G(r/a), \quad G(1) = 1. \tag{2.19}$$

The exact form of G depends on the initial structure. We take the form for axial velocity to be

$$w_0 = W(s,t) + \frac{\Gamma}{b}\chi(r/a), \qquad \text{with} \quad \overline{\chi} = 0. \tag{2.20}$$

Here b is a length scale which can be determined from a specified profile of w_0. The average axial velocity W is given by

$$W = \frac{2}{a^2}\int_0^a r w_0 \, \mathrm{d}r. \tag{2.21}$$

Further we write

$$a^2\overline{w^2} = a^2W^2 + \frac{a^2\Gamma^2}{b^2}\nu, \qquad \nu = 2\int_0^1 \eta\chi^2 \mathrm{d}\eta, \tag{2.22}$$

where ν is a constant determined from the given initial conditions. The continuity equation within the core is

$$\frac{\partial\xi}{\partial s}\frac{\partial}{\partial t}\left(a^2\frac{\partial s}{\partial\xi}\right) + \frac{\partial}{\partial s}(a^2\overline{w}) = 0. \tag{2.23}$$

Using (2.20) and expanding we get

$$\frac{\partial a^2}{\partial t} + a^2\frac{\partial}{\partial t}\left(\ln\frac{\partial s}{\partial\xi}\right) + \frac{\partial}{\partial s}(a^2W) = 0. \tag{2.24}$$

Now the tangential component of the force balance equation gives

$$\pi\frac{\partial}{\partial s}\left[\frac{1}{2}a^2\overline{v^2} - a^2\overline{w^2}\right] - \pi\mathbf{V}_{||}\frac{\partial a^2\overline{w}}{\partial s} - 2\pi a^2\overline{w}\frac{\partial}{\partial t}\left(\ln\frac{\partial s}{\partial\xi}\right)$$
$$- \pi\frac{\partial}{\partial t}(a^2\overline{w}) - \frac{\Gamma^2}{8\pi}\frac{\partial}{\partial s}(\ln a^2) = 0. \tag{2.25}$$

Here, $V_{||} = \mathbf{s}\cdot\mathbf{V}$. Making use of the definitions of averaged quantities and using the continuity equation (2.24), equation (2.25) reduces to

$$a^2W\frac{\partial w}{\partial s} + \frac{\Gamma^2\nu}{b^2}\frac{\partial a^2}{\partial s} + V_{||}\frac{\partial a^2W}{\partial s} + a^2W\frac{\partial}{\partial t}\left(\ln\frac{\partial s}{\partial\xi}\right) + a^2\frac{\partial W}{\partial t} + \frac{\Gamma^2}{8\pi^2}\frac{\partial}{\partial s}(\ln a^2) = 0. \tag{2.26}$$

We now specialize to a straight filament. We further assume that there is no externally imposed velocity. Then $V_{||} = 0$ and we can take $\xi = s$. The continuity equation (2.23) and equation (2.26) become

$$\frac{\partial a^2}{\partial t} + \frac{\partial}{\partial s}(a^2W) = 0, \tag{2.27}$$

$$a^2\left(\frac{\partial W}{\partial t}+W\frac{\partial W}{\partial s}\right)=-\frac{\partial}{\partial s}\left[\frac{\Gamma^2}{8\pi^2}\ln a^2+\frac{\Gamma^2\nu a^2}{b^2}\right]. \tag{2.28}$$

Lundgren & Ashurst (1989; referred to as LA) obtain the same set of equations (2.27) and (2.28) except the term involving ν in the second equation. They assume slug flow in the core. They model the vortex filament as a space curve along which a mass $\varrho A(s,t)$ per unit length and a velocity $\mathbf{U}(s,t)$ are prescribed at some time. Here, $A=\pi a^2$ is the area of cross-section of the vortex, $\mathbf{U}$ is taken to be the average velocity over a cross-section and ϱ is the fluid density. The conservation of mass is *modeled* by

$$\lambda a^2=a_0^2, \tag{2.29}$$

where a_0 is the initial core radius which is assumed constant and λ is the local stretch ratio defined by

$$\lambda=\frac{\mathrm{d}s}{\mathrm{d}\eta}, \tag{2.30}$$

where η is a Lagrangian variable (different from ξ). The Lagrangian variable η is assumed constant for a slug of fluid moving along the vortex tube with a velocity equal to the local tangential velocity within the core, i.e., the axial velocity. LA write without derivation the equation of motion of an element of the vortex as

$$\varrho A\frac{\partial \mathbf{U}}{\partial \mathbf{t}}=-\varrho A\left(\frac{\partial \mathbf{u}_T}{\partial t}-\mathbf{u}\cdot\mathbf{s}\frac{\partial \mathbf{u_T}}{\partial s}\right)+\varrho\Gamma\mathbf{s}\wedge\mathbf{u}-\frac{\varrho\Gamma^2}{8\pi A}\frac{\partial A}{\partial s}\mathbf{s}-A\nabla P_B, \tag{2.31}$$

where $\mathbf{u}=\mathbf{U}-\mathbf{U}_B$ is the velocity of the vortex relative to the surrounding fluid, $\mathbf{U}_B$ is the self induced velocity given by the Biot-Savart law (evaluated on the centerline), and $\mathbf{u}_T=\mathbf{u}-\mathbf{s}\ \ \mathbf{u}\cdot\mathbf{u}$ is the transverse part of $\mathbf{u}$. Clearly, the left hand side of equation (2.31) is a simplified version of (2.15). However, LA recognize that (2.27) and (2.28) are similar to 1-D gas dynamics equations. Equation (2.27) is identified with the mass conservation equation and the equation (2.28) is identified with the momentum equation. There is however no equation for the internal energy. This then becomes a special case of 1-D gas dynamics equations. The core area takes the role of density while the term in brackets on the right hand side of (2.28) takes the

role of pressure. If we define c to be the "sound speed" then from the theory of gas dynamics we have

$$c^2 = \frac{d\,(pressure)}{d\,(density)}.$$

Using a for density and the pressure term from equation (2.28) we get

$$c^2 = \frac{\Gamma^2\nu}{b^2} + \frac{\Gamma^2}{8\pi^2a^2}. \tag{2.32}$$

Then any infinitesimal disturbance would travel at this sound speed. Thus if the flow velocity w exceeds the sound speed, we have the situation of a supersonic flow resulting in a shock. Thus the condition for shock formation is

$$\frac{w}{V_m} > \sqrt{\frac{4\pi^2a^2\nu}{b^2} + \frac{1}{2}} \tag{2.33}$$

where $V_m = \Gamma/2\pi a$ is *defined* by LA to be the maximum swirl velocity. As noted by LA, these equations are also analogous to the shallow water equations. Steepening of wave-like perturbations due to nonlinearities results in the formation of a hydraulic jump. When the solutions do break, the conditions upstream and downstream of the breakdown region can be related via the shock jump conditions. This theory thus displays a strong similarity with the vortex breakdown theory proposed by Benjamin (1962, 1967). We have already noted that according to Benjamin, the vortex breakdown phenomenon is a finite transition between two steady states of axisymmetric swirling flow which coexist as conjugate states. The flow upstream, say A, of the breakdown point is assumed to be cylindrical and supercritical ("supersonic" state). Thus, no stationary linear waves can be supported by A. The flow downstream, say B, is also cylindrical but subcritical ("subsonic" state). The flow B is termed 'conjugate' to A. The cylindrical flow upstream is determined by the specification of the total head H and the distribution of circulation C on the stream-surface. The conjugate states are related by preservation of the total head and the circulation across the transition region. Because the equations derived here are averaged over the core structure, nothing can be said about the preservation of dependence of H and C.

We now wish to make a note on the effect of ν, the parameter which accounts for the variations across the core. Equation (2.22) can be rewritten as

$$\nu = \frac{b^2}{\Gamma^2} N, \qquad N = 2\int_0^1 \eta w_0^2(\eta) \mathrm{d}\eta - w^2. \tag{2.34}$$

Thus ν is a measure of deviation of mean-square of w_0 from its average. Thus the effect of ν is expected to be small for a vortex with large swirl velocity compared to the axial velocity. We expect the effect to be significant for the case of a jet with weak swirl.

Numerical comparison may be made with a wave speed computation of Maxworthy, Mory and Hopfinger (1983). They consider the following velocity profiles

$$v_0(r) = \frac{\Gamma}{2\pi}\left(1 - e^{-\alpha y}\right)/\sqrt{2y}, \qquad w_0(r) = W_m(1 - \beta y)e^{-\beta y}, \tag{2.35}$$

where W_m is the maximum axial velocity, $y = r^2/2$ and α and β are parameters determined by fitting the profiles to the experimental distribution. By considering the linear disturbance and long wave limit of this basic flow, Maxworthy *et al.* obtain the speed of the waves to be $0.93W_m \pm 0.72V_m$ for $\beta = 4$ cm^{-2}, $\alpha = 25$ cm^{-2}, $W_m = 60$ cm/sec and $\Gamma = 265$ cm^2/sec. As in equation (2.33) we define $V_m = \Gamma/2\pi a$. The core radius is $a = 0.32$ cm. Our calculations give, for the same choice of parameters, the wave speed to be $0.82W_m \pm 0.709V_m$, while the speed computed neglecting ν (LA) is $W_m \pm 0.707V_m$. The speeds measured with respect to a frame fixed to the laboratory are (150.7 cm/sec, −39.1 cm/sec), (153.2 cm/sec, −33.2 cm/sec), (143.2 cm/sec, −43.6 cm/sec) for Maxworthy *et al.*, LA and MS cases respectively. By considering a sinusoidal perturbation with wave number κ on a vortex with base flow profiles given by (2.35) and then numerically approaching the limit of a long wave ($\kappa \to 0$), we obtained the wave speeds to be (139.9 cm/sec, −53.3 cm/sec). These speeds disagree with the speeds reported by Maxworthy *et al.* The source of this diagreement could be due to numerical errors.

Notice that the wave speed predicted by MS theory depends only on the total circulation Γ and not on the details of distribution of the circulation within the core.

However, the actual distribution of the swirl profile and therefore that of circulation within the core affects the long wave speed on a columnar vortex.

Maxworthy *et al.* (1983) measured the speed of a wave on a vortex core experimentally. They report only one wave speed of -76 cm/sec. The negative value implies that the wave moves against the axial velocity. The theoretical wave speeds shown above were computed for the profiles (2.35) fitted with this experiment. Though the wave speeds do not greatly disagree among the three theoretical values, they are too far off from the experimental value. No decisive conclusions can be drawn as to the validity of MS or LA theories.

Prior to the discussion of the numerical implementation of MS equations, we wish to summarize the theoretical aspects. We have shown that in the case of a straight axisymmetric flow, the MS equations indeed contain the fast scales which drive the core waves. Further we have seen that the MS equations allow for arbitrary structure inside the core and therefore yield generalizations of the LA equations. However, the scope of the equations derived here is still limited in view of the assumed profiles for the axial and swirl velocities given by (2.19) and (2.20). As a result of these assumptions, the swirl component does not play any role in the dynamics represented by (2.27) and (2.28) which describe the evolution of the core and the axial velocity. This need not be true for a general case as will be seen in the numerical simulations in the following chapters.

The mechanism of vortex breakdown represented by these equations is similar to the wave breaking process. A wave like disturbance does not grow in its amplitude but it steepens and ultimately breaks. The region of breaking is represented by a shock. Across the shock, the axial velocity must necessarily undergo deceleration. Although this does not lead us to conclude that this is associated with the bubble of recirculating region (since the structure in the radial direction is averaged out), it does agree with the description that a vortex breakdown occurs when the fluid decelerates to form a stagnation point on the axis followed by the appearance of a recirculating

bubble (Garg & Leibovich, 1979, Stuart, 1989). Thus these equations have the merit of predicting deceleration of axial velocity which probably should be viewed as a basic requirement for breakdown. But, as in Benjamins theory, the upstream and downstream regions of breakdown represent some sort of cylindrical configuration.

2.3 Linear waves

We now consider linear solutions of equations (2.27) and (2.28). We do this in preparation for the numerical implementation of the fully nonlinear equations. Let the axis of the vortex be aligned with the z-axis. Let A and a be the area of cross section and the radius of cross section of the vortex respectively. Then

$$A(z,t) = \pi a^2(z,t). \tag{2.36}$$

Let

$$A(z,0) = A_0, \quad W(z,0) = W_0, \tag{2.37}$$

be the unperturbed base solution of (2.27) and (2.28). Now consider a perturbation to the base flow of the form

$$A(z,t) = A_0 + \varepsilon A_1 e^{i(\kappa z - \sigma t)}, \tag{2.38a}$$

$$w(z,t) = W_0 + \varepsilon w_1 e^{i(\kappa z - \sigma t)}, \tag{2.38b}$$

where κ is a given real number and $\varepsilon \ll 1$ is a parameter. A_1, w_1 and σ are numbers to be found. Substituting (2.38) into (2.27) and (2.28) and neglecting all the terms $O(\varepsilon^2)$ and higher we get

$$(\kappa W_0 - \sigma)A_1 + \kappa A_0 W_1 = 0, \tag{2.39a}$$

$$\left(\frac{\Gamma^2\kappa}{8\pi} + \frac{\Gamma^2\nu\kappa}{b^2}A_0\right)A_1 + (\kappa W_0 - \sigma)w_1 = 0. \tag{2.39b}$$

A non-trivial solution exists for (2.39) only if

$$\frac{\sigma}{\kappa} = W_0 \pm c_0, \tag{2.40}$$

where

$$c_0 = \sqrt{\frac{\Gamma^2}{8\pi A_0} + \frac{\Gamma^2 \nu}{b^2}}. \tag{2.41}$$

Since σ is real and is linearly proportional to the disturbance wave number κ, any linear disturbance of arbitrary shape propagates with speed given by (2.40). This was, of course, expected from the linear theory of gas dynamics. If $W_0 > c_0$ then (2.40) yields only positive values for σ and the waves propagate only to the right. That is, the flow is supercritical (Benjamin, 1962). In the following section we consider the numerical evolution of an initially nonlinear disturbance.

2.4 Numerical integration

As before, we assume that the axis of the vortex is aligned with the z-axis. Let x denote a co-ordinate moving along the z axis at constant speed. We choose the speed of the moving frame such that

$$x = \kappa z - \sigma_1 t, \tag{2.42}$$

where κ is a given real number and σ_1 is found from the linear analysis outlined in section 2.3. We consider numerical solutions of (2.27) and (2.28) in a moving frame. We are primarily interested in wave propagation on vortex cores. We consider an initial disturbance and follow its development in time. For simplicity the initial disturbance will be taken to be wave like so that we may consider the flow to be periodic in the axial direction. The variable κ can then be used to control the length of the axial domain. The assumption of periodicity also enables us to decompose the flow variables in to a Fourier series. Further, we add an artificial viscous term to the momentum equation (2.28). This is done in order to suppress unnecessary growth of high frequency oscillations that arise primarily due to numerical errors.

We rewrite (2.27) and (2.28) as

$$\frac{\partial A}{\partial t} = F + \sigma_1 \frac{\partial A}{\partial x}, \tag{2.43a}$$

$$\frac{\partial w}{\partial t} = G + \sigma_1 \frac{\partial w}{\partial x} + \mu_1 \kappa^2 \frac{\partial^2 w}{\partial x^2}, \tag{2.43b}$$

where μ_1 is the coefficient of viscosity and

$$F = -\kappa \frac{\partial Aw}{\partial x}, \tag{2.44a}$$

$$G = -\kappa\, w \frac{\partial w}{\partial x} - \kappa\, \frac{1}{A}\, \frac{\partial}{\partial x} \left[\frac{\Gamma^2}{8\pi} \ln A + \frac{\Gamma^2 \nu A}{b^2} \right]. \tag{2.44b}$$

We decompose A and w into a truncated Fourier series given by

$$A(x,t) = \sum_{\ell=0}^{m} A_\ell^e(t) \cos(\ell x) + \sum_{\ell=1}^{m} A_\ell^o(t) \sin(\ell x), \tag{2.45a}$$

$$w(x,t) = \sum_{\ell=0}^{m} w_\ell^e(t) \cos(\ell x) + \sum_{\ell=1}^{m} w_\ell^o(t) \sin(\ell x). \tag{2.45b}$$

The Fourier modes of F and G are computed by evaluating the nonlinear products appearing in (2.44) in the physical domain. A fast Fourier transform (FFT) is employed to compute the modal coefficients. We separate the Fourier components in (2.43) to give the following evolution equations for the Fourier modes,

$$\frac{\partial A_\ell^e}{\partial t} = F_\ell^e + \sigma_1 \ell A_\ell^o, \tag{2.46a}$$

$$\frac{\partial A_\ell^o}{\partial t} = F_\ell^o - \sigma_1 \ell A_\ell^e, \tag{2.46b}$$

$$\frac{\partial w_\ell^e}{\partial t} = G_\ell^e + \sigma_1 \ell w_\ell^o - \mu_1 (\kappa \ell)^2 w_\ell^e, \tag{2.46c}$$

$$\frac{\partial w_\ell^o}{\partial t} = G_\ell^o - \sigma_1 \ell w_\ell^e - \mu_1 (\kappa \ell)^2 w_\ell^o. \tag{2.46d}$$

Equations (2.46) represent a set of $(4m + 2)$ ordinary differential equations. These equations are integrated numerically using a combination of Adams-Bashforth and Crank-Nicolson schemes. If the solution at times t and $t - \Delta t$ is known, where Δt is the increment in time, then the solution at time $t + \Delta t$ can be found from

$$\frac{1}{\Delta t} \left[A_\ell^e(t + \Delta t) - A_\ell^e(t) \right] = \frac{3}{2} F_\ell^e(t) - \frac{1}{2} F_\ell^e(t - \Delta t) + \frac{\ell \sigma_1}{2} \left[A_\ell^o(t + \Delta t) + A_\ell^o(t) \right], \tag{2.47a}$$

$$\frac{1}{\Delta t} \left[A_\ell^o(t + \Delta t) - A_\ell^o(t) \right] = \frac{3}{2} F_\ell^o(t) - \frac{1}{2} F_\ell^o(t - \Delta t) - \frac{\ell \sigma_1}{2} \left[A_\ell^e(t + \Delta t) + A_\ell^e(t) \right], \tag{2.47b}$$

$$\frac{1}{\Delta t}\left[w_\ell^e(t+\Delta t)-w_\ell^e(t)\right]=\frac{3}{2}F_\ell^e(t)-\frac{1}{2}F_\ell^e(t-\Delta t)+\frac{\ell\sigma_1}{2}\left[w_\ell^o(t+\Delta t)+w_\ell^o(t)\right]$$
$$-\frac{\mu_1\kappa^2\ell^2}{2}\left[w_\ell^e(t+\Delta t)+w_\ell^e(t)\right], \tag{2.47c}$$

$$\frac{1}{\Delta t}\left[w_\ell^o(t+\Delta t)-w_\ell^o(t)\right]=\frac{3}{2}F_\ell^o(t)-\frac{1}{2}F_\ell^o(t-\Delta t)-\frac{\ell\sigma_1}{2}\left[w_\ell^e(t+\Delta t)+w_\ell^e(t)\right]$$
$$-\frac{\mu_1\kappa^2\ell^2}{2}\left[w_\ell^o(t+\Delta t)+w_\ell^o(t)\right]. \tag{2.47d}$$

These equations are readily solved for the unknowns at time $t+\Delta t$. We get

$$A_\ell^e(t+\Delta t)=\frac{1}{D_f}\left(F_{1_\ell}+\frac{1}{2}\Delta t\ \sigma_1\ell F_{2_\ell}\right), \tag{2.48a}$$

$$A_\ell^o(t+\Delta t)=\frac{1}{D_f}\left(F_{1_\ell}-\frac{1}{2}\Delta t\ \sigma_1\ell F_{2_\ell}\right), \tag{2.48a}$$

$$w_\ell^e(t+\Delta t)=\frac{1}{D_g}\left[\left(1+\frac{1}{2}\Delta t\kappa^2\ell^2\mu_1\right)G_{1_\ell}+\frac{1}{2}\Delta t\ \sigma_1\ell G_{2_\ell}\right], \tag{2.48c}$$

$$w_\ell^o(t+\Delta t)=\frac{1}{D_g}\left[\left(1+\frac{1}{2}\Delta t\kappa^2\ell^2\mu_1\right)G_{1_\ell}-\frac{1}{2}\Delta t\ \sigma_1\ell G_{2_\ell}\right], \tag{2.48d}$$

where

$$D_f=1+\frac{1}{4}\Delta t^2\sigma_1^2\ell^2, \tag{2.49a}$$

$$D_g=\left(1+\frac{1}{2}\kappa^2\ell^2\mu_1\Delta t\right)^2+\frac{1}{4}\Delta t^2\sigma_1^2\ell^2, \tag{2.49b}$$

and

$$F_{1_\ell}=A_\ell^e(t)+\Delta t\left[\frac{3}{2}F_\ell^e(t)-\frac{1}{2}F_\ell^e(t-\Delta t)\right]+\frac{\Delta t}{2}\ell\sigma_1A_\ell^o(t), \tag{2.50a}$$

$$F_{2_\ell}=A_\ell^o(t)+\Delta t\left[\frac{3}{2}F_\ell^o(t)-\frac{1}{2}F_\ell^o(t-\Delta t)\right]-\frac{\Delta t}{2}\ell\sigma_1A_\ell^e(t), \tag{2.50b}$$

$$G_{1_\ell}=w_\ell^e(t)+\Delta t\left[\frac{3}{2}G_\ell^e(t)-\frac{1}{2}G_\ell^e(t-\Delta t)\right]+\frac{\Delta t}{2}\left[\ell\sigma_1w_\ell^o(t)-\kappa^2\ell^2\mu_1w_\ell^e(t)\right], \tag{2.50c}$$

$$G_{2_\ell}=w_\ell^o(t)+\Delta t\left[\frac{3}{2}G_\ell^o(t)-\frac{1}{2}G_\ell^o(t-\Delta t)\right]-\frac{\Delta t}{2}\left[\ell\sigma_1w_\ell^e(t)+\kappa^2\ell^2\mu_1w_\ell^o(t)\right]. \tag{2.50d}$$

The equations stated above are applicable to all the Fourier modes $\ell=0,\ldots m$. However, since we employ the FFT, the m^{th} sine mode in the representation (2.45)

is not resolved. As a result, the evolution equations (2.46) are not strictly valid for $\ell = m$. We circumvent this problem by simply dropping all the equations for $\ell = m$.

2.5 Results

Four different solutions are presented in Figures 2.1 through 2.4. For each of these cases, the initial conditions are assumed to be of the form

$$W(x) = W_0 + W_1^e \cos(x), \tag{2.51a}$$

$$A(x) = A_0 + A_1^e \cos(x), \tag{2.51b}$$

where W_0 is the average of the given undisturbed axial velocity profile and A_0 is the area of the vortex. If a_0 denotes the radius of the undisturbed vortex then $A_0 = \pi a_0^2$. We choose some axial velocity profile and compute the average W_0. We further choose some Γ and a_0. We next compute the linear wave speed σ_1. We choose some value for the perturbation W_1 and we compute the value of A_1 using the linear theory. From equation (2.39a) we get

$$A_1 = \frac{\kappa A_0}{\sigma_1 - \kappa W_0} W_1. \tag{2.52}$$

We define the Reynolds number for the flow to be

$$Re = \Gamma/\mu_1. \tag{2.53}$$

A linear wave moving with a speed of σ_1/κ with respect to a frame fixed at infinity takes a time of

$$T = \kappa\ 2\pi/\sigma_1, \tag{2.54}$$

to traverse a distance of 2π. We measure time in units of T.

In Figure 2.1.1a – 2.1.1c, the cross section of the vortex in the meridional plane (the plane defined by the radial and the axial co-ordinates) is shown for different times. The initial undisturbed axial velocity is taken to be uniform with $W_0 = 1.1$ and the radius is taken to be $a_0 = 1.0$. $\Gamma = 15.75$, $Re = 1575$ and $W_1 = 0.4$ were chosen. A modal resolution of $m = 64$ was used. The initial wave steepens resulting

in a shock that develops at about $t = 2.0$. The shock seems to persist up to $t = 4.0$. Beyond this time, numerical breakdown of the solution occurred. In Figure 2.1.2, the time development of the axial velocity is shown for $t = 0$ to $t = 4$. The axial velocity shows a greater sensitivity to numerical oscillations than the core area.

An axial velocity of the form

$$w_0(r) = W_m e^{-r^2/L^2}, \tag{2.55}$$

was chosen with $W_m = 10.0$ and $L = 1.0$ for the solution presented in Figure 2.2. The average of (2.55) gives a value of $W_0 = 6.32$. The rest of the parameters consisted of $\Gamma = 15.75$, $a_0 = 1.0$, $Re = 1575$ and $W_1 = 0.5$. A modal resolution of $m = 128$ was used. A shock forms at about $t = 4.0$ - later than in the previous case. The axial velocity is shown in Figure 2.2.2 and it shows numerical breakdown at about $t = 5$.

An axial velocity of the form

$$w_0(r) = W_m \left(1 - \beta r^2/2\right) e^{-\beta r^2/r}, \tag{2.56}$$

was chosen with $W_m = 60$ and $\beta = 4$ for the solution presented in Figure 2.3 as well as Figure 2.4. The profile and the parameters were chosen to match the experiments of Maxworthy *et al.* The average axial velocity of $W_0 = 8.12$ was computed from given parameters. The rest of the parameters consisted of $\Gamma = 265$, $a_0 = 1$ and $W_1 = 30$. The only difference in the solutions presented in Figure 2.3 and 2.4 is the Reynolds number. They are $Re = 2650$ and 5300 for Figures 2.3 and 2.4 respectively. A modal resolution of $m = 256$ was chosen. In both the cases, the shock forms rather quickly, at about $t = 0.6$. The effect of increase in the Reynolds number appears to be negligible on the core shape. But, the numerical oscillations in the axial velocity are greatly enhanced.

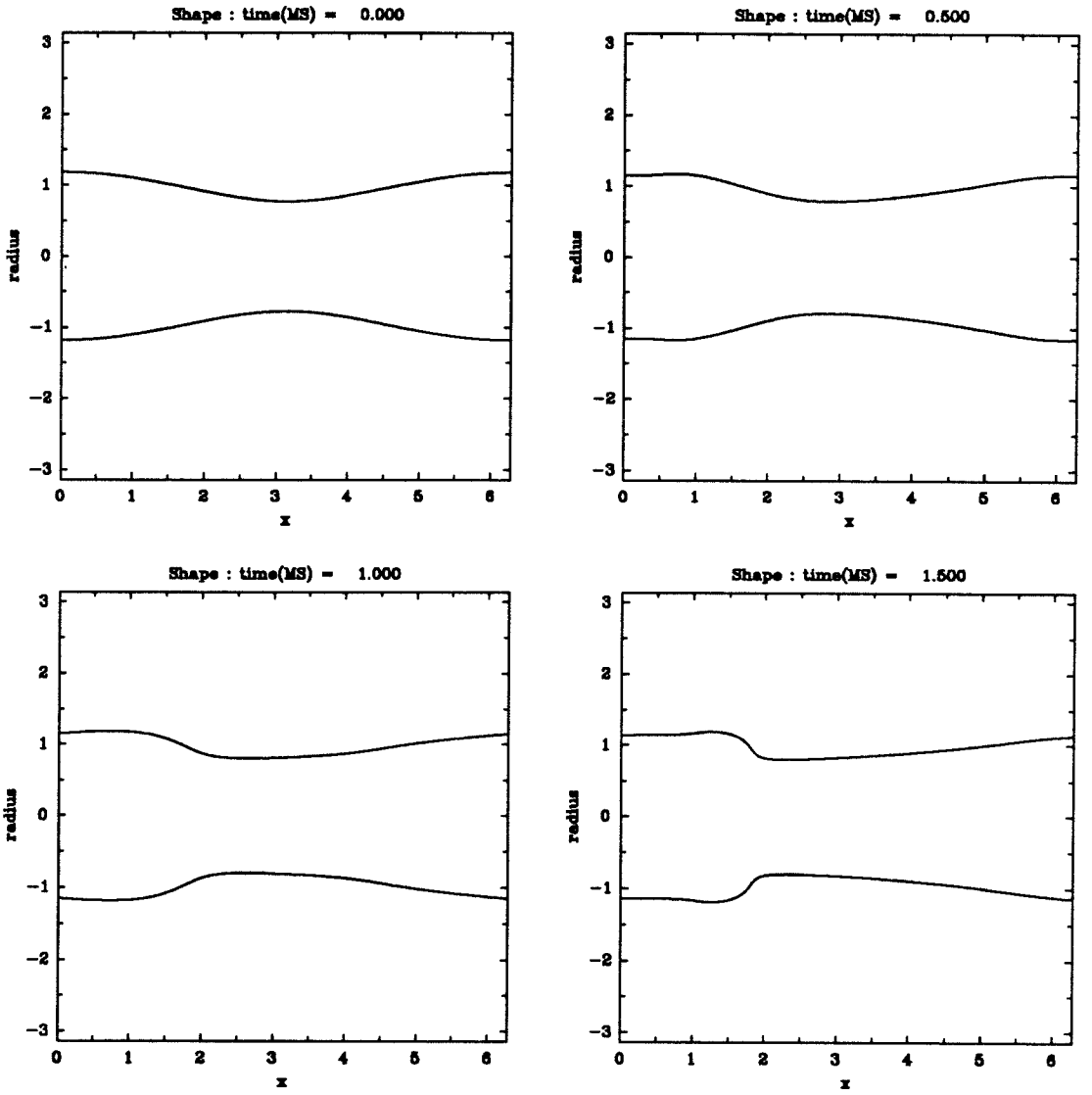

Fig. 2.1.1a The cross section of the vortex filament in the meridional plane is shown for $t = 0.0,\ 0.5,\ 1.0$, and 1.5. An uniform axial velocity profile with $W_0 = 1.1$ and core radius of $a_0 = 1$ was used for the base flow. The other parameters were $\Gamma = 15.75$, $Re = 1575$, $W_1 = 0.4$ and $m = 64$.

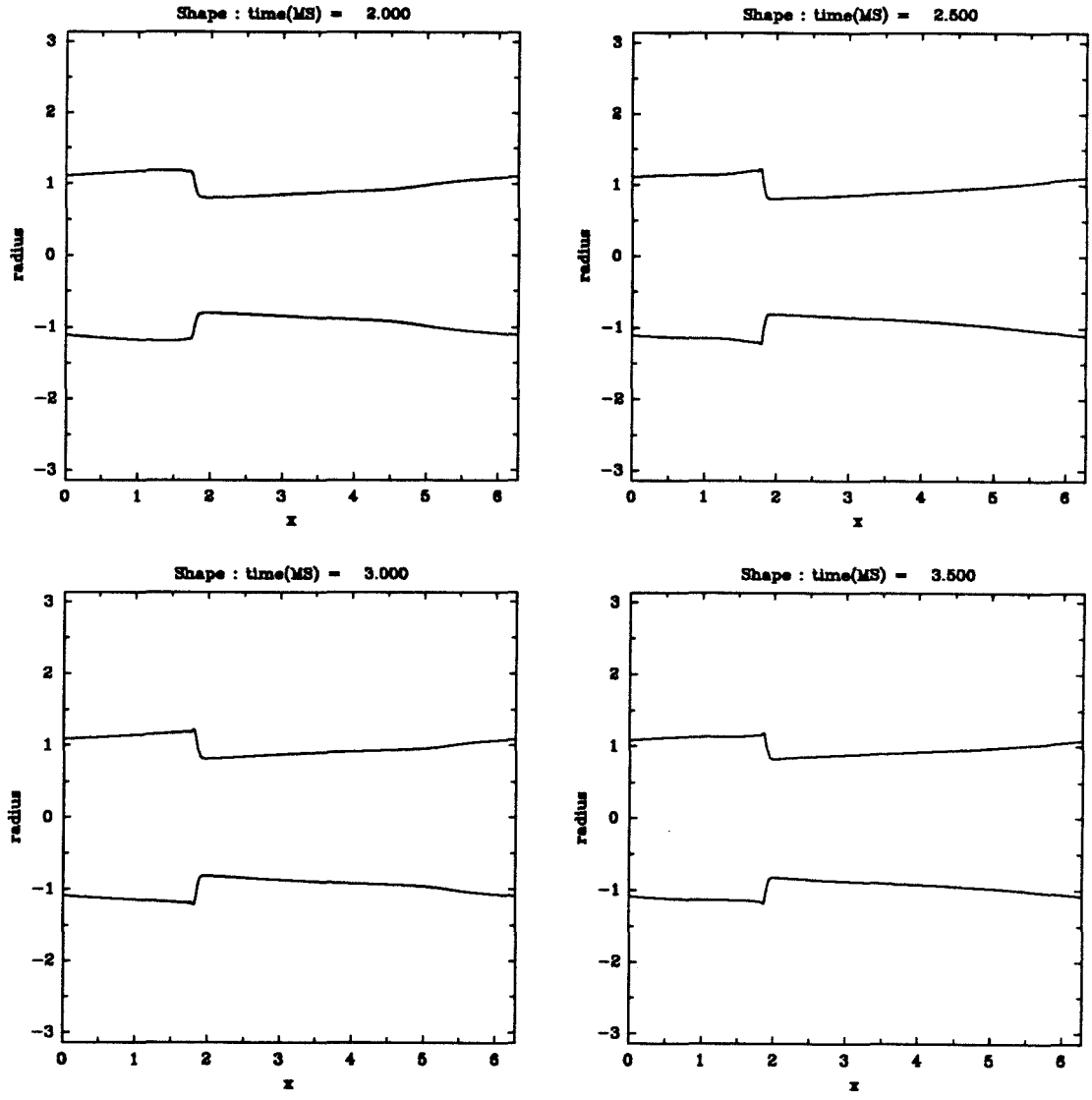

Fig. 2.1.1b The cross section of the vortex filament in the meridional plane is shown for $t = 2.0,\ 2.5,\ 3.0$, and 3.5. An uniform axial velocity profile with $W_0 = 1.1$ and core radius of $a_0 = 1$ was used for the base flow. The other parameters were $\Gamma = 15.75$, $Re = 1575$, $W_1 = 0.4$ and $m = 64$.

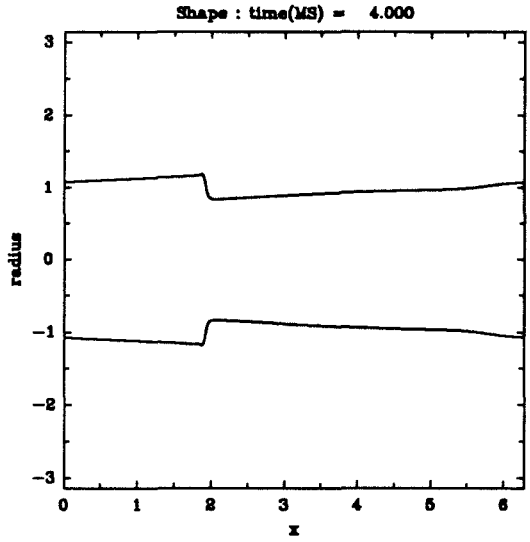

Fig. 2.1.1c The cross section of the vortex filament in the meridional plane is shown for $t = 4.0$. An uniform axial velocity profile with $W_0 = 1.1$ and core radius of $a_0 = 1$ was used for the base flow. The other parameters were $\Gamma = 15.75$, $Re = 1575$, $W_1 = 0.4$ and $m = 64$.

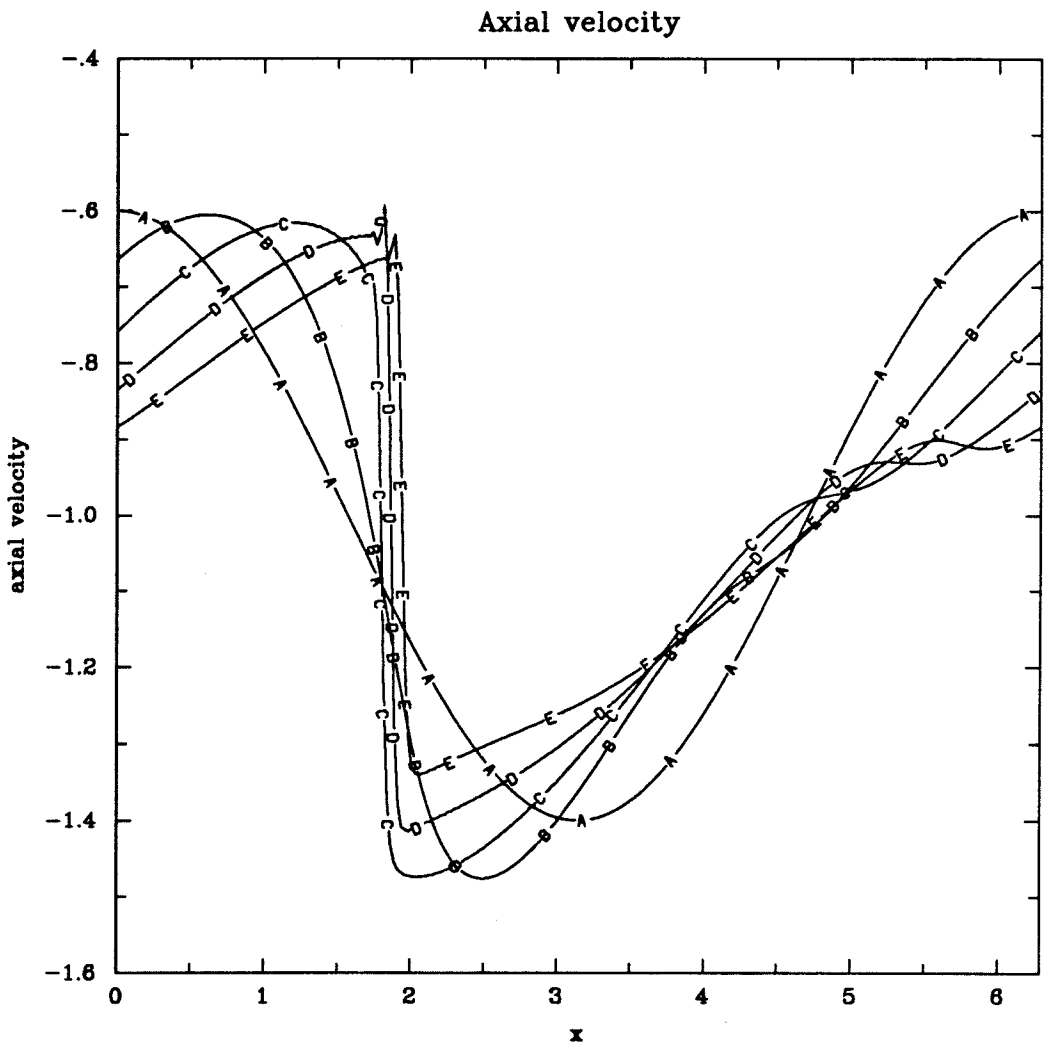

Fig. 2.1.2 The axial velocity as a function of x is shown for various time. Shown here are A. $t = 0$, B. $t = 1$, C. $t = 2$, D. $t = 3$, and E. $t = 4$. The parameters are listed in Figure 2.1.1.

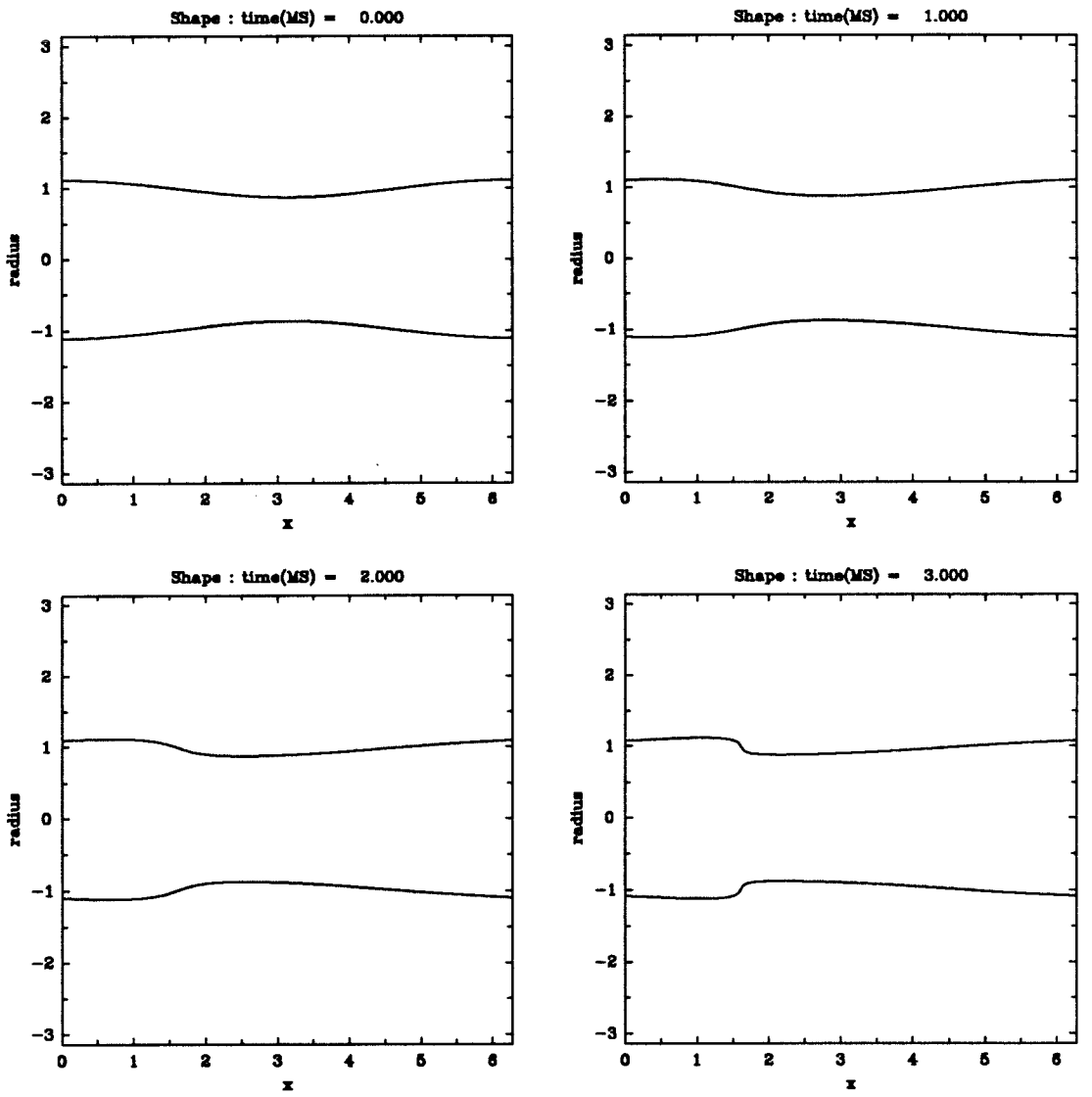

Fig. 2.2.1a The cross section of the vortex filament in the meridional plane is shown for $t = 0,\ 1,\ 2$, and 3. An exponential velocity profile (equation 2.55) with $W_m = 10$, $L = 1$ and core radius of $a_0 = 1$ was used for the base flow. The other parameters were $\Gamma = 15.75$, $Re = 1575$, $W_1 = 0.5$ and $m = 128$.

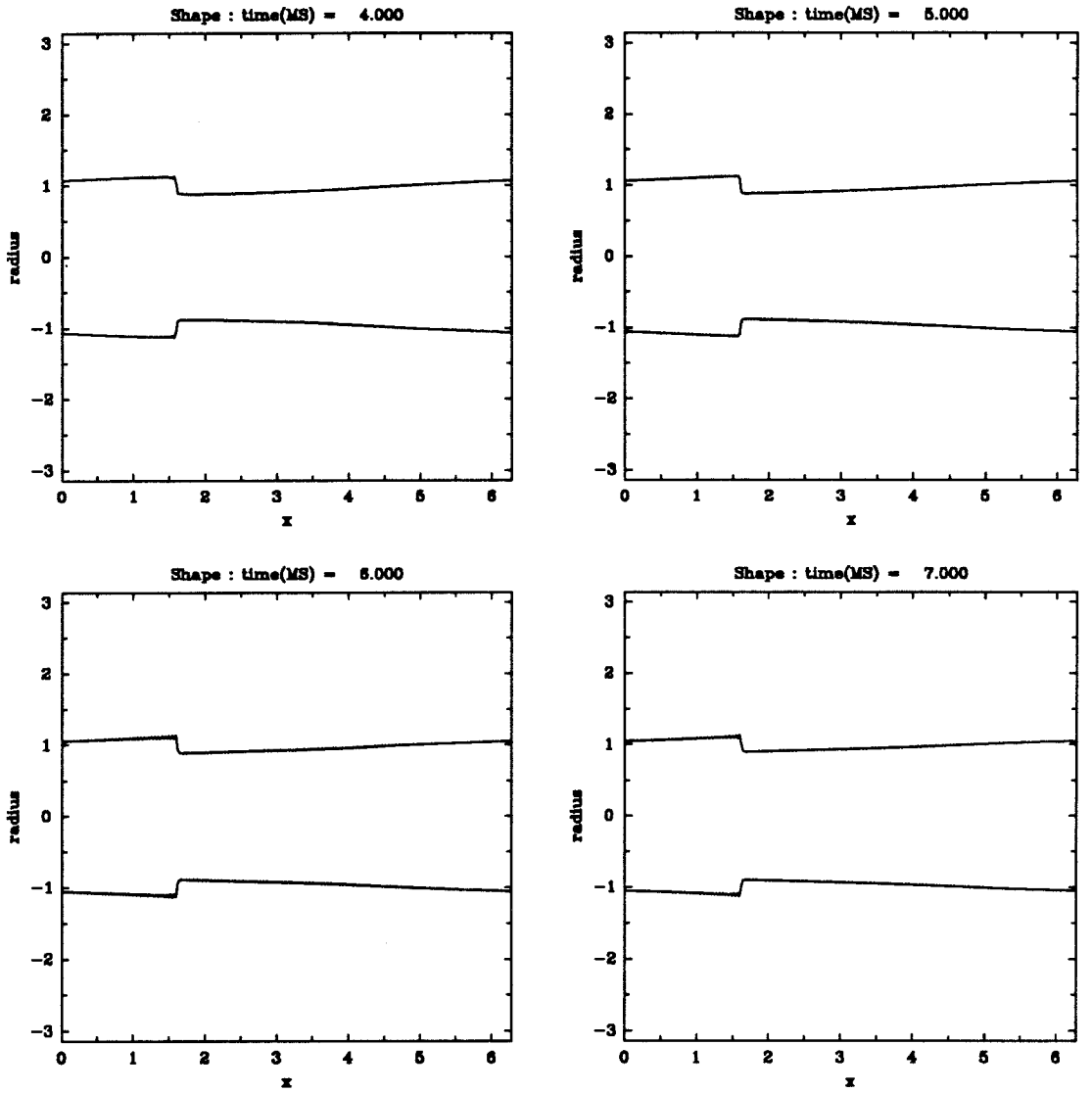

Fig. 2.2.1b The cross section of the vortex filament in the meridional plane is shown for $t = 4,\ 5,\ 6$, and 7. An exponential velocity profile (equation 2.55) with $W_m = 10$, $L = 1$ and core radius of $a_0 = 1$ was used for the base flow. The other parameters were $\Gamma = 15.75$, $Re = 1575$, $W_1 = 0.5$ and $m = 128$.

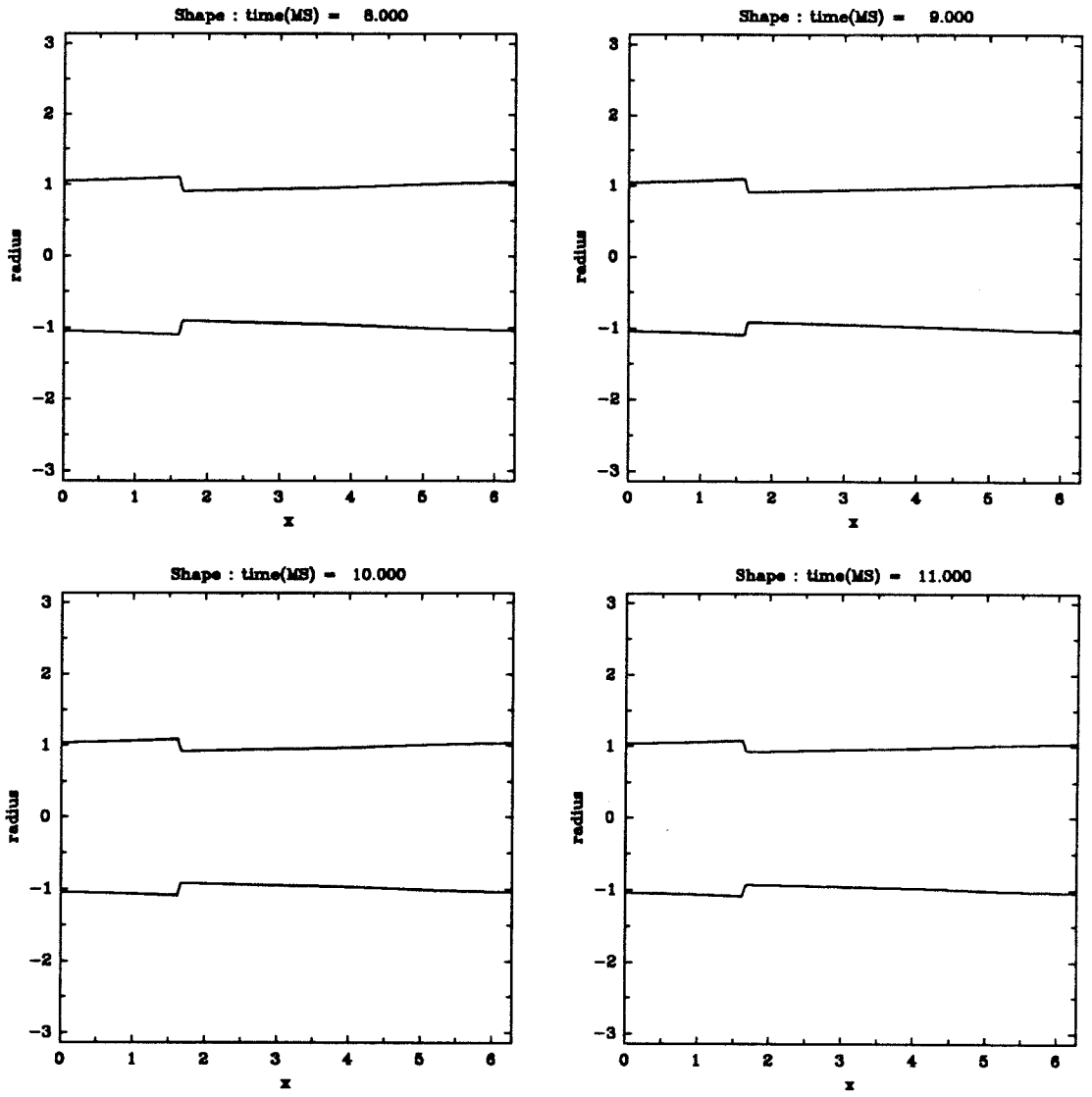

Fig. 2.2.1c The cross section of the vortex filament in the meridional plane is shown for $t = 8,\ 9,\ 10$, and 11. An exponential velocity profile (equation 2.55) with $W_m = 10$, $L = 1$ and core radius of $a_0 = 1$ was used for the base flow. The other parameters were $\Gamma = 15.75$, $Re = 1575$, $W_1 = 0.5$ and $m = 128$.

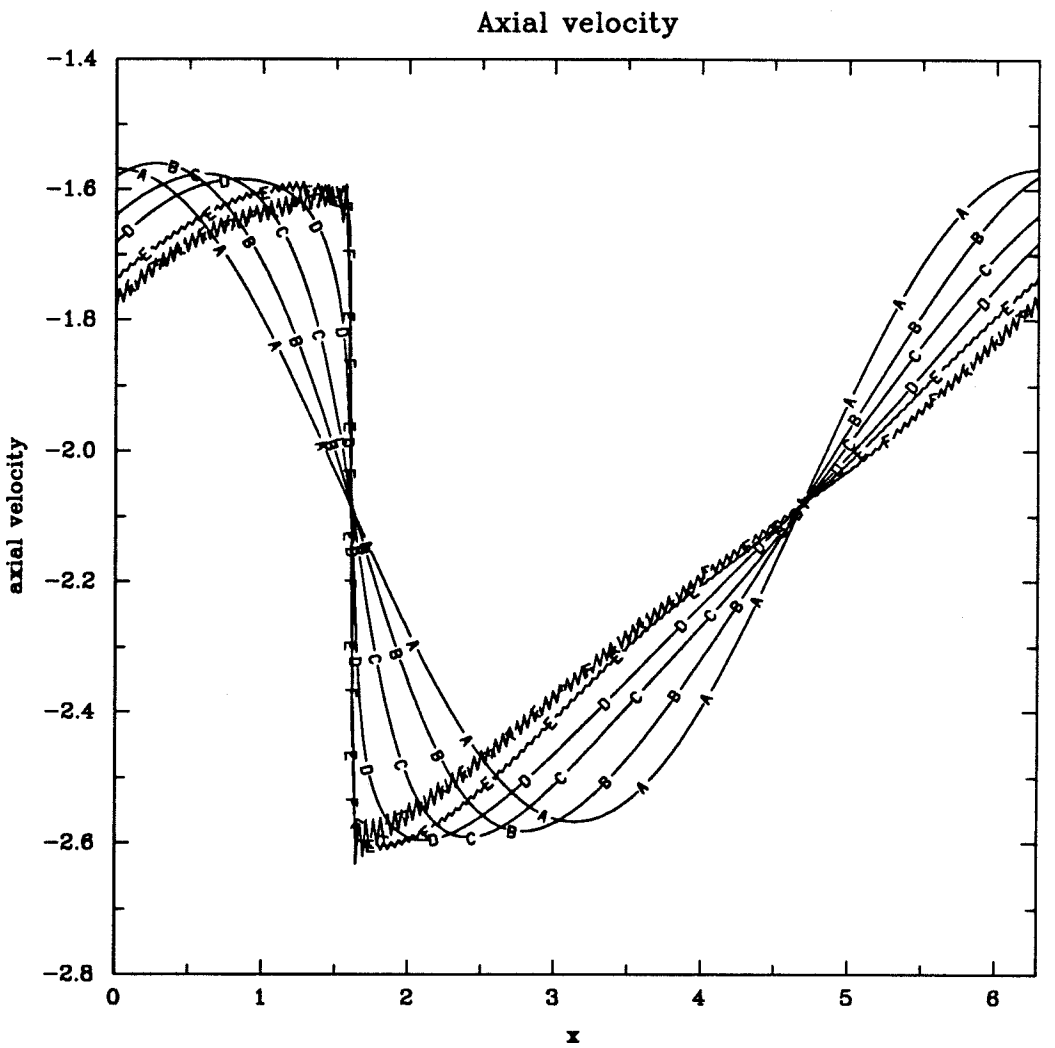

Fig. 2.2.2 The axial velocity as a function of x is shown for various time. Shown here are A. $t = 0$, B. $t = 1$, C. $t = 2$, D. $t = 3$, E. $t = 4$, and F. $t = 5$. The parameters are listed in Figure 2.2.1.

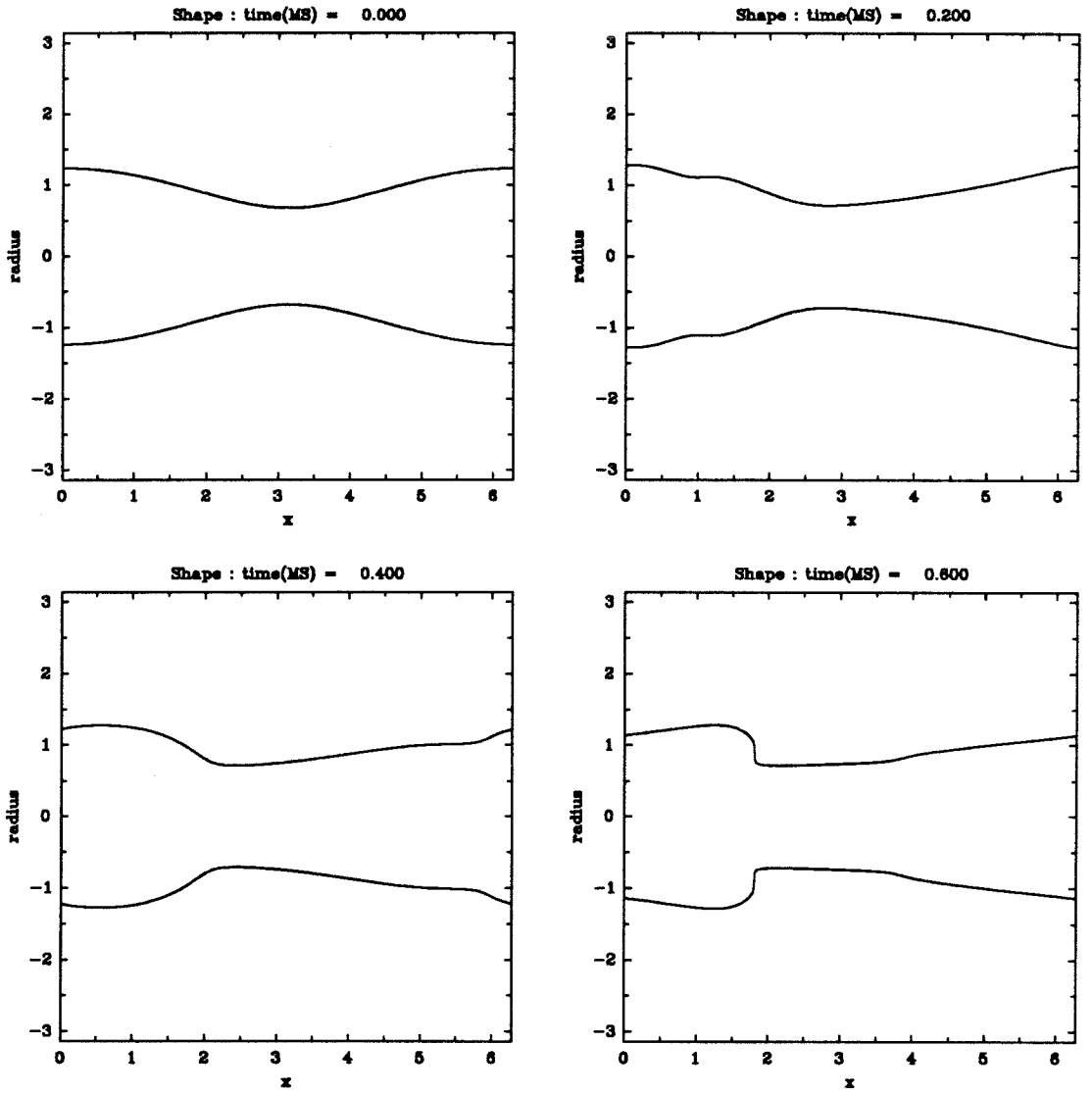

Fig. 2.3.1 The cross section of the vortex filament in the meridional plane is shown for $t = 0.0,\ 0.2,\ 0.4$, and 0.6. An exponential velocity profile (equation 2.56) with $W_m = 60$, $\beta = 4$ and core radius of $a_0 = 1$ was used for the base flow. The other parameters were $\Gamma = 265$, $Re = 2650$, $W_1 = 30$ and $m = 256$.

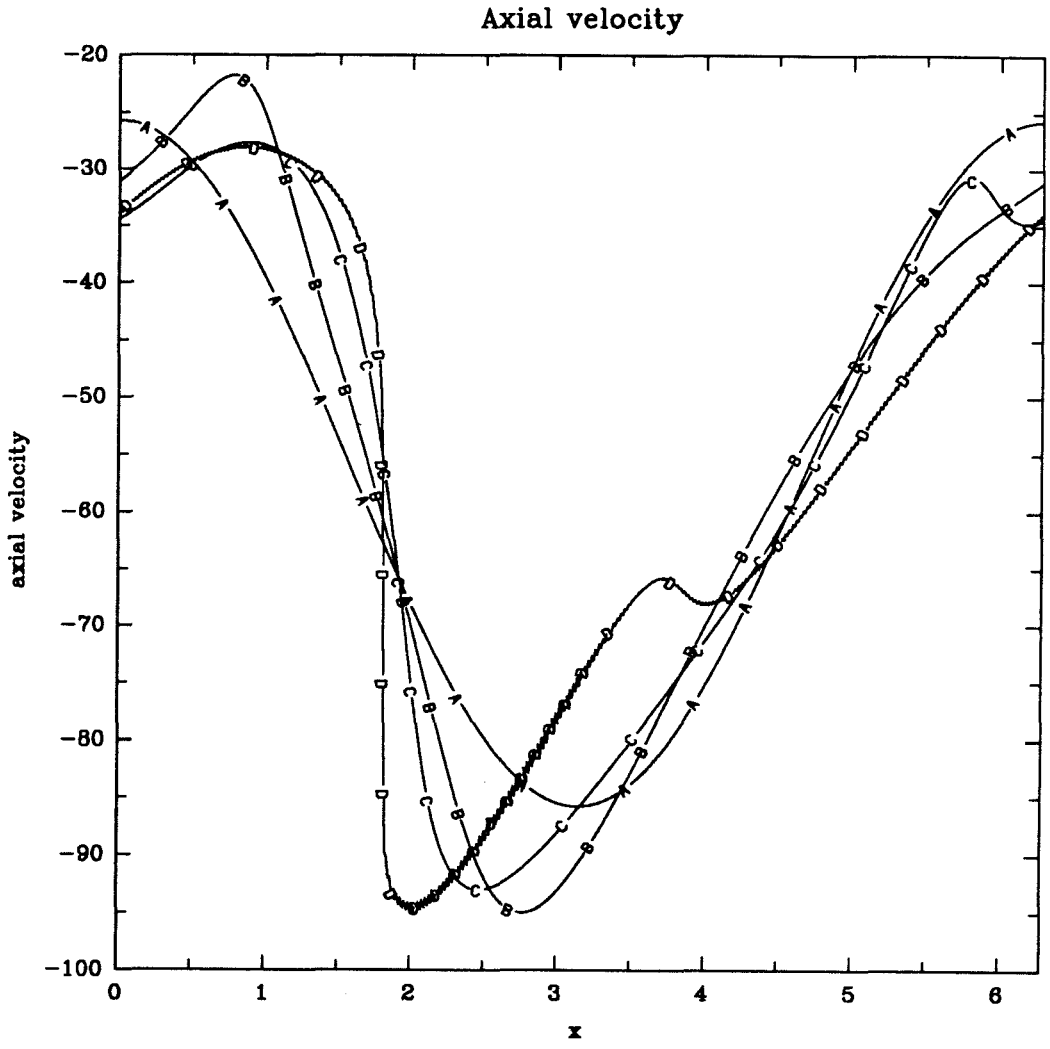

Fig. 2.3.2 The axial velocity as a function of x is shown for various time. Shown here are A. $t = 0.0$, B. $t = 0.2$, C. $t = 0.4$, and D. $t = 0.6$. The parameters are listed in Figure 2.3.1.

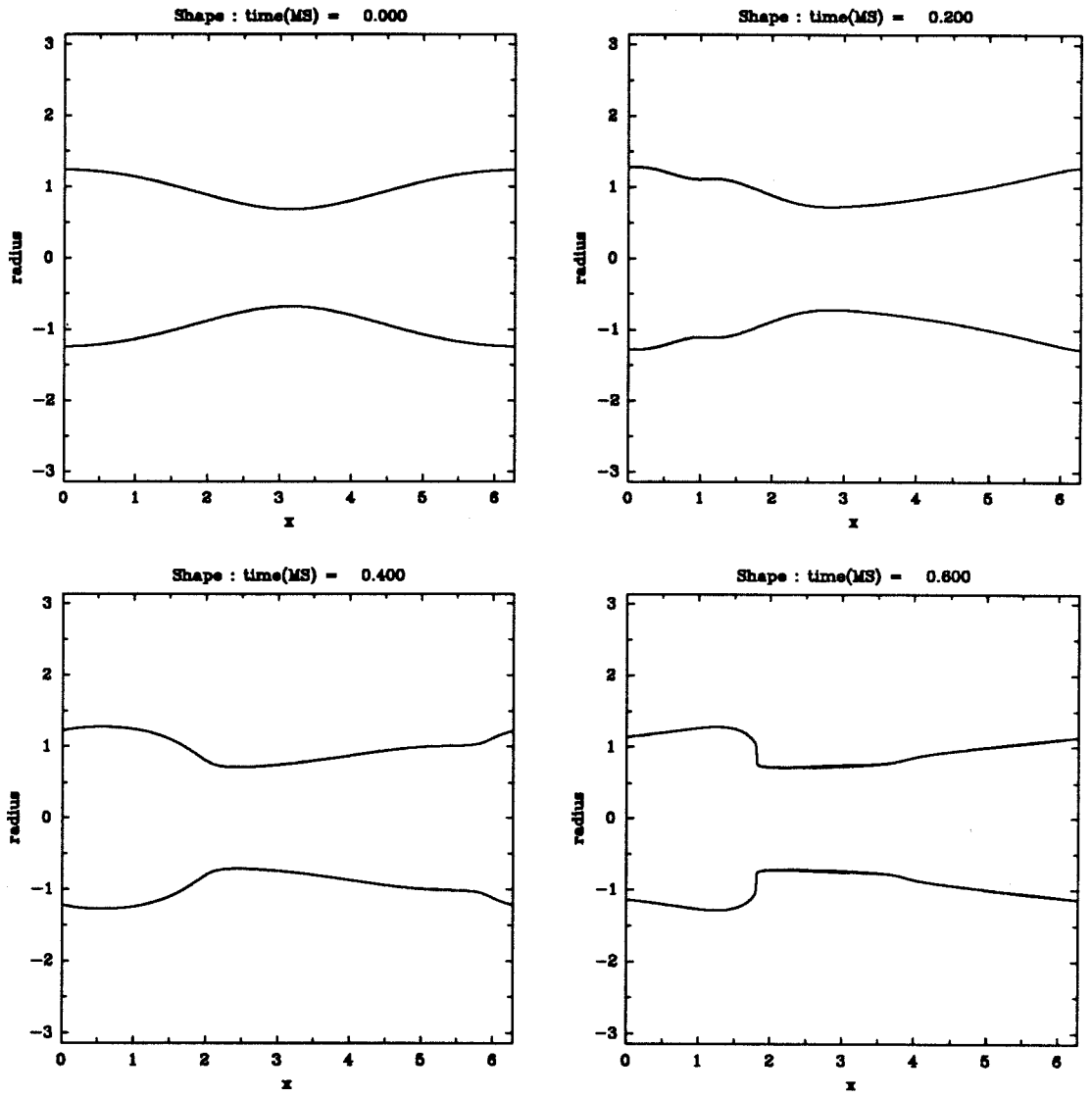

Fig. 2.4.1 The cross section of the vortex filament in the meridional plane is shown for $t = 0.0,\ 0.2,\ 0.4$, and 0.6. The parameters are the same as in Figure 2.3.1 except $Re = 5300$.

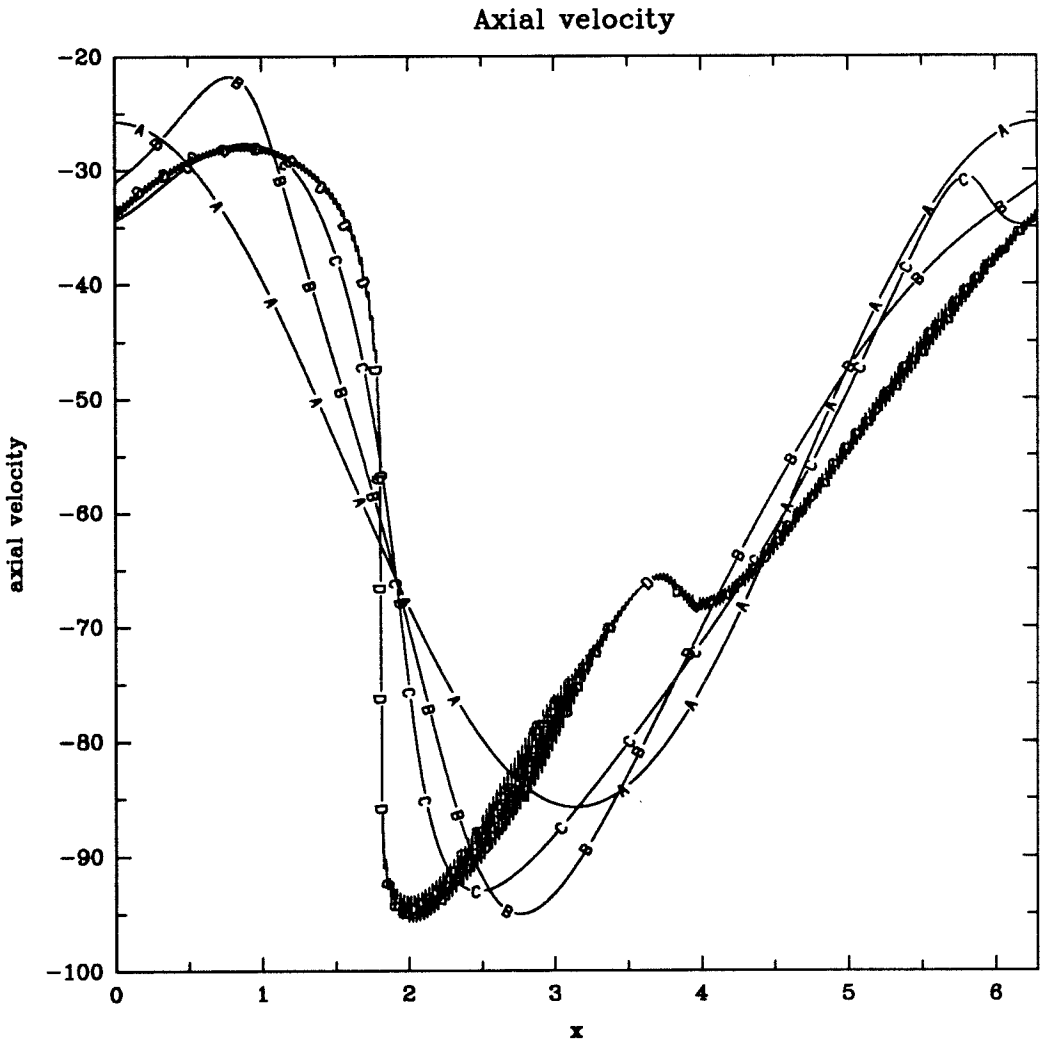

Fig. 2.3.2 The axial velocity as a function of x is shown for various time. Shown here are A. $t = 0.0$, B. $t = 0.2$, C. $t = 0.4$, and D. $t = 0.6$. The parameters are listed in Figure 2.4.1.

CHAPTER 3

Computational Aspects of Core Dynamics

3.1 Introduction

We have seen in the previous chapter that the MS equations contain the fast scale motion governing the deformation of the vortex core. We have also seen that they are of more general form compared to the LA equations. More importantly, these equations are hyperbolic in nature and therefore predict existence of shocks. Formation of shocks can be viewed as a result of steepening of wave like disturbances resulting in breaking. Lundgren and Ashurst have advanced this shock formation as a possible mechanism of vortex breakdown. In this chapter we discuss the numerical implementation of the full nonlinear time dependent equations of motion. We consider the time dependent Navier-Stokes equations at high Reynolds number instead of the time dependent Euler equations so that high frequency oscillations that arise primarily due to numerical errors are suppressed by the presence of viscosity. This will enable us to integrate the equations for longer times. In particular, we are interested in knowing whether the initial conditions that lead to shocks in MS equations also lead to shocks in the Euler equations. In this context, a shock in the Euler solutions means that the "core" area jumps at some axial location. At a given axial station, the core radius is defined as the radial location at which the swirl velocity is maximum.

We assume axisymmetry in our numerical solutions in order to compare with the axisymmetric solutions of LA. The radial direction is assumed to be unbounded. Boundary conditions in the radial direction away from the axis are derived by matching the solution to far field potential flow. This enables us to terminate the radial boundary at a finite distance. As our emphasis is on the wave motion occurring in the vortex core, we consider a periodic axial domain. This enables us to use the fast

Fourier transform thereby speeding up the numerical solution. We include in this chapter, a description of the algorithm used as well as the results of tests to validate the numerical procedure. The results of numerical simulation will be discussed in the next chapter.

3.2 Navier-Stokes equations

We consider the equations in cylindrical co-ordinates r, θ and z. The flow is assumed to be axisymmetric (independent of θ). Let the velocity components be denoted by u, v and w. The stream-function ψ and the circulation function Ω are defined by

$$u = -\frac{1}{r}\frac{\partial \psi}{\partial z}, \quad v = \frac{\Omega}{r}, \quad w = \frac{1}{r}\frac{\partial \psi}{\partial r}. \tag{3.1}$$

Let

$$x = \kappa z - \sigma_2 t, \tag{3.2}$$

where t denotes time. For some choice of κ and σ_2, the frame defined by the co-ordinates r, θ and x moves with speed σ_2/κ along the positive z axis with respect to the stationary frame defined by r, θ and z. We choose σ_2 to be the linear wave speed. The Navier-Stokes equations can be written

$$\frac{\partial \zeta}{\partial t} = f + \mu_2 D^2 \zeta, \tag{3.3a}$$

$$\frac{\partial \Omega}{\partial t} = g + \mu_2 D^2 \Omega, \tag{3.3b}$$

where

$$f = \sigma_2 \frac{\partial \zeta}{\partial x} - \frac{2\kappa}{r^2}\Omega\frac{\partial \Omega}{\partial x} - \frac{\kappa}{r}\left(\frac{\partial \psi}{\partial r}\frac{\partial \zeta}{\partial x} - \frac{\partial \psi}{\partial x}\frac{\partial \zeta}{\partial r}\right) - \frac{2\kappa}{r^2}\frac{\partial \psi}{\partial x}\zeta, \tag{3.4a}$$

$$g = \sigma_2 \frac{\partial \Omega}{\partial x} - \frac{\kappa}{r}\left(\frac{\partial \psi}{\partial r}\frac{\partial \Omega}{\partial x} - \frac{\partial \psi}{\partial x}\frac{\partial \Omega}{\partial r}\right), \tag{3.4b}$$

$$\zeta = D^2\psi = \frac{\partial^2 \psi}{\partial r^2} - \frac{1}{r}\frac{\partial \psi}{\partial r} + \kappa^2 \frac{\partial^2 \psi}{\partial x^2}, \tag{3.5}$$

and μ_2 is the coefficient of viscosity. We assume ψ, Ω and ζ to be periodic in x. Without loss of generality, we assume the period to be 2π. The period in z is controlled

by the variable κ. We then decompose ψ, Ω and ζ into a truncated Fourier series given by

$$\psi(r,x,t) = \psi_0(r,t) + \sum_{\ell=1}^{m} \psi_\ell^e(r,t)\cos(\ell x) + \sum_{\ell=1}^{m} \psi_\ell^o(r,t)\sin(\ell x), \tag{3.6a}$$

$$\Omega(r,x,t) = \Omega_0(r,t) + \sum_{\ell=1}^{m} \Omega_\ell^e(r,t)\cos(\ell x) + \sum_{\ell=1}^{m} \Omega_\ell^o(r,t)\sin(\ell x), \tag{3.6b}$$

$$\zeta(r,x,t) = \zeta_0(r,t) + \sum_{\ell=1}^{m} \zeta_\ell^e(r,t)\cos(\ell x) + \sum_{\ell=1}^{m} \zeta_\ell^o(r,t)\sin(\ell x). \tag{3.6c}$$

The zeroth mode is written separately for convenience. The subscripts on the Fourier modes represent the mode number and the superscripts denote parity (e is used for the even mode, if it is associated with cosine functions and o is used for the odd mode, if it is associated with sine functions). The superscript e/o will be used if the equations are same the for both odd and even modes. From equation (3.5) we obtain

$$\zeta_0(r,t) = \frac{\partial^2 \psi_0}{\partial r^2} - \frac{1}{r}\frac{\partial \psi_0}{\partial r}, \tag{3.7a}$$

$$\zeta_\ell^{e/o}(r,t) = \frac{\partial^2 \psi_\ell^{e/o}}{\partial r^2} - \frac{1}{r}\frac{\partial \psi_\ell^{e/o}}{\partial r} - (\kappa\ell)^2 \psi_\ell^{e/o}, \quad l = 1,\ldots,m. \tag{3.7b}$$

We substitute (3.6) into (3.4) and separate the modes. The nonlinear terms f and g take on similar forms as (3.6). To compute the Fourier modes of f and g, we take the so-called pseudo-spectral approach. In this approach, we compute the indicated products in the physical domain. This is accomplished by first computing ψ, Ω and ζ via a fast Fourier transform (FFT). We compute f and g and transform back using the FFT once again. We treat the Fourier modes of ζ and Ω as the unknowns. The equations describing their time evolution are

$$\frac{\partial \zeta_\ell^{e/o}}{\partial t} = f_\ell^{e/o} + \mu_2 D_\ell^2 \zeta_\ell^{e/o}, \tag{3.8a}$$

$$\frac{\partial \Omega_\ell^{e/o}}{\partial t} = g_\ell^{e/o} + \mu_2 D_\ell^2 \Omega_\ell^{e/o}, \tag{3.8b}$$

where we define,

$$D_\ell^2 = \frac{\partial^2}{\partial r^2} - \frac{1}{r}\frac{\partial}{\partial r} - (\ell\kappa)^2. \tag{3.9}$$

These equations are integrated numerically. We use a combined Adams-Bashforth and Crank-Nicolson scheme for time stepping. We treat the non-linear terms f and g using the Adams-Bashforth scheme and treat the viscous terms using the Crank-Nicolson scheme. Thus, if the solution at time t is known, then the solution at time $t + \Delta t$ is obtained from

$$\frac{\zeta(t+\Delta t)-\zeta(t)}{\Delta t} = \frac{3}{2}f(t) - \frac{1}{2}f(t-\Delta t) + \frac{\mu_2}{2}\left[D^2\zeta(t+\Delta t) + D^2\zeta(t)\right], \qquad (3.10a)$$

$$\frac{\Omega(t+\Delta t)-\Omega(t)}{\Delta t} = \frac{3}{2}g(t) - \frac{1}{2}g(t-\Delta t) + \frac{\mu_2}{2}\left[D^2\Omega(t+\Delta t) + D^2\Omega(t)\right]. \qquad (3.10b)$$

Here we have suppressed the r dependence of all the functions and also the superscripts and subscripts for convenience. Solving for the unknowns at time $t + \Delta t$ we get

$$\left[1 - \frac{\mu_2\Delta t}{2}D^2\right]\zeta(t+\Delta t) = \left[1 + \frac{\mu_2\Delta t}{2}D^2\right]\zeta(t) + \frac{\Delta t}{2}\left(3f(t) - f(t-\Delta t)\right), \quad (3.11a)$$

$$\left[1 - \frac{\mu_2\Delta t}{2}D^2\right]\Omega(t+\Delta t) = \left[1 + \frac{\mu_2\Delta t}{2}D^2\right]\Omega(t) + \frac{\Delta t}{2}\left(3g(t) - f(t-\Delta t)\right). \quad (3.11b)$$

These equations represent $2m + 1$ ordinary differential equations for each variable ζ and Ω. However, the FFT is incapable of resolving the m^{th} sine mode. This gives rise to an inconsistency in accurately evolving the last modes, both sine and cosine, since the products in f and g couple the last sine and cosine modes. This is overcome by simply dropping the m^{th} equations. Thus the reduced set of equations are to be solved subject to the following boundary conditions.

About $r = 0$ we assume that the solution is regular and the vorticity distribution is like that of solid body rotation. This implies that $\psi \sim r^2$ and $\Omega \sim r^2$ as $r \to 0$. It is easily seen from (3.5) that $\zeta \sim r^2$ near the axis. We then take

$$\zeta_\ell^{e/o}(t+\Delta t) = 0, \quad \Omega_\ell^{e/o}(t+\Delta t) = 0, \quad \ell = 0,\ldots,m, \quad \text{at} \quad r = 0. \qquad (3.12)$$

Since the vorticity decays rapidly as $r \to \infty$, we assume that

$$\frac{\partial\Omega_\ell^{e/o}(r, t+\Delta t)}{\partial r} = 0, \quad \text{as} \quad r \to \infty, \quad \ell = 0,\ldots,m. \qquad (3.13)$$

The condition (3.13) accounts for the decay of both radial and axial vorticity. The rapid decay of the swirl component of vorticity gives

$$\zeta_\ell^{e/o}(t+\Delta t) = 0, \quad \text{as} \quad r \to \infty, \quad \ell = 0, \ldots, m. \tag{3.14}$$

For numerical purposes, we assume

$$\frac{\partial \zeta_\ell^{e/o}(r, t+\Delta t)}{\partial r} = 0, \quad \text{as} \quad r \to \infty, \quad \ell = 0, \ldots, m. \tag{3.15}$$

From the given ζ values, we compute the streamfunction by inverting the relations (3.7). For this we require boundary conditions on ψ. We get

$$\psi_\ell^{e/o}(t+\Delta t) = 0, \quad \ell = 0, \ldots, m, \quad \text{at} \quad r = 0. \tag{3.16}$$

The behavior of Fourier components of ψ for large r is obtained by solving (3.14). For $\ell = 0$, we get

$$\psi_0 = a_0\, r^2 + b_0, \quad \text{as} \quad r \to \infty. \tag{3.17a}$$

We take $b_0 = 0$ since the streamfunction is arbitrary up to an additive constant. The value of a_0 is related to the axial velocity at infinity. We fix it to be the same as the value at the initial time. For $\ell = 1, \ldots, m$, we get

$$\psi_\ell^{e/o}(t+\Delta t) = a_\ell^{e/o}\ \ell\ \kappa\ r\ K_1(\ell\kappa r) + b_\ell^{e/o}\ \ell\ \kappa\ r\ I_1(\ell\kappa r), \quad \text{as} \quad r \to \infty. \tag{3.17b}$$

Here, I_1 and K_1 are the modified Bessel functions and a_ℓ and b_ℓ are arbitrary functions of time. We take $b_\ell = 0, \quad \ell \neq 0$, since the Bessel function I_1 grows exponentially with r. At any given time, the functions a_ℓ can be eliminated by differentiating equations (3.17) once. This yields,

$$\frac{\partial \psi_\ell^{e/o}(t+\Delta t)}{\partial r} + d_\ell(\kappa, r)\ \psi_\ell^{e/o}(t+\Delta t) = 0, \tag{3.18}$$

where

$$d_\ell(\kappa, r) = \ell\ \kappa\ \frac{K_0(\kappa\ell r)}{K_1(\kappa\ell r)}, \quad \ell = 1, \ldots, m. \tag{3.19}$$

The equations (3.11) that describe the evolution of ζ and Ω subject to the boundary conditions (3.12), (3.13) and (3.15) and the equations (3.7) that relate ψ and ζ subject to the boundary conditions (3.16) and (3.18) are now solved in a radial domain which is cut off at some convenient distance. We further consider a grid transformation so that grid points are closely spaced within the "core" of the vortex. For the present we understand the "core" to be the region close to the axis in which the vorticity is significant. A formal definition of the core and a procedure to compute the core boundary is given later. Within the core, vortex lines can stretch resulting in enhancement of vorticity. This in turn can cause large velocity gradients within the core region. A finer grid is thus necessary in this region. Outside the core, the flow quantities are expected to decay fairly rapidly. Thus the grid need not be very fine in this region. We consider a grid transformation and its inverse denoted by

$$r = r(\rho), \quad \rho = \rho(r). \tag{3.20}$$

We consider a uniform grid in the new variable ρ. We let

$$\frac{\mathrm{d}r}{\mathrm{d}\rho} = \delta_g + \frac{1}{2}\left(1 + \tanh\frac{\rho - a_g}{\beta_g}\right), \tag{3.21}$$

where δ_g, a_g and β_g are the grid parameters. When $\rho < a_g$, the grid spacing in r tends to δ_g times the spacing in ρ. By choosing appropriate values for the grid parameters, we can make the spacing within the vortex core as small as we please. For large ρ, the spacing in r is about $1+\delta_g$ times the spacing in ρ. This gives sufficient control for our purpose. The radial derivatives are replaced by

$$\frac{\partial}{\partial r} = \frac{\partial \rho}{\partial r}\frac{\partial}{\partial \rho}, \quad \frac{\partial^2}{\partial r^2} = \left(\frac{\partial \rho}{\partial r}\right)^2 + \frac{\partial \rho}{\partial r}\frac{\partial}{\partial \rho}\left(\frac{\partial \rho}{\partial r}\right). \tag{3.22}$$

We rewrite (3.9) as

$$D_\ell^2 = P(\rho)\frac{\partial^2}{\partial \rho^2} + Q(\rho)\frac{\partial}{\partial \rho} - (\kappa\ell)^2, \tag{3.23}$$

where

$$P(\rho) = \left(\frac{\partial \rho}{\partial r}\right)^2, \quad Q(\rho) = \frac{\partial \rho}{\partial r}\frac{\partial}{\partial \rho}\left(\frac{\partial \rho}{\partial r}\right) - \frac{1}{r(\rho)}\frac{\partial \rho}{\partial r}. \tag{3.24}$$

We now discuss the structure of the discrete equations to be solved.

3.3 Discrete equations

In this section we describe the discretization and the method of solution of the equations stated above. We take the distance at which we apply far field boundary conditions to be R. We consider a uniform grid in ρ given by

$$\rho_j = j\Delta\rho, \quad j = 0, \ldots, J, \tag{3.25}$$

where we take

$$\Delta\rho = \frac{\rho(R)}{J}, \tag{3.26}$$

for some J. We replace the continuous derivatives by central difference approximations. Thus for some quantity q we write

$$\left(\frac{\partial q}{\partial \rho}\right)_j = \frac{q_{j+1} - q_{j-1}}{2\Delta\rho}, \tag{3.27a}$$

$$\left(\frac{\partial^2 q}{\partial r^2}\right)_j = \frac{q_{j+1} - 2q_j + q_{j-1}}{\Delta\rho^2}, \quad j = 1, \ldots, J-1. \tag{3.27b}$$

The error introduced by the central differences is $O(\Delta\rho^2)$. For the outer boundary point we take a one sided difference given by

$$\left(\frac{\partial q}{\partial \rho}\right)_J = \frac{3q_J - 4q_{J-1} + q_{J-2}}{2\Delta\rho}. \tag{3.27c}$$

We now put the equations to be solved in a matrix form. We proceed first by collecting the quantities evaluated on the grid into the following column vectors

$$\vec{\psi}_\ell = \left\{\psi_{\ell,0}, \psi_{\ell,1}, \ldots, \psi_{\ell,J}\right\}^\top, \quad \vec{\Omega}_\ell = \left\{\Omega_{\ell,0}, \Omega_{\ell,1}, \ldots, \Omega_{\ell,J}\right\}^\top,$$

and

$$\vec{\zeta}_\ell = \left\{\zeta_{\ell,0}, \zeta_{\ell,1}, \ldots, \zeta_{\ell,J}\right\}^\top \tag{3.28}$$

Further we define a matrix A with entries

$$A_{j-1,j} = \frac{P_j}{\Delta\rho^2} - \frac{Q_j}{2\Delta\rho}, \quad A_{j,j} = -\frac{2P_j}{\Delta\rho^2},$$

$$A_{j+1,j} = \frac{P_j}{\Delta\rho^2} + \frac{Q_j}{2\Delta\rho}, \quad j = 1, \ldots, J-1,$$

$$A_{i,j} = 0 \quad \text{otherwise.} \tag{3.29}$$

Now we define the matrices I_1 and I_2 with elements

$$I_{1_{j,j}} = 1, \quad j = 0, \ldots, J-1, \tag{3.30a}$$

$$I_{1_{J,J-2}} = \frac{1}{2\Delta\rho}, \quad I_{1_{J,J-1}} = -\frac{2}{\Delta\rho}, \quad I_{1_{J,J}} = \frac{3}{2\Delta\rho}, \tag{3.30b}$$

$$I_{2_{j,j}} = 1, \quad j = 1, \ldots, J-1. \tag{3.31}$$

The remainder of the matrix elements are zero. The matrix form of (3.11) becomes

$$\left(I_1 - \frac{\mu_2\Delta t}{2}\left(A - (\kappa\ell)^2 I_2\right)\right)\vec{\zeta}_\ell(t+\Delta t) = \left(I_2 + \frac{\mu_2\Delta t}{2}\left(A - (\kappa\ell)^2 I_2\right)\right)\vec{\zeta}_\ell(t) + \frac{\Delta t}{2}\left(3\vec{f}_\ell(t) - \vec{f}_\ell(t-\Delta t)\right), \tag{3.32a}$$

$$\left(I_1 - \frac{\mu_2\Delta t}{2}\left(A - (\kappa\ell)^2 I_2\right)\right)\vec{\Omega}_\ell(t+\Delta t) = \left(I_2 + \frac{\mu_2\Delta t}{2}\left(A - (\kappa\ell)^2 I_2\right)\right)\vec{\Omega}_\ell(t) + \frac{\Delta t}{2}\left(3\vec{g}_\ell(t) - \vec{g}_\ell(t-\Delta t)\right), \tag{3.32b}$$

where the vectors $\vec{f}$ and $\vec{g}$ are given by

$$\vec{f}_\ell = \{0, f_{\ell\,1}, f_{\ell\,2}, \ldots, f_{\ell\,J-1}, 0\}^\top, \quad \vec{g}_\ell = \{0, g_{\ell\,1}, g_{\ell\,2}, \ldots, g_{\ell\,J-1}, 0\}^\top. \tag{3.33}$$

The inversion of the relation between ψ and ζ represented by equation (3.7) subject to the boundary conditions (3.16) and (3.18) can be written in the following matrix form

$$B_\ell\,\vec{\psi}_\ell = I_2\vec{\zeta}_\ell, \quad \ell = 0, \ldots, m, \tag{3.34}$$

where we define the matrices B_ℓ with the following entries,

$$B_{\ell_{1,1}} = 1, \tag{3.35a}$$

$$B_{\ell_{j-1,j}} = \frac{P_j}{\Delta\rho^2} - \frac{Q_j}{2\Delta\rho}, \quad B_{\ell_{j,j}} = -\frac{2P_j}{\Delta\rho^2} - (\kappa\ell)^2, \tag{3.5b}$$

$$B_{\ell_{j+1,j}} = \frac{P_j}{\Delta\rho^2} + \frac{Q_j}{2\Delta\rho}, \quad j = 1, \ldots, J-1, \quad \ell = 0, \ldots, m, \tag{3.35c}$$

$$B_{\ell_{J,J-2}} = \frac{1}{2\Delta\rho}\left(\frac{\partial\rho}{\partial r}\right)_J, \quad B_{\ell_{J,J-1}} = -\frac{2}{\Delta\rho}\left(\frac{\partial\rho}{\partial r}\right)_J, \tag{3.35d}$$

and finally

$$B_{\ell_{J,J}} = \frac{3}{2\Delta\rho}\left(\frac{\partial\rho}{\partial r}\right)_J + d_\ell, \quad \text{if} \quad \ell \neq 0 \tag{3.35e}$$

$$B_{0_{J,J}} = \frac{3}{2\Delta\rho}\left(\frac{\partial\rho}{\partial r}\right)_J - \frac{2}{r_J}. \tag{3.35f}$$

3.4 Computation of core shape

Now we give a definition of the vortex "core" and also give a procedure to compute the core size as a function of the axial position. We define the location of the core at some given x to be the radial distance at which the swirl profile attains its maximum. We first find an index p such that $v(r_p) = v_p$ is maximum on the grid. We consider two adjacent points on either side of p and assume a parabolic profile for the swirl to find a more precise location for the core boundary. In the neighborhood of point r_p we assume

$$v(r) = c_0 + c_1\, r + c_2\, r^2. \tag{3.36}$$

Letting a denote the core size, we compute it as the value of r at which the local parabolic swirl profile (3.36) attains its maximum. We get

$$a = -\frac{c_1}{2c_2} = \frac{1}{2}\frac{C_1}{C_2}, \tag{3.37}$$

where C_1 and C_2 are the following determinants,

$$C_1 = \begin{bmatrix} 1, & v_{p-1}, & r_{p-1}^2 \\ 1, & v_p, & r_p^2 \\ 1, & v_{p+1}, & r_{p+1}^2 \end{bmatrix}, \quad C_2 = \begin{bmatrix} 1, & r_{p-1}, & v_{p-1}^2 \\ 1, & r_p, & v_p^2 \\ 1, & r_{p+1}, & v_{p+1}^2 \end{bmatrix}. \tag{3.38}$$

This procedure is repeated for every x station to obtain a as a function of x.

3.5 Tests

Results of test runs are shown in Figure 3.2 and 3.3. The evolution equations (3.8) were integrated using the method described above with an initial condition of the form

$$\psi(r,x) = 0 + \varepsilon\psi_1^e(r)\cos(x), \tag{3.39a}$$

$$\Omega(r,x) = \Omega_0 + \varepsilon\Omega_1^e(r)\cos(x), \tag{3.39b}$$

where the profiles of Ω_0, ψ_1^e and Ω_1^e are shown in Figure 3.1. $\varepsilon = 0.2$ was chosen. The radial domain length of $R = 5$ with a radial resolution of $J = 50$ and a modal resolution of $m = 16$ were used. The viscocity coefficient was taken to be $\mu_2 = 10^{-4}$. The equations (3.8) were integrated up to time $t = 5$ using three different step sizes of $\Delta t = 0.001, 0.0005, 0.00025$. The axial velocity on the axis at $t = 5$ using these step sizes is plotted on the same graph. Differences, if any, are seen to be negligible.

A nonlinear steady state solution of the form

$$\overline{\psi}(r,x) = \sum_{\ell=0}^{m_1} \overline{\psi}_\ell \cos(\ell x), \tag{3.40a}$$

$$\overline{\Omega}(r,x) = \sum_{\ell=0}^{m_1} \overline{\Omega}_\ell \cos(\ell x), \tag{3.40b}$$

was used as an initial condition for the results shown in Figure 3.3. The axial velocity on the axis at $t = 0$, 5 and 10 is plotted on the same graph showing negligible dependence of the solution on time. The time $t = 10$ corresponds to about two wave periods of the steady state solution. The steady state solution (3.40) was generated using the method described in Chapter 6. A modal resolution of $m_1 = 4$ was used for the steady state solution. However, a total of 32 modal coefficients were used in the evolution equations. This was done in order to minimize the aliasing errors since the pseudo-spectral approach was used for the time dependent solution whereas the steady state solution was computed using a Galerkin approach.

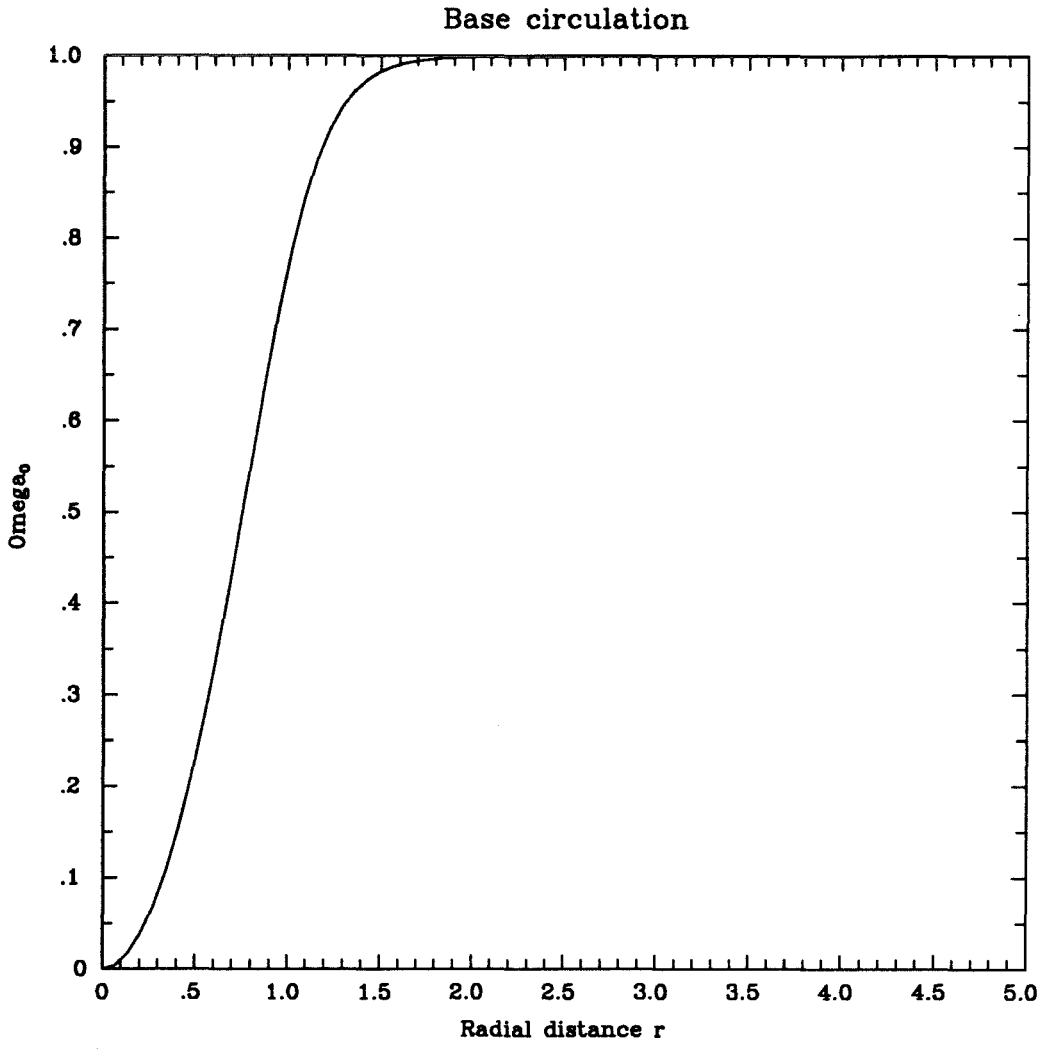

Fig. 3.1a The profile of the circulation function for the unperturbed vortex used in the test run is shown here for $R = 5$ and $J = 50$.

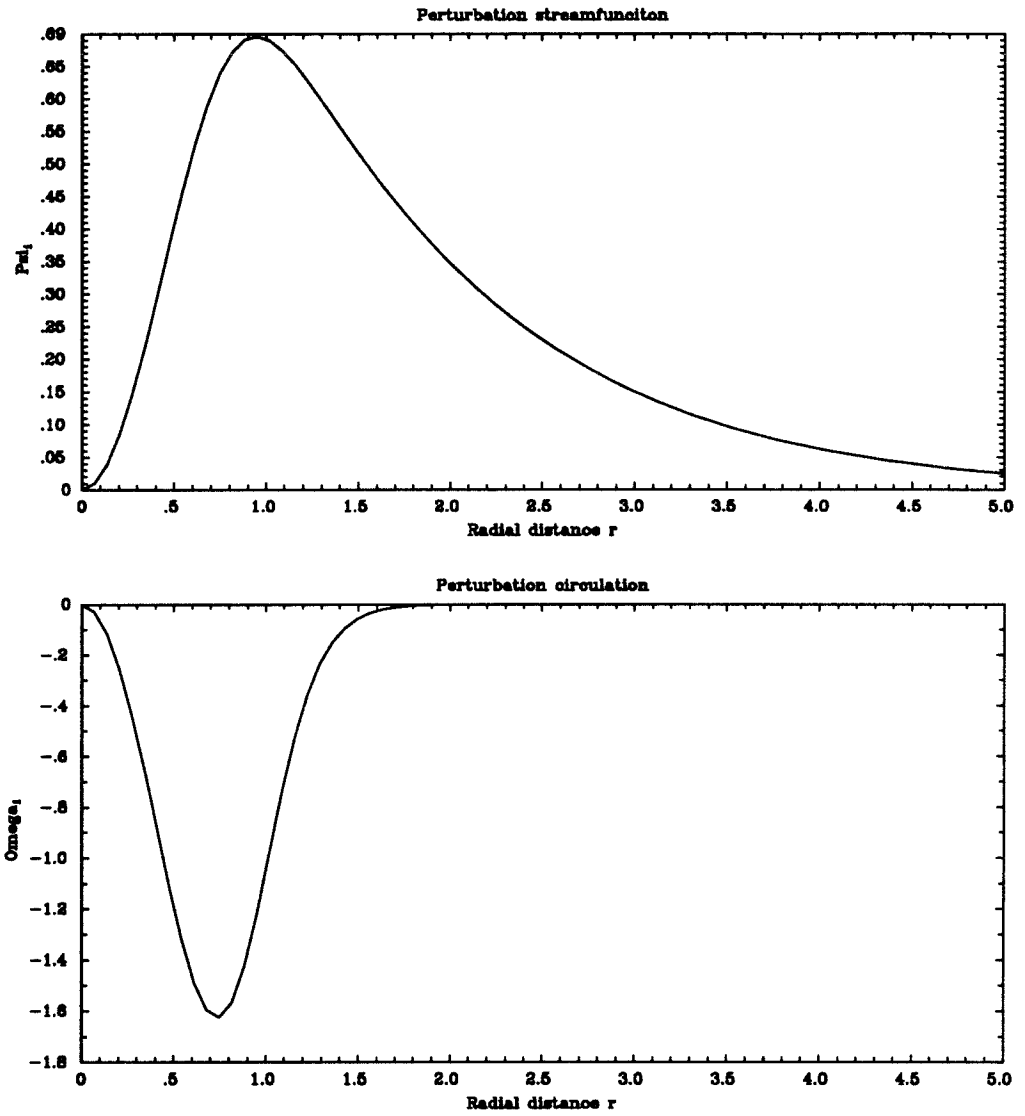

Fig. 3.1b Profiles of the perturbation stream function ψ_1^e and the perturbation circulation function Ω_1^e are shown here for $R = 5$ and $J = 50$.

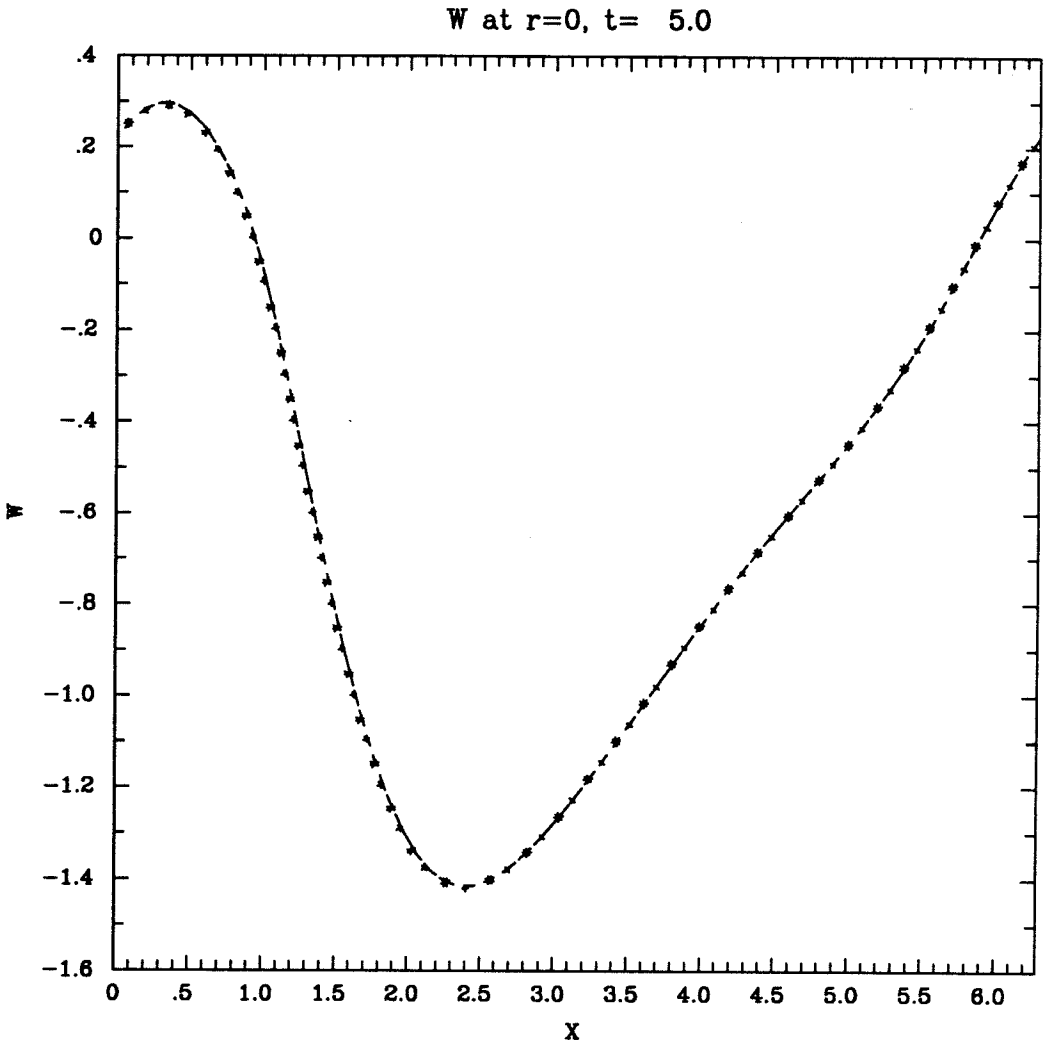

Fig. 3.2 The axial velocity on the axis at $t = 5$ is plotted for different values of Δt. Here, 1) '$---$', $\Delta t = 0.001$, 2) '$-+-$', $\Delta t = 0.0005$, and 3) '$-*-$', $\Delta t = 0.00025$. A grid resolution of $J = 50$ with $R = 5$ and $m = 16$ were used for each run.

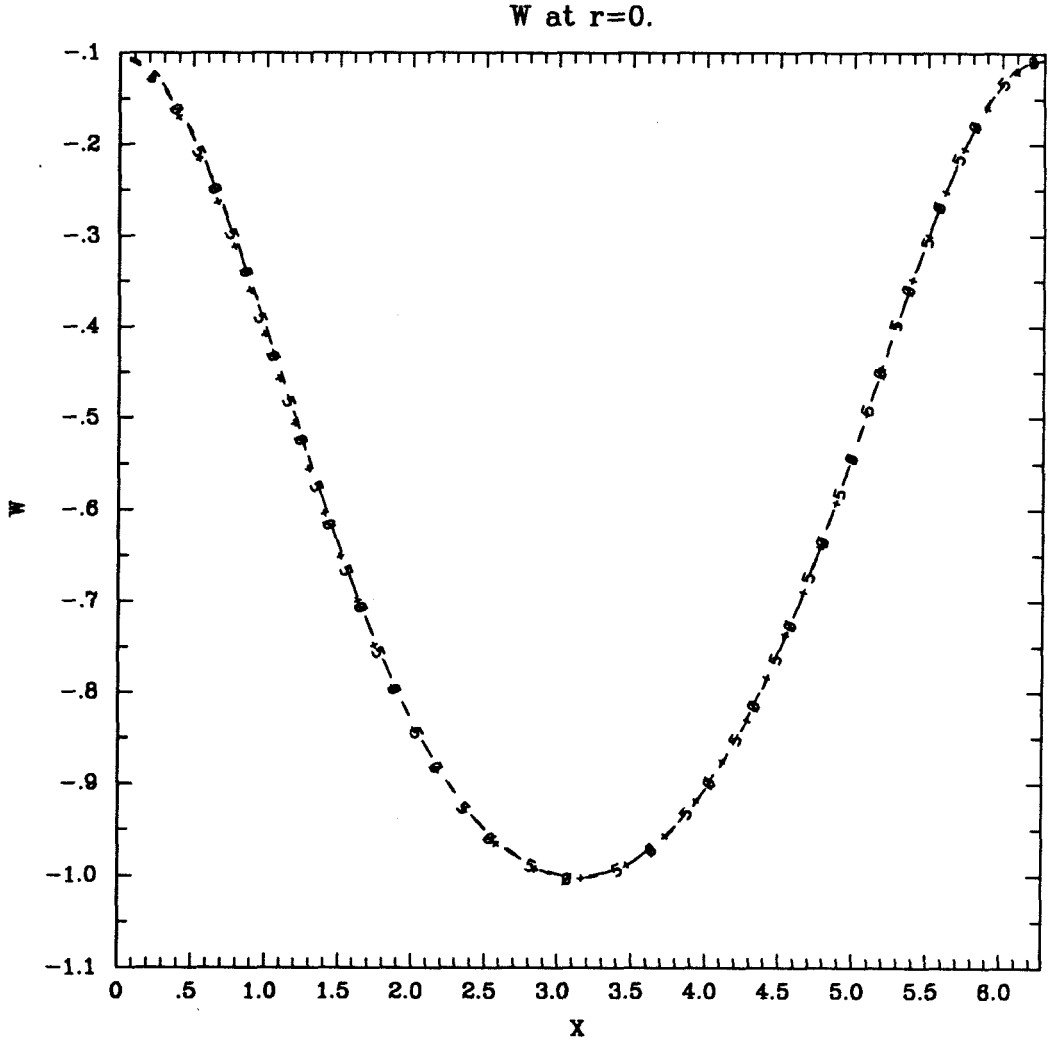

Fig. 3.3 The axial velocity on the axis for an initial steady state solution is plotted for 1) '−0−', $t = 0$, 2) '−5−', $t = 5$, and 3) '− + −', $t = 10$. Negligible variations are seen showing that the steady state is well maintained by the time dependent code.

CHAPTER 4

Numerical Results

4.1 Introduction

It was shown in Chapter 2 that the Moore-Saffman (MS) equations lead to shock formation on vortex cores for a variety of initial conditions. Since the MS equations are only approximate, the fact that a shock forms may not necessarily indicate that a shock also forms in the solutions of the Euler equations. Therefore, we try to establish whether a shock forms in the solutions of the Euler equations via numerical simulations of the Navier-Stokes (N-S) equations at high Reynolds number. The reason for using the N-S equations instead of the Euler equations is given in the previous chapter. The shock in this context is identified by a jump in the radius of the vortex core. As observed in the previous chapter, the formation of a shock on vortex cores in the solutions of MS equations is a result of steepening of a wave-like disturbance. Therefore, we choose as our initial condition for the N-S equations a cylindrical vortex with a wave-like perturbation imposed on it. In order to seek a comparison between the solutions of MS and N-S, we establish an equivalent initial condition for the MS problem. We do this by averaging the initial conditions of the N-S problem. This appears to be the best possible comparison we can get. We integrate the equations forward in time for both the problems and compare the shape of the vortex core.

There are two important differences in the MS equations and the N-S equations worth noting. First, the MS equations describe evolution of quantities that are averaged in the radial direction. The second difference is the role of circulation. In the MS case, the circulation plays a "passive" role in the dynamics since it appears only as the total circulation which does not vary along the vortex axis. The circulation is

dynamically uncoupled with the axial velocity. Therefore, it does not influence the evolution of the axial velocity or the vortex core shape. But this is not the case with the N-S equations. The axisymmetric Navier-Stokes equations can be thought of as describing the evolution of circulation and azimuthal vorticity. These two quantities fully describe the state of the flow. In general, the circulation field is as important as the vorticity field within the vortex core.

In this chapter we first describe the initial conditions used for the N-S problem and the MS problem. Then we present results of simulation for three cases. In the first case, we consider a vortex with a very small perturbation. The vortex is seen to evolve slowly in the sense that the vortex undergoes small changes in the structure of the flow within the core. The wave-like perturbation shows no evidence of wave steepening for the N-S problem. However, the MS solution is seen to develop a shock in the core area. In the second case, a vortex with a stronger perturbation is considered. In this case, the N-S stokes solution shows development of a region with a recirculating bubble. The bubble eventually collapses. But, as in the small perturbation case, the initial wave does not steepen. On the other hand, the MS solution develops a shock in the core area. In the third case, a vortex with still stronger perturbation is considered. The N-S solution is seen to develop a jump in the core area and so does the MS solution. But the jump in the N-S stokes solution is opposite in sense to the jump in the MS solution.

4.2 Initial conditions

Let r and z denote the radial and the axial co-ordinates respectively. Let u, v and w denote the radial, swirl and the axial components of velocity respectively. The axisymmetric stream function ψ and the circulation function Ω are defined by

$$u = -\frac{1}{r}\frac{\partial \psi}{\partial z}, \quad v = \frac{\Omega}{r}, \quad w = \frac{1}{r}\frac{\partial \psi}{\partial r}. \tag{4.1}$$

We consider an unperturbed cylindrical vortex defined by

$$\psi = \psi_0(r), \quad \Omega = \Omega_0(r). \tag{4.2}$$

The radius of the core a_0 is computed following the definition and procedure given in the previous chapter. Next we compute the average axial velocity W_0 using

$$W_0 = \frac{2}{a_0^2} \int_0^{a_0} w_0(r)\, r\, dr, \tag{4.3}$$

where

$$w_0(r) = \frac{1}{r} \frac{d\psi_0}{dr}, \tag{4.4}$$

specifies the distribution of the axial velocity. The area of the vortex core is given by

$$A_0 = \pi a_0^2. \tag{4.5}$$

The total circulation Γ is given by

$$\Gamma = 2\pi\, \Omega_\infty, \tag{4.6}$$

where

$$\Omega_\infty = \lim_{r \to \infty} \Omega_0(r). \tag{4.7}$$

Next we consider a perturbed vortex of the form

$$\psi(r, x) = \psi_0(r) + \varepsilon \psi_1(r) \cos(x), \tag{4.8a}$$

$$\Omega(r, x) = \Omega_0(r) + \varepsilon \Omega_1(r) \cos(x), \tag{4.8b}$$

where

$$x = \kappa z, \tag{4.9}$$

and ε is a parameter. The wave number κ is used here to control the wavelength in the axial direction. We adjust it so that the wavelength is relatively large compared to the core size of the vortex. Since the core size is $O(1)$, a value of $\kappa = 1$ is sufficient for our purpose. If $\varepsilon \ll 1$, then we know from linear theory that the disturbance given in (4.8) moves without change of form with a fixed speed when $O(\varepsilon^2)$ changes in the solution are neglected. Denote this speed by σ_2/κ. We compute σ_2 and the eigenfunctions ψ_1 and Ω_1 using the linear theory. With some choice of ε, the evolution

of the disturbed vortex given by (4.8) is computed via the Navier-Stokes equations in a frame moving with speed σ_2/κ.

For the MS problem, we assume that the axial velocity and the core area of the perturbed vortex has the form

$$W(x) = W_0 + \varepsilon W_1 \cos(x), \tag{4.10a}$$

$$A(x) = A_0 + \varepsilon A_1 \cos(x). \tag{4.10b}$$

The perturbation axial velocity W_1 is computed by averaging the perturbed axial velocity for the N-S problem stated in equation (4.8). We get

$$W_1 = \frac{2}{a_0^2} \int_0^{a_0} w_1(r)\, r\, dr, \tag{4.11a}$$

where the profile $w_1(r)$ is the perturbed axial velocity for the N-S problem and is given by

$$w_1(r) = \frac{1}{r} \frac{\mathrm{d}\psi_1}{\mathrm{d}r}. \tag{4.11b}$$

The quantity A_1 is computed from the linearized MS equation (see section 2.3, Chapter 2). We have

$$A_1 = \frac{A_0}{\sigma_1/\kappa - W_0} W_1, \tag{4.12}$$

where

$$\sigma_1/\kappa = W_0 + \sqrt{\frac{\Gamma^2}{8\pi A_0} + \frac{\Gamma^2 \nu}{b^2}}, \tag{4.13}$$

and

$$\frac{\Gamma^2 \nu}{b^2} = \frac{2}{a_0^2} \int_0^{a_0} w_0^2\, r\, dr - W_0^2. \tag{4.14}$$

The evolution of the disturbed vortex given by (4.10) is computed via the MS equations in a frame moving with speed σ_1/κ.

The time in either case is measured in units of linear wave periods T_1 and T_2 for the MS and Navier-Stokes equations respectively. In terms of σ_1 and σ_2 we compute

$$T_1 = 2\pi \frac{\kappa}{\sigma_1}, \quad T_2 = 2\pi \frac{\kappa}{\sigma_2}. \tag{4.15}$$

The Reynolds number for the flow is defined by

$$Re = \frac{\Gamma}{\mu}, \tag{4.16}$$

where μ is the coefficient of viscosity. We denote the coefficient of viscosity for the MS case by μ_1 and for the Navier-Stokes case by μ_2. For the results presented here we select the parameters so that $Re \gg 1$. Typical values of μ_1 and μ_2 used here are $O(10^{-4})$ and the circulation function Ω is $O(1)$ at infinity which gives a value of $\Gamma = O(2\pi)$.

The Navier-Stokes equations and the MS equations are integrated using the initial conditions described above.

4.3 Results

The solutions of the MS equations suggest that presence of an initial axial velocity component is not essential for the formation of a shock. It does, however, affect the time required for a shock to form. Since we are interested in the formation of the shock and not the time it takes to form a shock, we simply choose $\psi_0 = 0$ in our initial conditions. With a smaller value of ε, it will take a longer time before a shock forms.

Even though the initial conditions of the MS problem are derived from the initial conditions of the N-S problem, a quantitative comparison of the solutions does not appear to be within the reach of MS theory. This is suggested by the comparison of the linear wave speeds for the two problems. Table 4.1 shows the values of σ_1 and σ_2 for a cylindrical vortex of different core sizes. The circulation distribution $\Omega_0(r)$ for the computation of σ_2 used is that of a Kelvin type vortex with $\beta = 0.005$ (see section 6.4.1, Chapter 6 for details). This profile gives nearly constant axial vorticity for $0 \leq r \leq a_0$ and zero vorticity for $r \geq a_0$. The fact that the values of σ_1 and σ_2 are nearly the same for $a_0 = 1$ is merely a coincidence. In general, the values differ from each other. The speed of the linear wave for the MS case is smaller than the speed of the linear wave for the N-S case when the core size is small. The trend is

Table 4.1 Comparison of linear wave speeds.

The table shows σ_1 and σ_2 for the MS and the N-S cases respectively. Total circulation $\Omega_\infty = 1$ and disturbance wavenumber $\kappa = 1$ were used.

a_0	σ_1	σ_2
1/2	1.4142	1.5611
1	0.7071	0.7059
2	0.3536	0.2852
3	0.2357	0.1560

reversed when the core size is increased.

In Figures 4.1 through 4.10 the numerical results for a run with $\epsilon = 0.02$ are presented. The initial profiles of Ω_0, ψ_1, Ω_1 and ζ_1 are shown in Figure 4.1. The radial domain was taken to be $R = 2.5$ with a resolution of $J = 200$ radial points. The initial core size was $a_0 = 0.5$. A modal resolution of $m = 64$ was used for the N-S case and a resolution of $m = 128$ was used for the MS case. The viscosity coefficients were taken to be $\mu_1 = \mu_2 = 10^{-4}$. The Reynolds number for the flow was $Re = \Gamma/\mu = 62830$. Note that the Reynolds number based on typical velocity and core size is much less – about 8000. The high value for Re based on the total circulation is due to the factor 2π in the definition of Γ (see equation 4.6).

The development of the shape of the vortex core is shown in Figure 4.2 for the MS case. Gradual steepening of the core wave occurs as time passes. At about $t = 5.0$, a jump in the core area begins to form. In Figure 4.3 the maximum value of the $|\partial a(x,t)/\partial x|$, where a is the core radius, is plotted as a function of time. It gives a better indication of the steepening of the wave. It shows that the slope increases monotonically with time. Numerical oscillations are evident in Figure 4.2 which depict the shape of the vortex core. The development of the axial velocity is shown in Figure 4.4. The profile marked with A is at $t = 0$. For profiles marked with B through H, the time increases in steps of about 1.0. Steepening of the initial wave is clearly indicated. After the shock formation around $t = 5$ the axial velocity showed numerical errors which increased with time.

The development of the core shape for the N-S case is shown in Figure 4.5. The

core shows minimal distortion in shape with passage of time. The core wave does not steepen to form a shock when the solution has progressed to about $t = 11.8$ which is more than twice the time in which the MS solution develops a well defined shock. The maximum value of $|\partial a/\partial x|$ is shown in Figure 4.6. This shows qualitatively very different motion of the core wave. The core wave undergoes periodic flattening and steepening. The apparent small oscillations are due to the fact that the maximum value of the slope occurs at a different axial position. In Figure 4.7, the radial average of the axial velocity at various x locations is computed and plotted for different times. The profiles show no evidence of steepening.

The contours of constant ψ are presented in Figure 4.8 for later times ($t = 10.12$, 10.97, and 11.81). The contours of constant Ω and the contours of constant ζ are shown in Figure 4.9 and Figure 4.10 respectively. Throughout the motion, ψ and Ω show very minimal changes. Relatively greater changes are evident in the ζ field. A minor amount of concentration of constant ζ lines near the axis of the vortex is evident.

Next we describe the results of a run for a vortex with stronger perturbation.

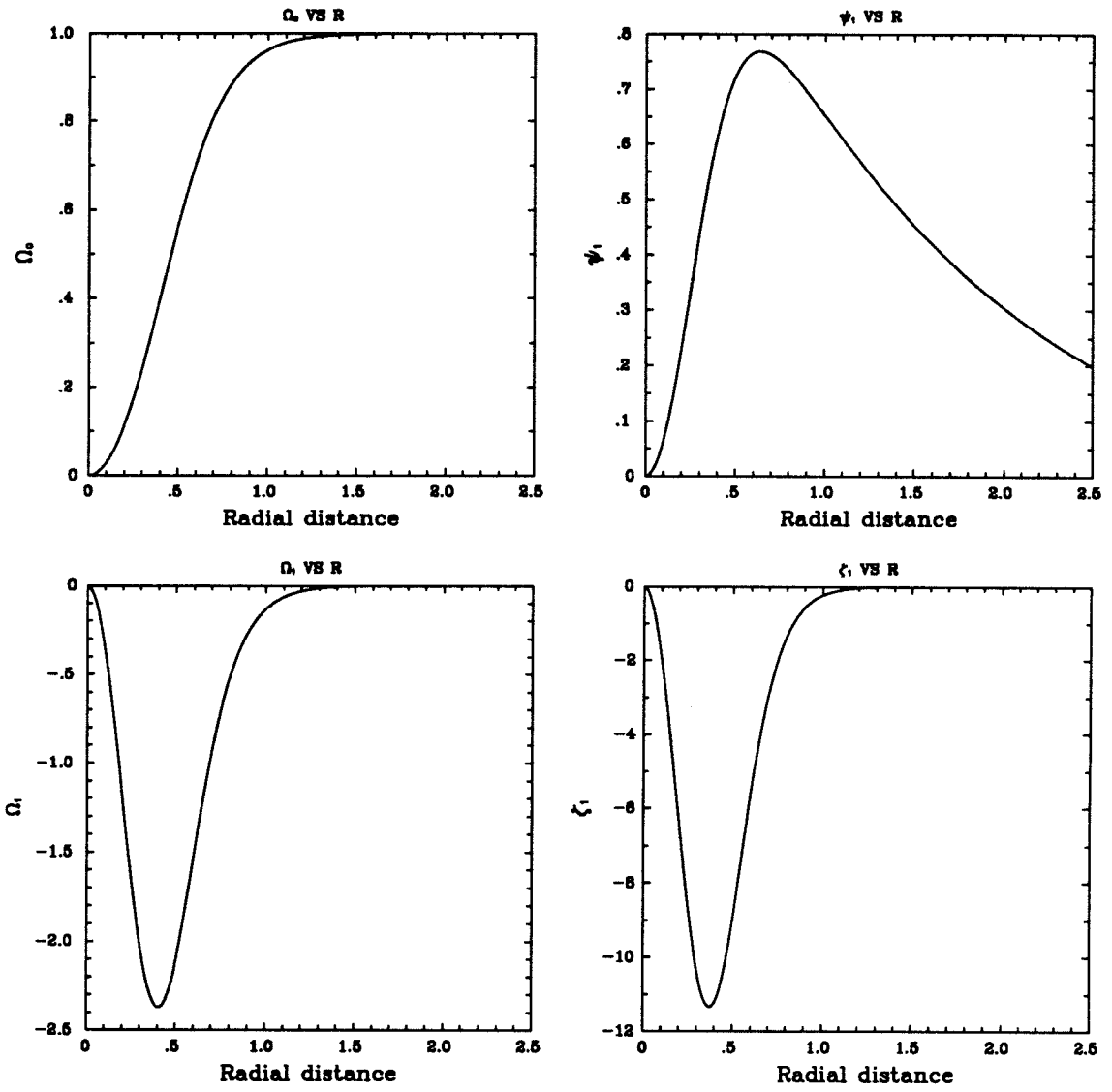

Fig. 4.1 The profiles of the circulation for the base flow Ω_0 and the perturbation components ψ_1, Ω_1 and ζ_1. Radial resolution of $J = 200$ with $R = 2.5$ is used. The size of the core radius is $a = 0.5$.

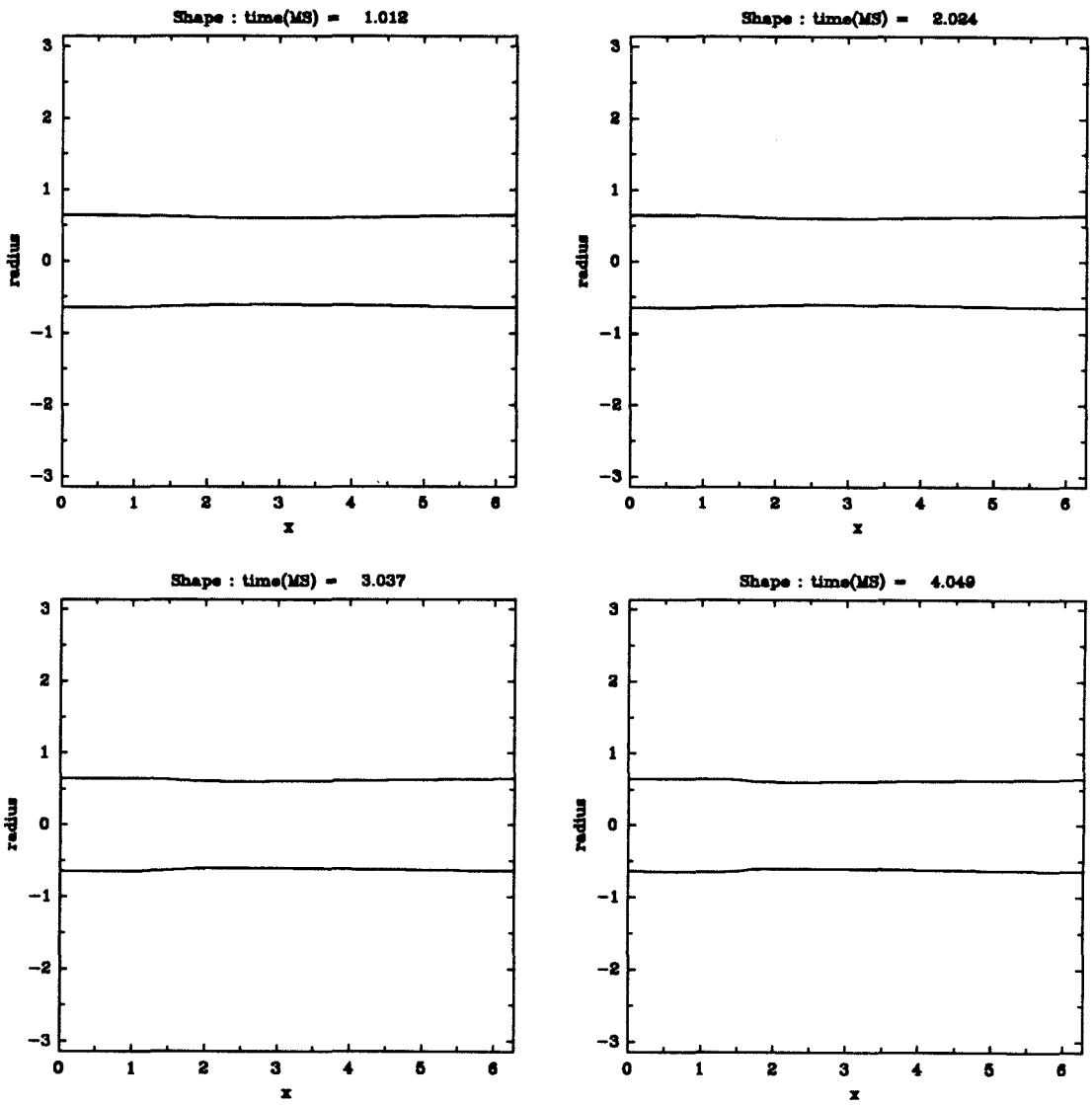

Fig. 4.2a The shape of the vortex as a function of time for the MS problem. The times are indicated on each plot.

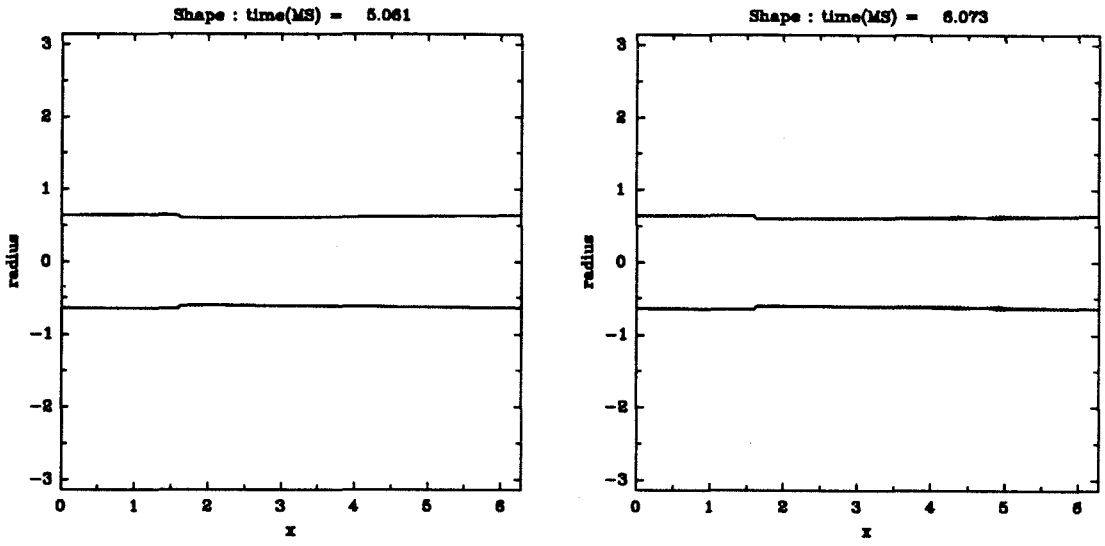

Fig. 4.2b The shape of the vortex as a function of time for the MS problem. The times are indicated on each plot.

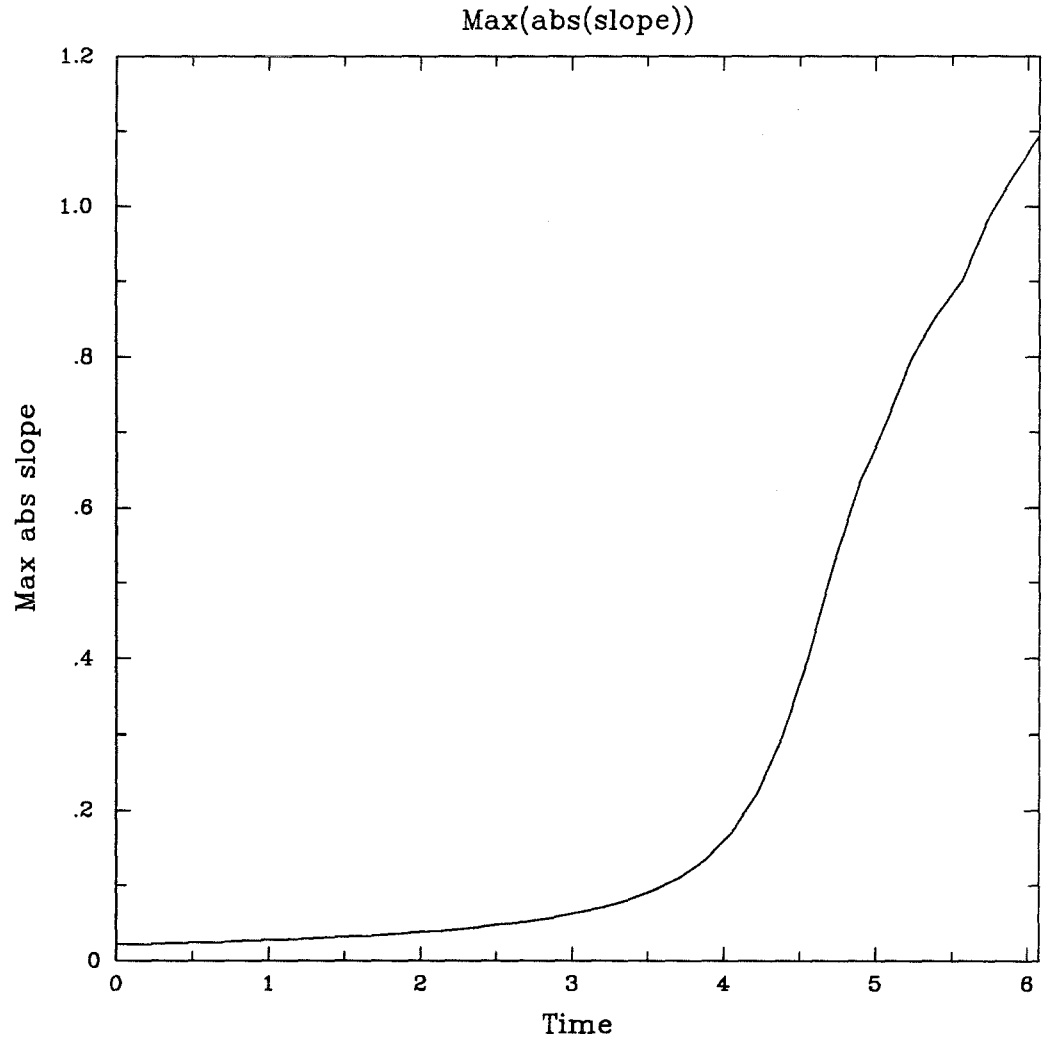

Fig. 4.3 Variation of maximum value of $|\partial a(x,t)/\partial x|$ as a function of time for the MS problem.

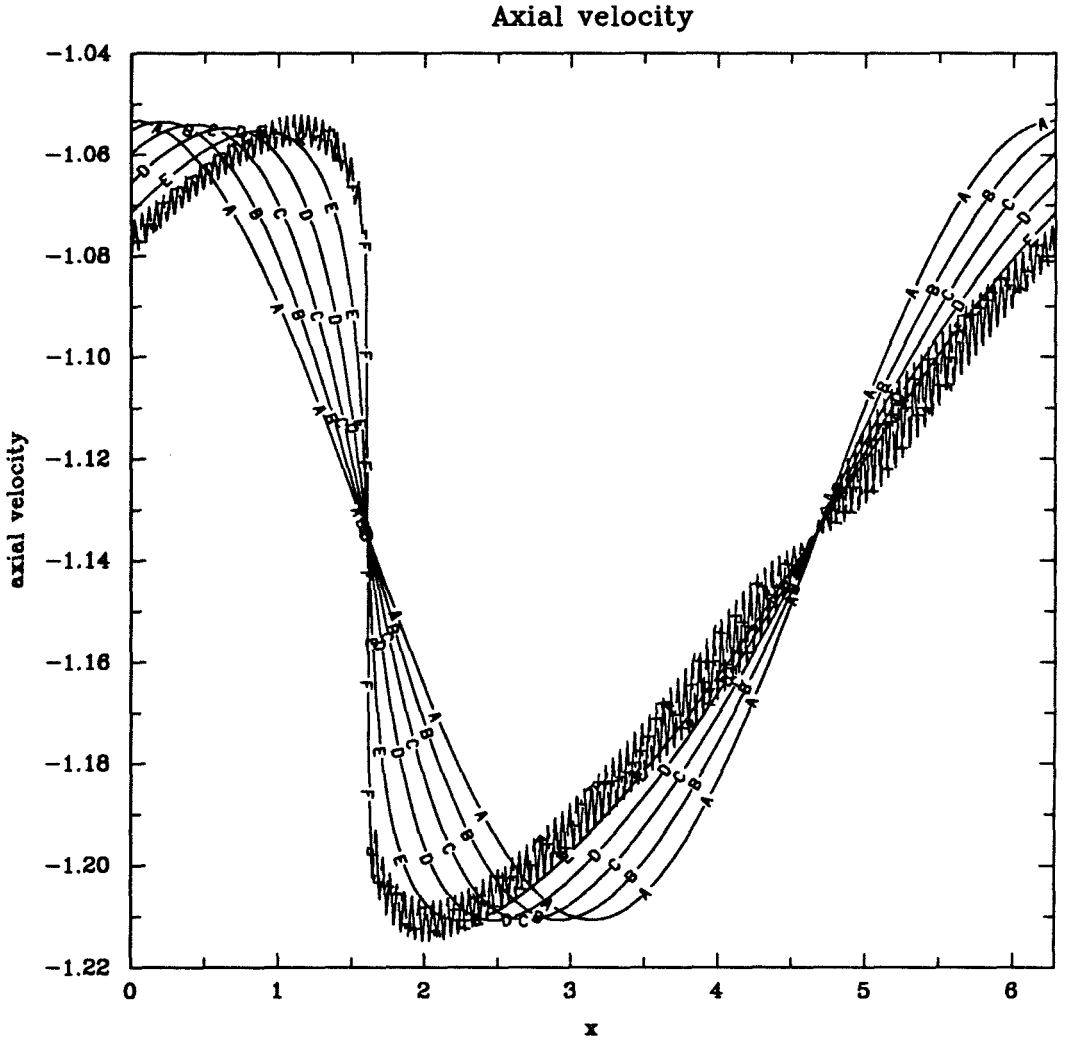

Fig. 4.4 Axial velocity as a function of x is shown for A. $t = 0.0$, B. $t = 1.012$, C. $t = 2.024$, D. $t = 3.037$, E. $t = 4.049$, and F. $t = 5.061$. This shows the solution of MS equations.

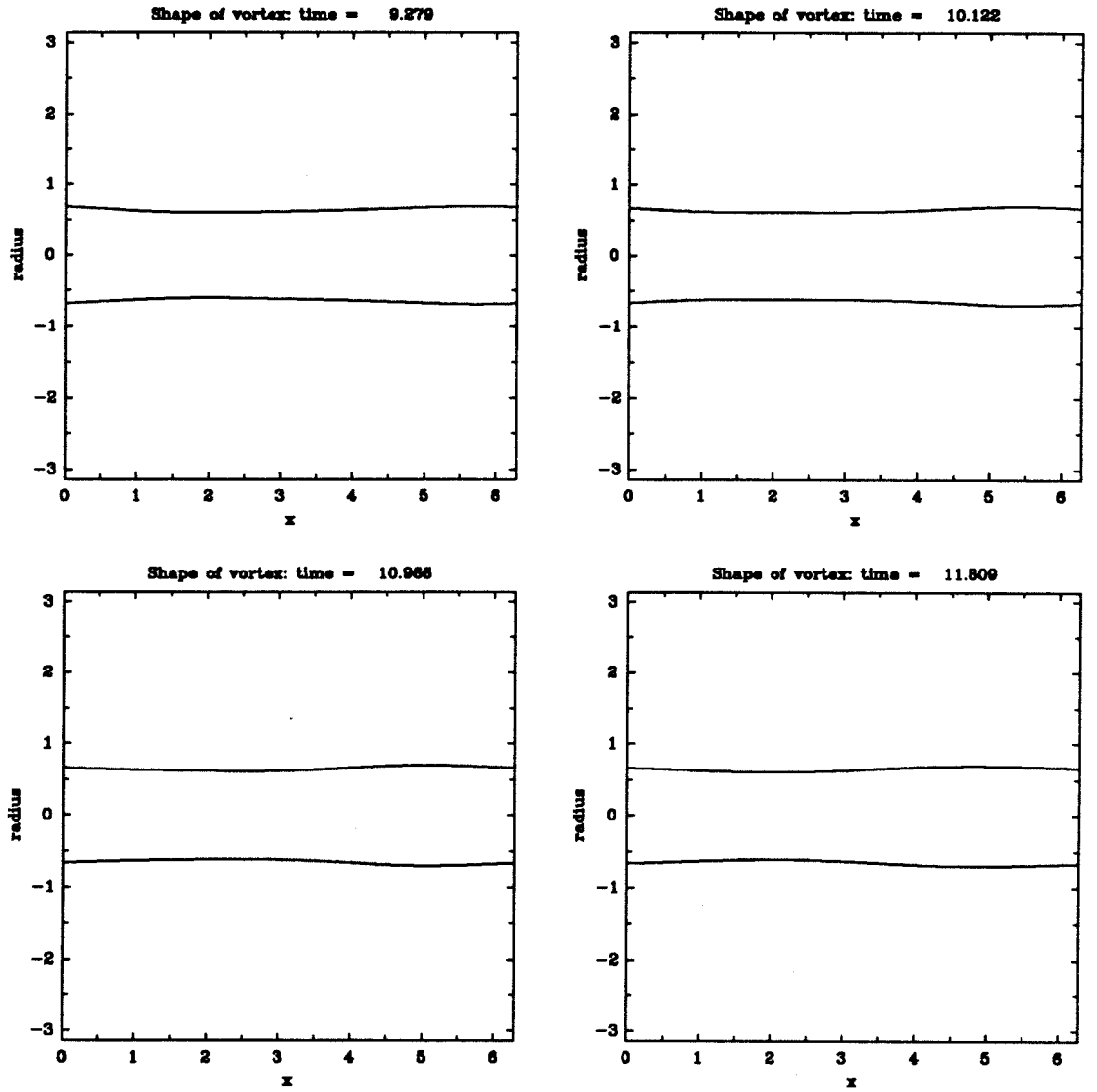

Fig. 4.5 The shape of the vortex as a function of time for the N-S problem. The times are indicated on each plot.

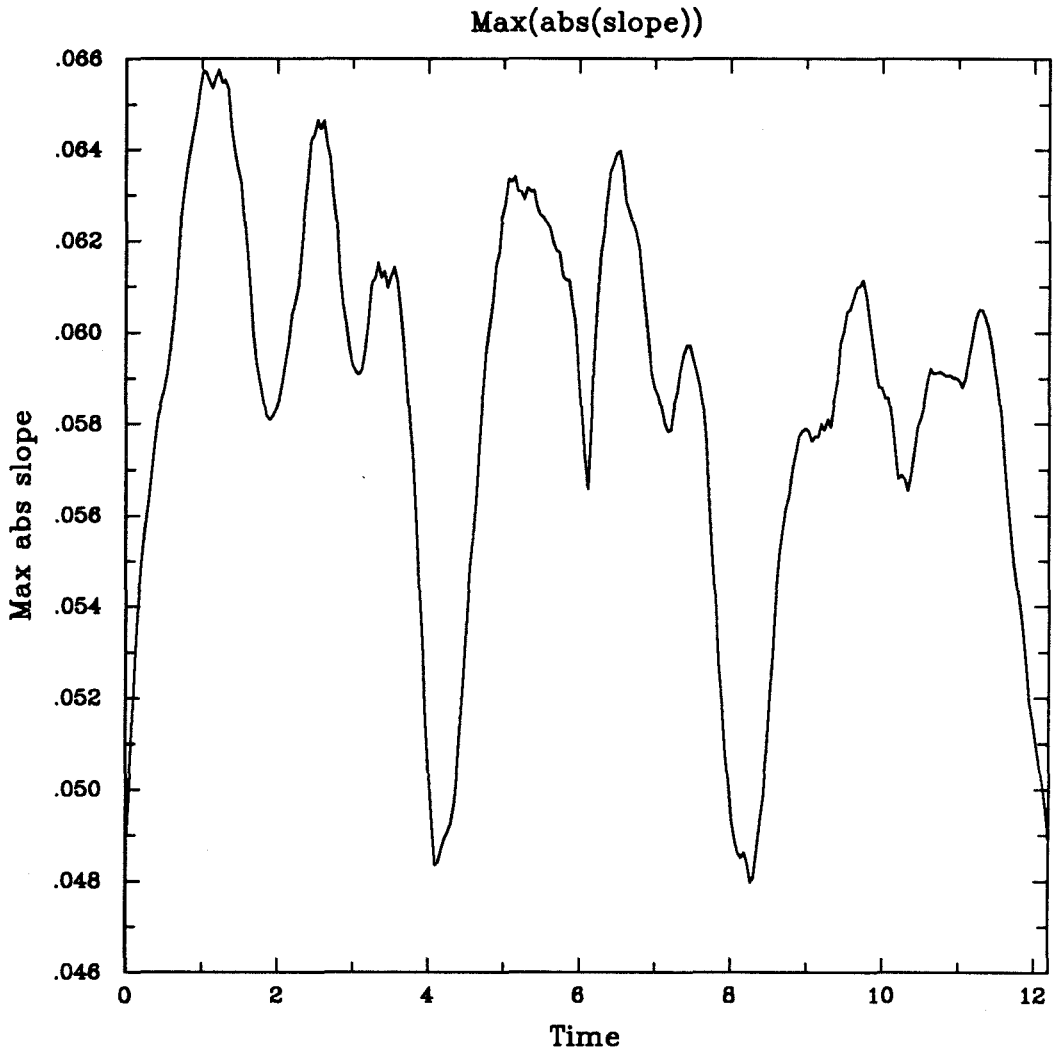

Fig. 4.6 Variation of maximum value of $|\partial a(x,t)/\partial x|$ as a function of time for the N-S problem.

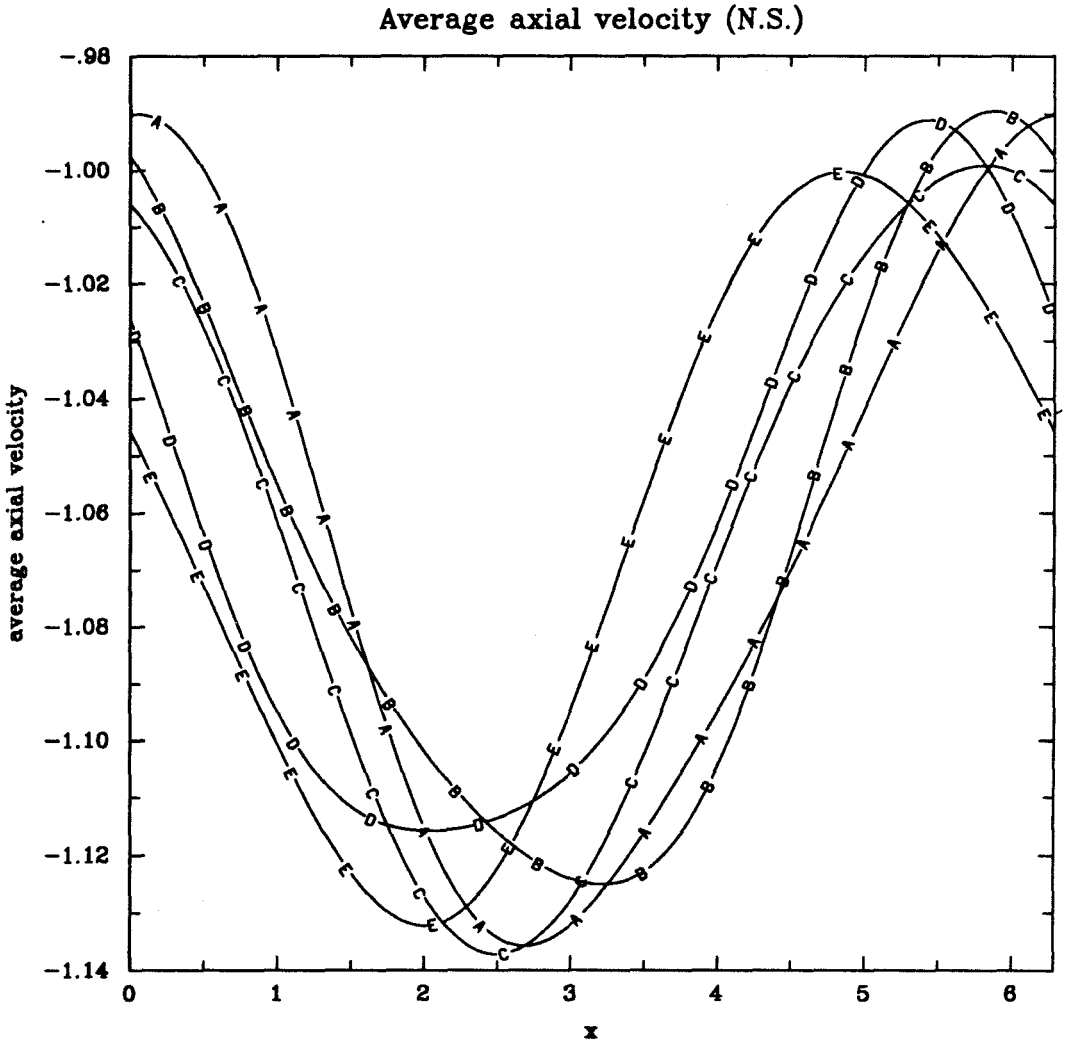

Fig. 4.7 Average axial velocity as a function of x is shown for A. $t = 5.061$, B. $t = 6.748$, C. $t = 8.435$, D. $t = 10.122$, and E. $t = 11.809$. This shows the solution of N-S equations.

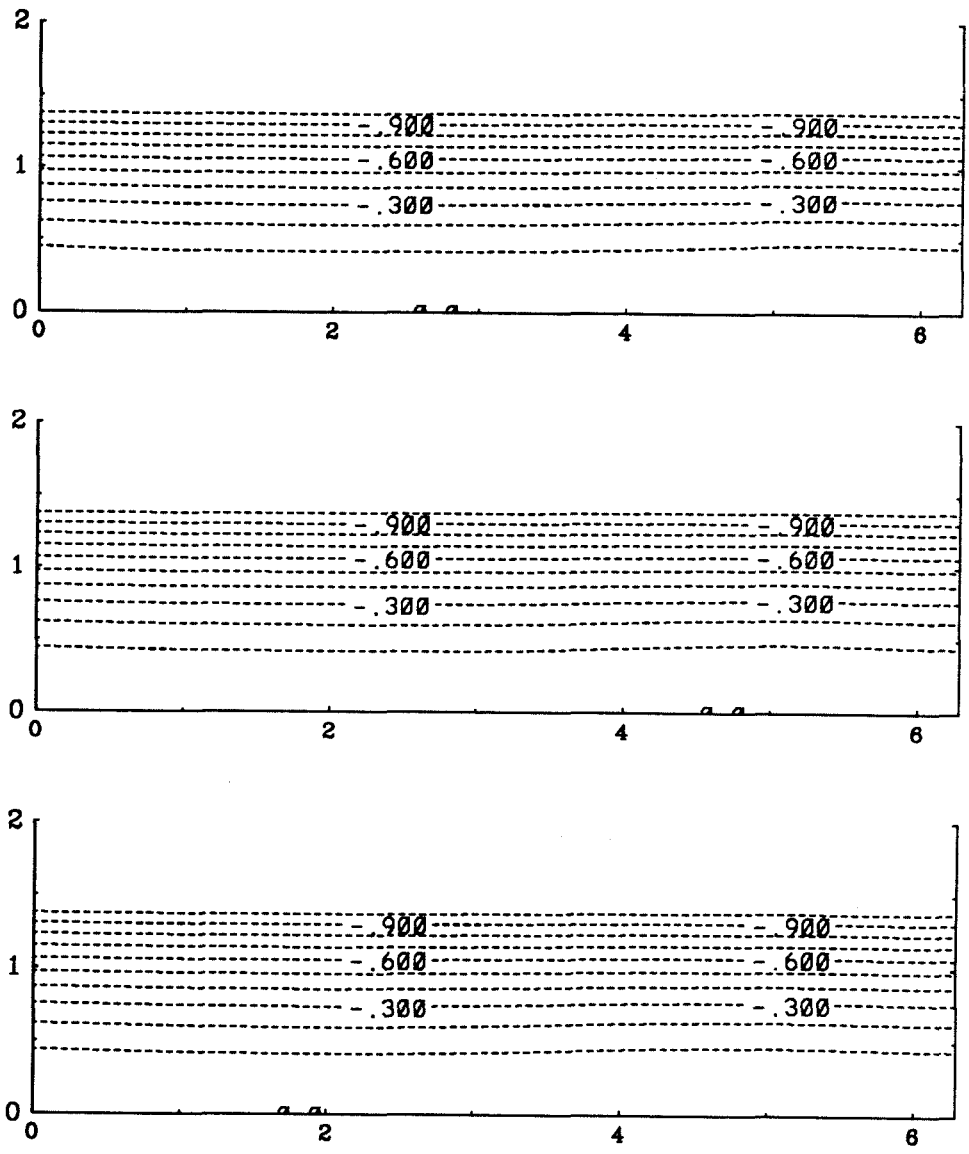

Fig. 4.8 Contours of constant ψ for $t = 10.122$, 10.966 and 11.809. Contour interval = 0.1. A dashed line is used for negative values.

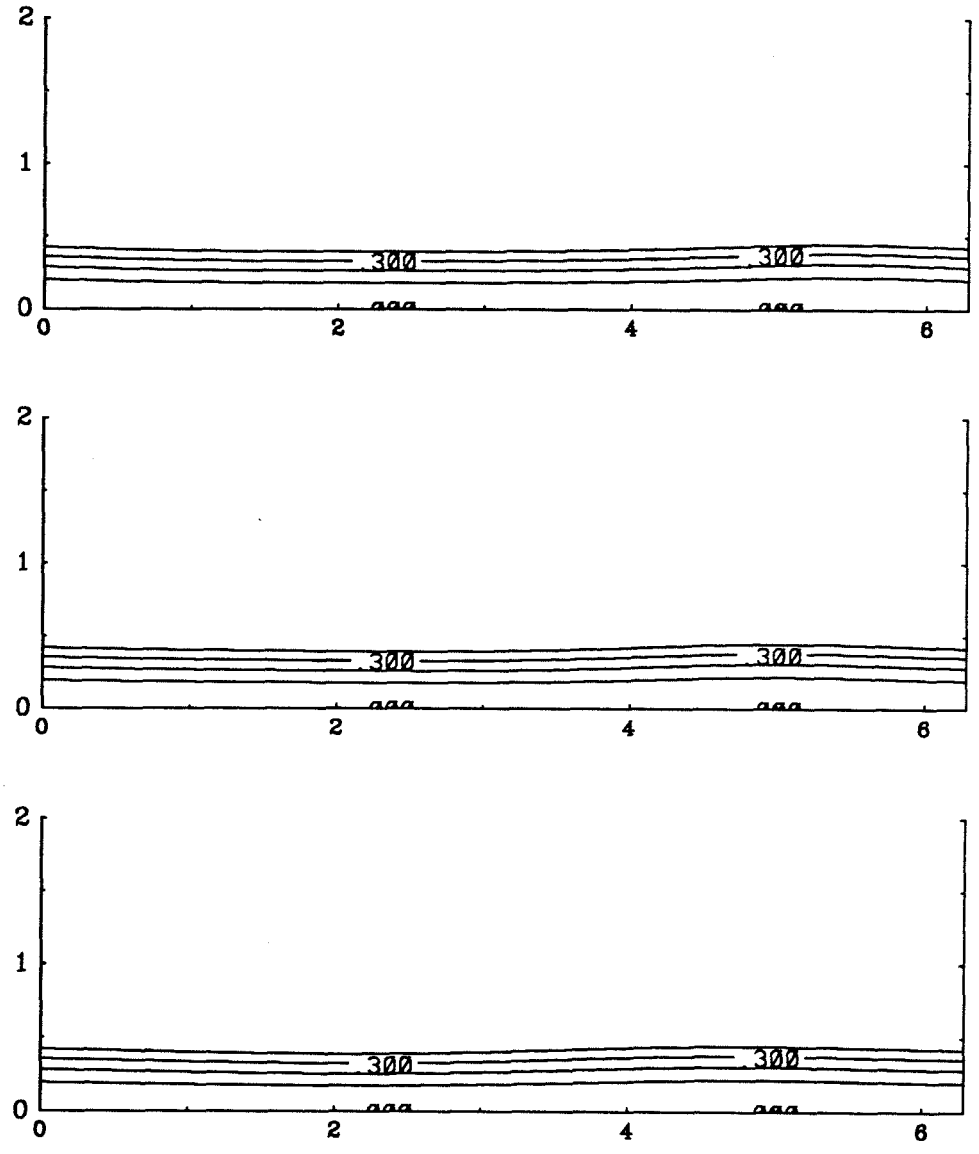

Fig. 4.9 Contours of constant Ω for $t = 10.122,\ 10.966$ and 11.809. Contour interval $= 0.1$. A dashed line is used for negative values.

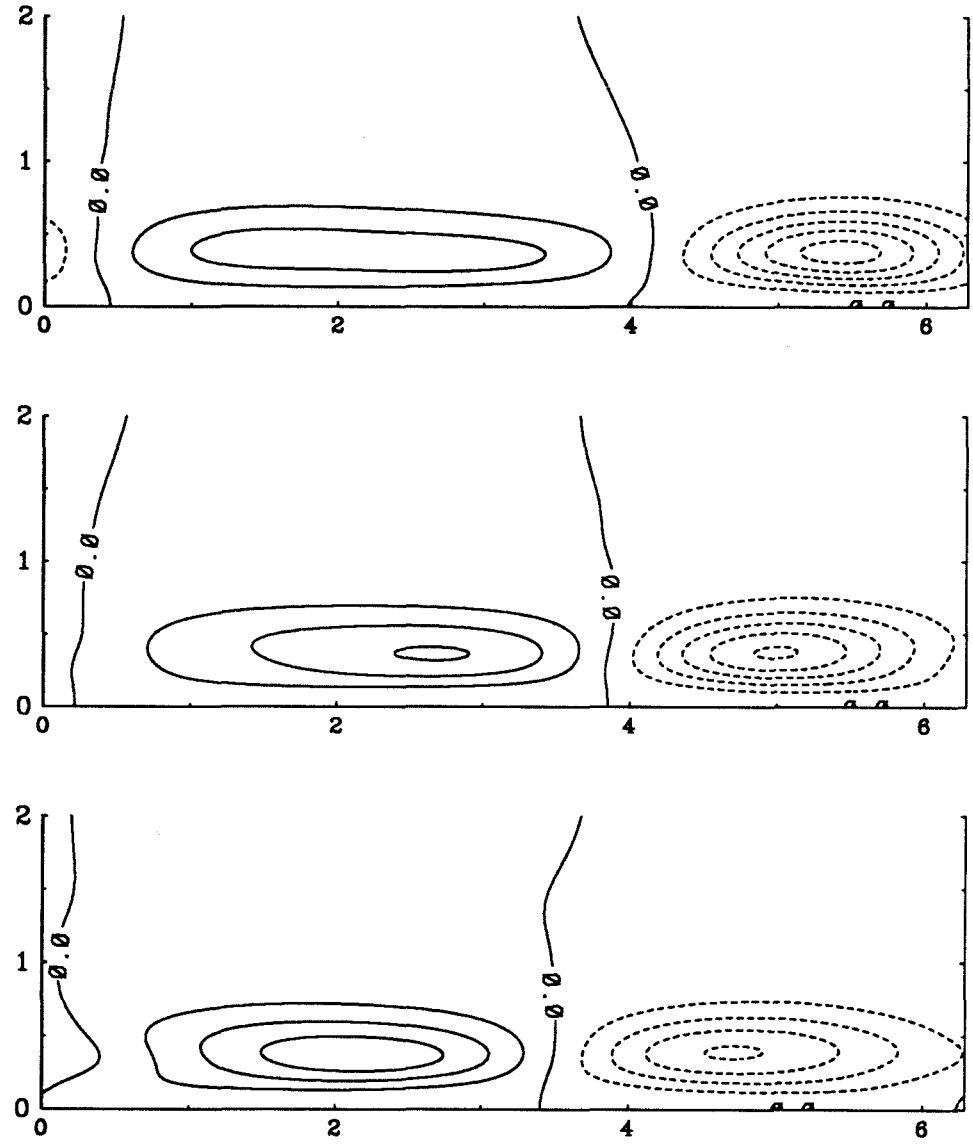

Fig. 4.10 Contours of constant ζ for $t = 10.122$, 10.966 and 11.809. Contour interval = 0.05. A dashed line is used for negative values.

In Figures 4.11 through 4.20 the numerical results for a run with $\varepsilon = 0.12$ are presented. Thus, the perturbation is stronger than the previous case. The initial profiles of Ω_0, ψ_1, Ω_1 and ζ_1 are shown in Figure 4.11. The radial domain was taken to be $R = 5$ with a resolution of $J = 320$ radial points. The initial core radius was about one. The radial resolution is comparable to the previous case. A modal resolution of $m = 64$ was used for the N-S case and a resolution of $m = 128$ was used for the MS case. The viscosity coefficients were taken to be $\mu_1 = \mu_2 = 10^{-4}$. The Reynolds number for the flow is the same as that of the previous run – $Re = \Gamma/\mu = 62830$.

The development of the shape of the vortex core is shown in Figure 4.12 for the MS case. Gradual steepening of the core wave occurs as time passes. At about $t = 1.36$, a jump in the core area begins to form. In Figure 4.13 the maximum value of the $|\partial a(x,t)/\partial x|$, where a is the core radius, is plotted as a function of time. It clearly indicates the the slope increases monotonically with time till $t = 1.6$. The apparent oscillations after this time are a result of numerical errors. Numerical oscillations are also evident in Figure 4.12 which depict the shape of the vortex core. The development of the axial velocity is shown in Figure 4.14. The profile marked with A is at $t = 0$. For profiles marked with B through H, the time increases in steps of 0.195. Steepening of the initial wave is clearly indicated. After the shock formation around $t = 1.5$ the axial velocity showed numerical errors which increased with time.

The development of the core shape for the N-S case is shown in Figure 4.15. The core bulges with passage of time. But the core wave does not steepen enough to form a shock. The maximum value of $|\partial a/\partial x|$ is shown in Figure 4.16. As in the small perturbation case, this shows qualitatively very different motion of the core wave. The core wave undergoes periodic flattening and steepening. In Figure 4.17, the radial average of the axial velocity at various x locations is computed and plotted for different times. Once again, the profiles fail to show any evidence of steepening.

The contours of constant ψ are presented in Figure 4.18. As time passes, the instantaneous streamlines begin to show a gradual bulging near $x = 0$ similar to the

core shape. The axial velocity on the axis begins to increase in magnitude near $x = 0$ but still remains of the same sign (negative) till slightly after $t = 1.4$. Beyond this time, a closed streamline appears on the axis signifying reversal of the axial flow on the axis. The bubble grows in size till $t = 1.8$ and then it begins to shrink in size. Then it detaches from the axis at about $t = 2.3$ and eventually collapses. The numerical solution could not be continued beyond this time because of numerical breakdown of the vorticity field.

The contours of constant Ω are shown in Figure 4.19. Throughout the motion, the circulation field shows minor changes. No reversal of circulation is seen in any part of the flow field. The lines show bulging similar to the contours of ψ.

The contours of constant ζ are shown in Figure 4.20. The initial elliptical contours are sheared by the action of fluid motion. This results in a clustering of contours in the flow domain around $x = 0$. The gradients in the vorticity field continually increase in this region. The domain within $x = 2$ and $x = 4$ shows relatively less concentration of contours. Most of the action is restricted to the region of flow about $x = 0$. This is also the region in which a bubble of reversed flow appears. The ζ field suffers numerical breakdown at about $t = 2$ because of lack of resolution.

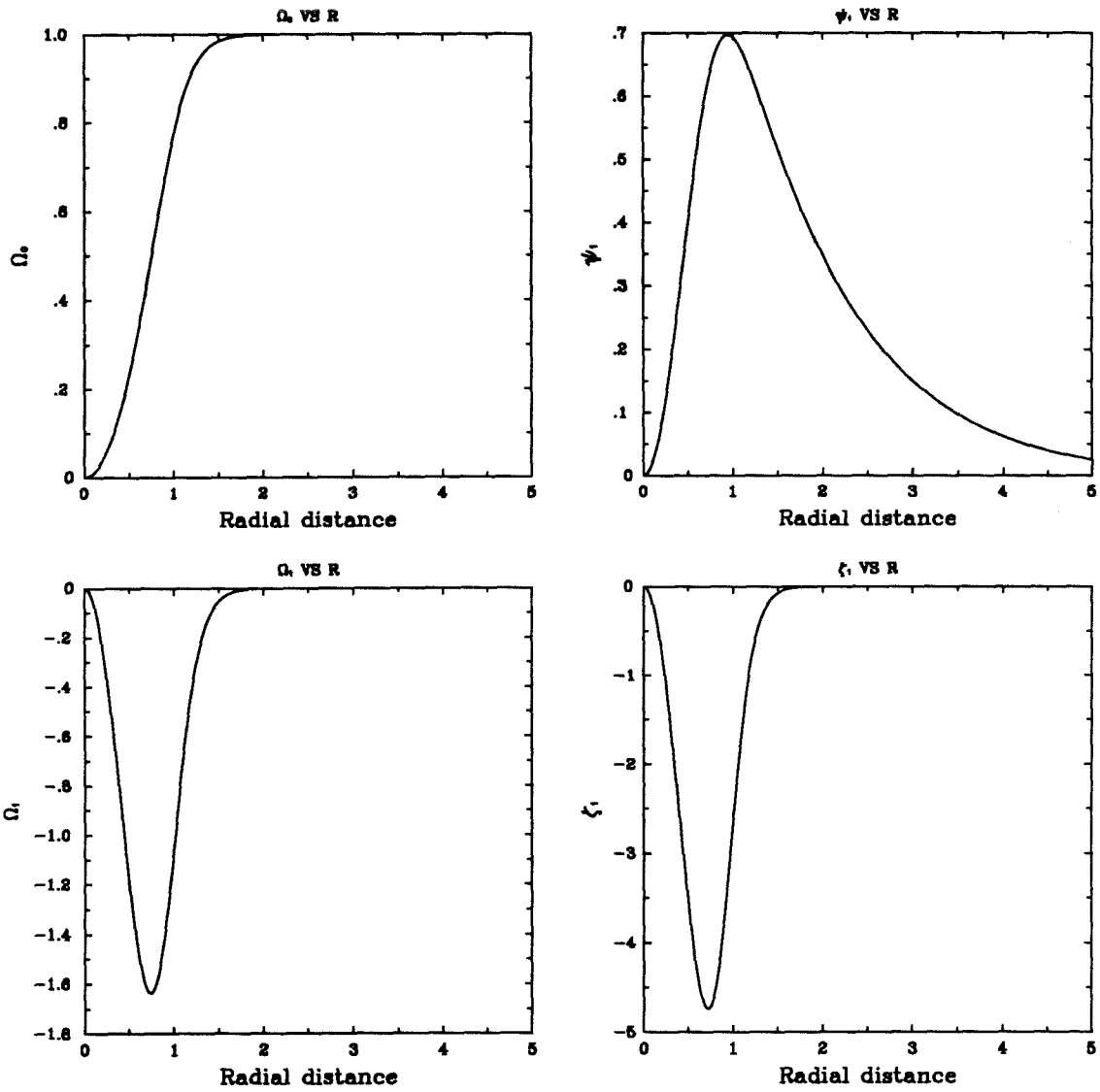

Fig. 4.11 The profiles of the circulation for the base flow Ω_0 and the perturbation components ψ_1, Ω_1 and ζ_1. Radial resolution of $J = 320$ with $R = 5$ is used. The size of the core radius is $a = 1$.

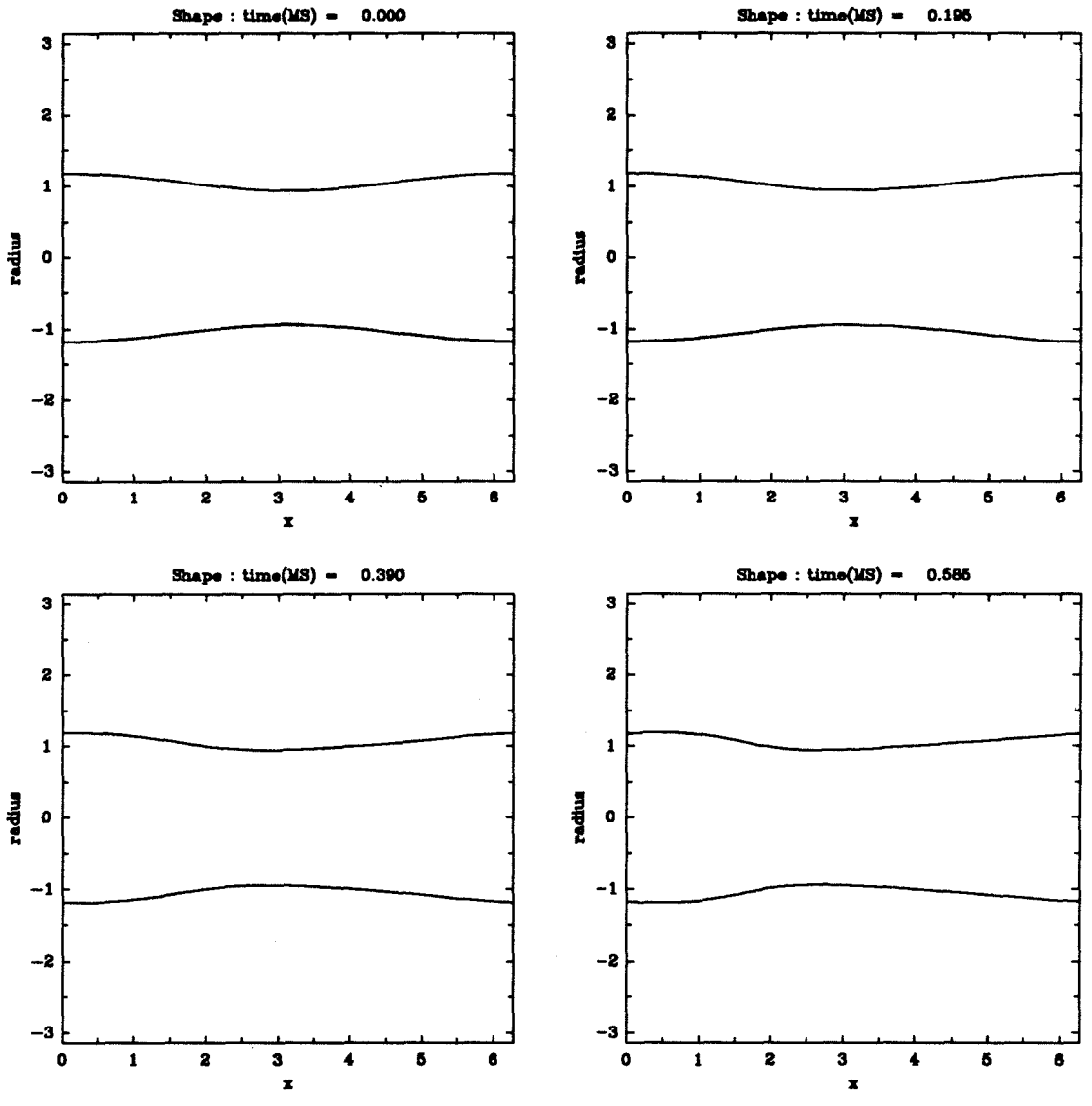

Fig. 4.12a The shape of the vortex as a function of time for the MS problem. The times are indicated on each plot.

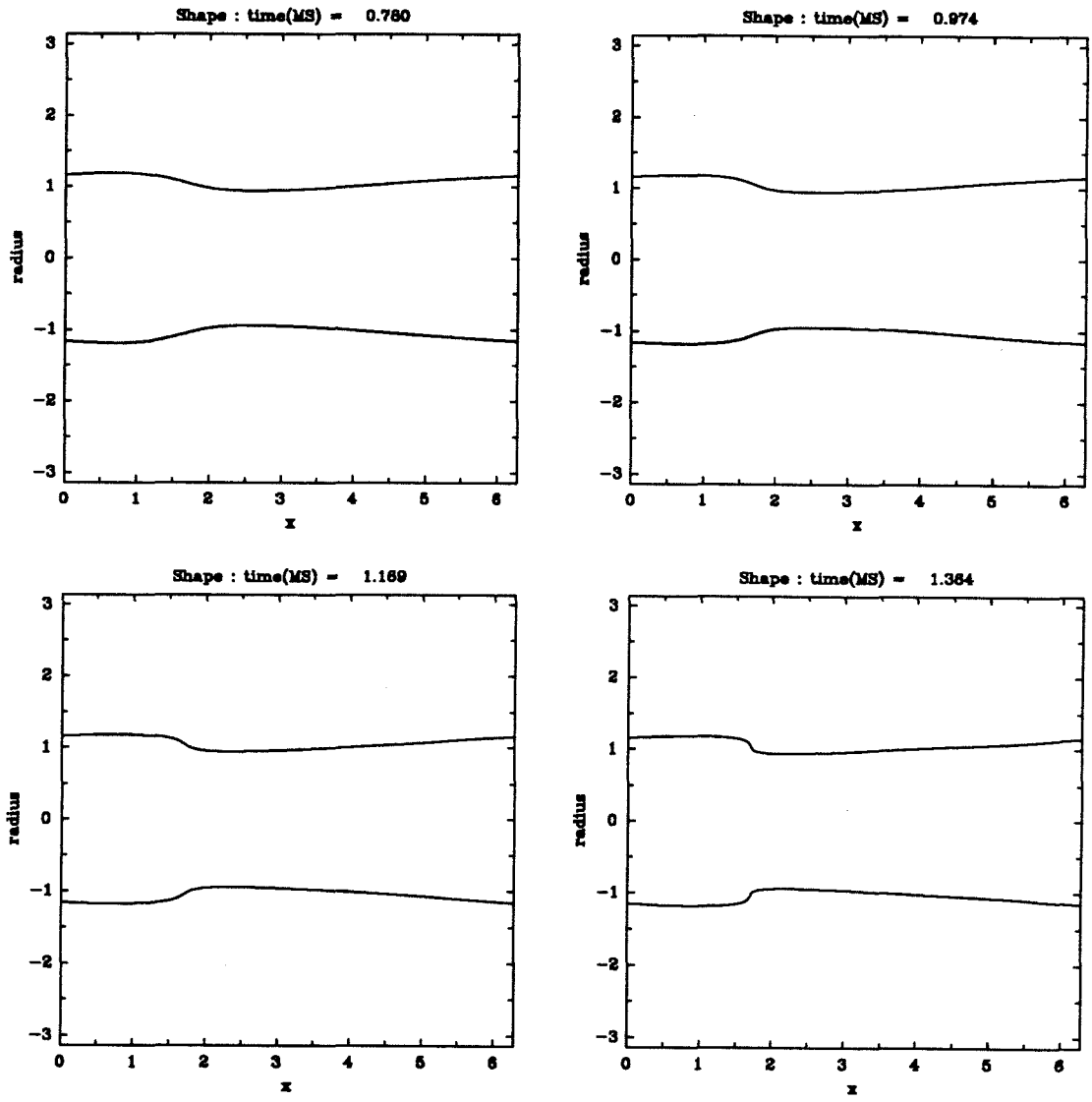

Fig. 4.12b The shape of the vortex as a function of time for the MS problem. The times are indicated on each plot.

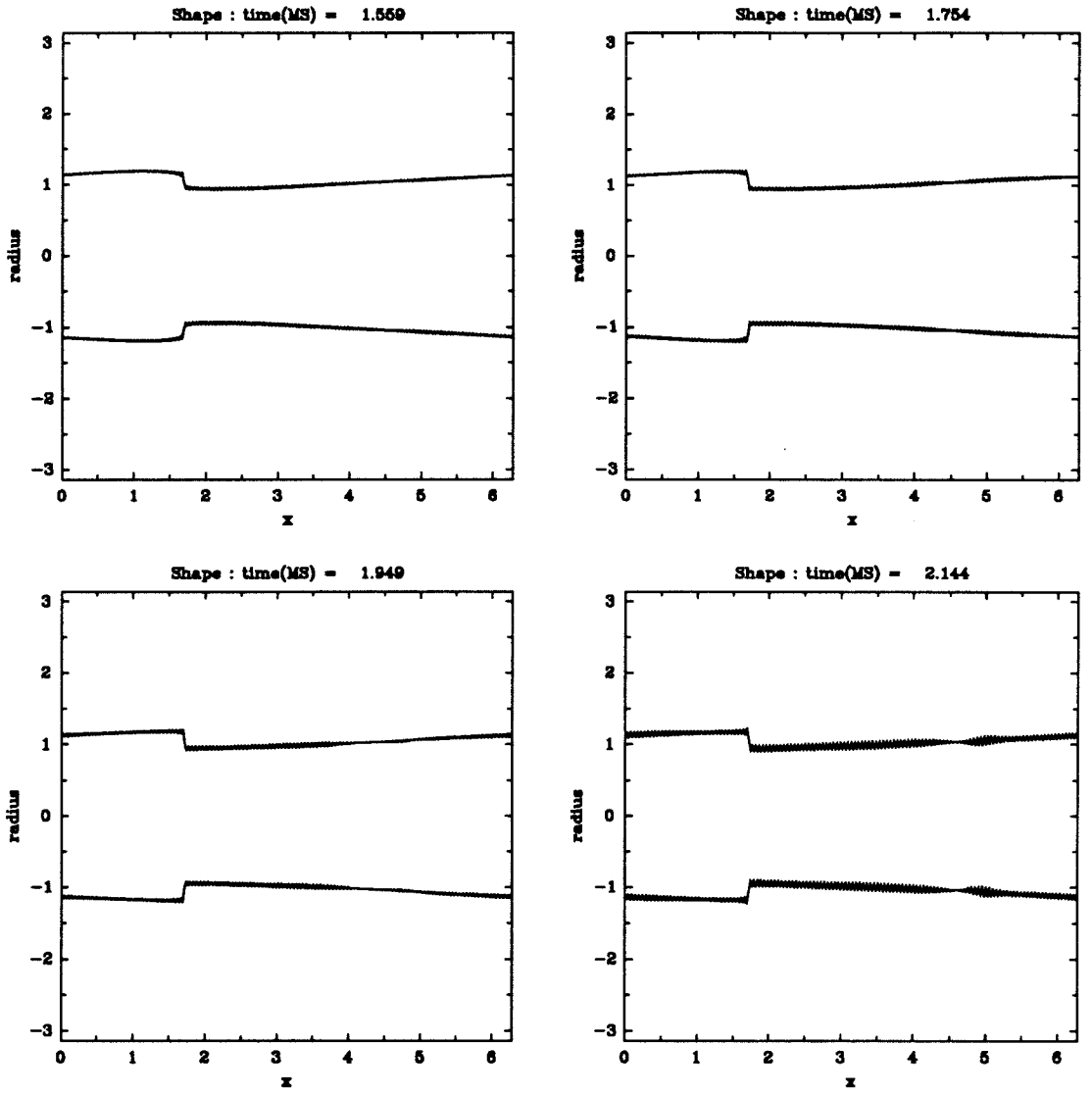

Fig. 4.12c The shape of the vortex as a function of time for the MS problem. The times are indicated on each plot.

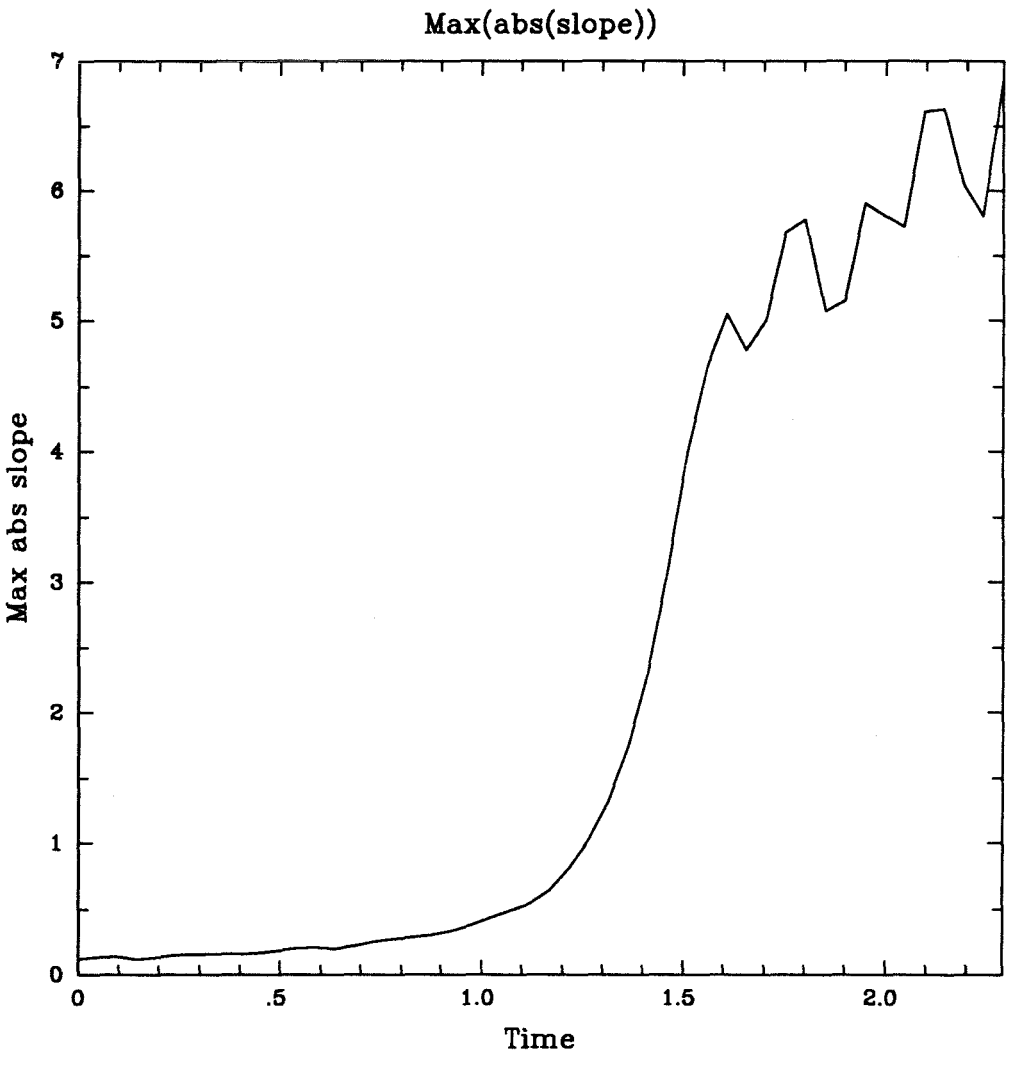

Fig. 4.13 Variation of maximum value of $|\partial a(x,t)/\partial x|$ as a function of time for the MS problem.

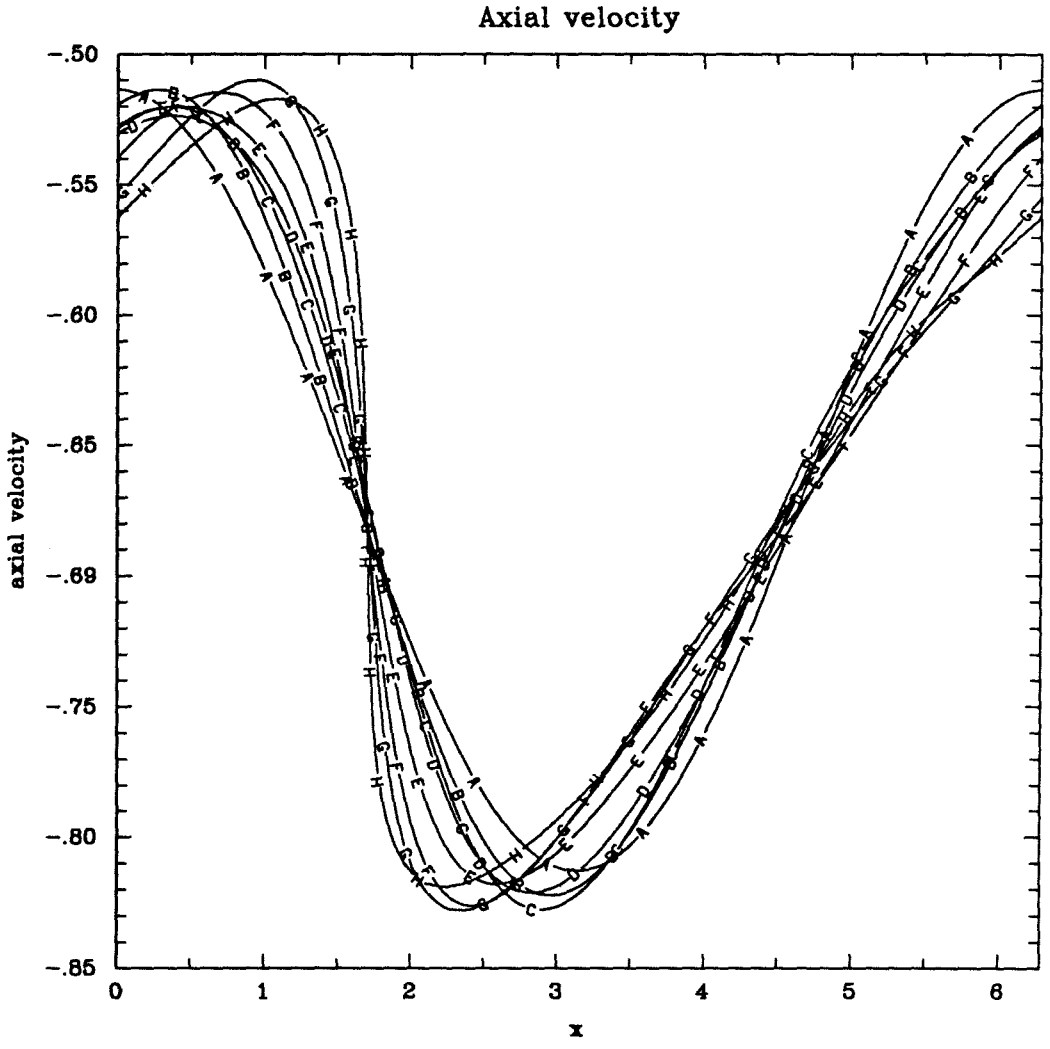

Fig. 4.14 Axial velocity as a function of x is shown for A. $t = 0.0$, B. $t = 0.195$, C. $t = 0.390$, D. $t = 0.585$, E. $t = 0.780$, F. $t = 0.974$, G. $t = 1.169$, and H. $t = 1.364$. This shows the solution of MS equations.

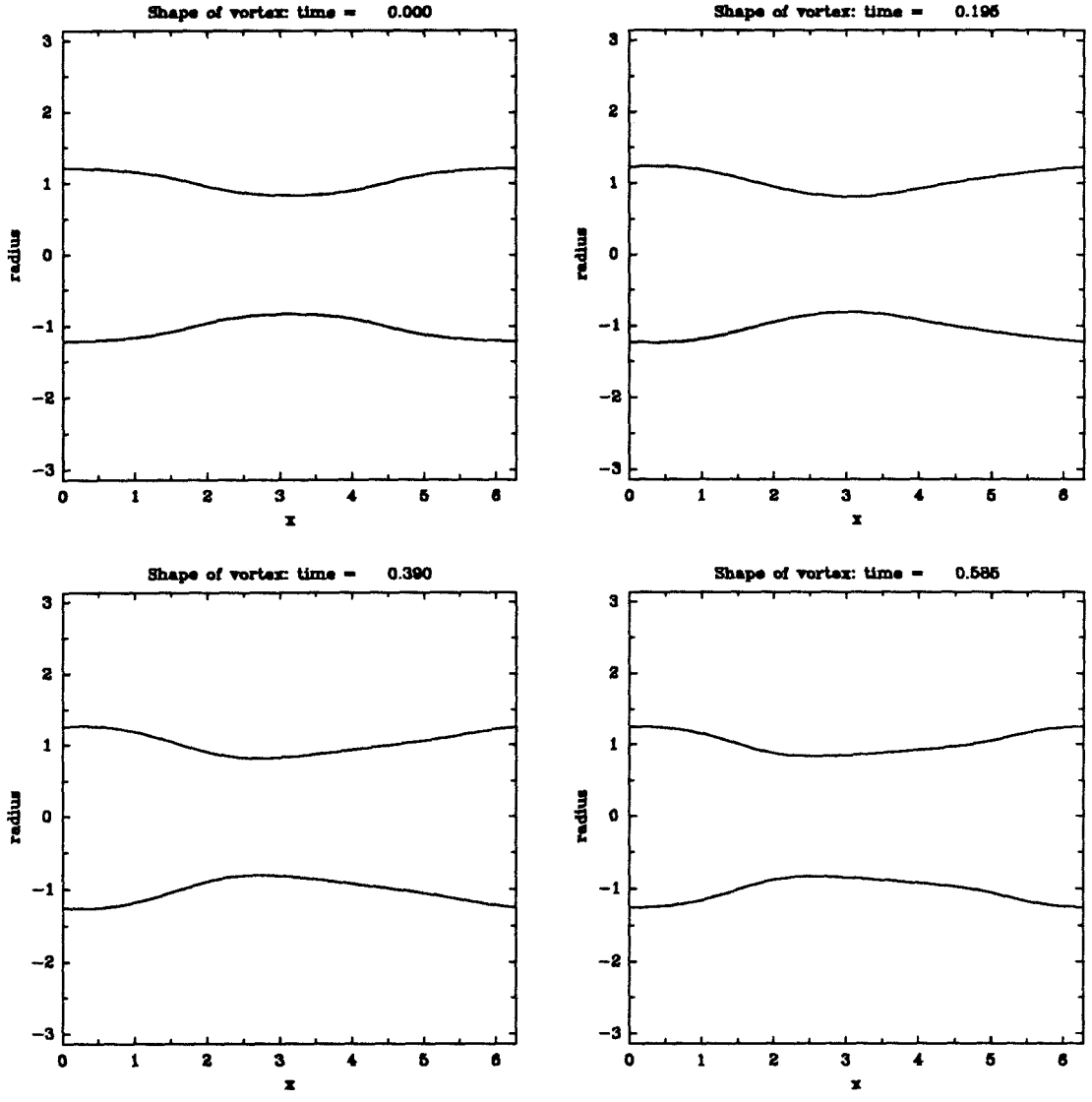

Fig. 4.15a The shape of the vortex as a function of time for the N-S problem. The times are indicated on each plot.

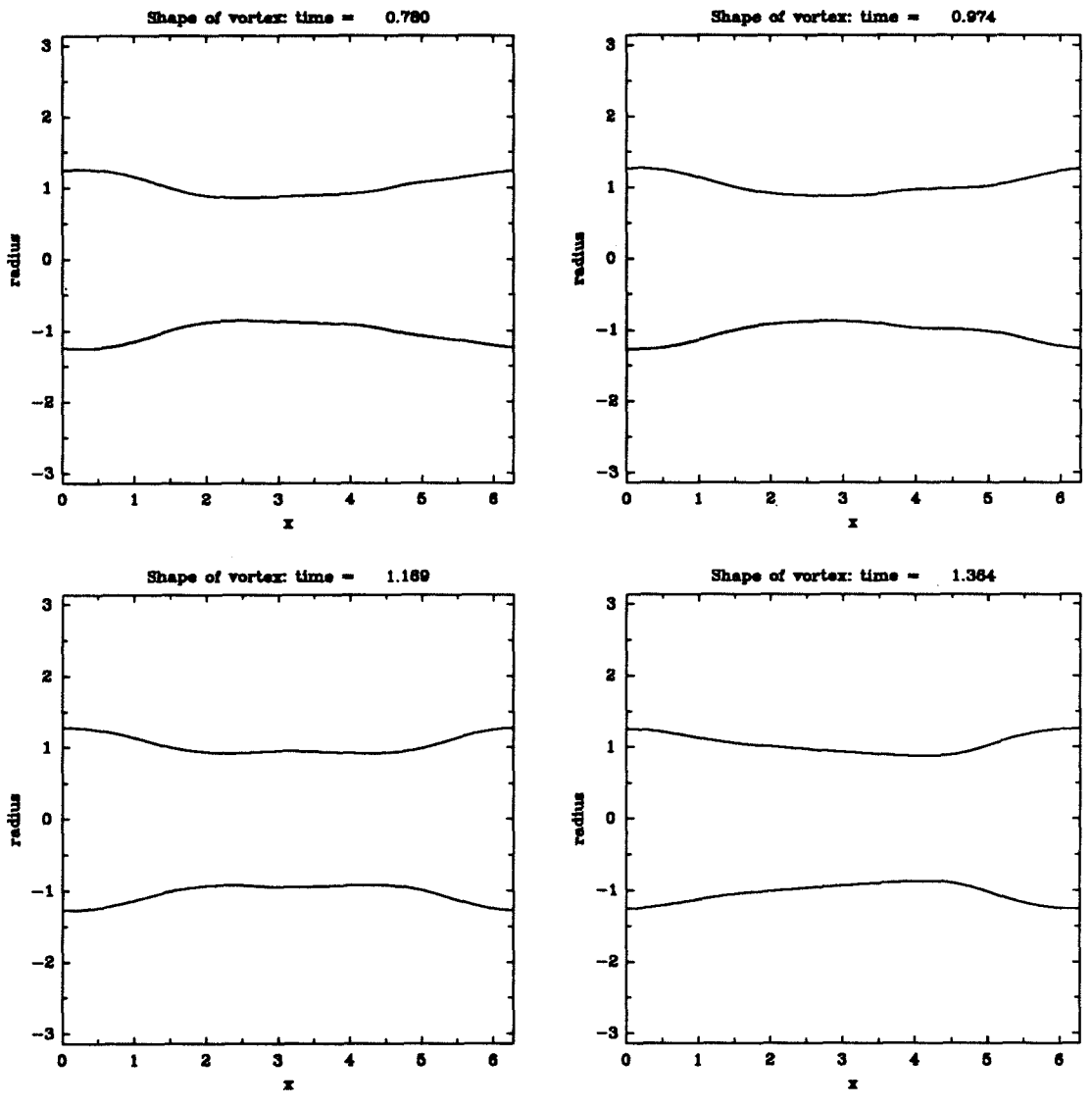

Fig. 4.15b The shape of the vortex as a function of time for the N-S problem. The times are indicated on each plot.

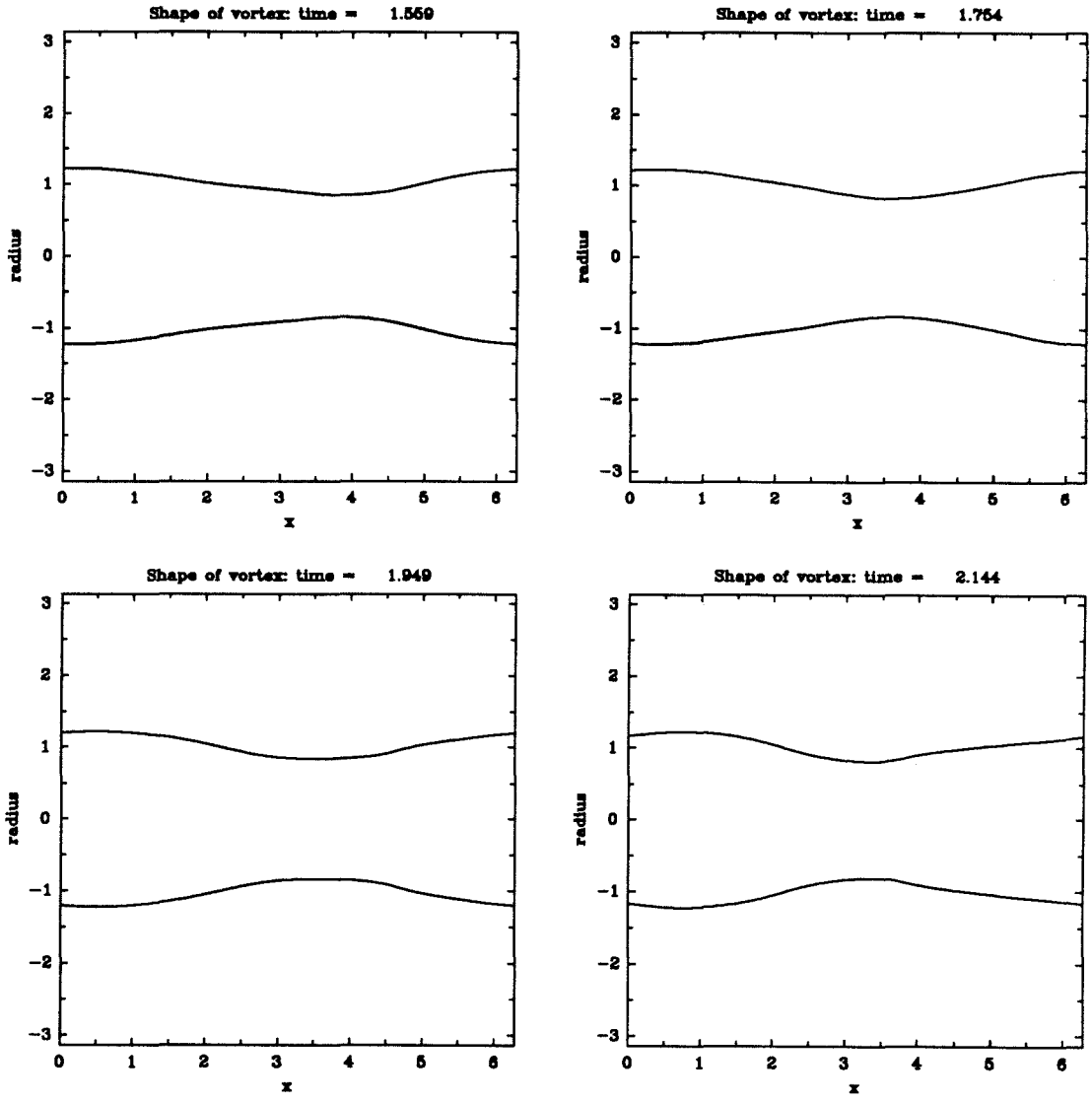

Fig. 4.15c The shape of the vortex as a function of time for the N-S problem. The times are indicated on each plot.

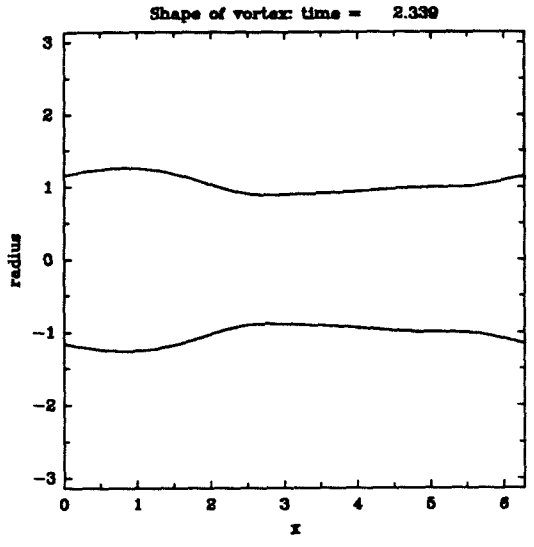

Fig. 4.15d The shape of the vortex as a function of time for the N-S problem. The times are indicated on each plot.

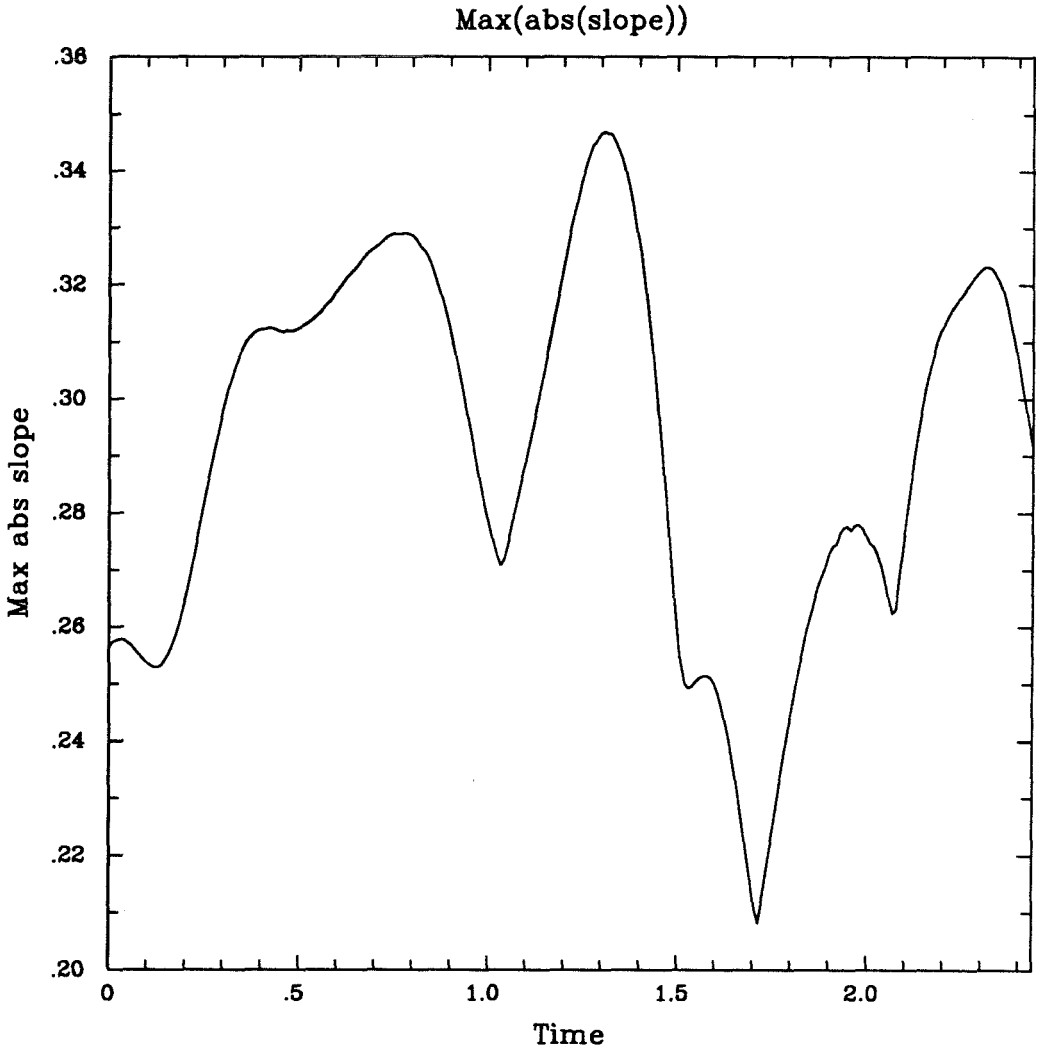

Fig. 4.16 Variation of maximum value of $|\partial a(x,t)/\partial x|$ as a function of time for the N-S problem.

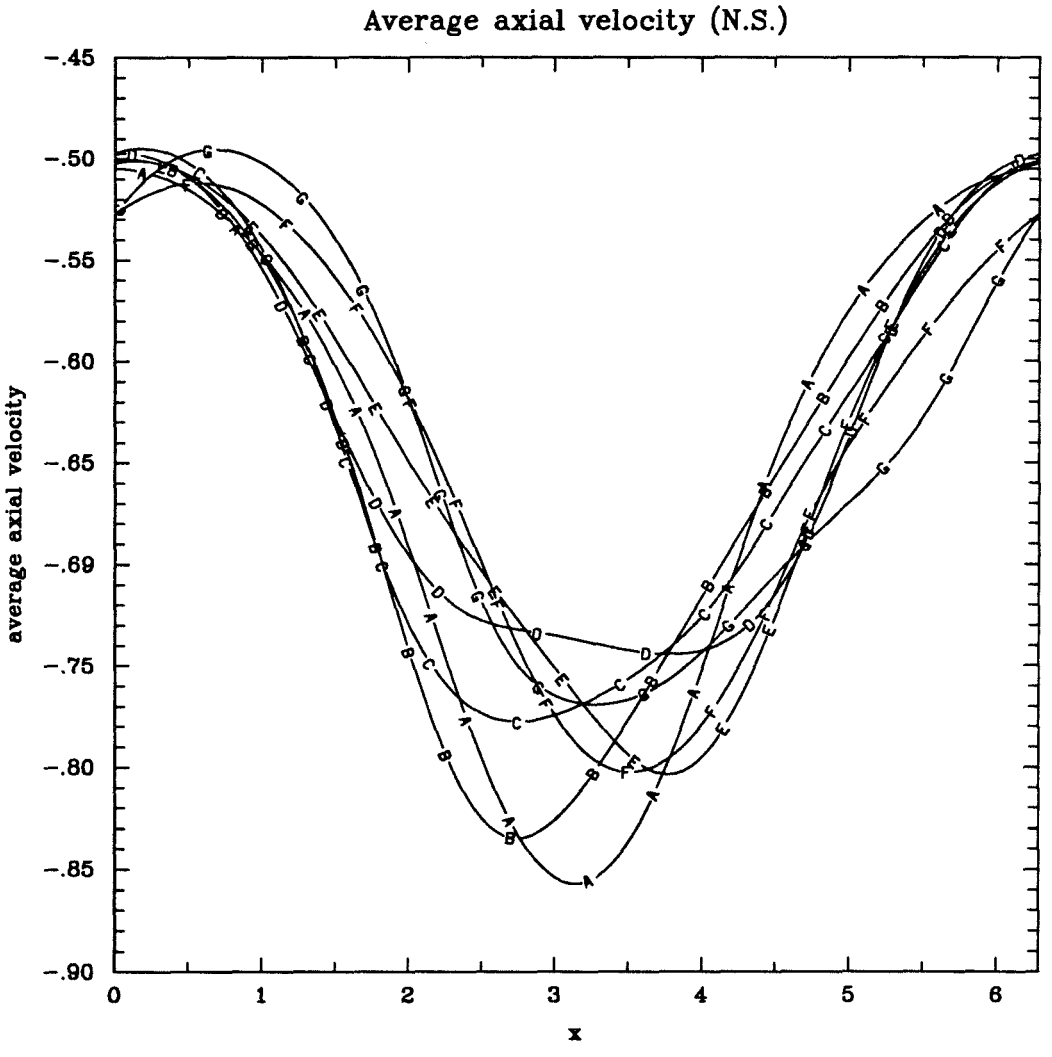

Fig. 4.17 Average axial velocity as a function of x is shown for A. $t = 0.0$, B. $t = 0.390$, C. $t = 0.780$, D. $t = 1.169$, E. $t = 1.559$, F. $t = 1.949$, and G. $t = 2.339$. This shows the solution of N-S equations.

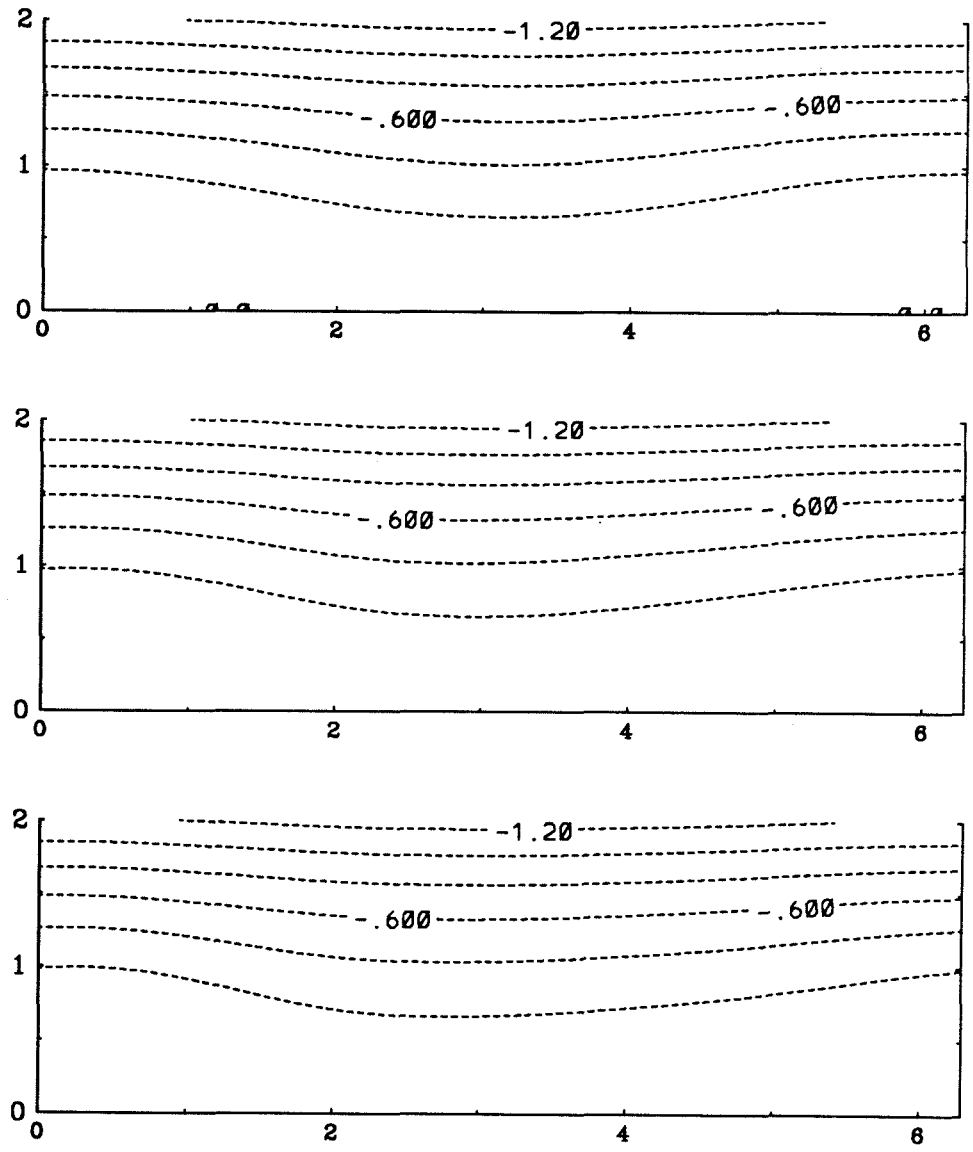

Fig. 4.18a Contours of constant ψ for $t = 0.0$, 0.195 and 0.390. Contour interval = 0.2. A dashed line is used for negative values.

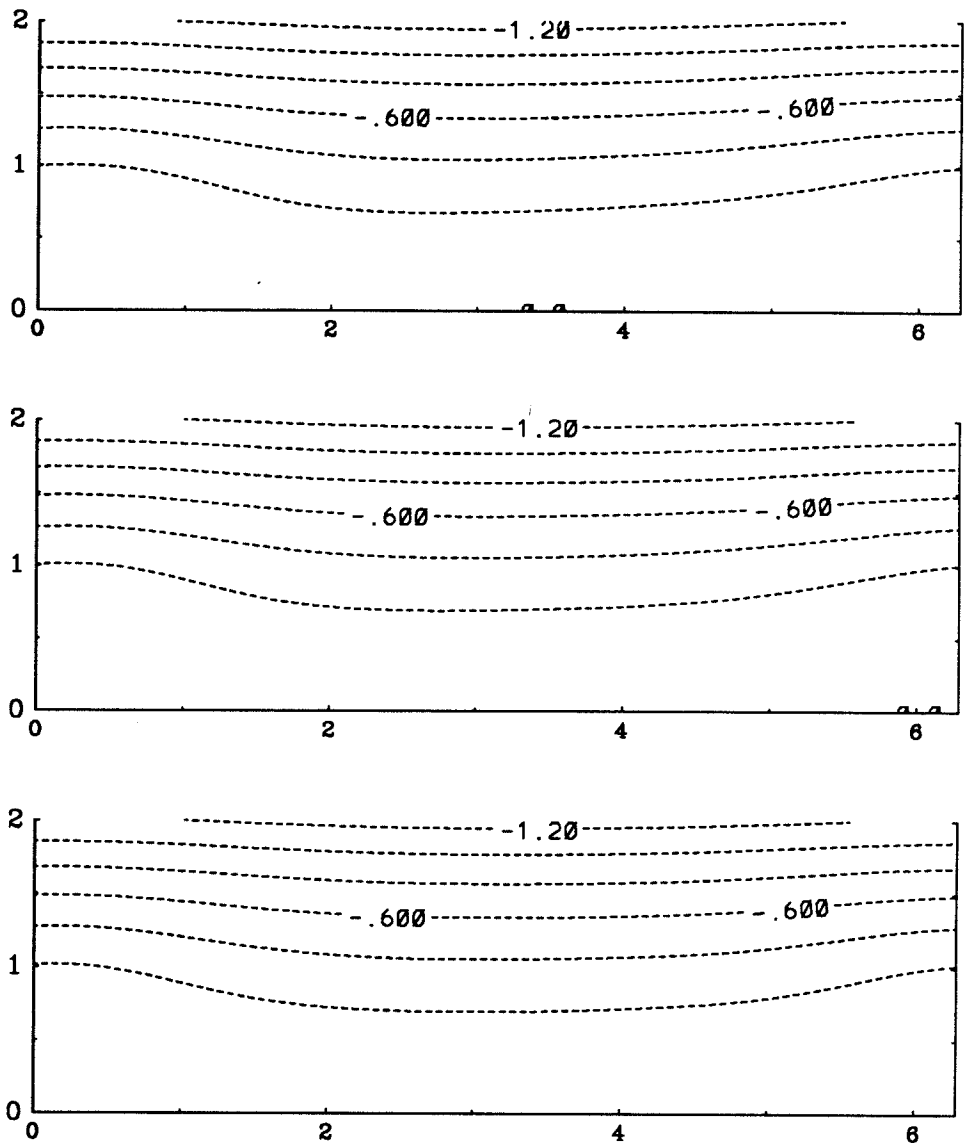

Fig. 4.18b Contours of constant ψ for $t = 0.585$, 0.780 and 0.974. Contour interval = 0.2. A dashed line is used for negative values.

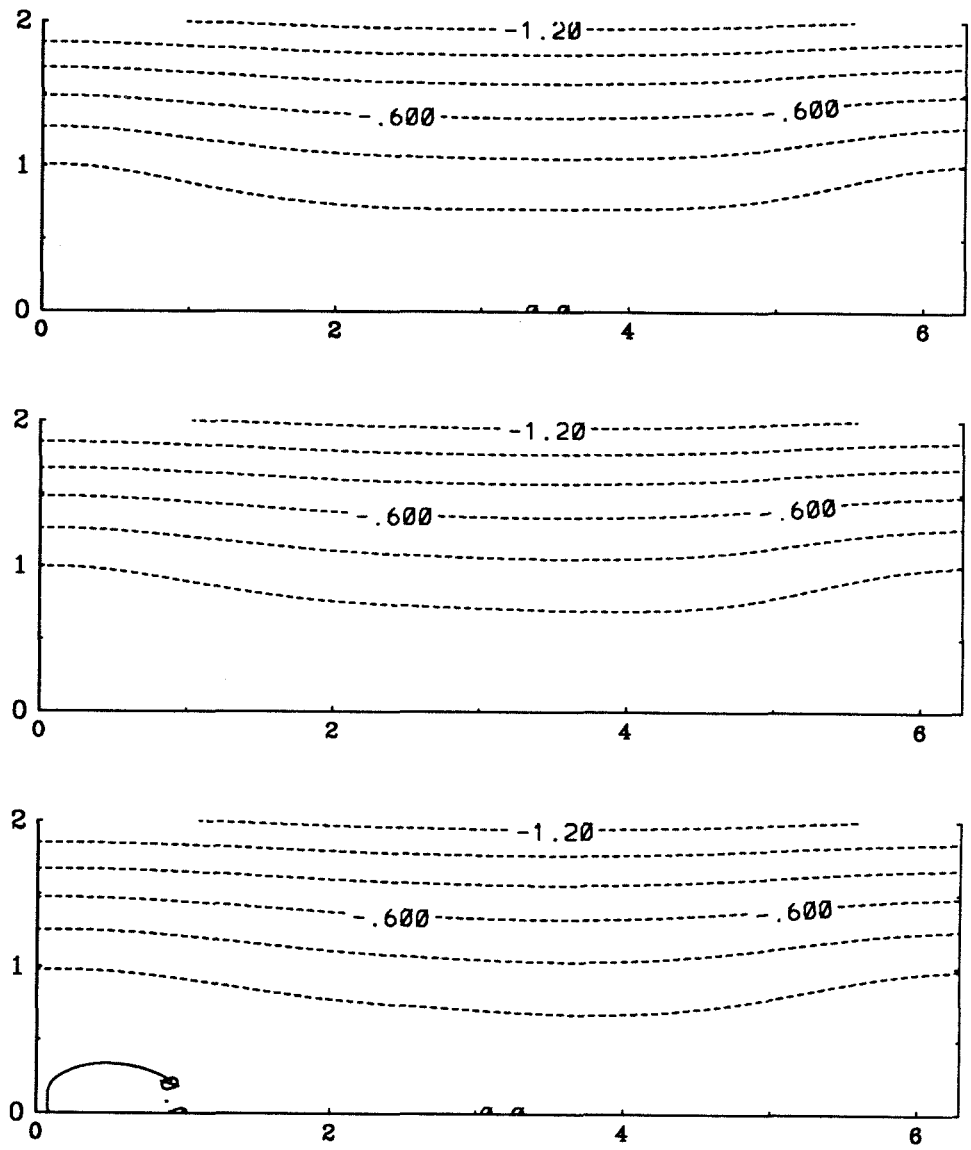

Fig. 4.18c Contours of constant ψ for $t = 1.169$, 1.364 and 1.559. Contour interval = 0.2. A dashed line is used for negative values.

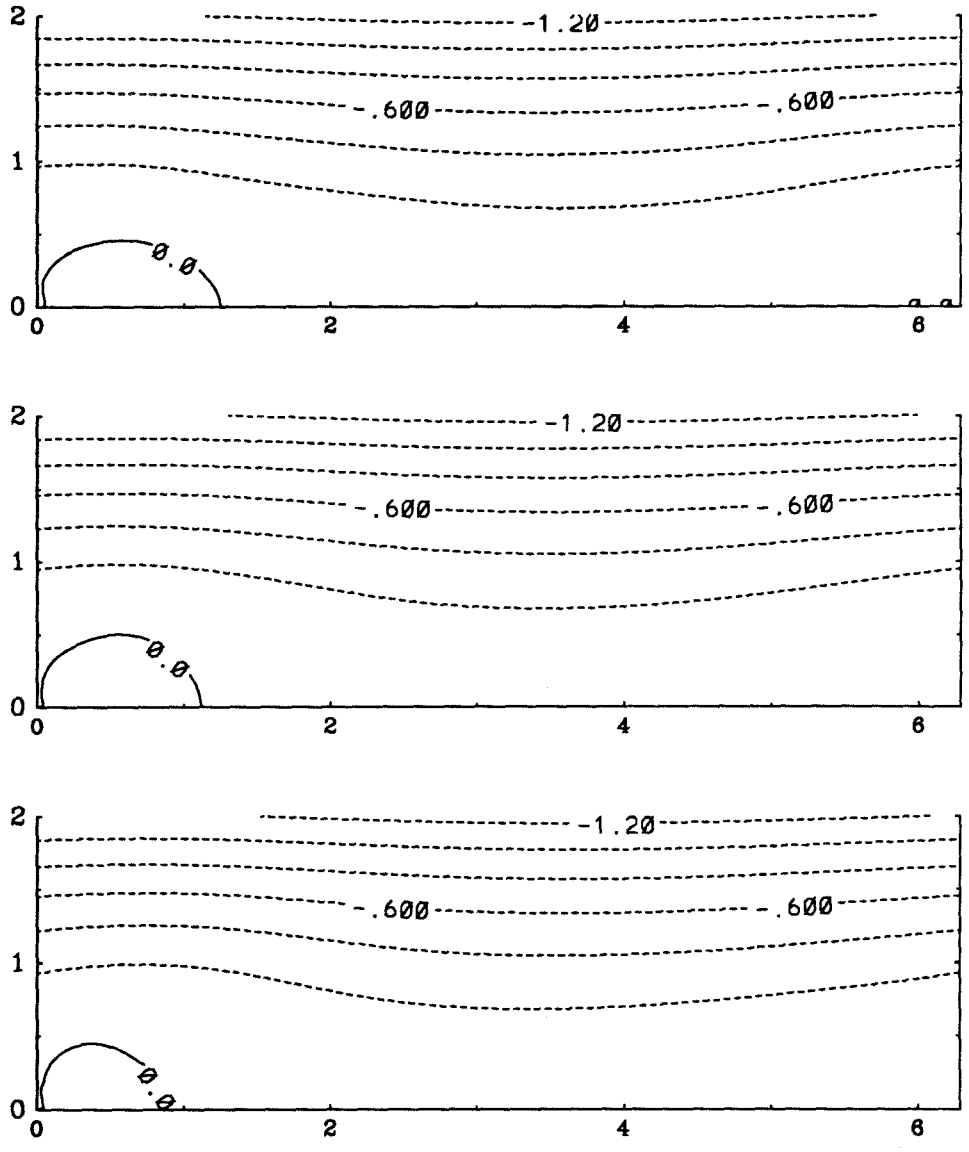

Fig. 4.18d Contours of constant ψ for $t = 1.754$, 1.949 and 2.144. Contour interval = 0.2. A dashed line is used for negative values.

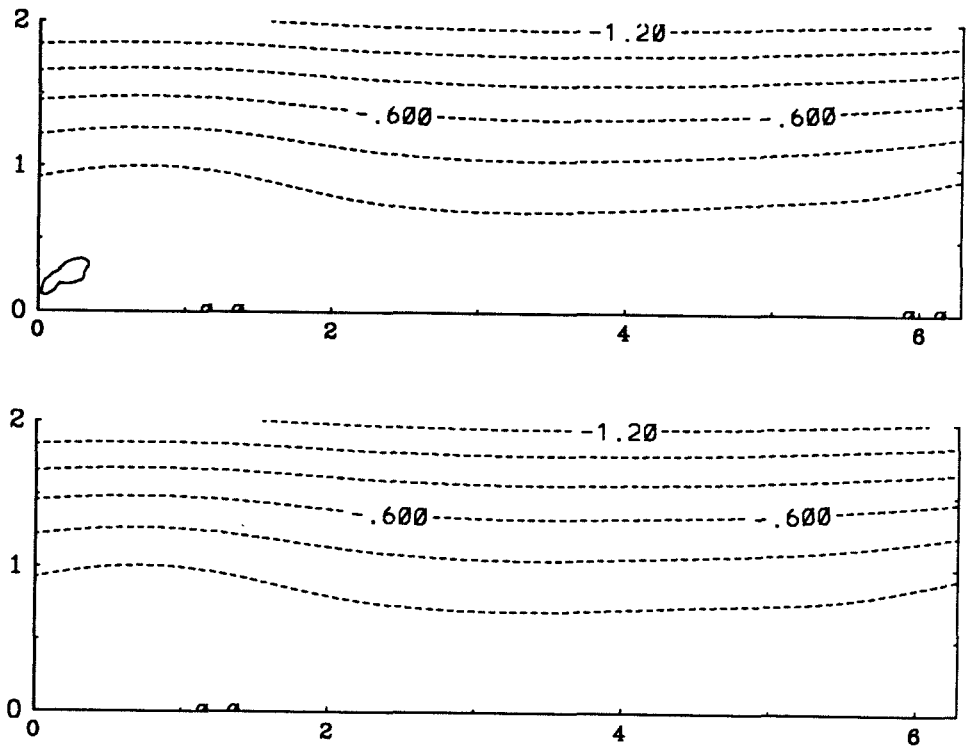

Fig. 4.18e Contours of constant ψ for $t = 2.339$ and 2.436. Contour interval = 0.2. A dashed line is used for negative values.

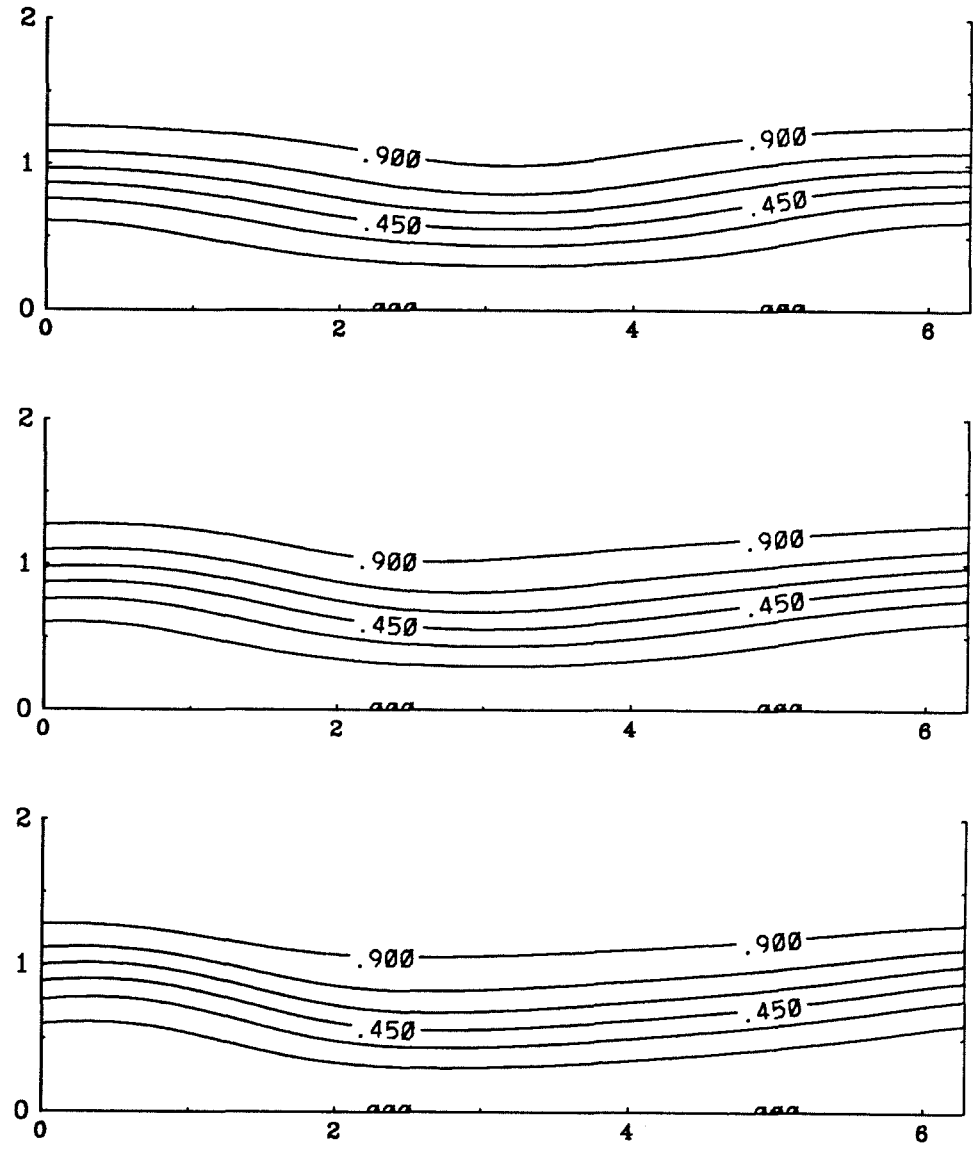

Fig. 4.19a Contours of constant Ω for $t = 0.0$, 0.195 and 0.390. Contour interval = 0.15. A dashed line is used for negative values.

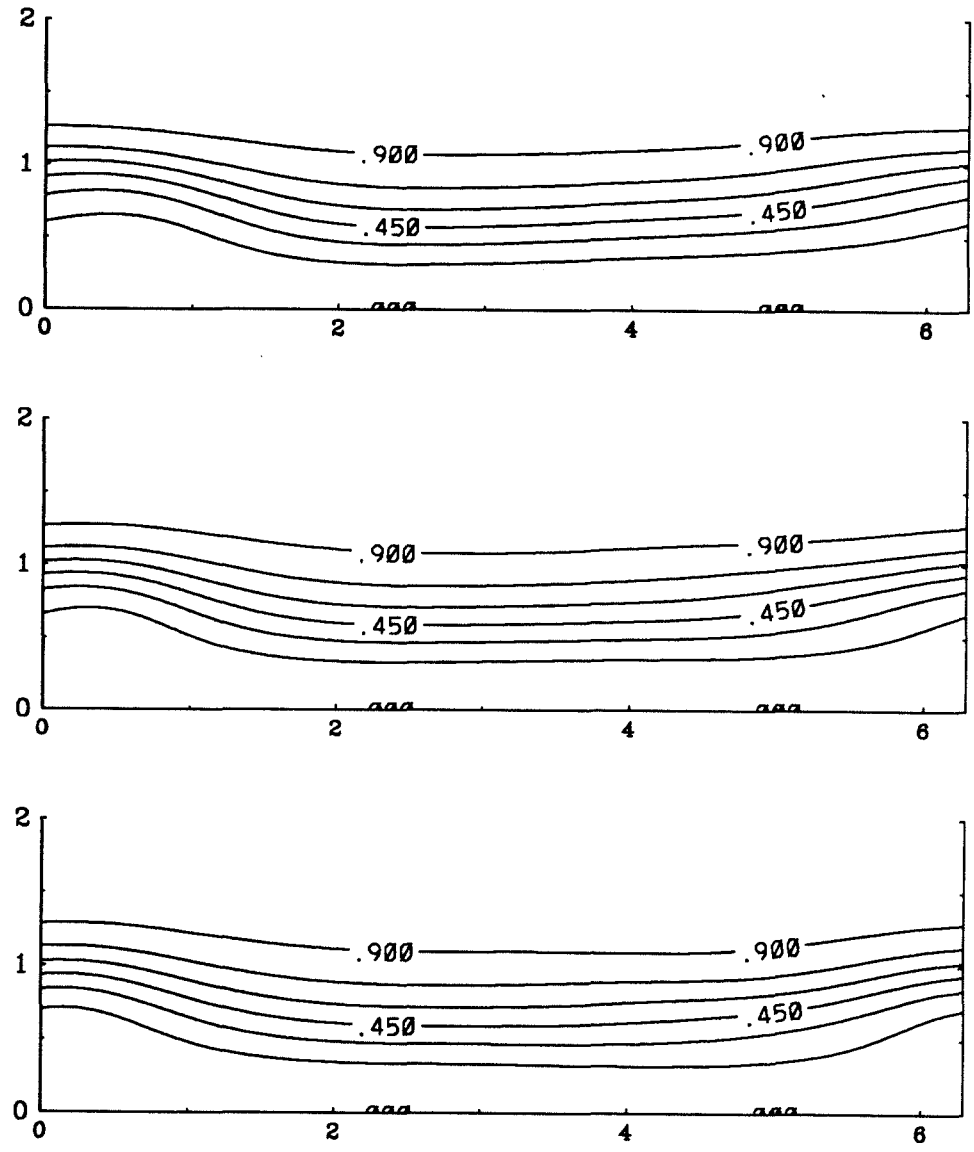

Fig. 4.19b Contours of constant Ω for $t = 0.585$, 0.780 and 0.974. Contour interval = 0.15. A dashed line is used for negative values.

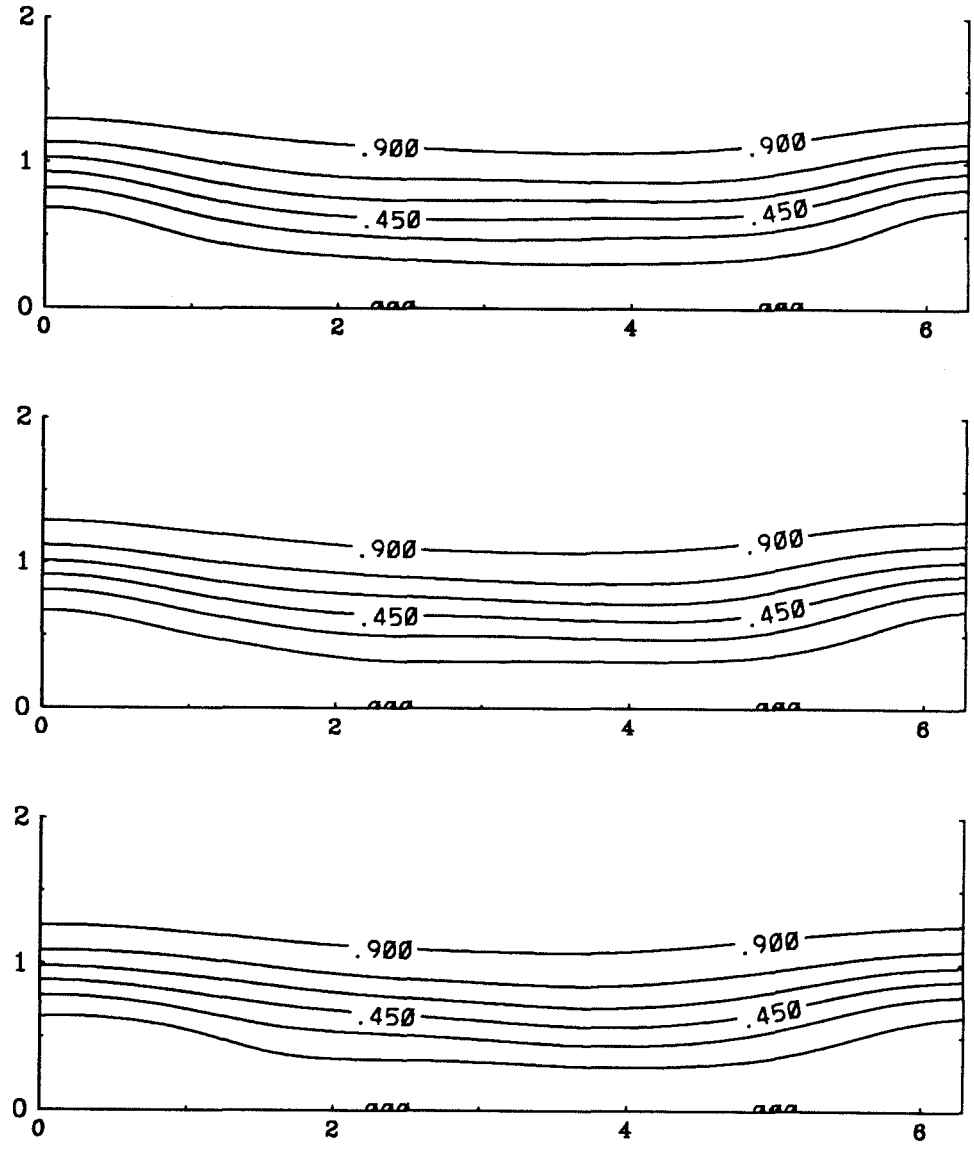

Fig. 4.19c Contours of constant Ω for $t = 1.169$, 1.364 and 1.559. Contour interval = 0.15. A dashed line is used for negative values.

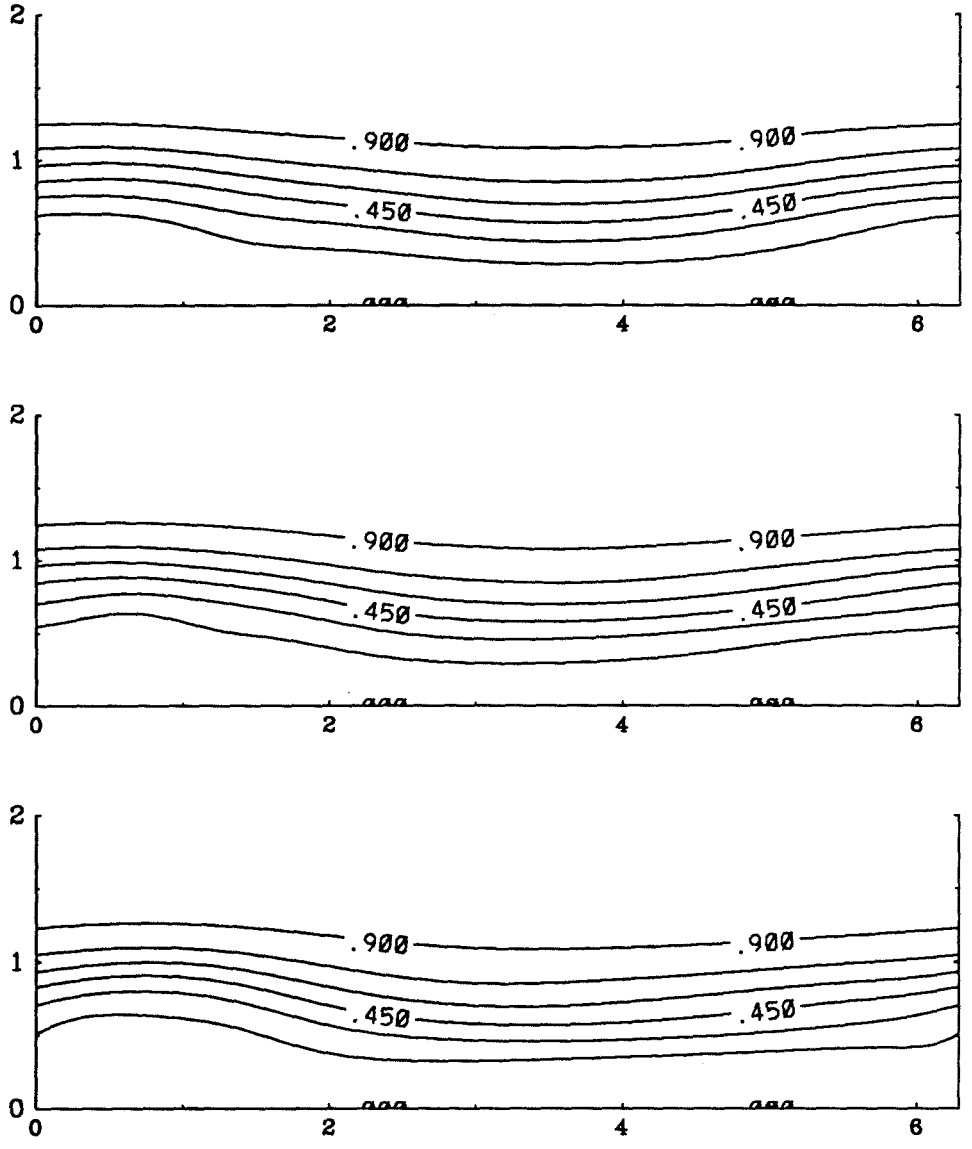

Fig. 4.19d Contours of constant Ω for $t = 1.754$, 1.949 and 2.144. Contour interval = 0.15. A dashed line is used for negative values.

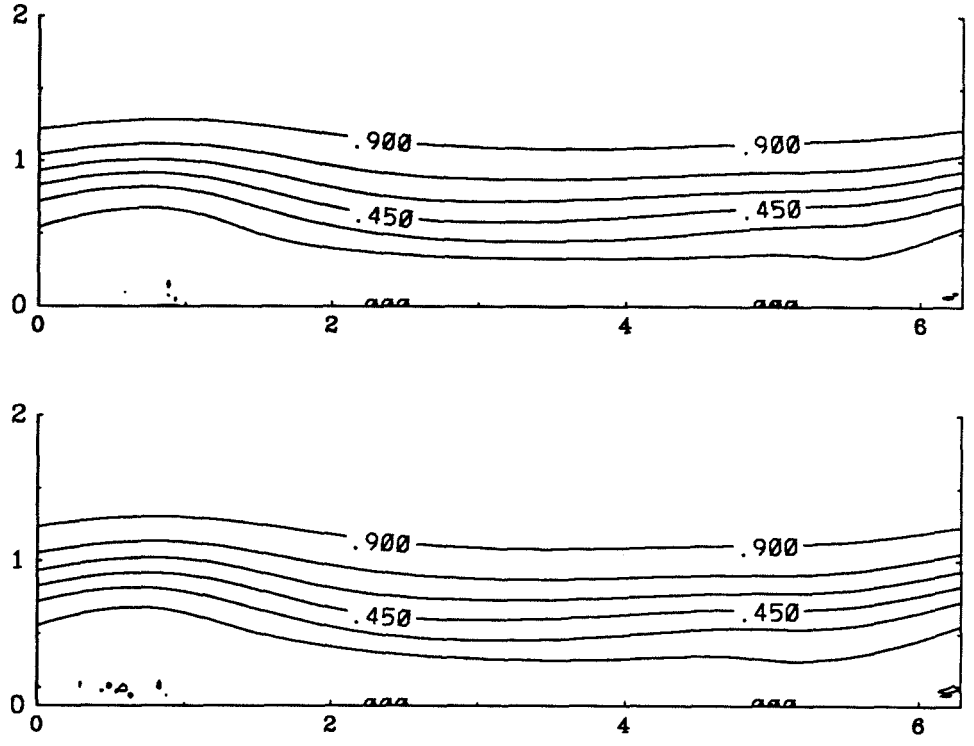

Fig. 4.19e Contours of constant Ω for $t = 2.339$ and 2.436. Contour interval = 0.15. A dashed line is used for negative values.

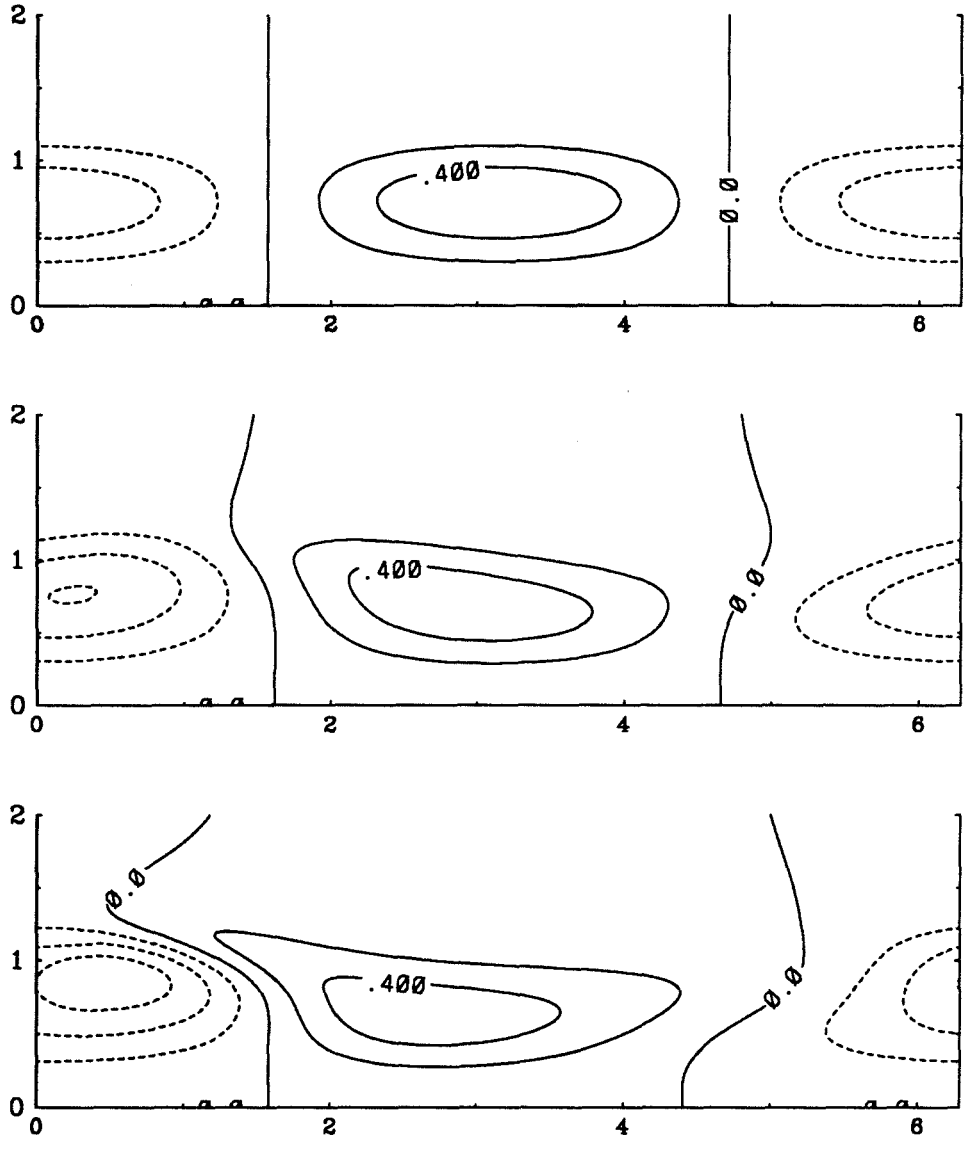

Fig. 4.20a Contours of constant ζ for $t = 0.0,\ 0.195$ and 0.390. Contour interval $= 0.2$. A dashed line is used for negative values.

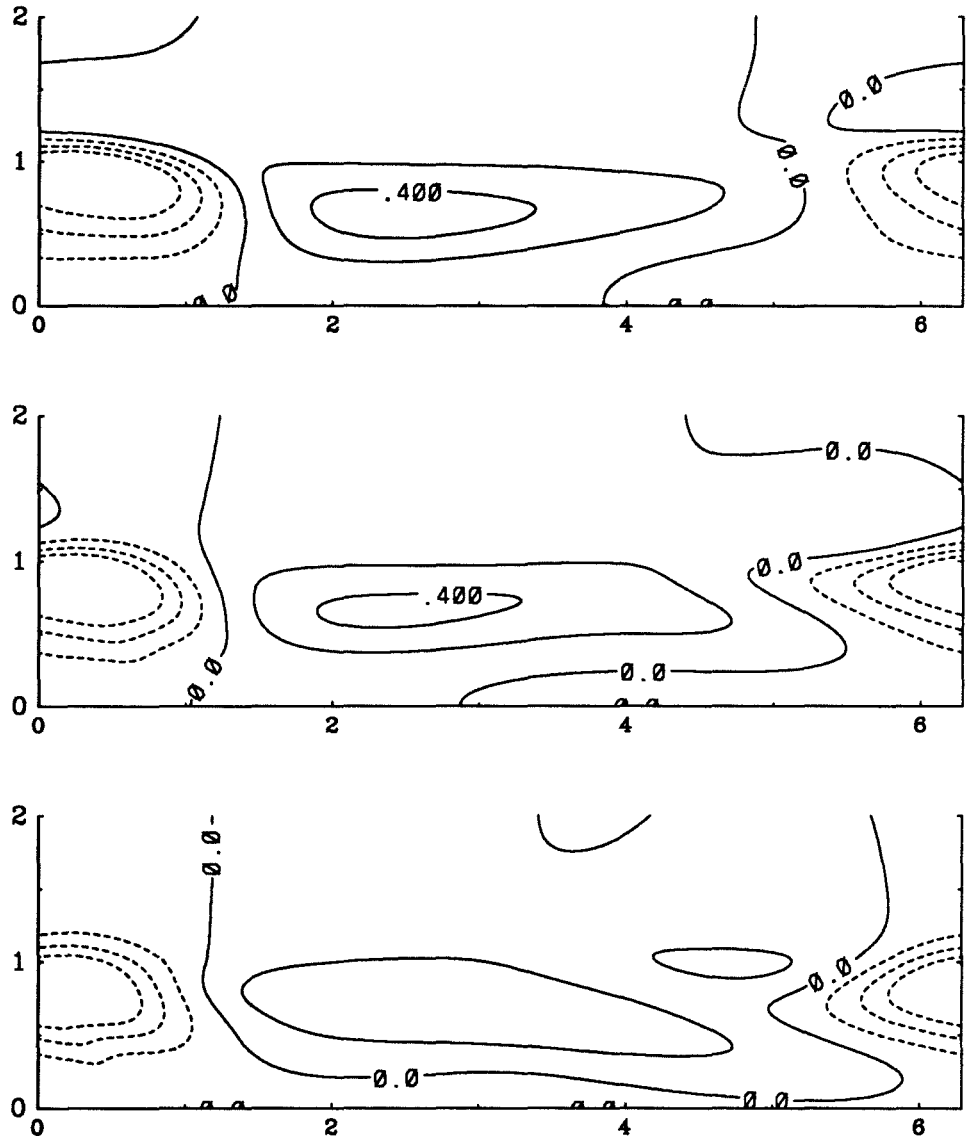

Fig. 4.20b Contours of constant ζ for $t = 0.585$, 0.780 and 0.974. Contour interval = 0.2. A dashed line is used for negative values.

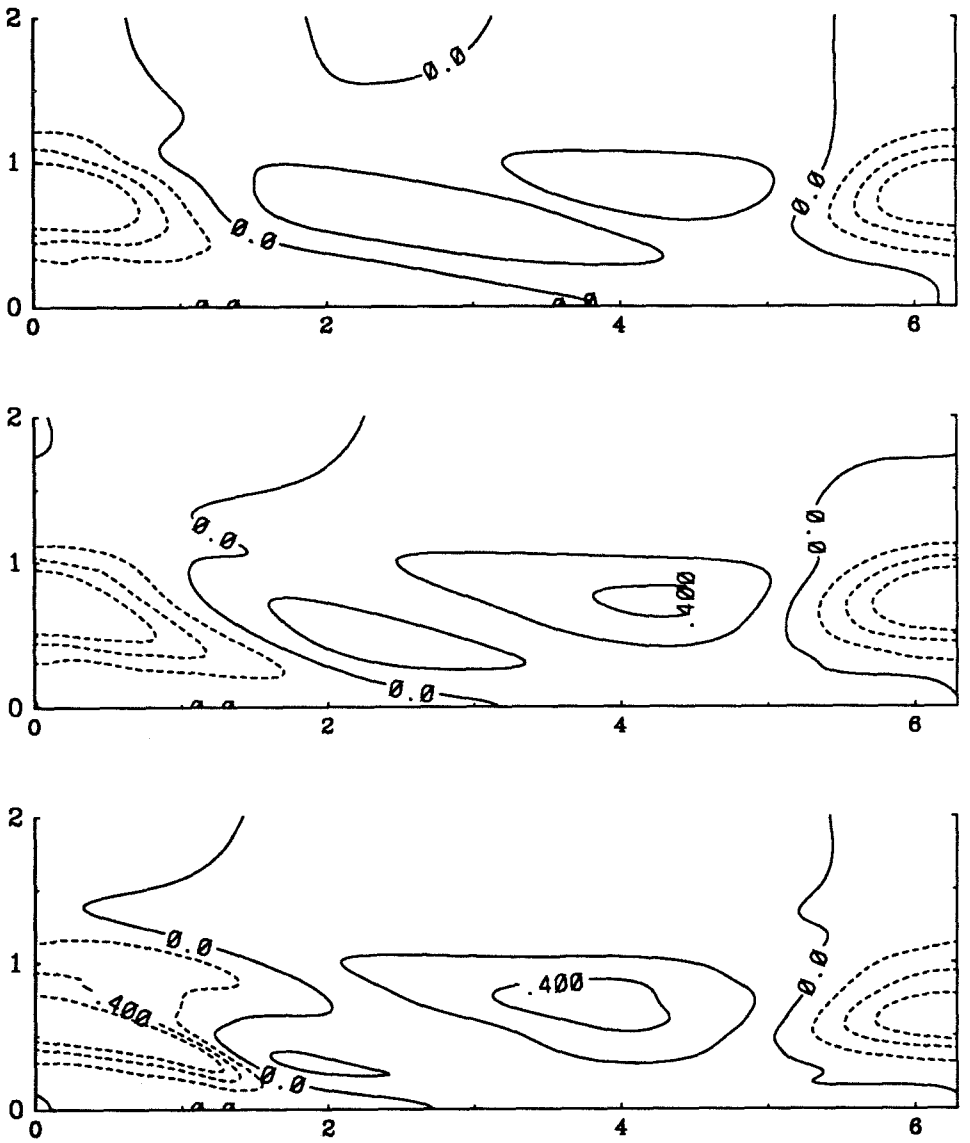

Fig. 4.20c Contours of constant ζ for $t = 1.169$, 1.364 and 1.559. Contour interval = 0.2. A dashed line is used for negative values.

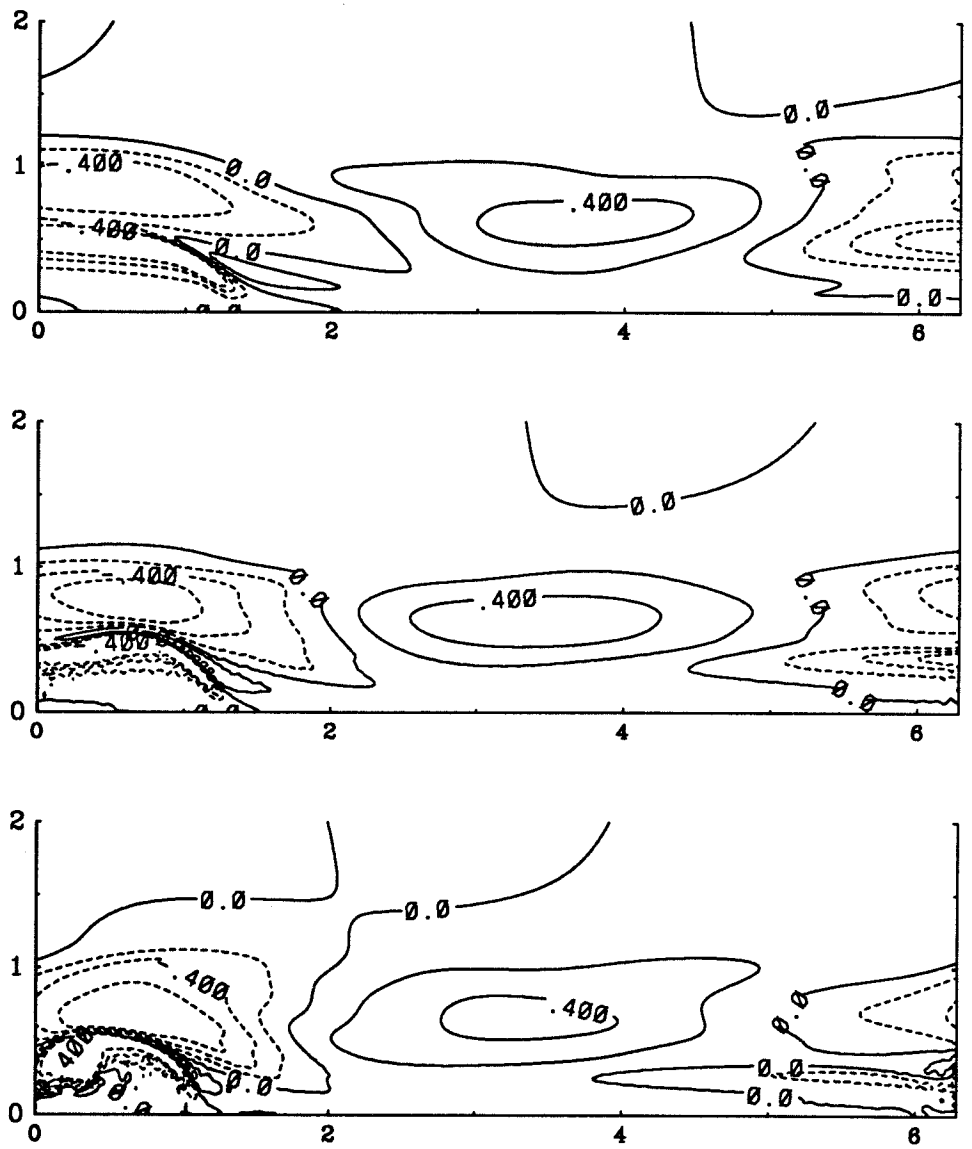

Fig. 4.20d Contours of constant ζ for $t = 1.754$, 1.949 and 2.144. Contour interval = 0.2. A dashed line is used for negative values.

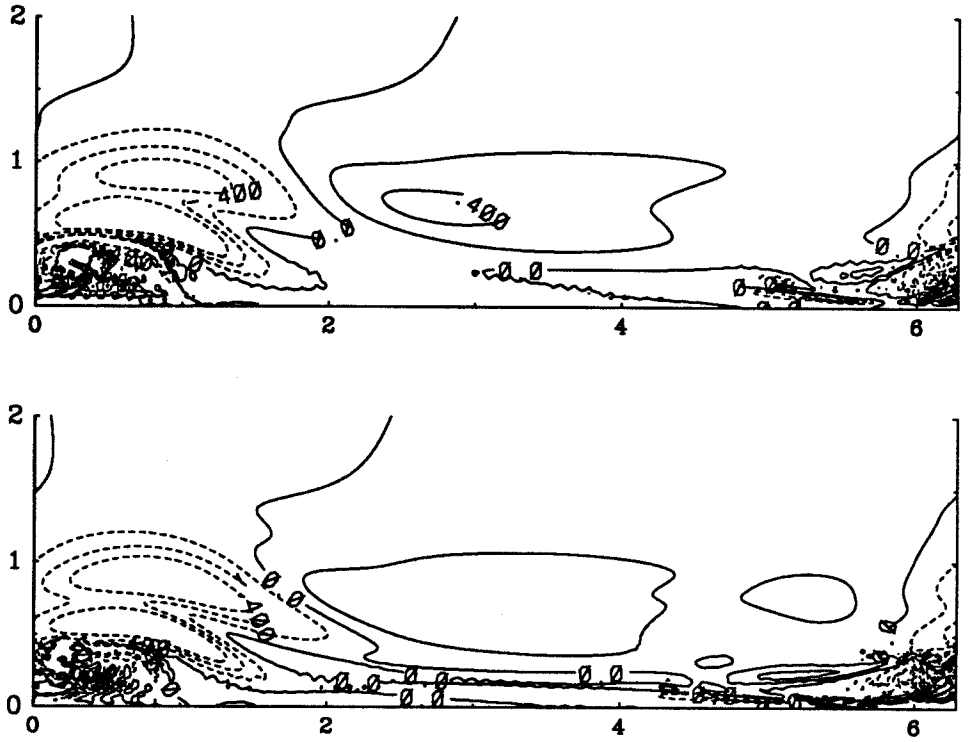

Fig. 4.20e Contours of constant ζ for $t = 2.339$ and 2.436. Contour interval = 0.2. A dashed line is used for negative values.

In Figures 4.21 through 4.30 the numerical results for a run with $\varepsilon = 0.2$ are presented. The initial profiles of Ω_0, ψ_1, Ω_1 and ζ_1 are shown in Figure 4.21. The radial domain was taken to be $R = 5$ with a resolution of $J = 160$ radial points. A modal resolution of $m = 128$ was used for the N-S case and a resolution of $m = 256$ was used for the MS case. Thus, this run is done at an improved axial resolution while the radial resolution is decreased compared to the previous run. A comparison of two runs for the previous case of $\varepsilon = 0.12$ with radial resolutions of $J = 160$ and $J = 320$ showed negligible difference in the solution. Thus, $J = 160$ appears to be sufficient. However, a jump in the core area may possibly form. A larger modal resolution is necessary. The viscosity coefficients were taken to be $\mu_1 = \mu_2 = 10^{-4}$. Therefore, the Reynolds number for the flow is the same as that of the previous runs - $Re = \Gamma/\mu = 62830$.

Because the perturbation parameter is greater in the present run compared to the previous run, we will refer to the present run as the "strong" case and the previous run as the "weak" case. The development of the shape of the vortex core is shown in Figure 4.22 for the MS case. As in the previous case, a gradual steepening of the core wave occurs as time passes. At about $t = 0.87$, a jump in the core area forms. In Figure 4.23 the maximum value of the $|\,\partial a(x,t)/\partial x\,|$, is plotted as a function of time. The monotonic increase of slope up to $t = 0.9$ is seen. This is qualitatively similar to the development of a shock in the previous cases. Soon after the shock forms, numerical errors tend to increase. The slope does not increase without bound because of restricted resolution. The development of the axial velocity is shown in Figure 4.24. The initial wave marked with A at $t = 0$ continues to steepen as time increases.

The development of the core shape for the N-S case is shown in Figure 4.25. The core bulges considerably with passage of time. The fattened core near $x = 0$ accommodates a bubble of reversed flow as can be seen from the contours of constant ψ in Figure 4.28. A jump in the core area forms around $t = 0.68$ behind the bubble

unlike the MS case in which the jump forms on the front side of the location where the bubble would be present. Also the jump is opposite in sense compared to the MS case. Unlike the previous cases, the maximum slope increases monotonically with time similar to the MS case. The slope reaches a maximum at about $t = 0.8$ for the N-S case and then it begins to decrease. The decrease is due to the action of viscosity. The average axial velocity is shown in Figure 4.27. The axial velocity steepens in the opposite sense and the steepening occurs between $x = 3$ and $x = 5$. The shock in the MS case, in contrast, occurs due to steepening of the axial velocity in the region $0 \leq x \leq 3$.

The contours of constant ψ are presented in Figure 4.28. As the Figure for $t = 0$ indicates, the perturbation is so strong that there is a bubble of reversed flow located symmetrically about $x = 0$. As time passes, the bubble moves to the right along the axis. The bubble deforms so that its axial extent decreases while the radial extent remains relatively unchanged. The bubble detaches from the axis at about $t = 0.78$ and moves off the axis as it collapses. A second bubble of reversed flow is seen to emerge between $t = 0.98$ and $t = 1.1$. It is seen to grow rapidly and occupies nearly half the axial domain by about $t = 1.27$. Since the ζ field does not seem to be well resolved during the emergence and growth of this second bubble of reversed flow region, this feature may be spurious. However, this feature was seen for various combinations of modal and radial resolutions.

The contours of constant Ω are shown in Figure 4.29. The Ω field also contains a bubble of reversed circulation region at the initial time. This bubble undergoes remarkable deformation as time passes. While the "leading" edge of the bubble (the edge to the right) remains bound to nearly the same axial location, the "trailing" edge (the edge to the left of the bubble) stretches enormously until it occupies nearly 80% of the axial domain.

The contours of constant ζ are shown in Figure 4.30. Similar to the weakly perturbed vortex, a concentration of contours near $x = 0$ is seen here also. The

contours indicate that the solution is not smooth beyond $t = 1.0$.

In summary, we have seen that a weakly perturbed vortex fails to develop any jump in the core area for the N-S case. The core wave periodically steepens and flattens for the N-S case while the MS case shows monotonic increase in the magnitude of the slope of the core radius. Therefore, there is a qualitative disagreement between the solutions of MS and N-S.

On the other hand, a strongly perturbed vortex develops a jump in the core area in both N-S and the MS solutions. Even though the sense of jump in the core area disagree, a similarity is seen in the way the core steepens. The time taken for a shock formation is about 0.87 for the MS case while it is about 0.68 for the N-S case. It is clear from the solutions for the strongly perturbed vortex that the circulation field plays an important role in the dynamics. However, it is not clear if this is responsible for the development of jump in the core area. An improved model in which further corrections due to changes in the internal structure may shed some light on this issue.

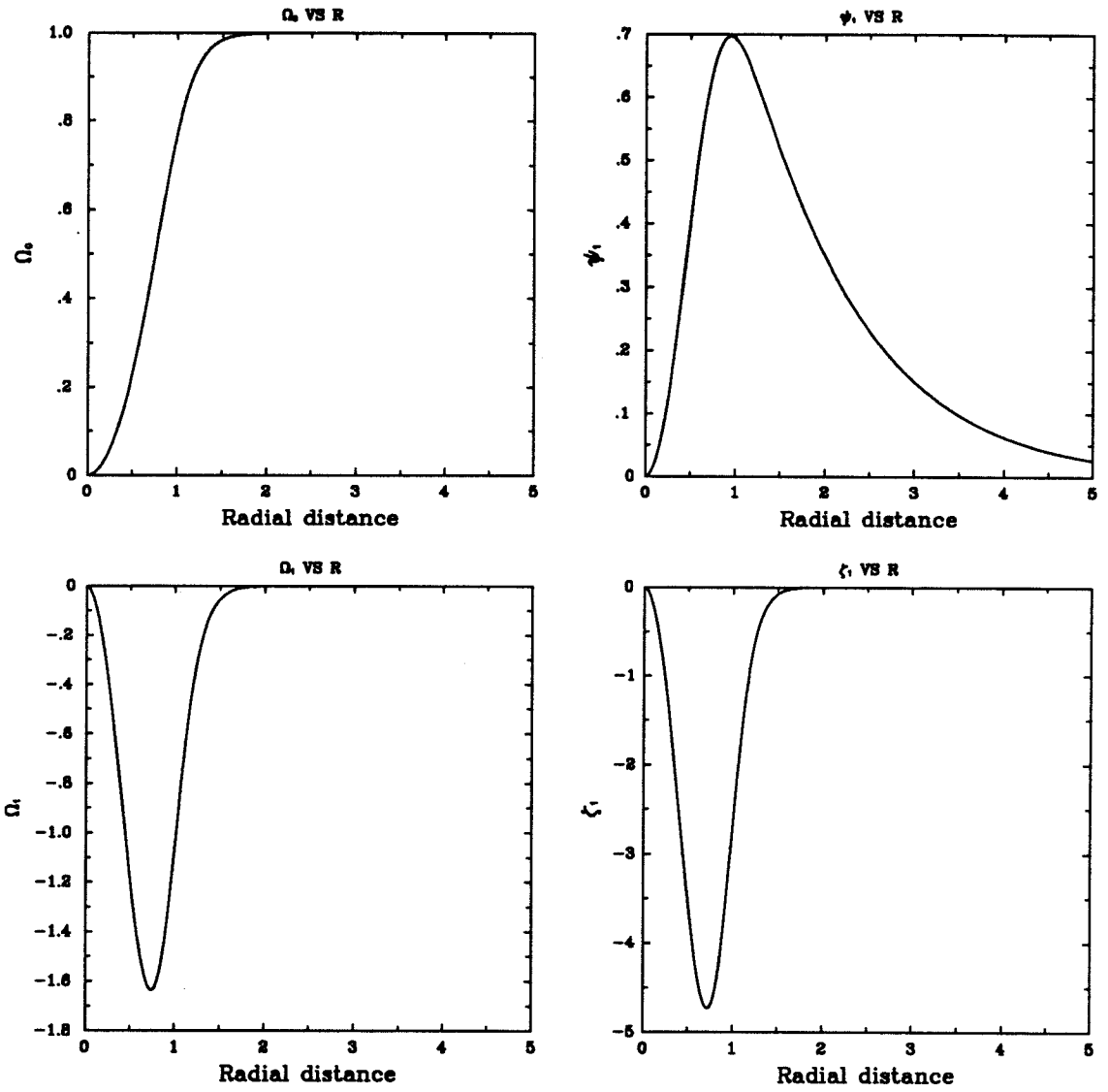

Fig. 4.21 The profiles of the circulation for the base flow Ω_0 and the perturbation components ψ_1, Ω_1 and ζ_1. Radial resolution of $J = 160$ with $R = 5$ is used. The size of the core radius is $a = 1$.

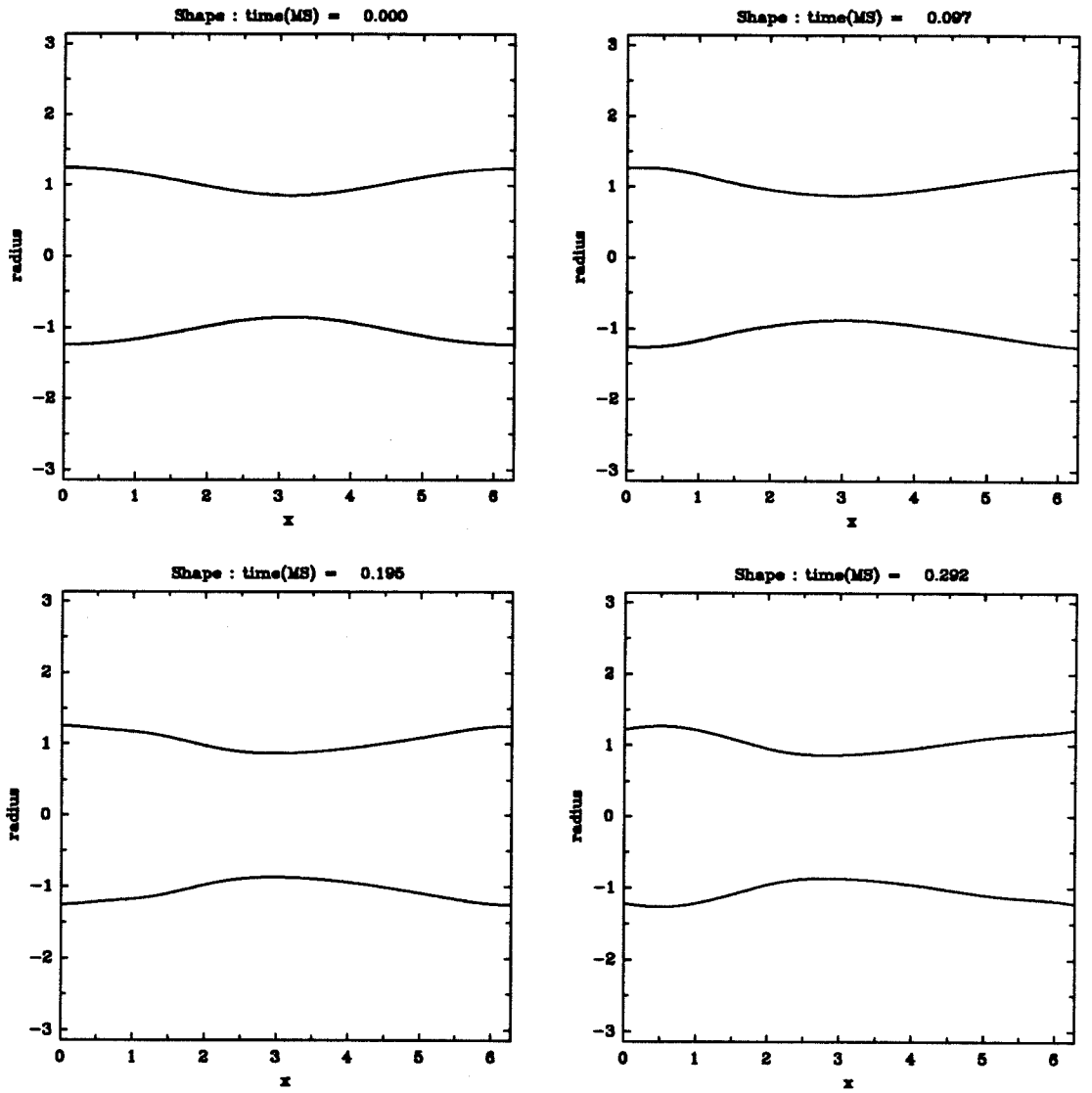

Fig. 4.22a The shape of the vortex as a function of time for the MS problem. The times are indicated on each plot.

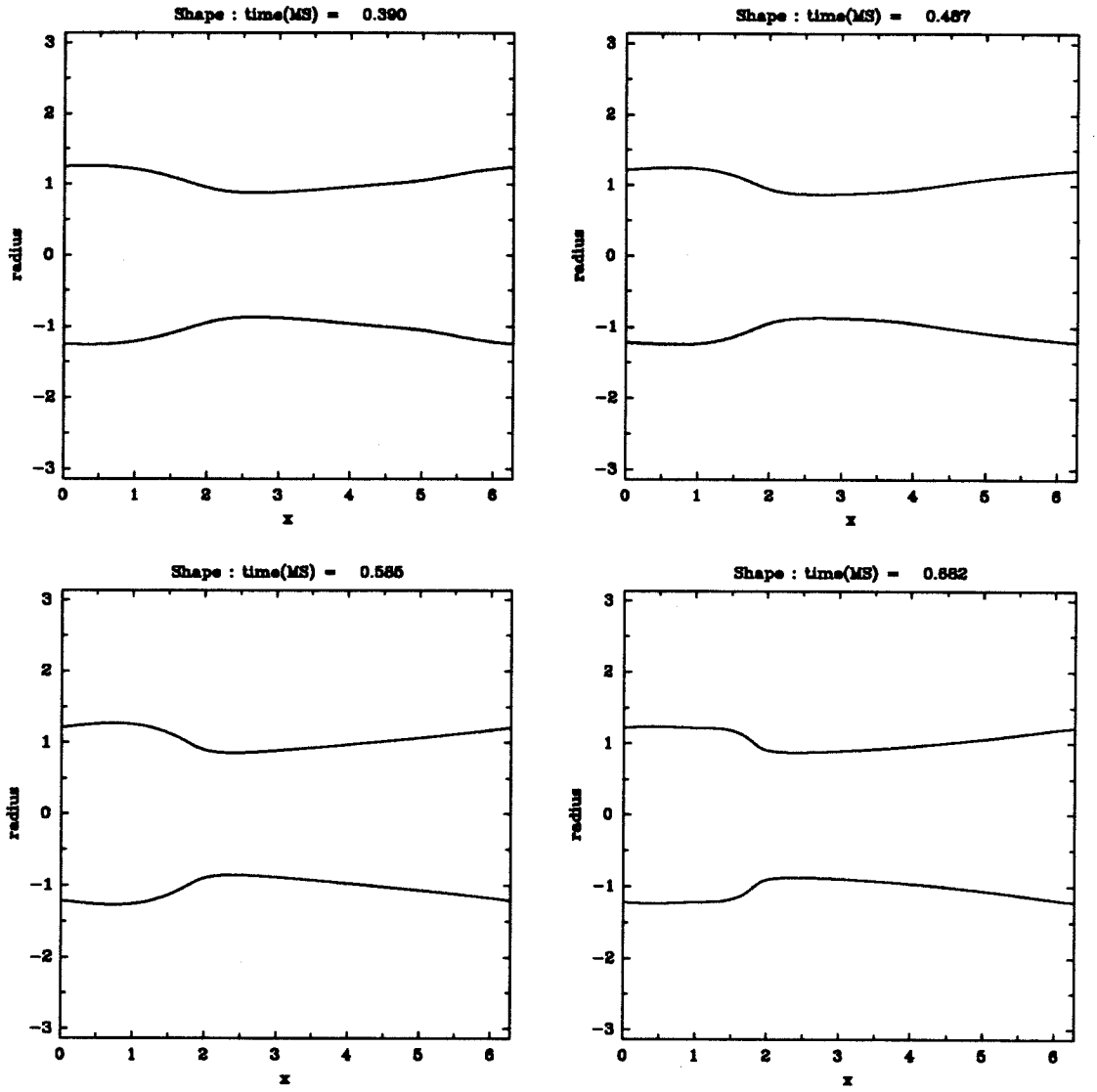

Fig. 4.22b The shape of the vortex as a function of time for the MS problem. The times are indicated on each plot.

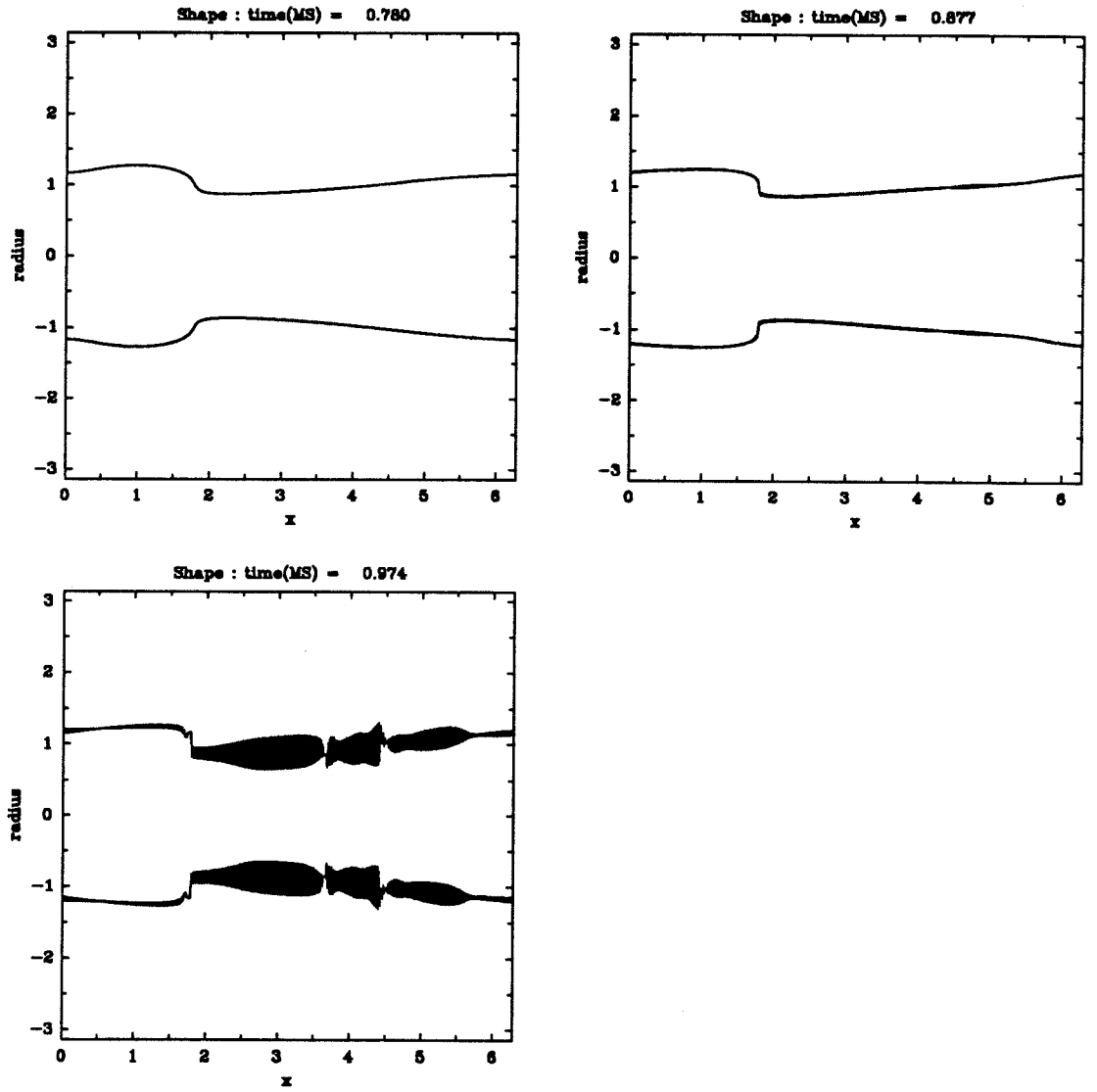

Fig. 4.22c The shape of the vortex as a function of time for the MS problem. The times are indicated on each plot.

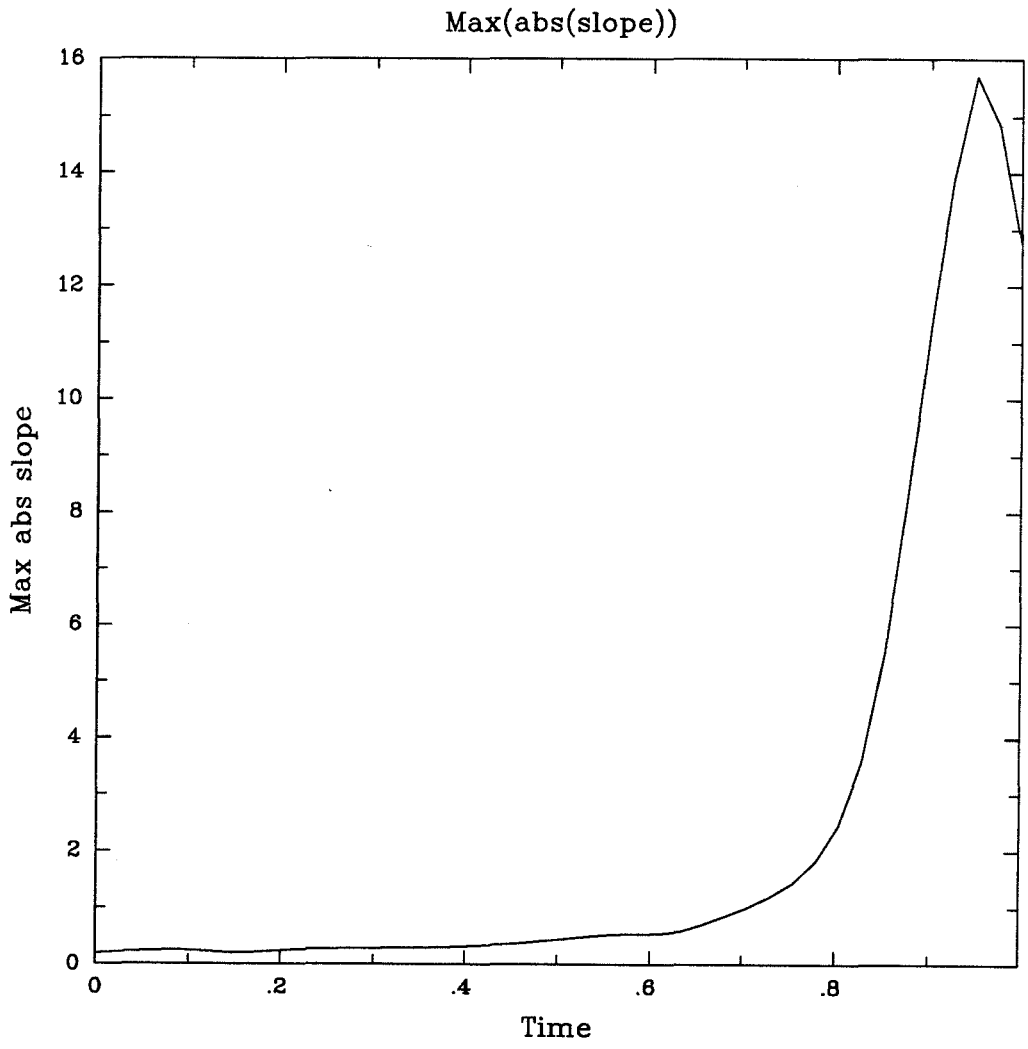

Fig. 4.23 Variation of maximum value of $|\,\partial a(x,t)/\partial x\,|$ as a function of time for the MS problem.

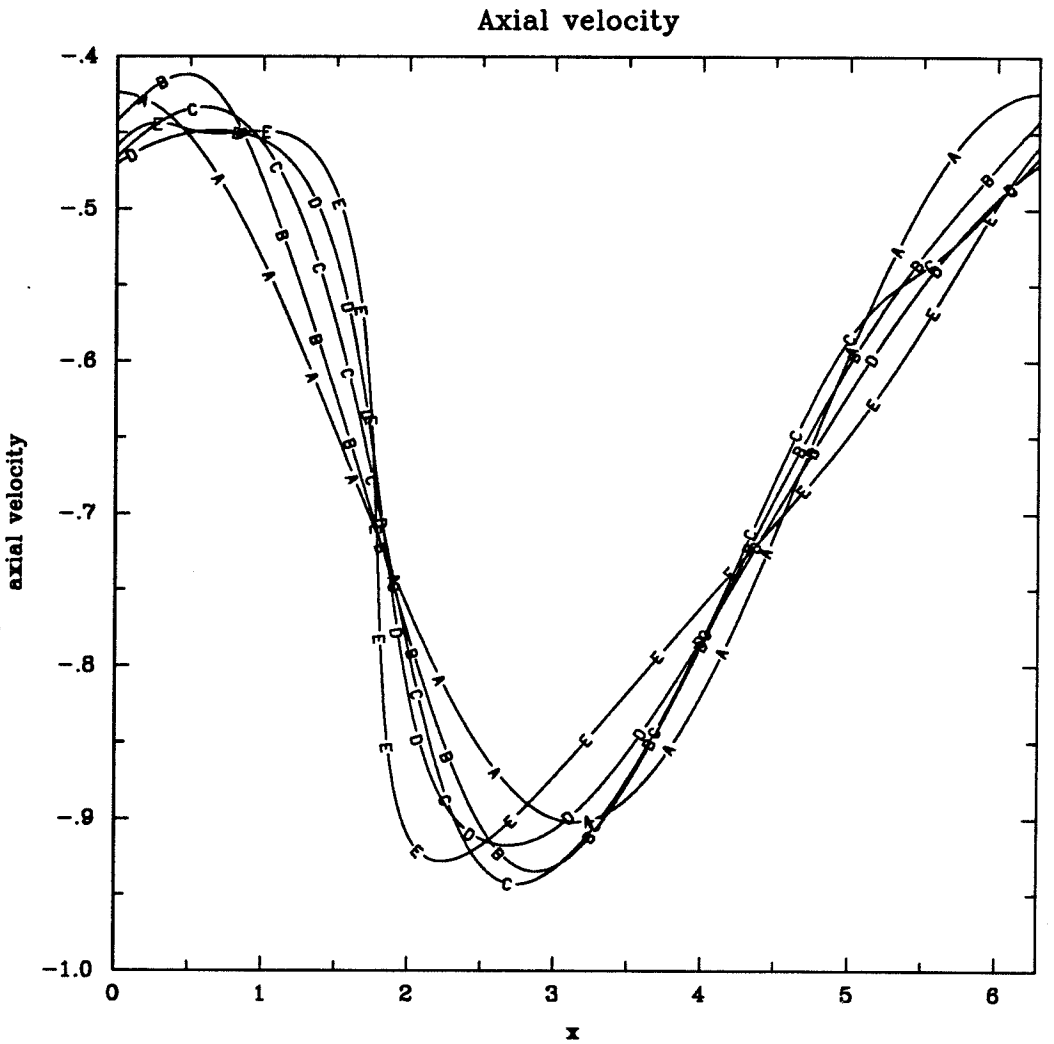

Fig. 4.24 Axial velocity as a function of x is shown for A. $t = 0.0$, B. $t = 0.195$, C. $t = 0.390$, D. $t = 0.585$ and E. $t = 0.780$. This shows the solution of MS equations.

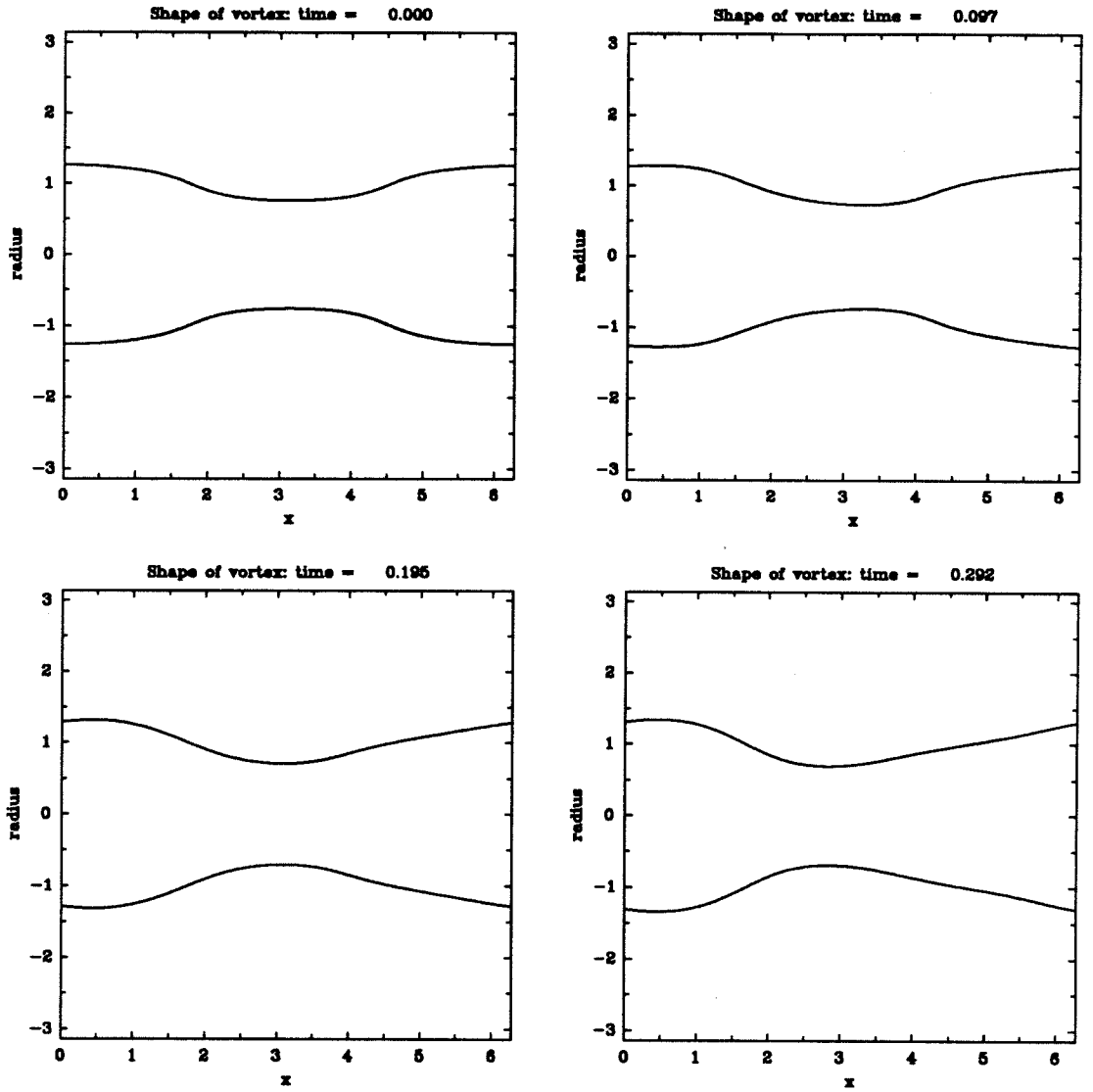

Fig. 4.25a The shape of the vortex as a function of time for the N-S problem. The times are indicated on each plot.

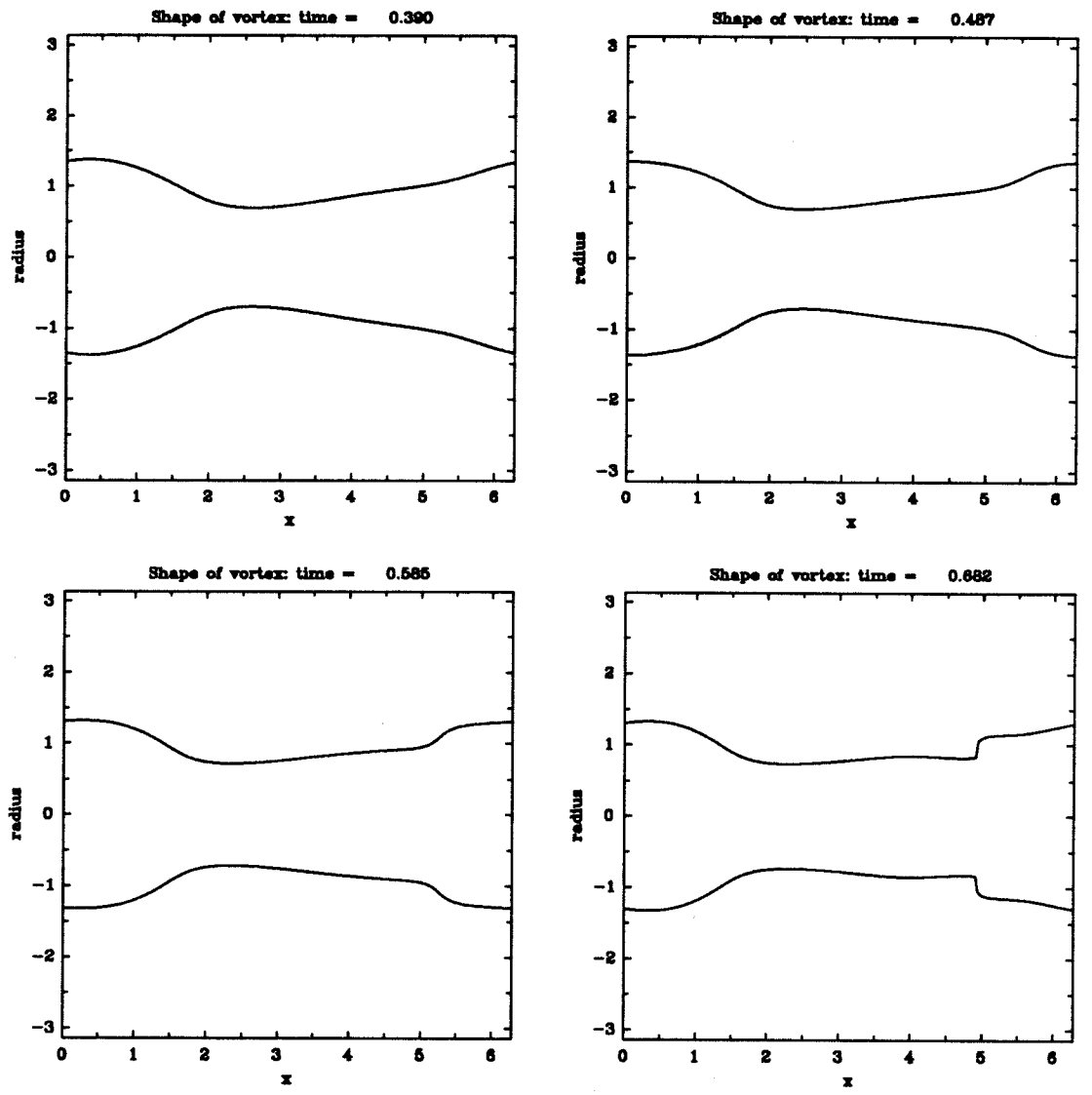

Fig. 4.25b The shape of the vortex as a function of time for the N-S problem. The times are indicated on each plot.

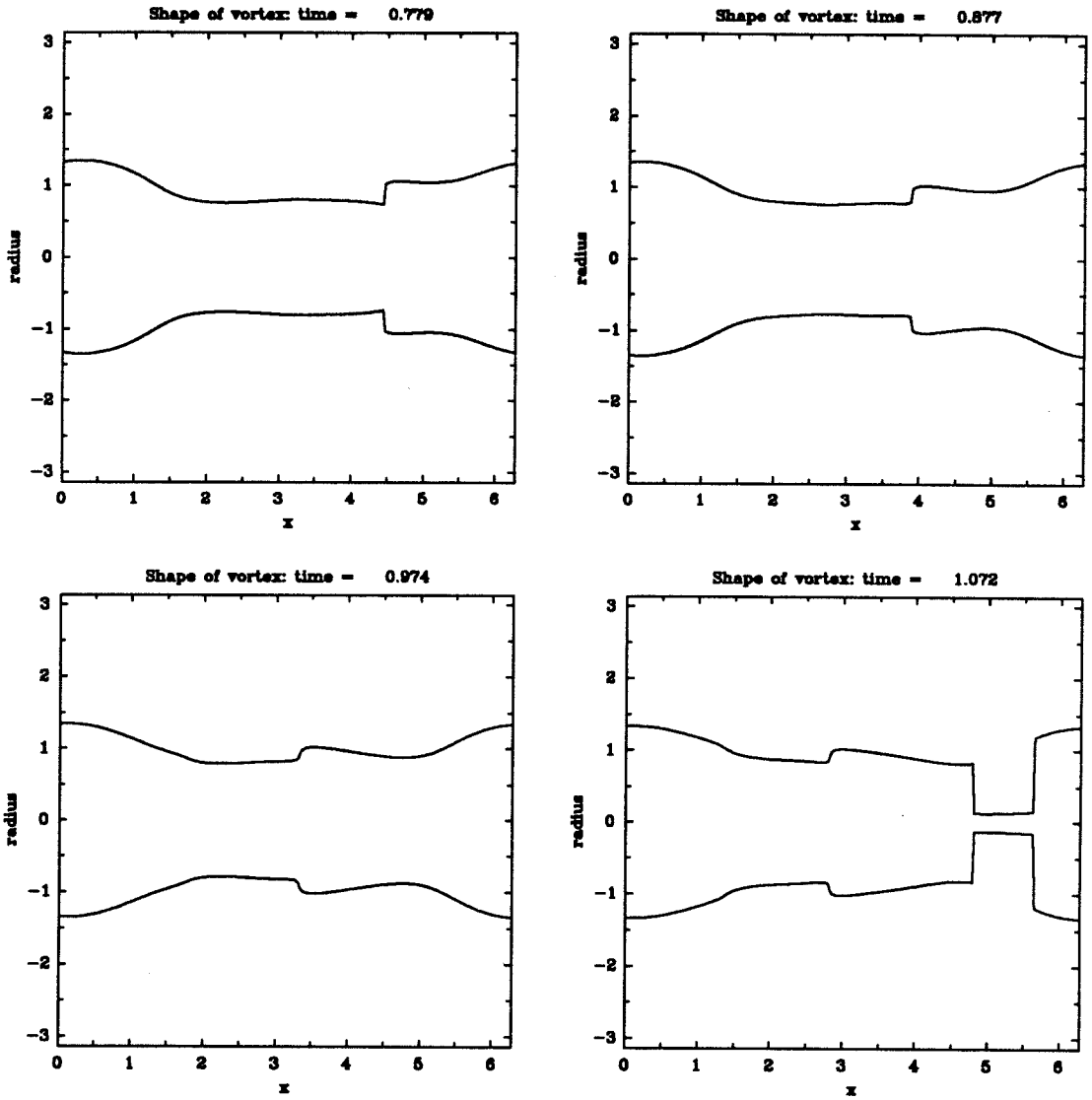

Fig. 4.25c The shape of the vortex as a function of time for the N-S problem. The times are indicated on each plot.

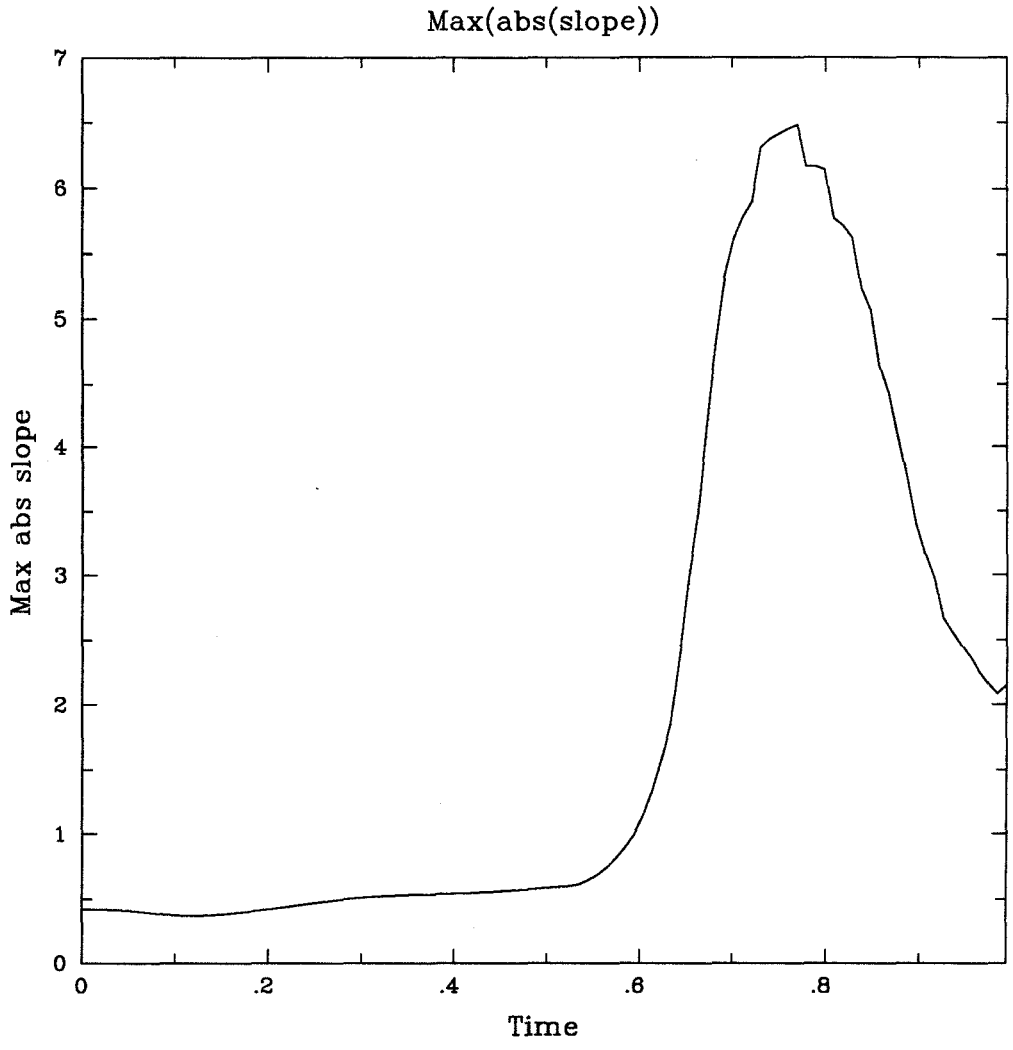

Fig. 4.26 Variation of maximum value of $|\,\partial a(x,t)/\partial x\,|$ as a function of time for the N-S problem.

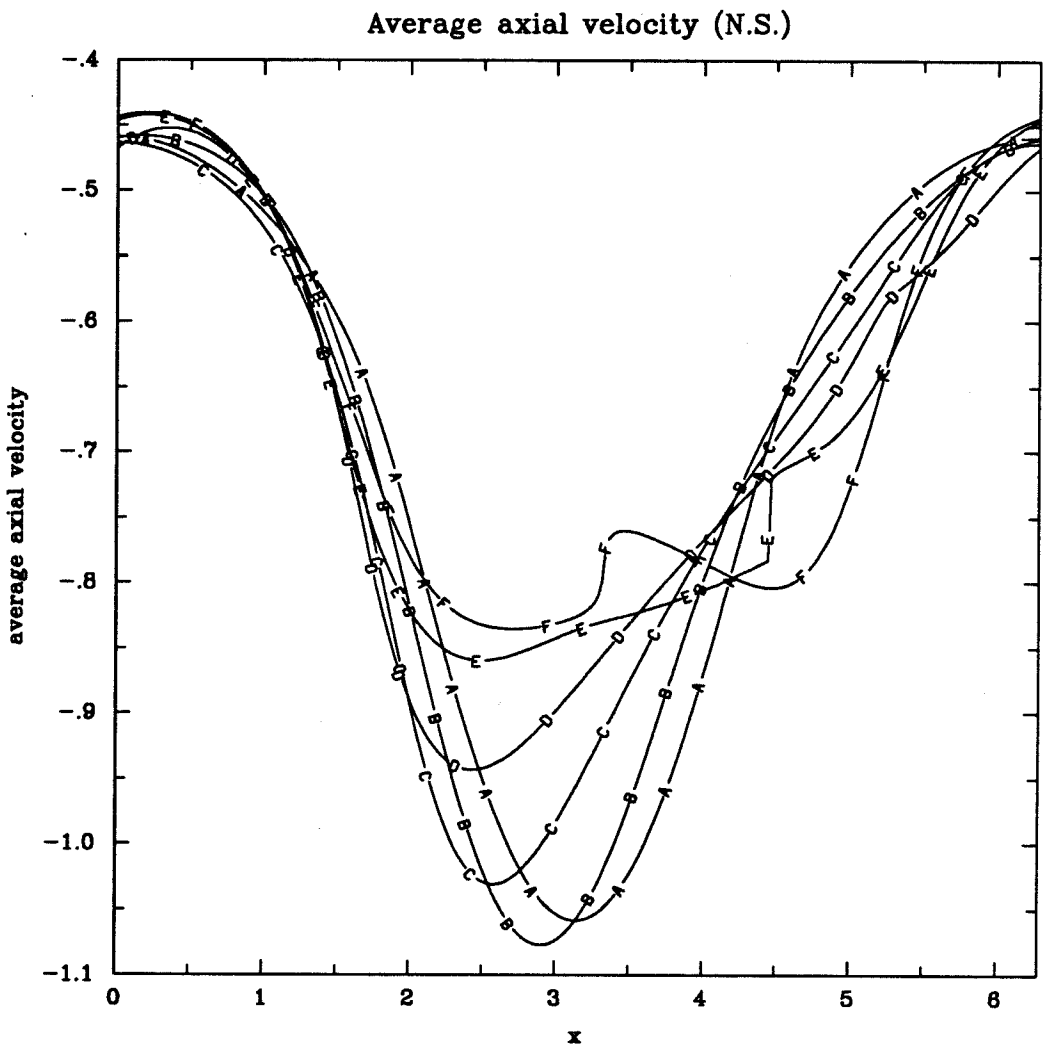

Fig. 4.27 Average axial velocity as a function of x is shown for A. $t = 0.0$, B. $t = 0.195$, C. $t = 0.390$, D. $t = 0.585$, E. $t = 0.779$ and F. $t = 0.974$. This shows the solution of N-S equations.

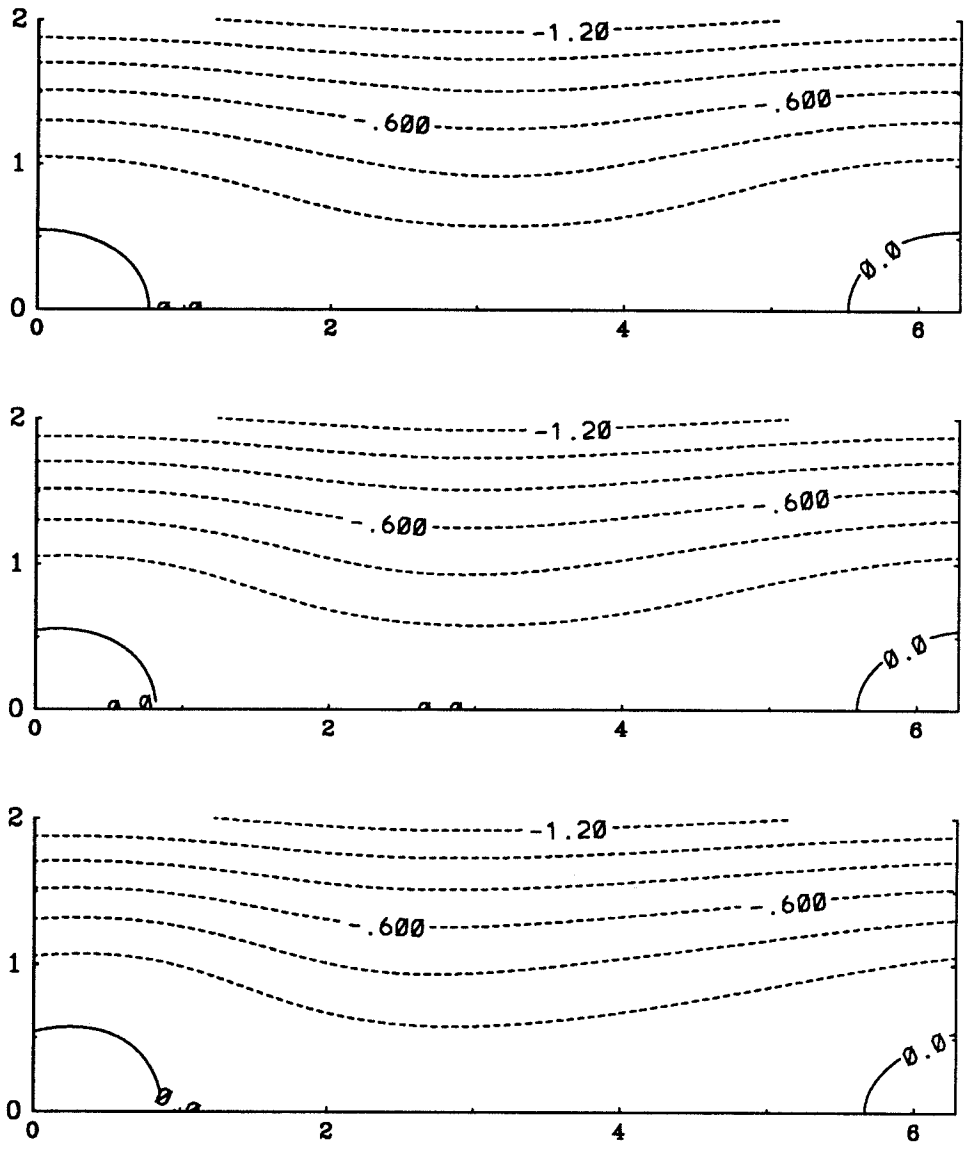

Fig. 4.28a Contours of constant ψ for $t = 0.0,\ 0.097$ and 0.195. Contour interval $= 0.2$. A dashed line is used for negative values.

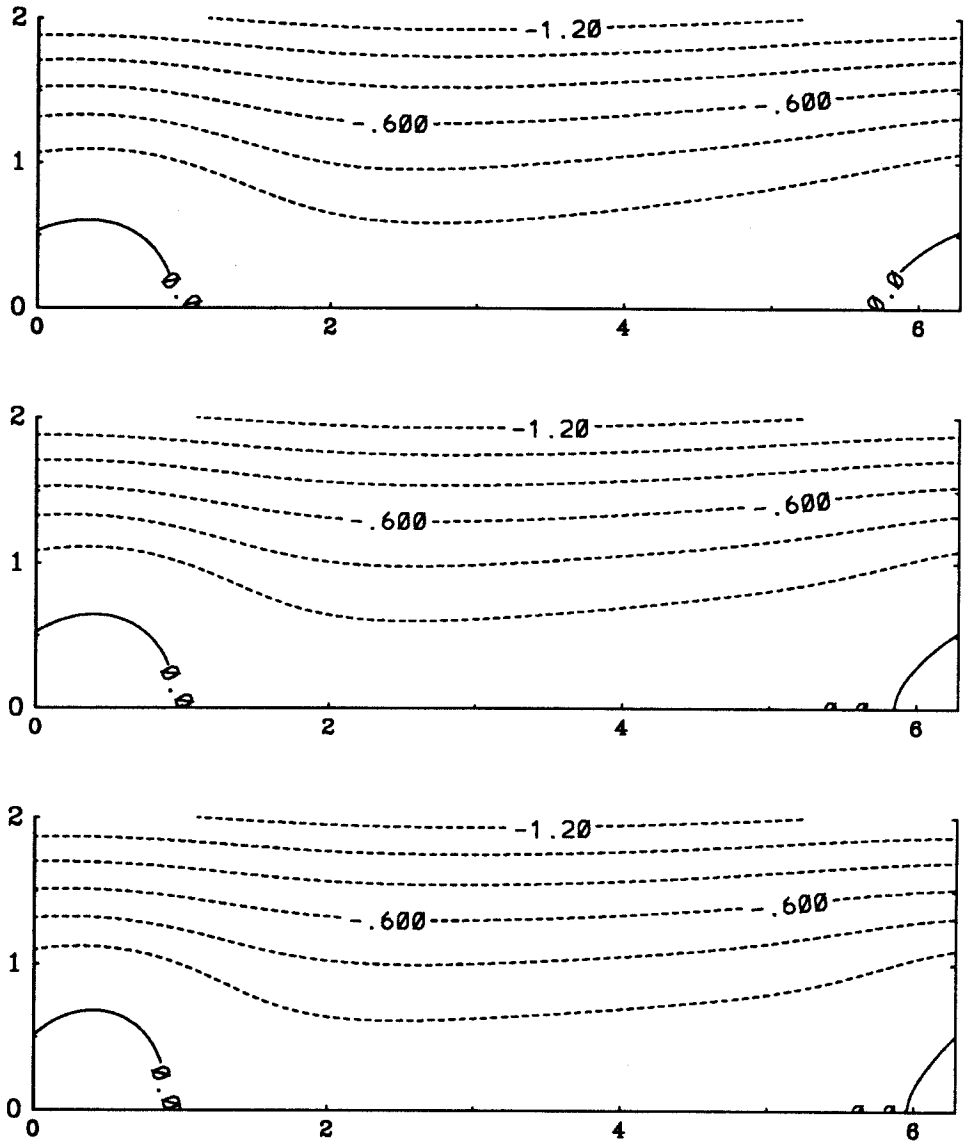

Fig. 4.28b Contours of constant ψ for $t = 0.292$, 0.390 and 0.487. Contour interval = 0.2. A dashed line is used for negative values.

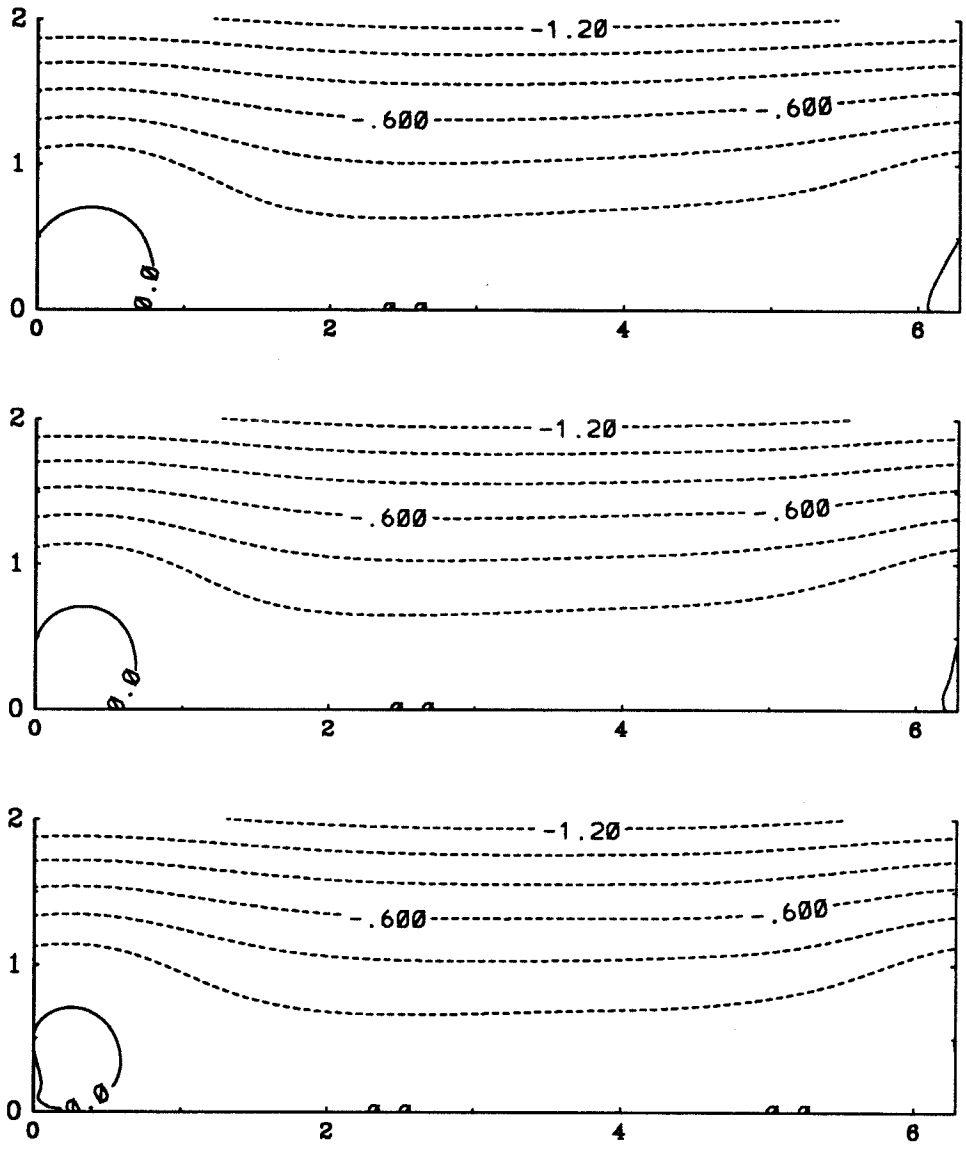

Fig. 4.28c Contours of constant ψ for $t = 0.585,\ 0.682$ and 0.779. Contour interval $= 0.2$. A dashed line is used for negative values.

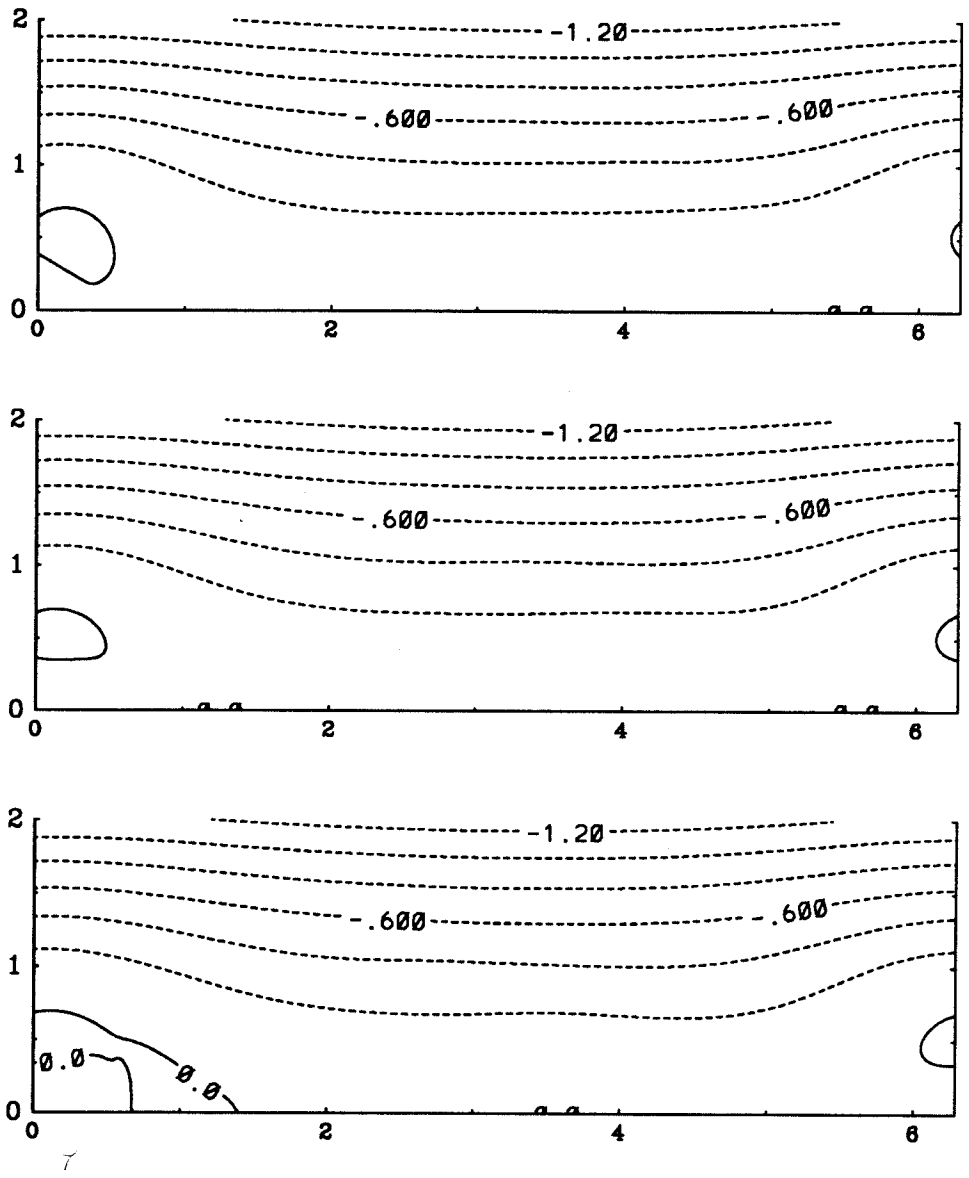

Fig. 4.28d Contours of constant ψ for $t = 0.877$, 0.974 and 1.072. Contour interval = 0.2. A dashed line is used for negative values.

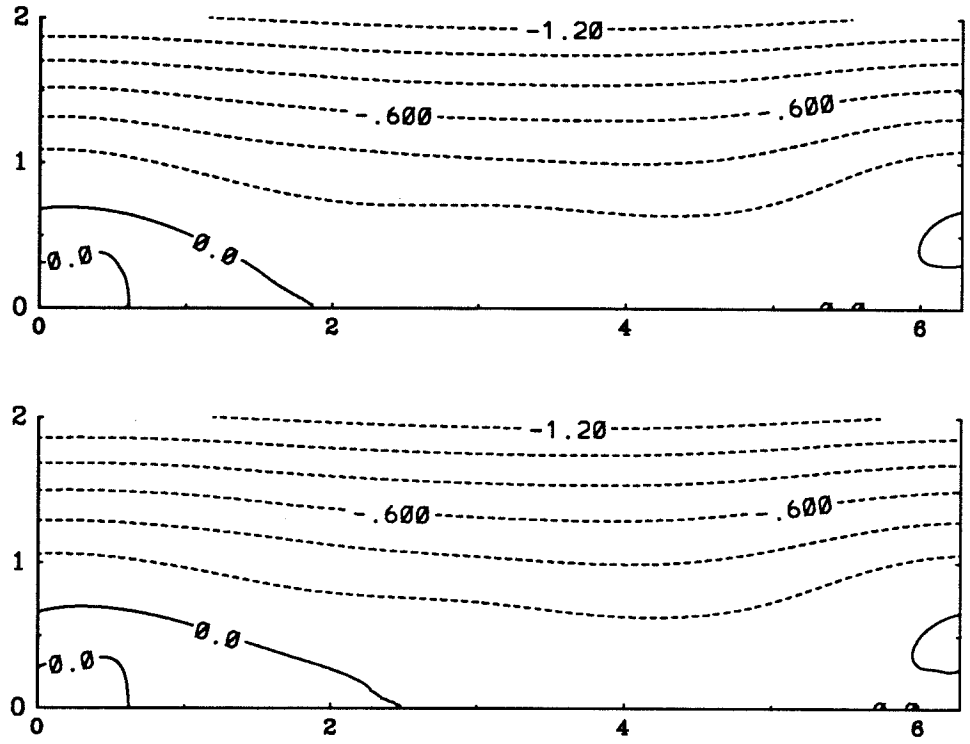

Fig. 4.28e Contours of constant ψ for $t = 1.169$ and 1.267. Contour interval = 0.2. A dashed line is used for negative values.

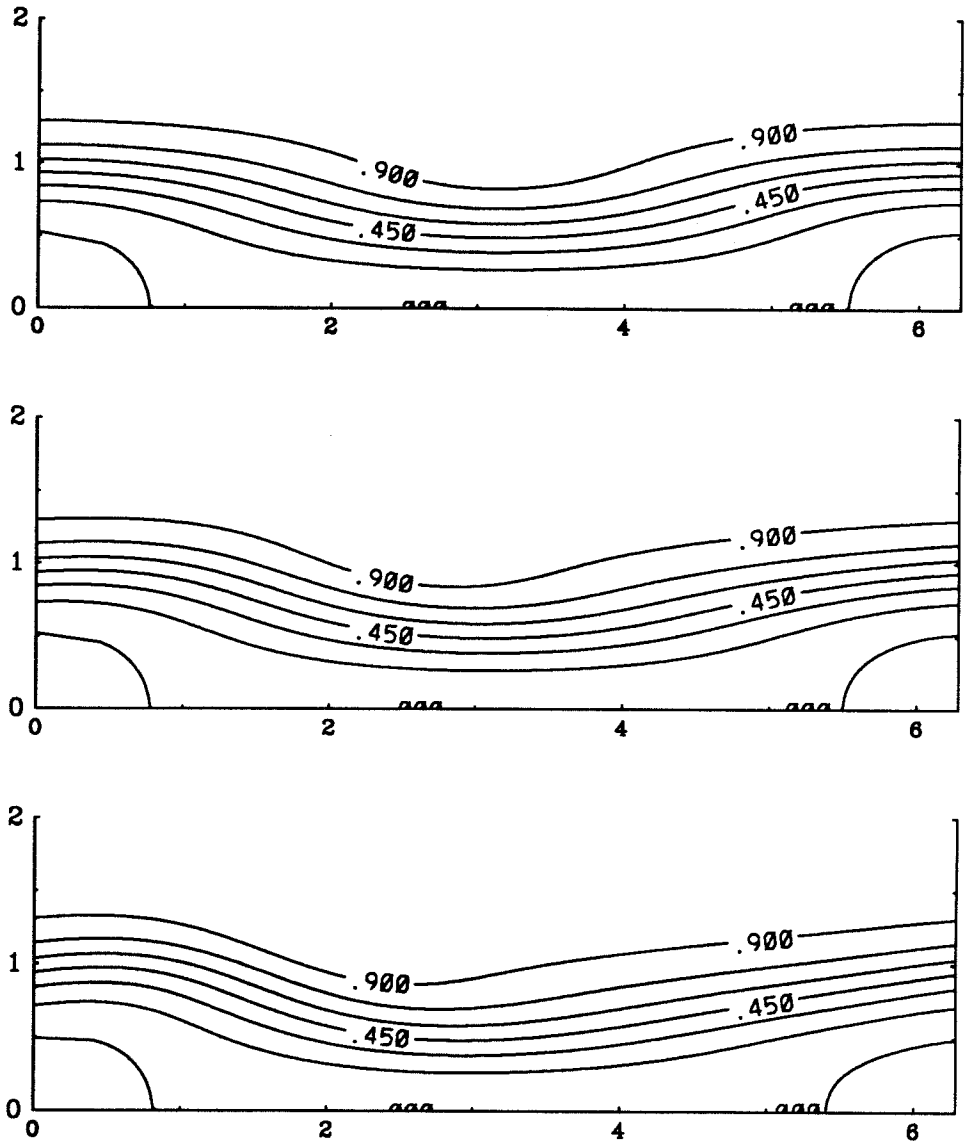

Fig. 4.29a Contours of constant Ω for $t = 0.0$, 0.097 and 0.195. Contour interval = 0.15. A dashed line is used for negative values.

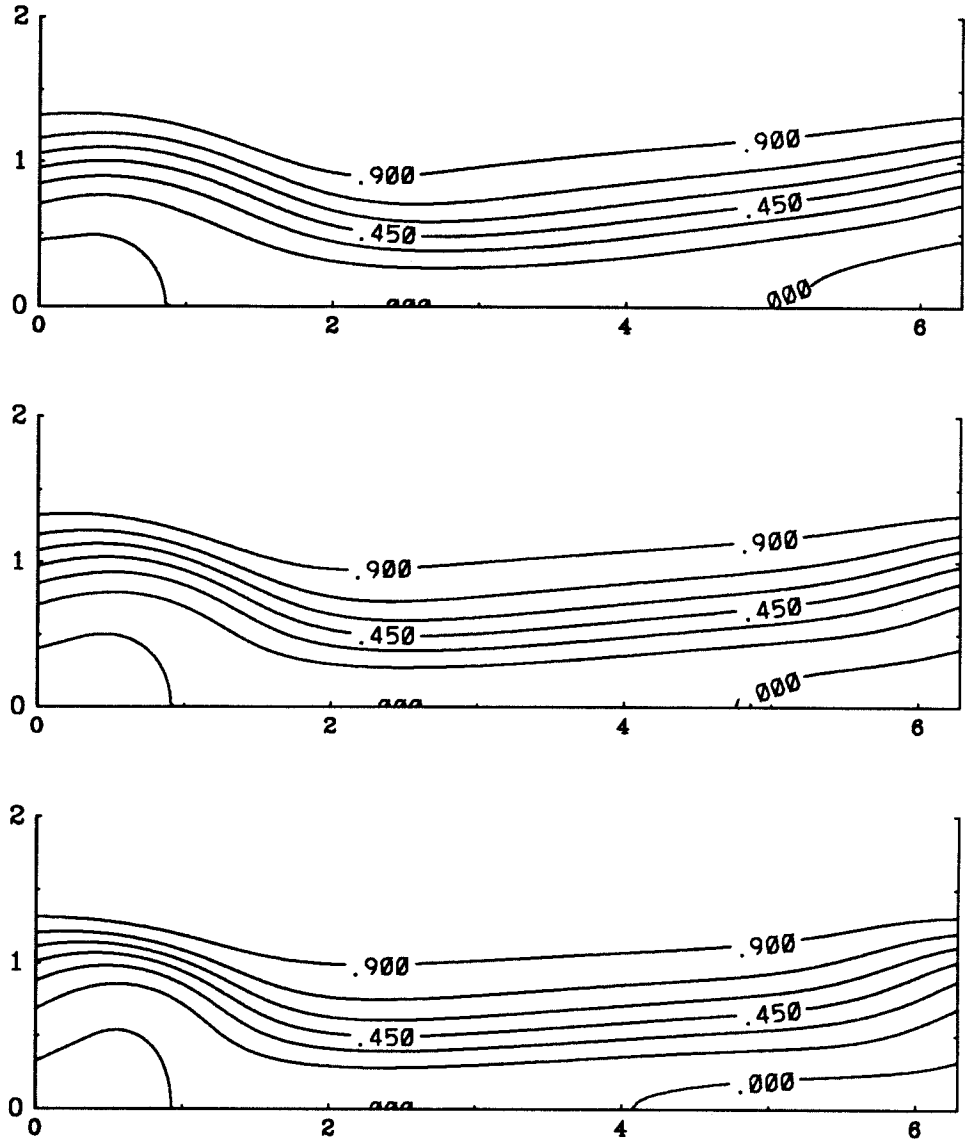

Fig. 4.29b Contours of constant Ω for $t = 0.292$, 0.390 and 0.487. Contour interval = 0.15. A dashed line is used for negative values.

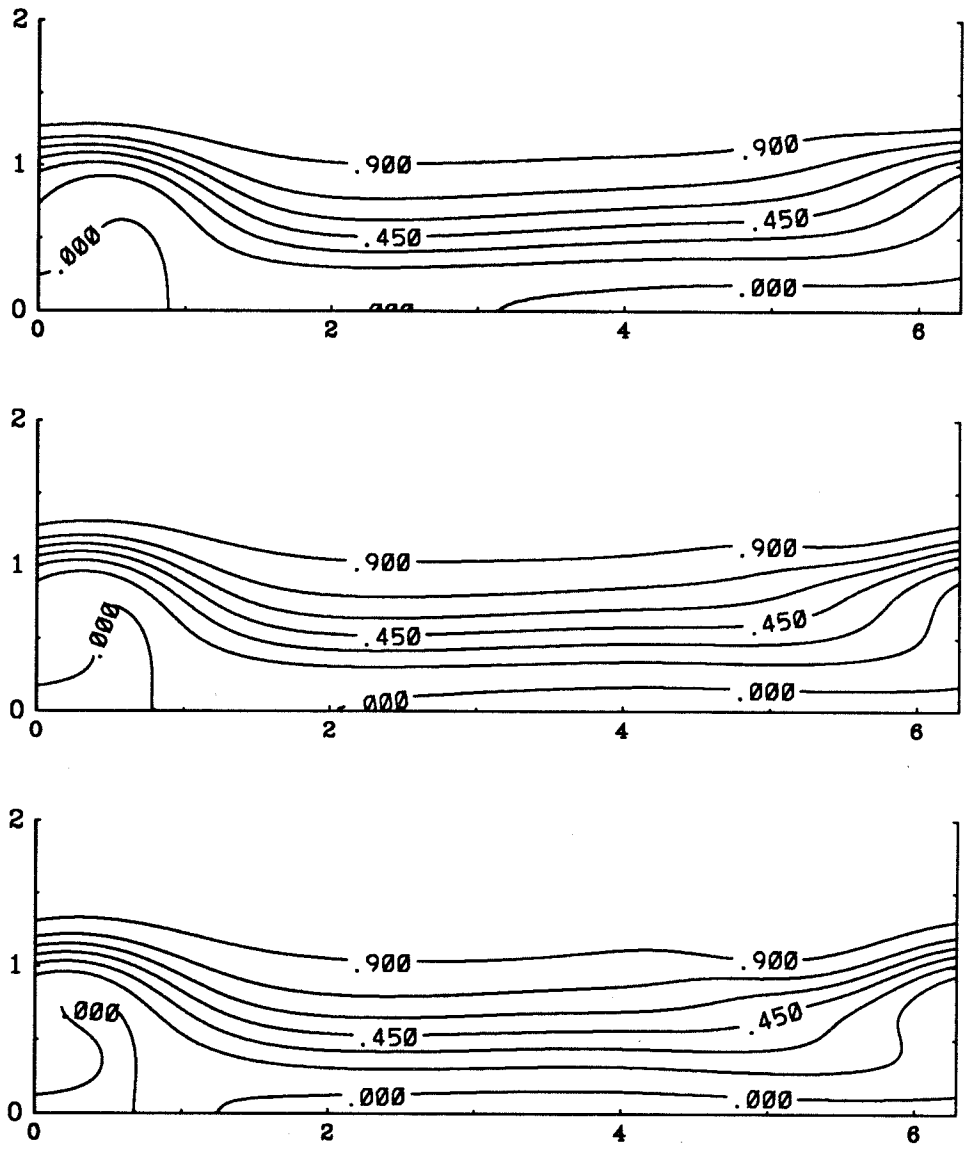

Fig. 4.29c Contours of constant Ω for $t = 0.585$, 0.682 and 0.779. Contour interval = 0.15. A dashed line is used for negative values.

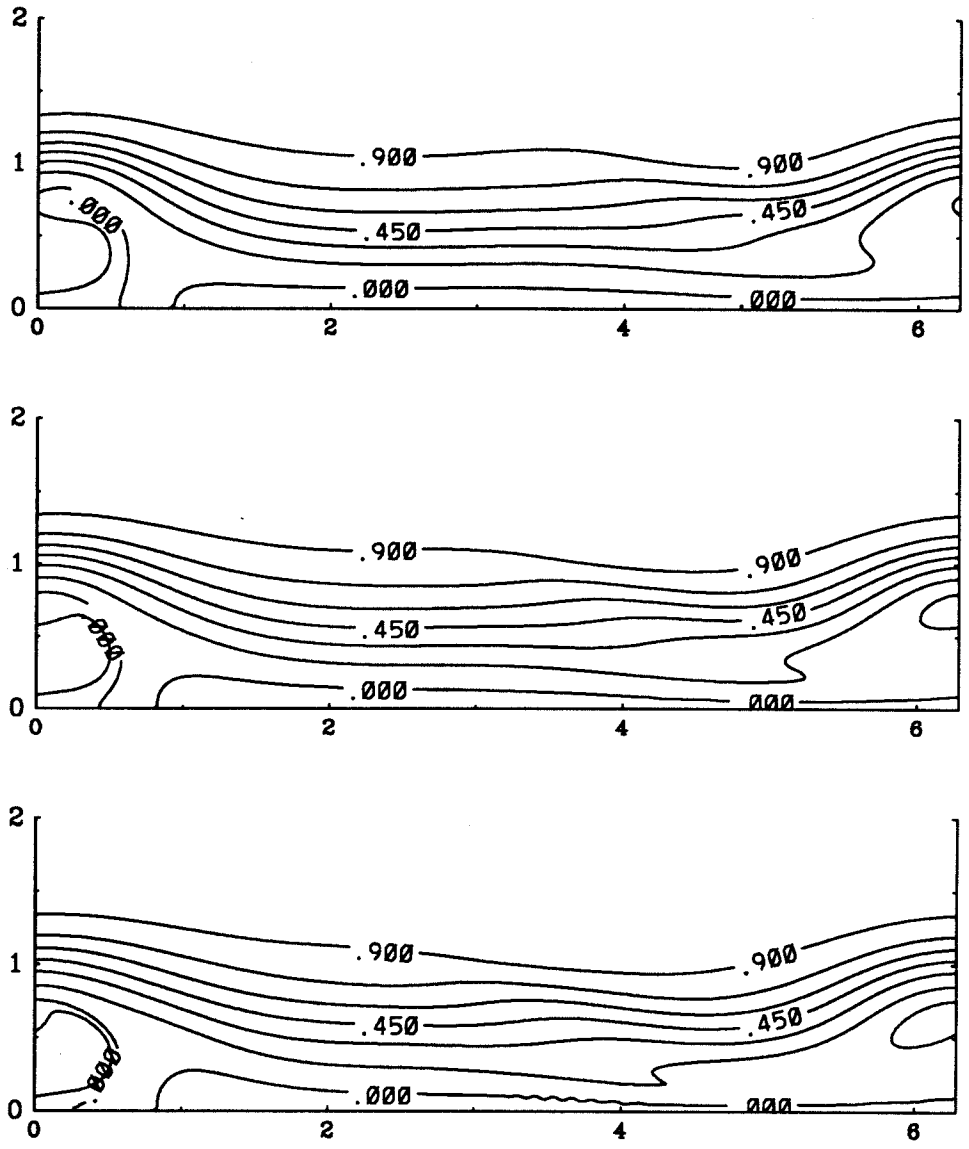

Fig. 4.29d Contours of constant Ω for $t = 0.877$, 0.974 and 1.072. Contour interval = 0.15. A dashed line is used for negative values.

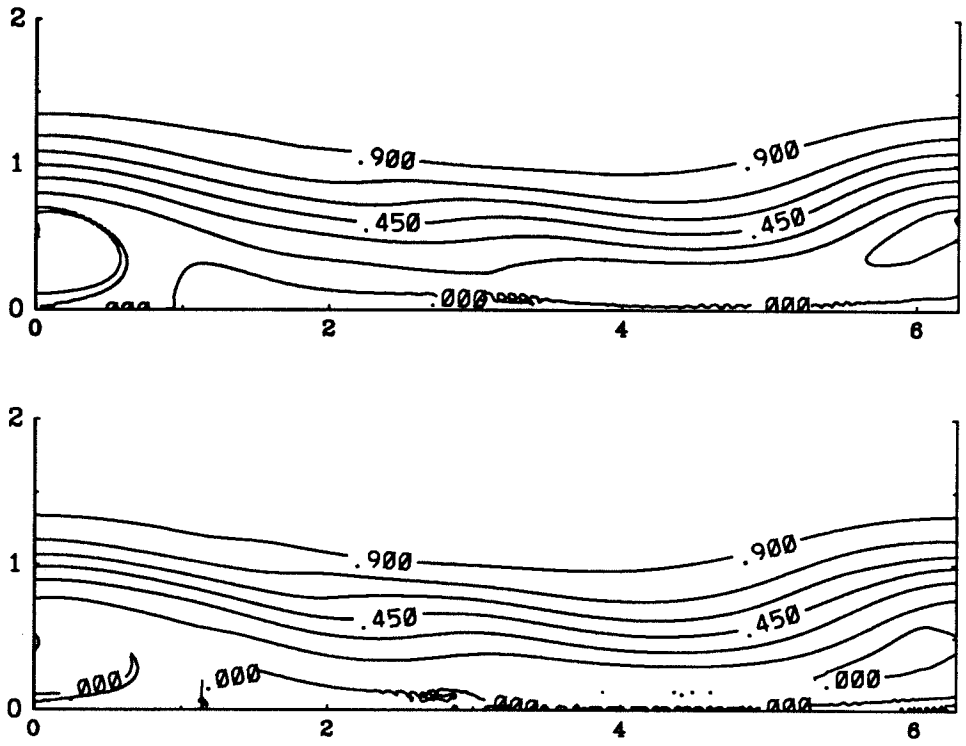

Fig. 4.29e Contours of constant Ω for $t = 1.169$ and 1.267. Contour interval = 0.15. A dashed line is used for negative values.

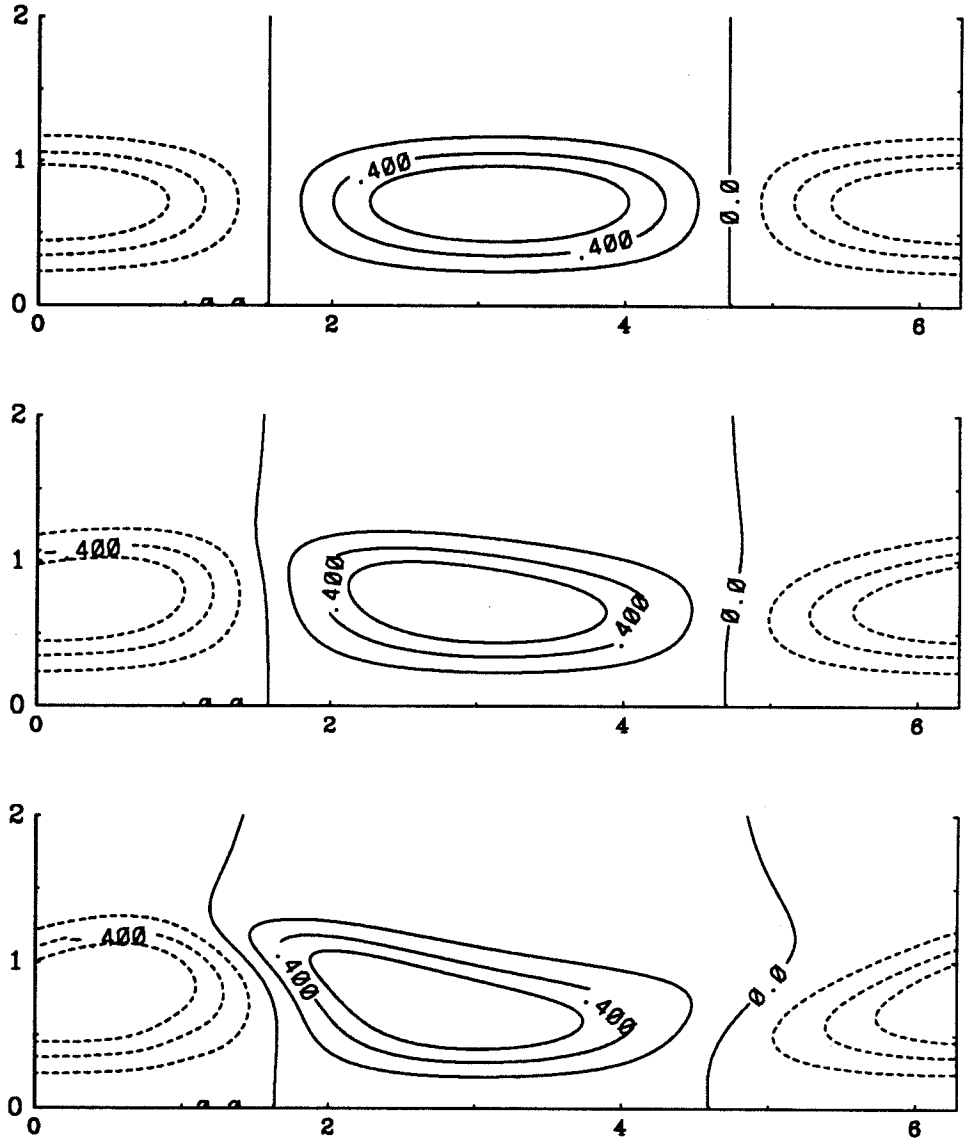

Fig. 4.30a Contours of constant ζ for $t = 0.0$, 0.097 and 0.195. Contour interval = 0.2. A dashed line is used for negative values.

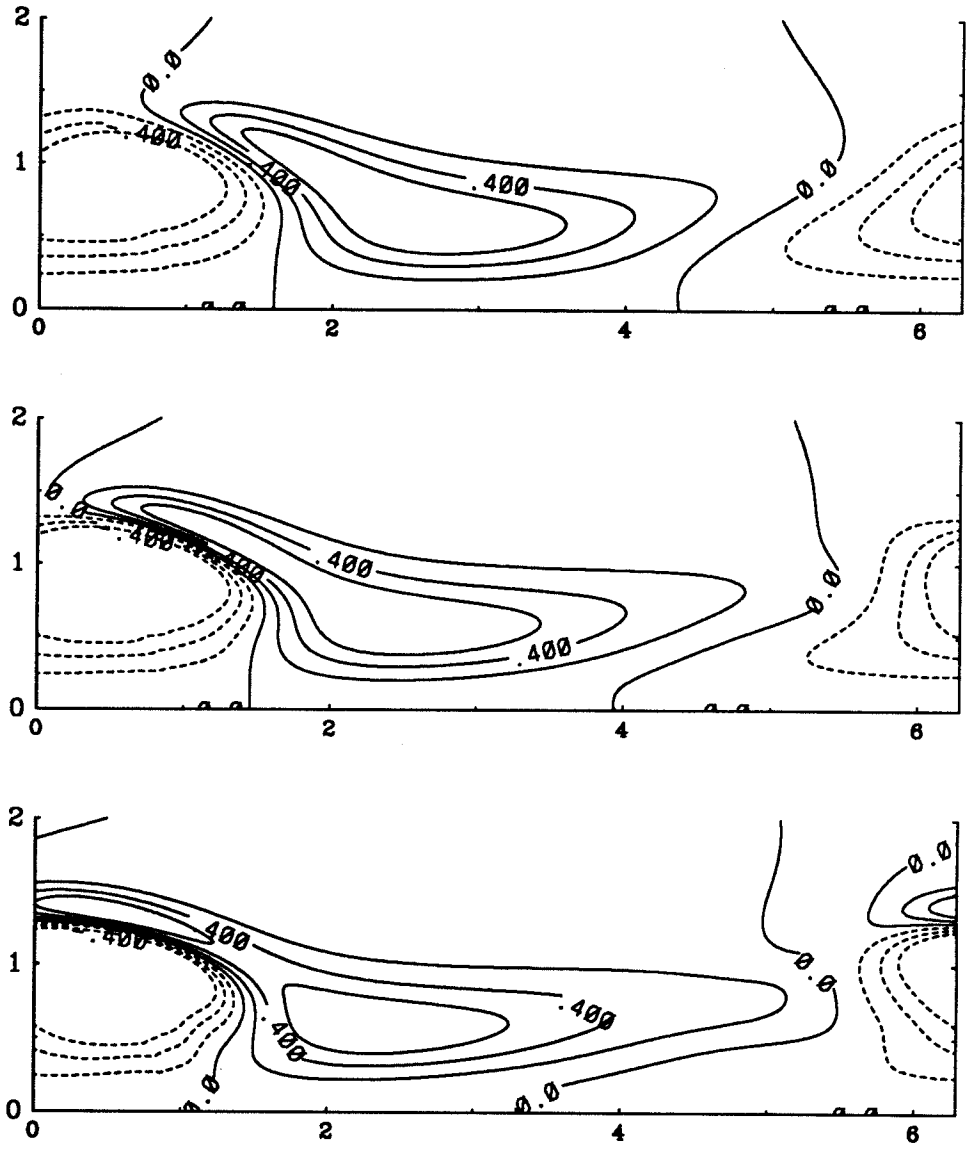

Fig. 4.30b Contours of constant ζ for $t = 0.292$, 0.390 and 0.487. Contour interval = 0.2. A dashed line is used for negative values.

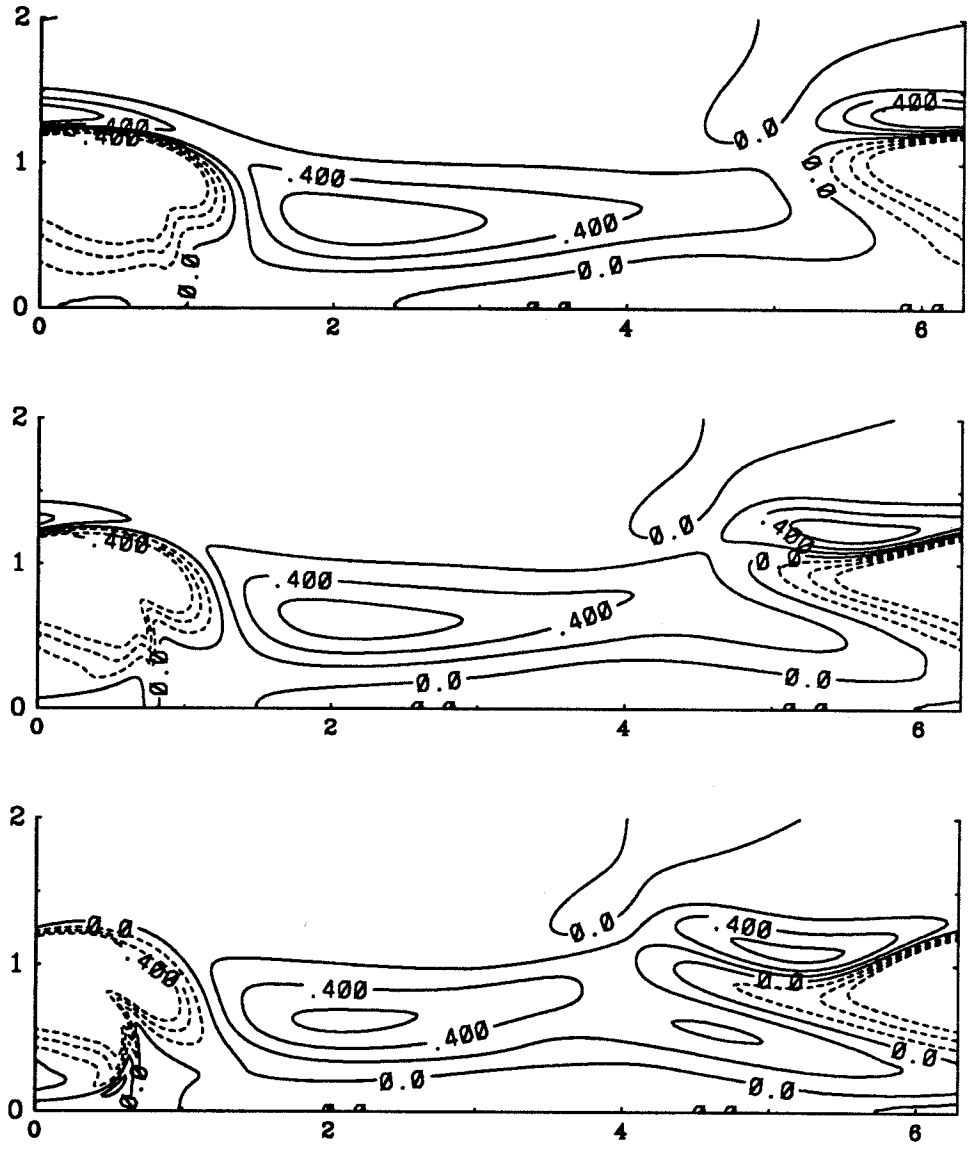

Fig. 4.30c Contours of constant ζ for $t = 0.585$, 0.682 and 0.779. Contour interval = 0.2. A dashed line is used for negative values.

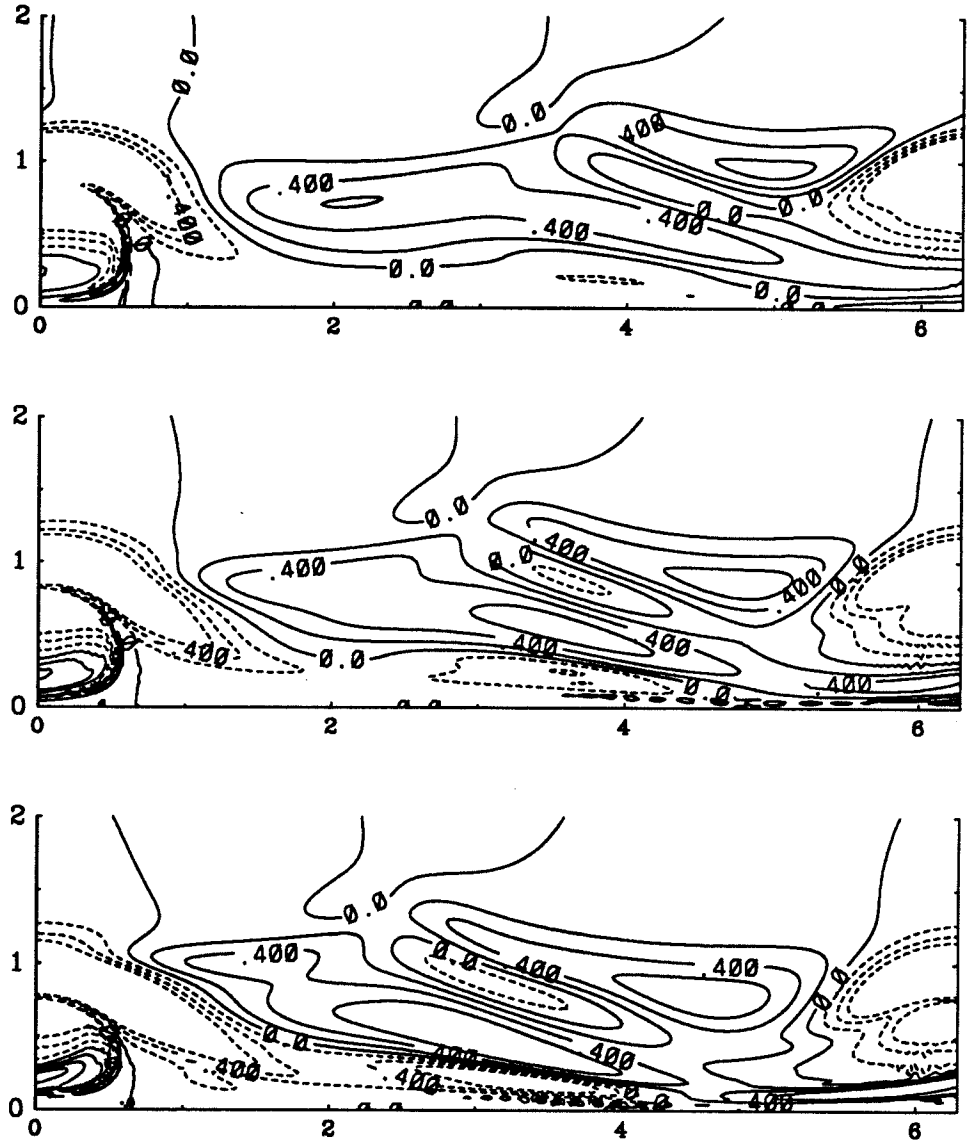

Fig. 4.30d Contours of constant ζ for $t = 0.877$, 0.974 and 1.072. Contour interval $= 0.2$. A dashed line is used for negative values.

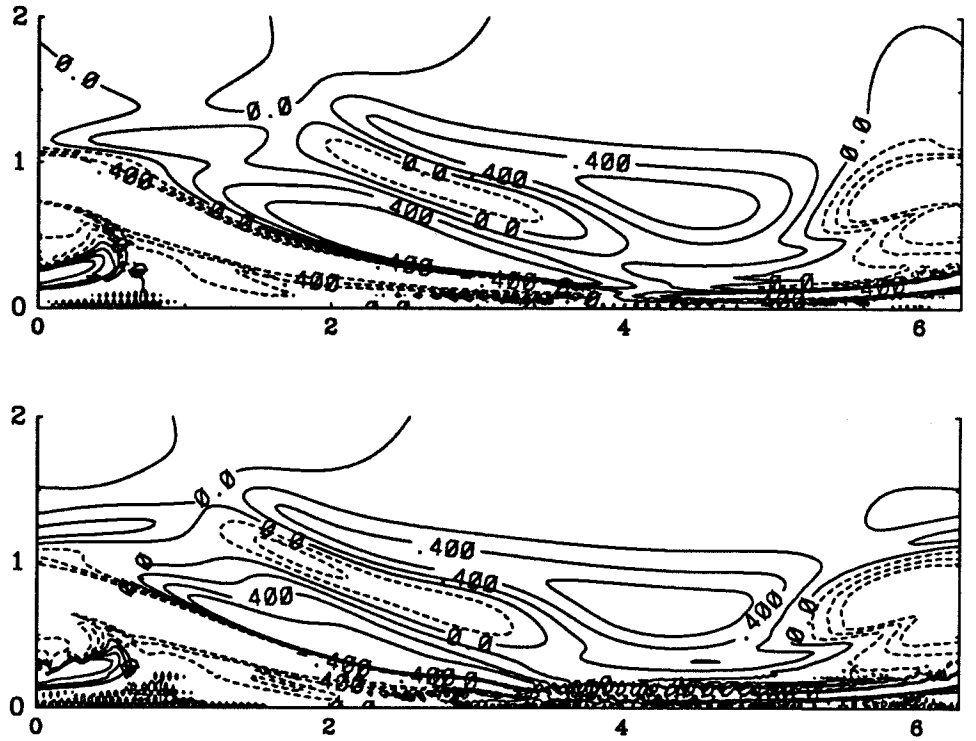

Fig. 4.30e Contours of constant ζ for $t = 1.169$ and 1.267. Contour interval = 0.2. A dashed line is used for negative values.

Part II

CHAPTER 5

Axisymmetric Nonlinear Kelvin Waves

5.1 Introduction

In 1880 Lord Kelvin considered linear stability of columnar vortices. Three different cases were considered by Kelvin. The first case consists of a uniformly rotating fluid between two cylindrical surfaces. The second case consists of a hollow vortex in a tube. Our interest lies in the third case which consists of a slightly disturbed vortex column in a region of infinite radial extent. The vortex column consists of a core of uniform vorticity surrounded by irrotational fluid with continuous velocity across the core boundary. We restrict ourselves to the axisymmetric disturbances of this basic vortex column. The results of linear analysis due to Kelvin show that there exist only neutral waves moving at a constant speed as seen in a frame at rest at infinity. The speed of propagation depends on the wave length of the perturbation. In this chapter we first consider extension of Kelvin's results to second order in an appropriately defined wave amplitude. This leads us to the question of uniqueness of solutions. We find that there exist infinitely many solutions at the second order itself. Determination of the second order solution consists of two components; an axially varying component and a mean component that corrects the base flow characterizing the vortex column. We find that the mean corrections cannot be determined uniquely. Thus there arises a need for extra conditions. At this point we notice that inviscid axisymmetric flows with swirl are characterized by two functions; the Bernoulli function H and the circulation function Ω (Batchelor, 1967). On a streamline given by ψ = constant, both H and Ω must be constant. Thus H and Ω are expressible as functions of ψ, the stream-function, alone. A particular solution is obtained by specifying the functional form of $H(\psi)$ and $\Omega(\psi)$ in some region of the

flow. The flow in the rest of the region is then automatically determined. We supply the required additional conditions by specifying the functional dependence of $H(\psi)$ and $\Omega(\psi)$. The choice of functional forms is dictated by the base flow itself. We find that the linear solution satisfies these constraints exactly. The particular choice of the functional dependence of these functions makes it possible to re-write the Euler equations into a single equation for the stream function. For the chosen distributions of $H(\psi)$ and $\Omega(\psi)$, we find that this equation is linear. We take advantage of this situation and compute the solution to arbitrary orders in wave amplitude. The perturbation procedure adopted here is similar to Stokes expansion in the study of water waves (Schwartz, 1974). However, the presence of vorticity makes the problem harder as the governing equation for the motion inside the core is no longer a simple Laplace's equation. This prohibits us from using a conformal map to transform the domain in which the geometry remains fixed at all amplitudes. Therefore we choose to work directly in the physical domain and determine, as part of the problem, the shape of the interface separating the fluid inside the core from the potential flow outside. A similar approach of finding a solution directly in the physical domain has been used by Holyer (1979) for the case of two dimensional water waves.

The basic motivation of performing these calculations is to determine if there exist solutions with a recirculating bubble. These solutions represent a bubble type of vortex breakdown.

5.2 Equations of motion

We consider the steady, incompressible Euler equations in primitive variables. Let r, ϕ and z denote the radial, swirl and the axial coordinates respectively. Let u, v and w denote the radial, swirl and axial components of velocity respectively. Let p denote the pressure. We consider a frame, fixed at infinity, in which the flow is steady. In such a frame, we assume a base flow consisting of a cylindrical vortex column with zero radial velocity, uniform axial velocity from right to left and a swirl velocity distribution that gives uniform axial vorticity in the cylindrical core and an

irrotational flow outside this core. The precise form of the base flow is given in (5.5). The formulation of the problem in this chapter differs from Kelvin's linear analysis. Lord Kelvin considers a vortex on which the linear waves move at constant speed with respect to a frame fixed at infinity. In our approach, we impose a uniform axial velocity which exactly opposes the linear waves and hence they become steady waves. The effect of nonlinearity in Kelvin's approach would result in a correction of the wave speed. In our approach, we find corrections to the imposed axial velocity.

We set $x = \kappa z$, where κ is the wavenumber of the disturbance imposed on the base flow. The problem is treated as being periodic in x, and we take, without any loss of generality, the period to be 2π. The equations of motion in cylindrical co-ordinates are given by

$$u_r + \frac{u}{r} + \kappa w_x = 0, \tag{5.1}$$

$$uu_r + \kappa w u_x - \frac{v^2}{r} = -p_r, \tag{5.2}$$

$$uv_r + \kappa w v_x + \frac{uv}{r} = 0, \tag{5.3}$$

$$uw_r + \kappa w w_x = -\kappa p_x, \tag{5.4}$$

where r denotes the radial co-ordinate. We have used subscripts to denote partial derivatives.

Now we specify the base flow. The radial and the axial velocities are of the form

$$u(r) = u_{00}(r) = 0, \quad 0 \leq r < \infty, \tag{5.5a}$$

$$w(r) = w_{00}(r) = -c_0 = -\alpha_0/\kappa, \quad 0 \leq r < \infty, \tag{5.5b}$$

where $c_0 = \alpha_0/\kappa$ is the amount of axial velocity at $r = \infty$ that is necessary to sustain a standing linear wave disturbance with wave number κ. The value of c_0 is determined as part of the solution. In particular, it is found from the linear theory. The quantity c_0 can be identified with the linear wave speed in Kelvin's analysis. We find the pressure by integrating the radial momentum equation. The swirl and the pressure

profiles are given by

$$v_{00_<} = T_0 r, \quad p_{00_<} = \frac{T_0^2 r^2}{2} \qquad \text{for} \quad r \leq a_{00}, \tag{5.5c}$$

$$v_{00_>} = \frac{T_0 a_{00}^2}{r}, \quad p_{00_>} = T_0^2 a_{00}^2 - \frac{T_0^2 a_{00}^4}{2r^2} \qquad \text{for} \quad r \geq a_{00}, \tag{5.5d}$$

where a_{00} denotes the radius of the undisturbed vortex core and T_0 is a known constant which is related to the strength of the vortex. From now on the subscripts $<$ and $>$ will be used to denote the solutions inside and outside the core respectively. When we consider disturbances of finite amplitude, the subscripts $<$ and $>$ will stand for $r < R$ and $r > R$ where R will be the perturbed boundary. Thus for the base flow, $R = a_{00}$. Also, the pressure is arbitrary up to a constant. We have chosen the convention that pressure is zero at the axis of the vortex.

Now we consider a deviation from the base flow and represent it as a Fourier series

$$u = \sum_{k=1}^{\infty} u_k(r)\sin(kx), \quad v = \sum_{k=0}^{\infty} v_k(r)\cos(kx), \tag{5.6a}$$

$$w = \sum_{k=0}^{\infty} w_k(r)\cos(kx), \quad p = \sum_{k=0}^{\infty} p_k(r)\cos(kx). \tag{5.6b}$$

The Fourier coefficients themselves are expanded into a power series given by

$$u_k = \varepsilon^k u_{k,k} + \varepsilon^{k+2} u_{k,k+2} + \cdots, \quad k = 1, 2, \ldots, \tag{5.7a}$$

$$v_k = \varepsilon^k v_{k,k} + \varepsilon^{k+2} v_{k,k+2} + \cdots, \quad k = 0, 1, 2, \ldots, \tag{5.7b}$$

$$w_k = \varepsilon^k w_{k,k} + \varepsilon^{k+2} w_{k,k+2} + \cdots, \quad k = 0, 1, 2, \ldots, \tag{5.7c}$$

$$p_k = \varepsilon^k p_{k,k} + \varepsilon^{k+2} p_{k,k+2} + \cdots, \quad k = 0, 1, 2, \ldots, \tag{5.7d}$$

where ε is an expansion parameter and the quantities u_{11}, u_{13} etc., are functions of r only. We will relate ε to the wave amplitude at a later stage. The particular form assumed in (5.6) and (5.7) is a consequence of the symmetry of the solution. The symmetry is such that the solution remains the same if we replace x by $x \pm \pi$ and ε by $-\varepsilon$. We substitute these expansions into the equations of motion and collect

Fourier modes and like powers of ε. Let, from now on, primes denote derivatives of various functions with respect to their arguments, i.e.,

$$q'(\cdot) = \frac{\mathrm{d}q(\cdot)}{\mathrm{d}(\cdot)}, \quad q''(\cdot) = \frac{\mathrm{d}^2 q(\cdot)}{\mathrm{d}(\cdot)^2}, \quad \text{etc.} \tag{5.8}$$

When the argument of the functions is suppressed, it is assumed to be r. The argument other than r appears later with the Bessel functions.

Equating the coefficients of $\varepsilon\cos(x)$ and $\varepsilon\sin(x)$ we get

$$u_{11}' + \frac{u_{11}}{r} - \kappa w_{11} = 0, \tag{5.9}$$

$$\alpha_0 u_{11} + \frac{2v_{00}}{r} v_{11} - p_{11}' = 0, \tag{5.10}$$

$$\alpha_0 v_{11} + B_{00} u_{11} = 0, \tag{5.11}$$

$$\alpha_0 w_{11} - \kappa p_{11} = 0. \tag{5.12}$$

Equating the coefficients of $\varepsilon^2\cos(2x)$ and $\varepsilon^2\sin(2x)$ we get

$$u_{22}' + \frac{u_{22}}{r} - 2\kappa w_{22} = 0, \tag{5.13}$$

$$2\alpha_0 u_{22} + \frac{2v_{00}}{r} v_{22} - p_{22}' = -\frac{1}{2} u_{11} u_{11}' + \frac{\kappa}{2} w_{11} u_{11} - \frac{1}{2}\frac{v_{11}^2}{r}, \tag{5.14}$$

$$2\alpha_0 v_{22} + B_{00} u_{22} = -\frac{1}{2} u_{11} v_{11}' + \frac{\kappa}{2} w_{11} v_{11} - \frac{1}{2r} u_{11} v_{11}, \tag{5.15}$$

and

$$2\alpha_0 w_{22} - 2\kappa p_{22} = -\frac{1}{2} u_{11} w_{11}' + \frac{\kappa}{2} w_{11}^2. \tag{5.16}$$

Finally, equating the coefficient of ε^2 we get,

$$p_{02}' - \frac{2v_{02}}{r} v_{02} = -\frac{1}{2} u_{11}' u_{11} - \frac{\kappa}{2} w_{11} u_{11} + \frac{1}{2}\frac{v_{11}^2}{r}. \tag{5.17}$$

We define

$$B_{00} = \left(v_{00}' + v_{00}/r\right), \tag{5.18}$$

in the equations above. We solve these equations in the two regions defined by $r \leq R$ and $r \geq R$, where R denotes the shape of the perturbed boundary separating the

fluid in the vortex core and the rest of the fluid which is irrotational. We assume the following form for the equation of this boundary.

$$R(x) = \sum_{k=0}^{\infty} a_k \cos(kx), \tag{5.19a}$$

where

$$a_k = \varepsilon^k a_{k,k} + \varepsilon^{k+2} a_{k,k+2} + \cdots, \quad k = 0, 1, 2, \ldots. \tag{5.19b}$$

The coefficients a_{02}, a_{22} etc are constants to be determined as part of the problem. The coefficient a_{11} is arbitrary and may be absorbed into the definition of ε. We retain it only for the purpose of automatic implementation of the perturbation procedure for large orders since the automatic expansion is done by a method based on the manipulation of the indices, i.e., the subscripts. The solutions to the above equations are to be matched across the core boundary. We may consider two types of matching conditions. We may either make the velocity vector continuous across the boundary or make the normal component of velocity and pressure continuous. The continuity of the normal velocity and the pressure is implied by the continuity of the velocity vector (see Saffman, 1991).

5.3 Boundary conditions

5.3.1 Conditions at the core boundary

We consider here continuity of the velocity across the boundary. The continuity of velocity implies that $u_<(R) = u_>(R)$, $v_<(R) = v_>(R)$ and $w_<(R) = w_>(R)$. Since the equation for R is itself unknown, we proceed by expanding all the quantities in a Taylor series about $r = a_{00}$. We then collect the coefficients of like powers of ε and separate out the modes. This procedure is assumed valid since we are looking for solutions which are continuous everywhere except perhaps at the boundary. A typical expansion takes the form

$$v(R) = v(a_{00}) + v_r(a_{00})(R - a_{00}) + v_{rr}(a_{00}) \frac{(R - a_{00})^2}{2!} + \cdots, \tag{5.20}$$

where,

$$v(a_{00}) = v_{00}(a_{00}) + \varepsilon^2 v_{02}(a_{00}) + \varepsilon v_{11}(a_{00})\cos(x) + \cdots,$$

$$v_r(a_{00}) = v_{00}'(a_{00}) + \varepsilon^2 v_{02}'(a_{00}) + \varepsilon v_{11}'(a_{00})\cos(x) + \cdots, \text{etc.}$$

We further expand $(R - a_{00})$, $(R - a_{00})^2$, etc., into a Taylor series about $\varepsilon = 0$ and substitute into (5.20). We evaluate expression (5.20) on either side of the core boundary. From the continuity of velocity at the interface, we get a set of conditions to be satisfied by the coefficients $u_{i,j}$, $v_{i,j}$ and $w_{i,j}$. They are stated below. We denote

$$\{Q\} = Q_>(a_{00}) - Q_<(a_{00}). \tag{5.21}$$

Then, the conditions on the linear terms (denoted by subscript 1,1) are

$$\{u_{11}\} = 0, \tag{5.22}$$

$$\left\{v_{11} + a_{11}v_{00}'\right\} = 0, \tag{5.23}$$

$$\{w_{11}\} = 0. \tag{5.24}$$

The conditions on the second order quantities associated with subscript (22) are

$$\left\{u_{22} + \frac{a_{11}}{2}u_{11}'\right\} = 0, \tag{5.25}$$

$$\left\{v_{22} + a_{22}v_{00}' + \frac{a_{11}}{2}v_{11}' + \frac{a_{11}^2}{4}v_{00}''\right\} = 0, \tag{5.26}$$

$$\left\{w_{22} + \frac{a_{11}}{2}w_{11}'\right\} = 0. \tag{5.27}$$

Finally, the conditions on the mean flow corrections associate with subscript (02) are

$$\left\{v_{02} + a_{02}v_{00}' + \frac{a_{11}}{2}v_{11}' + \frac{a_{11}^2}{4}v_{00}''\right\} = 0, \tag{5.28}$$

$$\left\{w_{02} + \frac{a_{11}}{2}w_{11}'\right\} = 0. \tag{5.29}$$

5.3.2 Conditions at $r = 0$ and $r = \infty$

Very close to the axis, we assume that flow tends to that of solid-body rotation. This means that the swirl must be linear in r. Since there is no source of fluid, there is no radial velocity present at the axis. This leads us to the boundary conditions

$$u(r = 0) = 0, \quad v(r = 0) = 0, \tag{5.30a}$$

and we assume that

$$w(r = 0) < \infty. \tag{5.30b}$$

As $r \to \infty$ we assume that the perturbations must decay.

5.4 Linear solution

We eliminate the pressure from (5.10) and (5.12) and solve for u_{11} and v_{11} in terms of w_{11}. We get

$$u_{11} = \frac{\alpha_0^2 w_{11}'}{\kappa D_{11}}, \qquad v_{11} = -B_{00}\frac{\alpha_0 w_{11}'}{\kappa D_{11}}, \tag{5.31}$$

where,

$$D_{11} = \alpha_0^2 - B_{00}2v_{00}/r. \tag{5.32}$$

Notice that D_{11} is a constant in the outer and inner regions. Eliminating the radial component of velocity in the continuity equation (5.9), we get an equation in w only. Evaluation of this equation in the inner and outer regions gives us,

$$w_{11_>}'' + \frac{1}{r}w_{11_>}' - \kappa^2 w_{11_>} = 0, \tag{5.33}$$

$$w_{11_<}'' + \frac{1}{r}w_{11_<}' + \nu_1^2 w_{11_<} = 0, \tag{5.34}$$

where

$$\nu_1^2 = \frac{\kappa^2(4T_0^2 - \alpha_0^2)}{\alpha_0^2}. \tag{5.35}$$

The consistent solutions are of the form

$$w_{11_<} = A_{11_<}J_0(\nu_1 r), \qquad w_{11_>} = A_{11_>}K_0(\kappa r), \tag{5.36}$$

where the constants $A_{11_<}$ and $A_{11_>}$ are to be determined and J_0 and K_0 are Bessel functions. We reject the other linearly independent solution of (5.33) because it grows exponentially as $r \to 0$ thus violating the boundary conditions. A similar argument holds for the solution outside the core. The constants may be computed by applying the conditions (5.22) through (5.24). Using (5.22) and (5.23) leads us to a homogeneous system of equations in the unknown constants. If a nontrivial solution to that system exists, then the determinant of the system must be zero. This leads us to a dispersion relation. Finally applying (5.24) determines the constants explicitly. We get,

$$A_{11_<} = a_{11} \frac{\kappa D_{11_<}}{\alpha_0 \nu_1 J_0'(\nu_1 a_{00})}, \qquad A_{11_>} = a_{11} \frac{\alpha_0}{K_0'(\kappa a_{00})}, \tag{5.37}$$

and the dispersion relation which determines α_0 is,

$$\frac{\alpha_0^2 \nu_1}{\kappa D_{11_<}} \frac{J_0'(\nu_1 a_{00})}{J_0(\nu_1 a_{00})} = \frac{K_0'(\kappa a_{00})}{K_0(\kappa a_{00})}. \tag{5.38}$$

Since only the square of α_0 enters into the problem, there are two solution branches corresponding to the left and right moving waves. For a given real κ, there are an infinite number of roots to (5.38) on each branch.

If ν_1^2 is negative, then the axial velocity inside the core is proportional to the Bessel function I_0 instead of J_0 as can be seen from the equation (5.34). This, however, fails to satisfy the boundary conditions. Therefore, the solution must be such that ν_1^2 is positive. Then from equation (5.35) we see that the quantity α_0 is bounded from above by

$$|\alpha_0| \leq 2T_0. \tag{5.39}$$

Further, all the roots of (5.38) are real and distinct with an accumulation point at zero. The eigenfunctions corresponding to the largest root exhibit no internal zeroes. Thus if we were to denote α_{0_p} to be the p^{th} root of (5.38), the corresponding eigenfunction has p internal zeroes and $p = 0$ corresponds to the largest root. Some roots (for the positive branch) are given in table 5.1.

It is mentioned by Lord Kelvin (1880) that the equality of u_{11} and w_{11} at $r = a_{00}$ (see equations 5.19 and 5.21) also implies equality of v_{11} at $r = a_{00}$. This, however,

Table 5.1 Roots of Kelvin's dispersion relation (5.38).

This table shows the values of α_0 computed from the equation (5.38) using $a_{00} = 1$ and $T_0 = 1$.

No	$k = 0.5$	$k = 1.0$	$k = 2.0$
1	0.39027755502169	0.70590520214049	1.1409768704885
2	0.17881709329998	0.34903848551704	0.65317764970197
3	0.11494037766721	0.22752214229761	0.44161072269100
4	$8.4561601890232\,10^{-02}$	0.16817372402080	0.33076942077432
5	$6.6854178045997\,10^{-02}$	0.13323687205356	0.26366406570569
6	$5.5268790200782\,10^{-02}$	0.11027049913461	0.21893714384469
7	$4.7101675816889\,10^{-02}$	$9.4037783116883\,10^{-02}$	0.18707674151658
8	$4.1035655843075\,10^{-02}$	$8.1961719668731\,10^{-02}$	0.16326035106466
9	$3.6352840385686\,10^{-02}$	$7.2629437942164\,10^{-02}$	0.14479664026559
10	$3.2628780505344\,10^{-02}$	$6.5202405153967\,10^{-02}$	0.13006994049018

is not true as can easily be seen from (5.23). Rewriting (5.23) in the expanded form we get

$$v_{11<} + a_{11} v'_{00<} = v_{11>} + a_{11} v'_{00>}, \tag{5.40}$$

where the quantities are evaluated at $r = a_{00}$. Using (5.5) we obtain

$$v_{11<}(a_{00}) - v_{11>}(a_{00}) = -2a_{11}T_0 \neq 0. \tag{5.41}$$

However, the swirl velocity is continuous at $r = a_{00} + \varepsilon a_{11}\cos(x)$.

5.5 Second order solution

Once again we may eliminate the pressure from (5.14) and (5.16) and using the known linear solution we get,

$$u_{22} = \frac{2\alpha_0^2}{\kappa}\,\frac{w'_{22}}{D_{22}}, \qquad v_{22} = -\frac{\alpha_0 B_{00}}{\kappa}\,\frac{w'_{22}}{D_{22}}, \tag{5.42}$$

where

$$D_{22} = 4\alpha_0^2 - B_{00}\,\frac{2v_{00}}{r}. \tag{5.43}$$

Note that D_{22} is also a constant in the outer and inner regions. Substituting these into the continuity equation yields a second order ordinary differential equation in w_{22}. This turns out to be homogeneous too since both u_{22} and v_{22} do not depend on linear terms. We get,

$$w''_{22<} + \frac{1}{r}w'_{22<} - \nu_2^2 w_{22<} = 0, \tag{5.44}$$

$$w''_{22>} + \frac{1}{r} w'_{22>} - (2\kappa)^2 w_{22<} = 0, \tag{5.45}$$

where

$$\nu_2^2 = \frac{\kappa^2 D_{22<}}{\alpha_0^2}. \tag{5.46}$$

Thus the linear solution seemingly does not act as a forcing mechanism as is usual in most cases. It does, however, alter the pressure field and hence the second order velocities. Thus the effect is an indirect one.

The general solution to w_{22} depends on the sign of $D_{22<}$. The sign of $D_{22<}$ in turn depends on the core size and the magnitude of the axial vorticity of the unperturbed vortex. For example, $D_{22<}$ is found to be positive for $a_{00} = 2$ and $T_0 = 1/4$ and it is found to be negative for $a_{00} = 1$ and $T_0 = 1$. In Figure 5.1, contours on which $D_{22<}$ is constant is plotted for various values of the core size a_{00} and T_0. It shows that the value of $D_{22<}$ is zero at about $a_{00} = 1.6$ and is independent of T_0. The case of $D_{22<} = 0$ is not considered here.

If $D_{22<}$ is positive then we have,

$$w_{22<} = A_{22<} I_0(\nu_2 r), \qquad w_{22>} = A_{22>} K_0(2\kappa r). \tag{5.47}$$

Notice that the solution in the inner region is characteristically different from the linear solution. Using the conditions (5.25) and (5.27) we find

$$A_{22<} = -a_{11}^2 \frac{2\kappa T_0^2}{\alpha_0} \frac{K_0'(2\kappa a_{00})}{E}, \qquad A_{22>} = -a_{11}^2 \frac{4\alpha_0 T_0^2 \nu_2}{D_{22<}} \frac{I_0'(\nu_2 a_{00})}{E}, \tag{5.48}$$

where

$$E = -I_0(\nu_2 a_{00}) K_0'(2\kappa a_{00}) + \frac{2\alpha_0^2 \nu_2}{\kappa D_{22<}} I_0'(\nu_2 a_{00}) K_0(2\kappa a_{00}). \tag{5.49}$$

Using the remaining condition (5.26) we obtain,

$$a_{22} = -a_{11}^2 \left[\frac{1}{4a_{00}} + \frac{\nu_1}{2} \frac{J_0(\nu_1 a_{00})}{J_0'(\nu_1 a_{00})} + \frac{2T_0^2 \nu_2}{D_{22<}} \frac{I_0'(\nu_2 a_{00}) K_0'(2\kappa a_{00})}{E} \right]. \tag{5.50}$$

If the sign of $D_{22<}$ is negative, then the solution is found by simply replacing ν_2 by σ_2, where

$$\sigma_2^2 = -\nu_2^2, \tag{5.51}$$

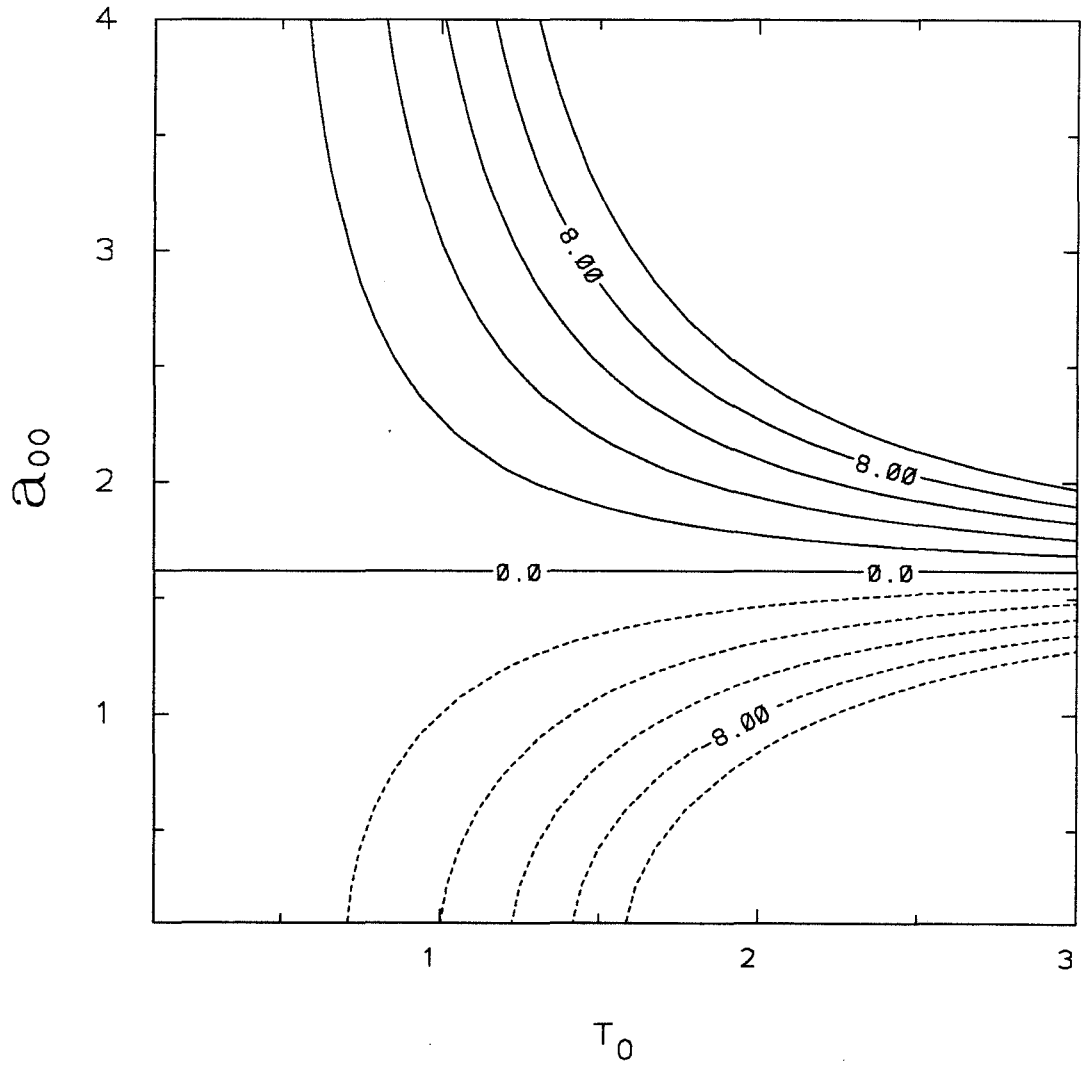

Fig. 5.1: Contours of constant $D_{22_<}$. It shows that the quantity $D_{22_<}$ becomes zero at about $a_{00} = 1.6$ and is independent of T_0.

and further replacing I_0 and I_0' by J_0 and J_0' respectively in equations (5.47) through (5.50).

A typical solution is shown in Figure 5.2. Figure 5.2a shows the linear eigenfunctions. While the radial and axial components are continuous, the swirl jumps at the unperturbed boundary. Figure 5.2b and 5.2c show the second order quantities for two possible cases arising from the sign of $D_{22<}$. The parameters used for each case are listed in the figure captions. When the quantity $D_{22<}$ is positive, the inner solution is non-oscillatory and when it is negative, the inner solution is oscillatory. The solution in Figure 5.1c is oscillatory with no internal zeroes.

5.6 Mean flow corrections

The corrections to mean flow (i.e., the quantities with subscripts 02) cannot be determined uniquely from the given conditions. Whether we consider continuity of velocity vector or the continuity of pressure and normal velocity as our conditions at the core boundary, we would have an undetermined function leading us to an infinity of solutions. As discussed already, this is reflected in the considerations of the Bernoulli (H) and circulation (Ω) functions. For the sake of completeness, we briefly recount the relation of H and Ω to the flow variables (see Batchelor, 1967). The Euler equation in the absence of any body forces can be written in the vector form as

$$\frac{\partial \mathbf{u}}{\partial t} + \mathbf{u} \cdot \nabla \mathbf{u} = -\nabla p, \tag{2.52}$$

where $\mathbf{u}$ is the velocity and p is the pressure. We have assumed the density to be unity. Using the vector identity

$$\frac{1}{2} \nabla(\mathbf{u} \cdot \mathbf{u}) = \mathbf{u} \cdot \nabla \mathbf{u} + \mathbf{u} \wedge \omega, \tag{2.53}$$

where ω = curl $\mathbf{u}$ is the vorticity and $\wedge$ denotes the vector cross product, we can rewrite the governing equation as

$$\mathbf{u} \wedge \omega - \frac{\partial \mathbf{u}}{\partial t} = \nabla \left(\frac{1}{2} \mathbf{u} \cdot \mathbf{u} + p \right). \tag{2.54}$$

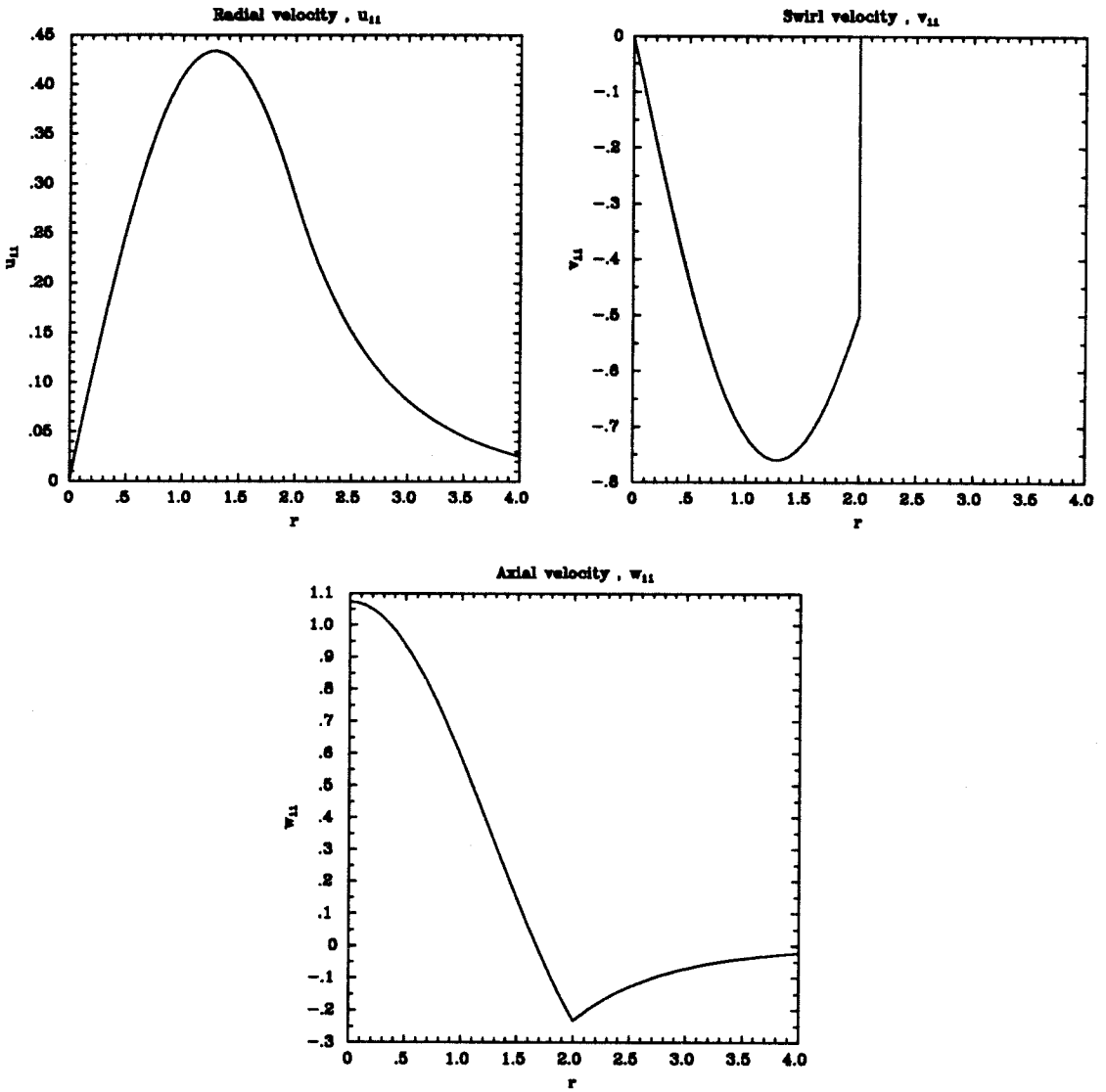

Fig. 5.2a: Linear eigenfunctions for inner and outer regions. The unperturbed boundary is at $a_{00} = 2$. $T_0 = 1/4$.

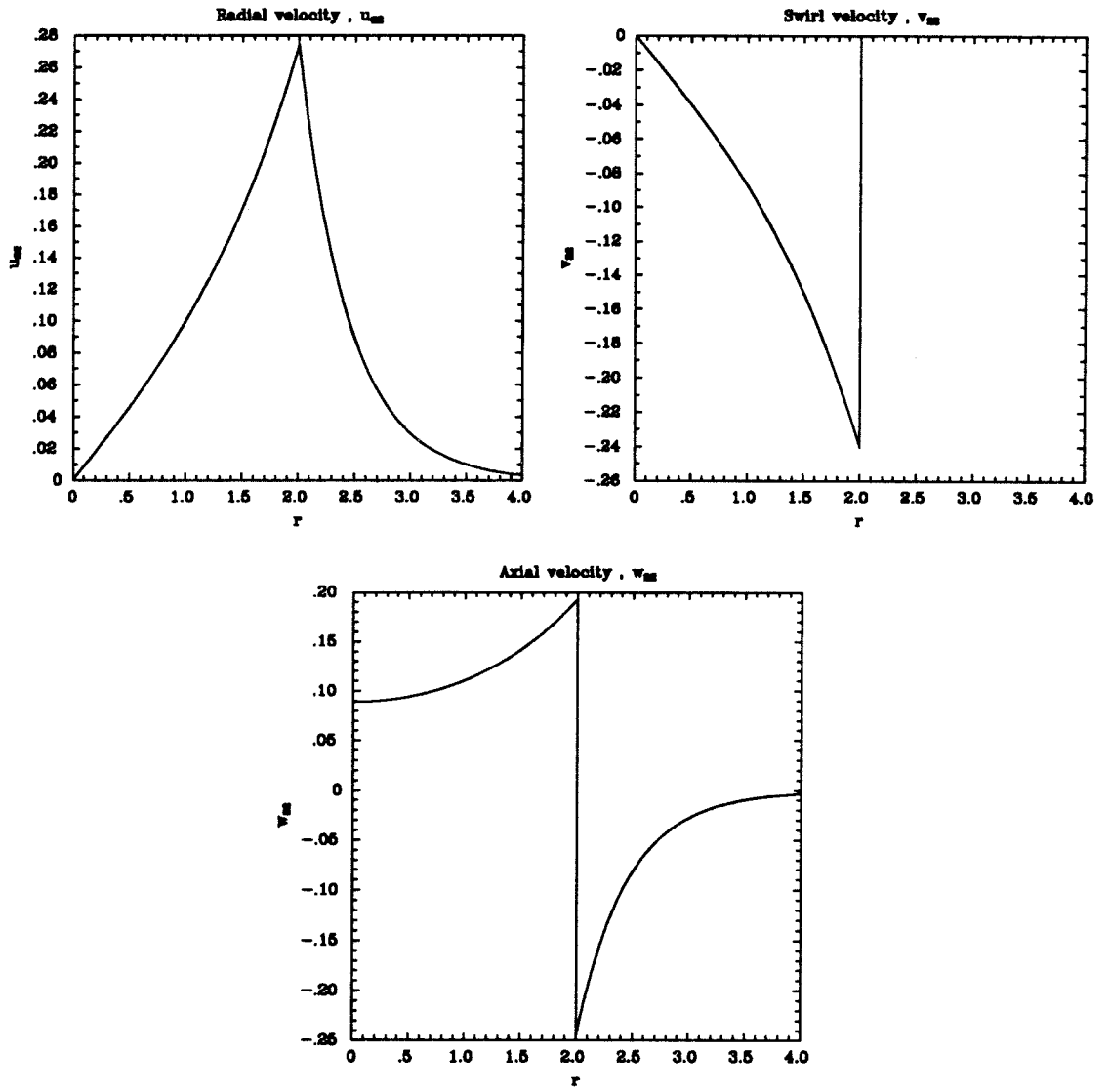

Fig. 5.2b: Second order solution for inner and outer regions. The unperturbed boundary is at $a_{00} = 2$. $T_0 = 1/4$. The quantity $D_{22<}$ is positive in this case.

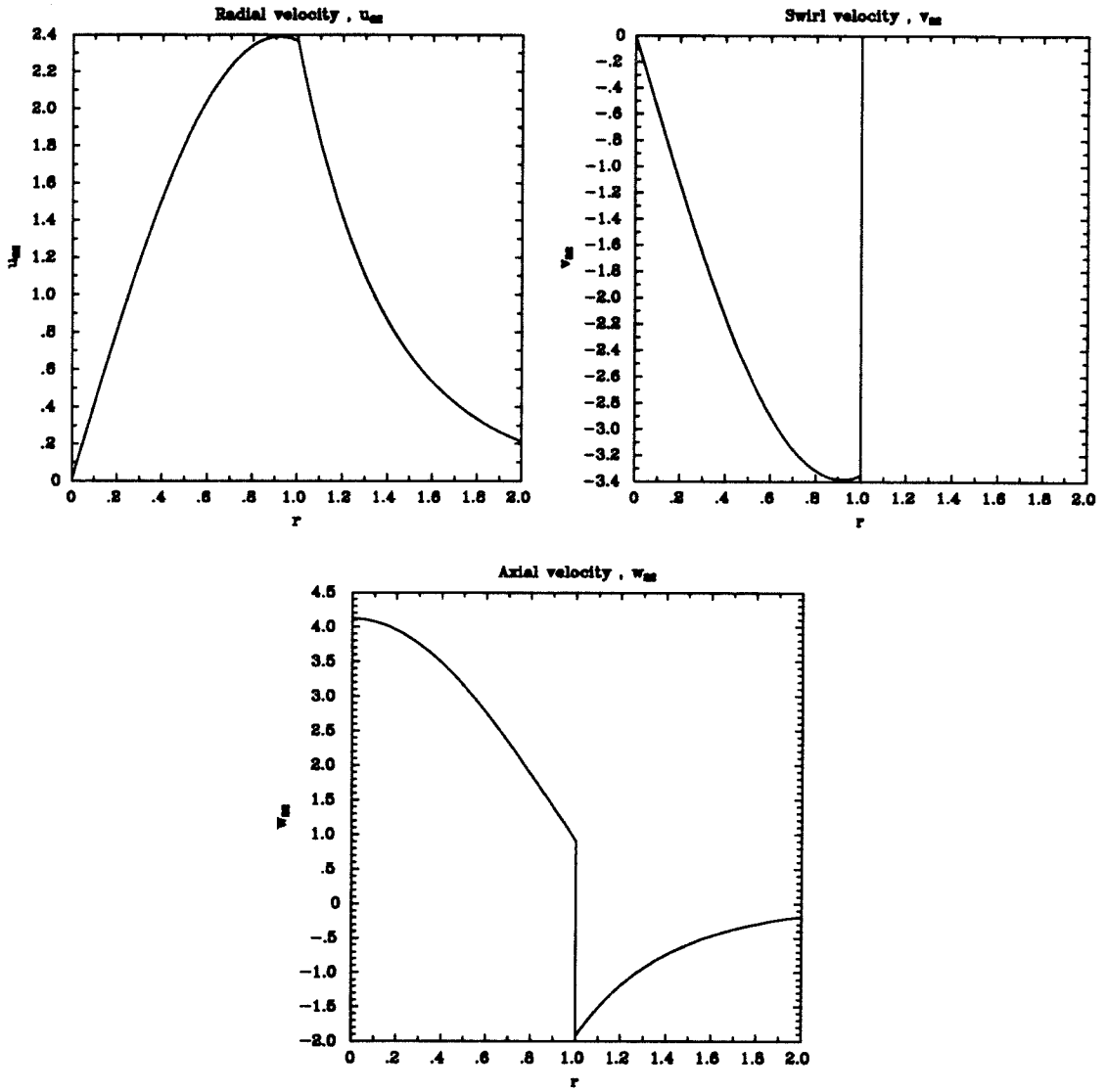

Fig. 5.2c: Second order solution for inner and outer regions. The unperturbed boundary is at $a_{00} = 1$. $T_0 = 1$. The quantity $D_{22<}$ is negative in this case.

We denote the quantity in the brackets on the right-hand-side of equation (2.54) by H, the Bernoulli function. The swirl component of the momentum equation (2.54) can be re-written in the form

$$\frac{D(rv)}{Dt} = 0, \tag{2.55}$$

where D/Dt represents the material derivative. We represent the quantity rv by Ω, the circulation function. Thus

$$H = p + \frac{1}{2}(u^2 + v^2 + w^2), \qquad \Omega = vr. \tag{5.56}$$

Equation (2.55) represents the constancy of the circulation round a material curve in the form of a circle centered on the axis of symmetry and normal to it. When the motion is steady, a material element moves along a streamline and thus moves on the surface of revolution formed by rotating the curve in the axial plane given by ψ = constant, about the axis of symmetry. Then, from Bernoulli's theorem and from (2.55), it follows that

$$p + \frac{1}{2}(u^2 + v^2 + w^2) = H(\psi), \qquad rv = \Omega(\psi), \tag{5.57}$$

where H and Ω are arbitrary functions of ψ. We determine the mean flow corrections by specifying the dependence of H and Ω on ψ.

We assume that the circulation of the perturbed filament is the same as that of the unperturbed one. This implies then

$$\Omega_> = rv_> = rv_{00_>} = T_0 a_{00}^2, \tag{5.58}$$

which is a constant. This immediately gives

$$v_{02_>} = 0. \tag{5.59}$$

Since the flow outside the core is irrotational, we require that the Bernoulli function be independent of r and x. Its value, however, differs from that of the base flow and depends on ε. We assume that

$$H_> = H_{00>} + \varepsilon^2 H_{02_>} + \cdots, \tag{5.60}$$

where $H_{02_>}$, $H_{04_>}$ etc., are constants to be determined. Substituting the assumed expansions for pressure and velocities into (5.60) we get,

$$p_{02_>} + w_{00_>} w_{02_>} + \frac{1}{4} u_{11_>}^2 + \frac{1}{4} w_{11_>}^2 = H_{02_>}. \tag{5.61}$$

We can show by integrating (5.17) that

$$p_{02_>} = -\frac{1}{4\kappa^2} w_{11_>}'^2 - \frac{1}{4} w_{11_>}^2 + A_{02_>}, \tag{5.62}$$

where $A_{02_>}$ is a constant. Upon eliminating the pressure between (5.61) and (5.62), we get

$$A_{02_>} - \frac{\alpha_0}{\kappa} w_{02_>} = H_{02_>}. \tag{5.63}$$

Since $A_{02_>}$ and $H_{02_>}$ are constants, it follows from (5.63) that $w_{02_>}$ is also a constant. This is consistent with the fact that the flow at infinity must be corrected for finite amplitude effects. In other words, this is equivalent to expanding the phase speed.

Now we consider the flow inside the core. Since this fluid is rotational, we know that both H and Ω are arbitrary functions of stream function ψ. The solution is made unique by fixing the form of this functional dependence of H and Ω on ψ. Since the base flow naturally selects a functional form, we will take that function to hold for all amplitudes. Now, from the definition of stream-function we have,

$$u = -\frac{\kappa}{r} \psi_x(r, x), \qquad w = \frac{1}{r} \psi_r(r, x). \tag{5.64}$$

Evaluating (5.56) for the base flow gives us,

$$\Omega_{00_<} = -\frac{2\kappa T_0}{\alpha_0} \psi_{00_<}, \qquad H_{00_<} = -\frac{2\kappa T_0^2}{\alpha_0} \psi_{00_<} + \frac{\alpha_0^2}{2\kappa^2}. \tag{5.65}$$

Now we make the assumption that the following be true for all orders of expansion,

$$\Omega_< = -\frac{2\kappa T_0}{\alpha_0} \psi_<, \qquad H_< = -\frac{2\kappa T_0^2}{\alpha_0} \psi_< + \frac{\alpha_0^2}{2\kappa^2}. \tag{5.66}$$

An expansion similar to (5.8) is assumed for the stream-function and is substituted into (5.66) to get,

$$r v_{02_<} = -\frac{2\kappa T_0}{\alpha_0} \psi_{02_<}. \tag{5.67}$$

By setting $v_{02<} = g'_{02<}$, we may integrate (5.17) to get

$$p_{02<} = -\frac{\alpha_0^2(\alpha_0^2+4T_0^2)}{4\kappa^2 D_{11<}^2} w''_{11<} - \frac{1}{4} w_{11<}^2 + 2T_0 g_{02<} + A_{02<}. \tag{5.68}$$

We evaluate $H_<$ using (5.56) and, as before, collect coefficients of like powers of ε and separate harmonics. We obtain,

$$H_{02<} = 2T_0 g_{02<} + A_{02<} + T_0 r v_{02<} - \frac{\alpha_0}{\kappa} w_{02<}. \tag{5.69}$$

By eliminating the stream-function using (5.66) we get $H_{02<} = T_0 r v_{02<}$. Using this in the equation above yields $w_{02<} = (2\kappa T_0/\alpha_0) g_{02<} + (\kappa/\alpha_0) A_{02<}$. Since by definition we have $w = \psi_r/r$, we can eliminate the axial component and obtain the following equation,

$$g''_{02<} + \frac{1}{r} g'_{02<} + \nu_0^2 g_{02<} = -\frac{2\kappa^2 T_0}{\alpha_0^2} A_{02<}, \tag{5.70}$$

where

$$\nu_0 = \frac{2\kappa T_0}{\alpha_0}. \tag{5.71}$$

The solution of (5.70) is given by,

$$g_{02<} = b_{02<} J_0(\nu_0 r) - \frac{A_{02<}}{2T_0}, \tag{5.72}$$

where $b_{02<}$ is a constant. Using this we may evaluate

$$w_{02<} = \frac{2\kappa T_0}{\alpha_0} b_{02<} J_0(\nu_0 r). \tag{5.73}$$

Now we use the boundary condition (5.29) to get

$$2T_0 b_{02<} J_0(\nu_0 a_{00}) - A_{02>} + H_{02>} = a_{11}^2 2T_0^2. \tag{5.74}$$

There remains now only one condition (5.28). Using this constraint and simplifying we get the correction to the Bernoulli constant outside the core to be

$$\begin{aligned} H_{02>} = A_{02>} &+ \frac{2T_0\alpha_0}{\kappa} J_0(\nu_0 a_{00}) a_{02} \\ &+ a_{11}^2 \left[2T_0^2 - \frac{T_0\alpha_0}{\kappa} \frac{J_0(\nu_0 a_{00})}{J'_0(\nu_0 a_{00})} \left(\nu_1 \frac{J_0(\nu_1 a_{00})}{J'_0(\nu_1 a_{00})} - \frac{1}{2a_{00}} \right) \right]. \end{aligned} \tag{5.75}$$

The constant associated with the pressure ($A_{02_>}$) can be absorbed into the Bernoulli constant. We still have an undetermined constant, *viz.*, a_{02}. This, however, is to be determined at the third order in the usual manner by requiring that the solution is free of any resonance.

Further we notice that the constant associated with pressure inside the core ($A_{02_<}$) dropped out of the equations. If we were to make pressure continuous across the interface, it would also get fixed.

The assumption made in (5.66) has been crucial in fixing the solution. This, however, is not the only way to fix the solution branch. We could assume any arbitrary functional dependence of H and Ω on ψ. Clearly, there are an infinite number of choices. Another possibility is that assumed by Hafez *et al.* (1986) or by Leibovich (1990) in which the circulation has a fixed functional form except for a scaling factor which depends on the amplitude. We adopt yet another method to fix the solution branch for the full nonlinear Euler equations in which the solution path is characterized by each solution having the same axial mean as that of the base flow. This forms the subject of the following chapter. If we restrict the solutions for the present case so that the solution correct to the second order in ε is to have the same axial mean as that of the base flow, we find that the continuity of velocity across the core boundary cannot be maintained. Specifically, the condition (5.29) cannot be satisfied. We can, however, find a solution such that the pressure and the normal velocity across the core boundary is continuous. This yields the same second order quantities with subscripts (2,2) as in the solution with velocity continuity condition across the core boundary. But the form of quantities with subscripts (0,2), i.e., the mean flow corrections, differ. It is shown in the next chapter that the solution with the axial mean the same as the base flow gives rise to a vortex sheet bound to the core boundary. We can extend the second order solution with continuous velocity across the core boundary to arbitrary order in ε. This is considered in the next section. The question of whether we can extend the solution that has the same axial mean

as the base flow to arbitrary orders in ε and with a vortex sheet bound to the core boundary, is not considered here. An answer to this question is not evident from the second order solution.

5.7 Extension to large orders

The solution procedure discussed above may be continued to any order in the expansion parameter ε. However, the algebra becomes too involved and it proves to be difficult to proceed by hand. We can make use of the conditions imposed on the Bernoulli function and the circulation function to extend the solution to large orders. When the flow is steady, the Euler equations may be restated in terms of the stream function as

$$\psi_{rr} - \frac{1}{r}\psi_r + \psi_{zz} = r^2 \frac{dH}{d\psi} - \Omega(\psi)\frac{d\Omega}{d\psi}. \tag{5.76}$$

The above equation is sometimes called the Bragg-Hawthorne equation or the Squire-Long equation (see Leibovich & Kribus, 1990 for a further account of this equation). For a simple derivation see Batchelor(1967). Since the functional forms of H and Ω are held fixed and given by (5.66), equation (5.76) becomes,

$$\psi_{rr} - \frac{1}{r}\psi_r + \kappa^2\psi_{xx} = \frac{2T_0^2}{W_0} r^2 - \frac{4T_0^2}{W_0^2}\psi, \qquad \text{for} \quad r < R(x), \tag{5.77}$$

where

$$W_0 = w_{00}, \tag{5.78}$$

and since the flow is irrotational outside the core we get,

$$\psi_{rr} - \frac{1}{r}\psi_r + \kappa^2\psi_{xx} = 0, \qquad \text{for} \quad r > R(x), \tag{5.79}$$

where $x = \kappa z$ and $R(x)$ defines the core boundary. We now assume the following form for the stream function

$$\psi(r,x) = \psi_0(r) + \sum_{k=1}^{\infty} \psi_k(r)\cos(kx). \tag{5.80}$$

Further, each of the modes is expanded in powers of ε and assumed to be of the form

$$\psi_k = \varepsilon^k \left(\psi_{k,k} + \varepsilon^2\psi_{k,k+2} + \cdots\right). \tag{5.81}$$

We substitute (5.80) in (5.77) and (5.79) and solve the resulting equations at each order. The solution inside the core is either proportional to rI_1 or rJ_1 depending on the sign of coefficient of $\psi_{k,l_<}$. This sign in turn depends on the choice of parameters a_{00}, T_0 and W_0. We get,

$$\psi_{kl_<} = A_{kl}\frac{r}{a_{00}}\frac{I_1(\theta_k r)}{I_1(\theta_k a_{00})}, \qquad \text{if} \quad W_0^2 > 4T_0^2/\kappa^2 k^2, \tag{5.82a}$$

$$\psi_{kl_<} = A_{kl}\frac{r}{a_{00}}\frac{J_1(\theta_k r)}{J_1(\theta_k a_{00})}, \qquad \text{if} \quad W_0^2 < 4T_0^2/\kappa^2 k^2, \tag{5.82b}$$

when $r < R(x)$ and

$$\psi_{kl_>} = B_{kl}\frac{r}{a_{00}}\frac{K_1(\kappa k r)}{K_1(\kappa k a_{00})}, \tag{5.83}$$

when $r > R(x)$. The constants A_{kl} and B_{kl} are to be determined by matching the velocity across the core boundary as before. Now we give the form of velocities. Inside the core we have

$$u_{kl_<} = A_{kl}\frac{\kappa k}{a_{00}}M_{1k}(r), \tag{5.84a}$$

$$v_{kl_<} = A_{kl}\frac{2T_0}{a_{00}W_0}M_{1k}(r), \tag{5.84b}$$

$$w_{kl_<} = A_{kl}\frac{\theta_k}{a_{00}}M_{2k}(a_{00})M_{0k}(r), \tag{5.84c}$$

and outside the core we have

$$u_{kl_>} = B_{kl}\frac{\kappa k}{a_{00}}N_{1k}(r), \tag{5.85a}$$

$$v_{kl_>} = 0, \tag{5.85b}$$

$$w_{kl_>} = B_{kl}\frac{\kappa k}{a_{00}}N_{2k}(a_{00})N_{0k}(r). \tag{5.85c}$$

If $W_0^2 > 4T_0^2/\kappa^2 k^2$ then,

$$M_{0k}(r) = \frac{J_0(\theta_k r)}{J_0(\theta_k a_{00})}, \quad M_{1k}(r) = \frac{J_1(\theta_k r)}{J_1(\theta_k a_{00})}, \quad M_{2k}(r) = \frac{J_0(\theta_k r)}{J_1(\theta_k r)}, \tag{5.86}$$

where

$$\theta_k = \left[(4T_0^2 - \kappa^2 k^2 W_0^2)/W_0^2\right]^{1/2}, \tag{5.87}$$

and, if $W_0^2 < 4T_0^2/\kappa^2 k^2$ then,

$$M_{0k}(r) = \frac{I_0(\theta_k r)}{I_0(\theta_k a_{00})}, \quad M_{1k}(r) = \frac{I_1(\theta_k r)}{I_1(\theta_k a_{00})}, \quad M_{2k}(r) = \frac{I_0(\theta_k r)}{I_1(\theta_k r)}, \tag{5.88}$$

where

$$\theta_k = \left[(\kappa^2 k^2 W_0^2 - 4T_0^2)/W_0^2\right]^{1/2}, \tag{5.89}$$

and finally,

$$N_{0k}(r) = \frac{K_0(\kappa k r)}{K_0(\kappa k a_{00})}, \quad N_{1k}(r) = \frac{K_1(\kappa k r)}{K_1(\kappa k a_{00})}, \quad N_{2k}(r) = \frac{K_0(\kappa k r)}{K_1(\kappa k r)}. \tag{5.90}$$

Note that (5.85b) is a result of our assumption that the filament has the same circulation. Also the eigenfunctions identically satisfy the boundary conditions at the origin and as $r \to \infty$.

If $k = 0$ the forms given by (5.85) need to be modified. The appropriate forms are,

$$u_{0l_>} = 0, \qquad w_{0l_>} = B_{kl}, \tag{5.91a}$$

and

$$v_{0l_>} = 0, \quad l \neq 0. \tag{5.91b}$$

5.8 Method of solution

The solution at various orders is found by matching the velocity at the core boundary. We proceed, as before, by expanding the velocities into a Fourier series and further expanding the Fourier coefficients into a power series in ε. We evaluate the velocities on the inner and outer side of the interface and equate them. As in section 5.3, this leads us to a set of conditions to be satisfied by the expansion coefficients of the velocities. The algebra is done via a FORTRAN code in this case. The jump conditions set out in (5.22) through (5.29) are carried out to arbitrary order. We skip the details of programming and focus on the structure of the linear systems to be solved at each stage.

When $k > 1$, we find

$$u_{kl_<} - u_{kl_>} = F_1, \tag{5.92a}$$

$$v_{kl<} - v_{kl>} + \left(v'_{00<} - v'_{00>}\right) a_{kl} = F_2, \tag{5.92b}$$

$$w_{kl<} - w_{kl>} = F_3, \tag{5.92c}$$

where, F_1, F_2 and F_3 are computed from the jump conditions and they depend on the lower order solution. Using the known forms for the eigenfunctions, we rewrite the above equations as,

$$\frac{\kappa k}{a_{00}} A_{kl} - \frac{\kappa k}{a_{00}} B_{kl} = F_1, \tag{5.93a}$$

$$\frac{2T_0}{a_{00} W_0} M_{2k}(a_{00}) A_{kl} + 2T_0 a_{kl} = F_2, \tag{5.93b}$$

$$\frac{\theta_k}{a_{00}} M_{2k}(a_{00}) A_{kl} + \frac{\kappa k}{a_{00}} N_{2k}(a_{00}) B_{kl} = F_3. \tag{5.93c}$$

The three equations in three unknowns, A_{kl}, B_{kl} and a_{kl} are easily solved for $k > 1$.

The cases $k = 0$ and $k = 1$ are treated separately. When $k = 1$, the system (5.93) becomes singular. When $k = 0$ we have three unknowns and only two constraints since the continuity of the radial velocity does not contribute. The two cases of $k = 1$ and $k = 0$ are solved simultaneously. First we note that when k is even, l is also even and when k is odd l is odd. We start with the linear solution which corresponds to $k = 1$ and $l = 1$. At the second order we first determine the constants $A_{2,2}$, $B_{2,2}$ and $a_{2,2}$. We next determine the third order constants $A_{3,3}$, $B_{3,3}$ and $a_{3,3}$. The constants $A_{0,2}$, $B_{0,2}$, $a_{0,2}$, $A_{1,3}$, $B_{1,3}$ and $a_{1,3}$ are determined simultaneously. This completes the solution to third order. Similarly we complete the solution to fifth order and so on to some order $l-2$ where $l-2$ is odd. Let $l = 2p+1$. We describe the determination of solution to order $l-1$ and l. Using (5.93), we find all constants except $A_{0,2p}$, $B_{0,2p}$ and $a_{0,2p}$. As noted, this system associated with subscript $(0, 2p)$ lacks an equation. We require an amplitude condition which defines the perturbation parameter ε. We use the semi-wave height given by

$$2\varepsilon = R(0) - R(\pi). \tag{5.94}$$

On using (5.19) and equating powers of ε we get

$$a_{11} = 1, \tag{5.95}$$

and

$$a_{1l} = -\left(a_{3l} + a_{5l} + \cdots + a_{ll}\right), \qquad l = 2p+1. \tag{5.96a}$$

The other two equations that result from continuity of velocity are

$$\frac{2T_0}{a_{00}W_0}\, A_{0,2p} + 2T_0\, a_{0,2p} = G_1, \tag{5.96b}$$

$$\frac{\theta_0}{a_{00}}\, M_{2,0}\, A_{0,2p} - \, B_{0,2p} = G_2. \tag{5.96c}$$

The system (5.96) is still not closed because we have four unknowns ($A_{0,2p}$, $B_{0,2p}$, $a_{0,2p}$ and $a_{1,2p+1}$) but only three equations. We solve this together with equations for the $(1, 2p+\ 1\ )$ system given by

$$\frac{\kappa}{a_{00}}\, A_{1,2p+1} - \frac{\kappa}{a_{00}}\, B_{1,2p+1} + \left(A_{11}\frac{\kappa}{a_{00}}\, M'_{11} - B_{11}\frac{\kappa}{a_{00}}\, N'_{11}\right)\, a_{0,2p} = G_3, \tag{5.96d}$$

$$\begin{aligned}\frac{2T_0}{W_0 a_{00}}\, A_{1,2p+1} + 2T_0\, a_{1,2p+1} + \frac{a_{11}2T_0}{W_0 a_{00}}\, M'_{1,0}\, A_{0,2p} \\ + \left[a_{11}(v''_{00<} - v''_{00>}) + (v'_{11<} - v'_{11>})\right]\, a_{0,2p} = G_4,\end{aligned} \tag{5.96e}$$

$$\begin{aligned}\frac{\theta_1}{a_{00}}\, M_{2,1}\, A_{1,2p+1} + \frac{\kappa}{a_{00}}\, N_{2,1}\, B_{1,2p+1} + \frac{\theta_0}{a_{00}}\, M_{2,1}M'_{0,1}\, A_{0,2p} \\ + \left[A_{11}\frac{\theta_1}{a_{00}}\, M_{2,1}M'_{0,1} + B_{11}\frac{\kappa}{a_{00}}\, N_{2,1}N'_{0,1}\right]\, a_{0,2p} = G_5.\end{aligned} \tag{5.96f}$$

Here, primes denote derivatives with respect to r. All the functions and their derivatives are evaluated at $r = a_{00}$. The quantities G_1 through G_5 are evaluated from the given jump conditions. Now the system (5.96) is closed with six equations and the six unknowns $A_{0,2p}$, $B_{0,2p}$, $a_{0,2p}$, $A_{1,2p+1}$, $B_{1,2p+1}$ and $a_{1,2p+1}$. If the system (5.96) is non-singular, then it gives a unique solution. There may be a set of parameters for which the system might become singular. We did not come across any for the cases tried. Since $W_0 = -\alpha_0/\kappa$ is an eigenvalue of the linear system, the coefficient of $a_{0,2p}$ in (5.96d) must vanish. This follows from the dispersion relation. Therefore, this

provides us with a check on the calculations. The system (5.96) is to be solved only after the constants $(3, l)$ through (l, l) are found. This restriction is due to (5.96a).

Once the coefficients $A_{i,j}$, $B_{i,j}$ and $a_{i,j}$ are found, the velocity coefficients $u_{i,j}$, $v_{i,j}$ and $w_{i,j}$ can be determined from (5.84), (5.85) and (5.91). As $r \to \infty$, the swirl and the radial components of the velocity vanish while the axial velocity reaches a value that is independent of x. From (5.91) it is easily seen that

$$\lim_{r\to\infty} w(r, x) = W_0 + \varepsilon^2 B_{0,2} + \varepsilon^4 B_{0,4} + \cdots.$$

A typical variation of axial velocity at infinity with the wave amplitude is shown in Figure 5.3. It shows that the axial velocity increases in magnitude with ε. The series summation is considered next.

5.9 Padé summation

Once the solution is determined in the form of coefficients of the perturbation series, we need to construct the solution at some value of ε at some physical location. This is performed by evaluating the sums by the method of Padé summation. This we describe here briefly. For details on this and an excellent algorithm for constructing the Padé approximants, we refer to Bender & Orszag (1978). Consider for example, the task of finding the value of the axial velocity at $r = 0$ and $x = 0$ for some value of ε. This would first require computation of the coefficients $w_{l<}$ for $l = 0, 1, \ldots m$. Now consider the computation of the coefficient $w_{0<}$ at $r = 0$. This term is given by the sum

$$w_{0<}(r = 0) = w_{0,0<}(0) + w_{0,2<}(0)\delta + w_{0,4<}(0)\delta^2 + \cdots, \tag{5.97}$$

where we have set $\delta = \varepsilon^2$. The sum represented by (5.97) is a power series in the variable δ with the known coefficients $w_{l,k}$. The idea of Padé summation is to replace the power series (5.97) by a sequence of rational functions of the form

$$P_M^N(\delta) = \frac{\sum_{n=0}^{N} a_n \delta^n}{\sum_{n=0}^{M} b_n \delta^n}, \quad b_0 = 1. \tag{5.98}$$

The coefficients a_n and b_n are found by matching the first $(M + N + 1)$ terms in the Taylor series expansion of P_M^N with the first $(M + N + 1)$ terms in the power series

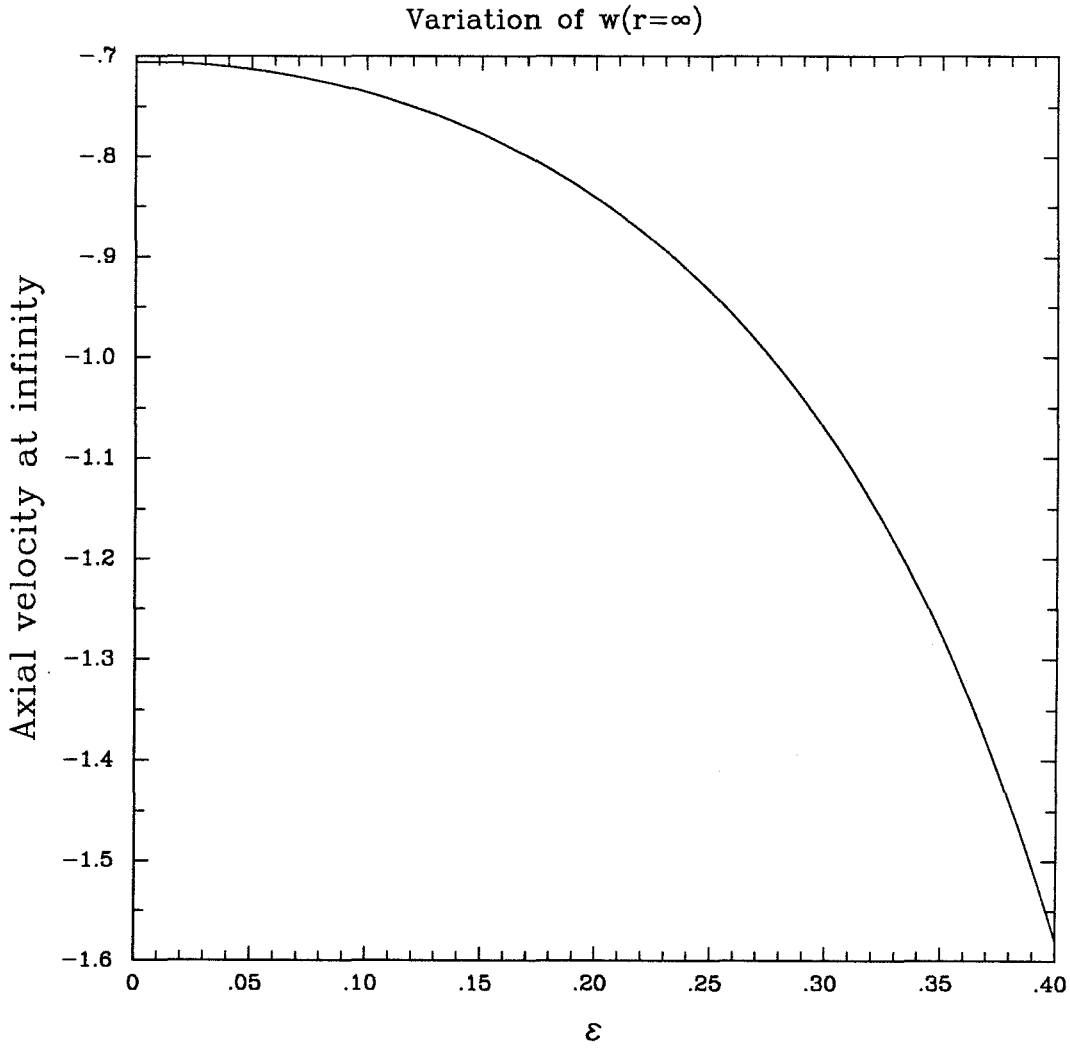

Fig. 5.3 The axial velocity at $r = \infty$ is shown here as a function of the semi-wave height ε for a vortex with core radius of $a_{00} = 1$ and a total circulation of one.

Table 5.2 Coefficients for $w_{0<}$ term.

The coefficients contributing to the term $w_{0<}$ are shown here. The parameters were $a_{00} = 1$, $T_0 = 1$, $\kappa = 1$.

j	$w_{0,j<}$
0	$-7.059052\ 10^{-1}$
2	$3.089275\ 10^{-1}$
4	$1.542953\ 10^{+1}$
6	$-1.935112\ 10^{+1}$
8	$4.009085\ 10^{+2}$
10	$-2.777568\ 10^{+3}$
12	$2.552956\ 10^{+4}$
14	$-2.324963\ 10^{+5}$
16	$2.205574\ 10^{+6}$
18	$-2.145395\ 10^{+7}$
20	$2.133385\ 10^{+8}$

Table 5.3 Convergence of the Padé Sequence.

The convergence of the Padé sequence for the coefficients shown in Table 5.2 is given here for the case of $\delta = \varepsilon^2 = 0.1$.

n	P_M^N	*Sum*
0	P_0^0	−0.7059052
1	P_1^0	−0.6763077
2	P_1^1	−0.7136389
3	P_2^1	−0.5618688
4	P_2^2	−0.5021175
5	P_3^2	−0.5162811
6	P_3^3	−0.5136962
7	P_4^3	−0.5143003
8	P_4^4	−0.5142114
9	P_5^4	−0.5142323
10	P_5^5	−0.5142278

(5.97). The rational function P_M^N so computed is known as the Padé approximant. The limit of P_M^N as N and $M \to \infty$ is the required sum represented by (5.97). Table 5.2 shows the coefficients occurring in (5.97) and Table 5.3 shows the approximants P_0^0, P_1^0, P_1^1, ... The summation was done with $\delta = 0.1$. The Padé sequence clearly converges. A smaller number of Padé approximants is needed for required convergence if the value of the perturbation parameter ε is smaller.

5.10 Results

The expansion coefficients were computed up to 21 orders in ε. For a given value of ε the expansion coefficients were summed using the Padé summation technique. The values of $R(x)$ were computed as follows. Define

$$\tilde{a}_k = a_{k,k} + a_{k,k+2}\delta + a_{k,k+4}\delta^2 + \cdots, \quad k = 0, 1, \ldots, m, \tag{5.99}$$

where $\delta = \varepsilon^2$. Now for a fixed value of x the location of the interface can be represented as a power series in ε given by

$$R(x) = \sum_{k=0}^{m} \tilde{b}_k \varepsilon^k, \tag{5.100}$$

where the coefficients are given by

$$\tilde{b}_k = \tilde{a}_k \cos(kx). \tag{5.101}$$

We compute the values of $\tilde{a}_k$ by employing the Padé summation on the series (5.99) in the variable δ and then compute the coefficients $\tilde{b}_k$. We repeat the Padé summation on the series (5.100) in the variable ε. All other quantities such as ψ, u, v, w, etc., are summed in a similar way for a given r and x location.

We present some of the results in Figures 5.4 and 5.5. In each case a value of the core radius a_{00} is chosen and a total circulation of unity is assumed. All the solutions found here are such that there is no velocity discontinuity anywhere in the flow field including the core boundary.

In Figure 5.4a, the shape of the boundary for various values of ε for the case of $a_{00} = 1$ is shown. It shows bulging of the core about $x = 0$ and flattening about $x = \pi$. The length of the flattened trough was more pronounced for smaller values of a_{00} and less so for larger values. This appears to be similar to the surface waves on a 2 dimensional layer of uniform vorticity of height h as calculated by Broadbent and Moore (1985). The core radius a_{00} plays the role of h in our case. But for larger values of layer thickness, Broadbent and Moore observe development of a cusp in the wave profile. This was not observable in our calculations. The reason could be that we do

not have enough coefficients or that such a cusp in fact never develops. One could compute the singularities of the series represented by (5.100) which will move around in the (r, x) space as the amplitude ε is varied and perhaps make a better prediction about the formation of a cusp, if it forms at all. This was not done, however, because of the complexity as well as lack of availability of enough perturbation coefficients.

Figure 5.4b shows the axial velocity as a function of the radial distance at $x = 0$ for the case of $a_{00} = 1$, and clearly shows that flow reversal occurs when ε is between 0.1 and 0.15. The profile also clearly shows the continuity of w across the interface thus serving as a check on the accuracy of calculations.

Figure 5.5 shows the streamlines for various values of a_{00} and ε. The stream-function was computed on a uniform grid extending from $x = -\pi$ to π and $r = 0$ to $R(0)$. In general, the recirculating bubble, after making its first appearance, grows with ε. The separating streamline is nearly circular in all the cases. Also a larger bubble was formed for a vortex with a thicker core radius. A bubble was not formed for the case of $a_{00} = 3$. The indications are that a bubble will not form since the stream-line closest to the axis does not tend to become more concave near $x = 0$ while the stream-lines in the mid core region appear to do so.

The solution in the given region was found upon specifying the dependence of the Bernoulli function (H) and the circulation function (Ω) on ψ. We only need to specify the dependence at some region of the flow (say in the vicinity of $x = \pi$). The rest of the flow is exactly determined in all cases except when the recirculating bubble appears. This is accompanied by the formation of closed streamlines inside the bubble. These closed streamlines are isolated from the streamlines outside the bubble. Therefore, the solution inside the bubble need not necessarily be governed by the same dependence of H and Ω that govern the flow outside. In principle one can find an infinity of solutions each giving a different flow field inside the bubble. In the cases considered here, the region inside the bubble is also governed by the same

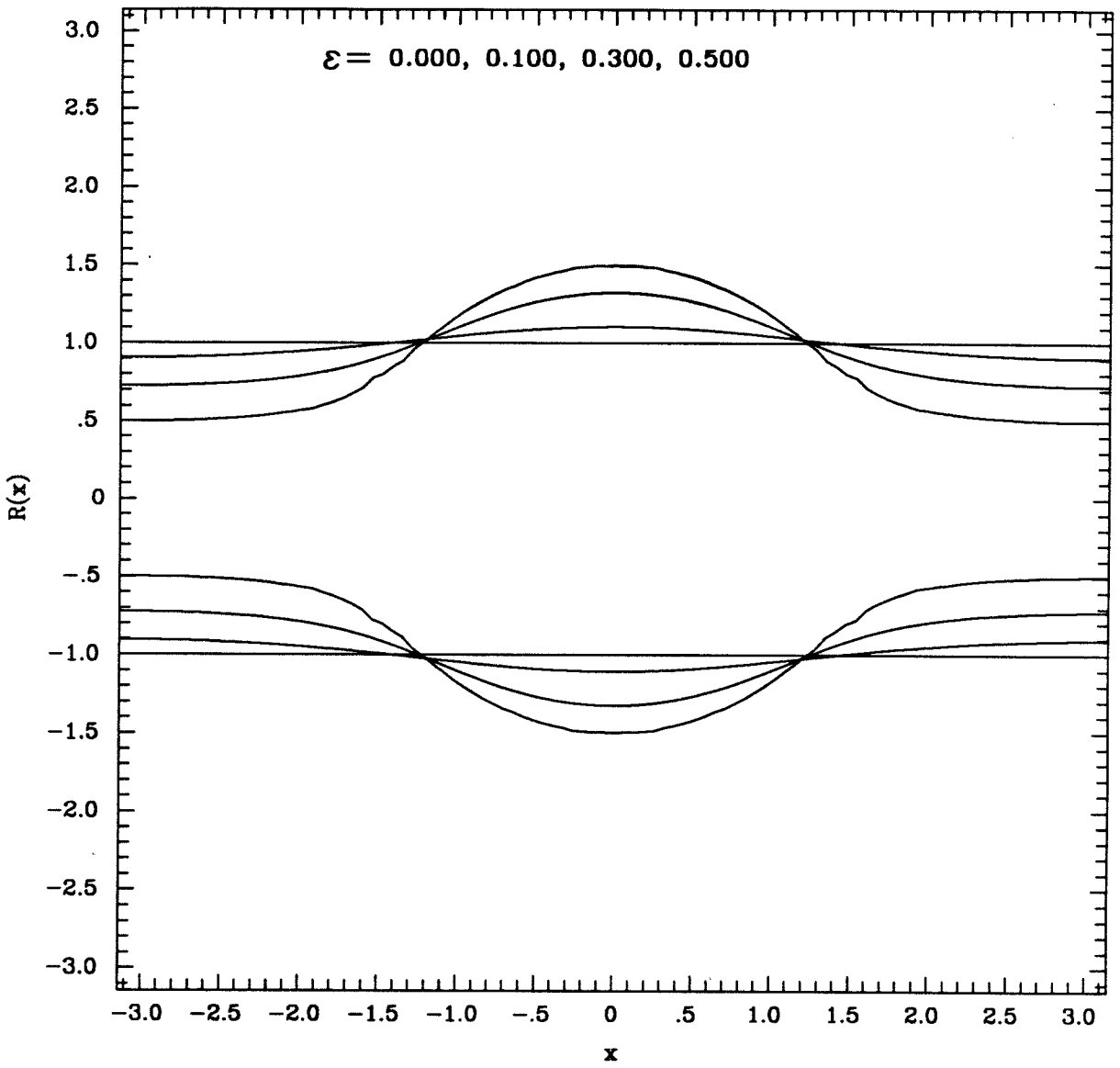

Fig. 5.4a Shape of the boundary of the vortex is shown here as a function of x for different values of ε. The symmetrically located curves on the negative side of the ordinate are drawn to give the impression of a cross section. The parameters consisted of $a_{00} = 1$ and $T_0 = 1$.

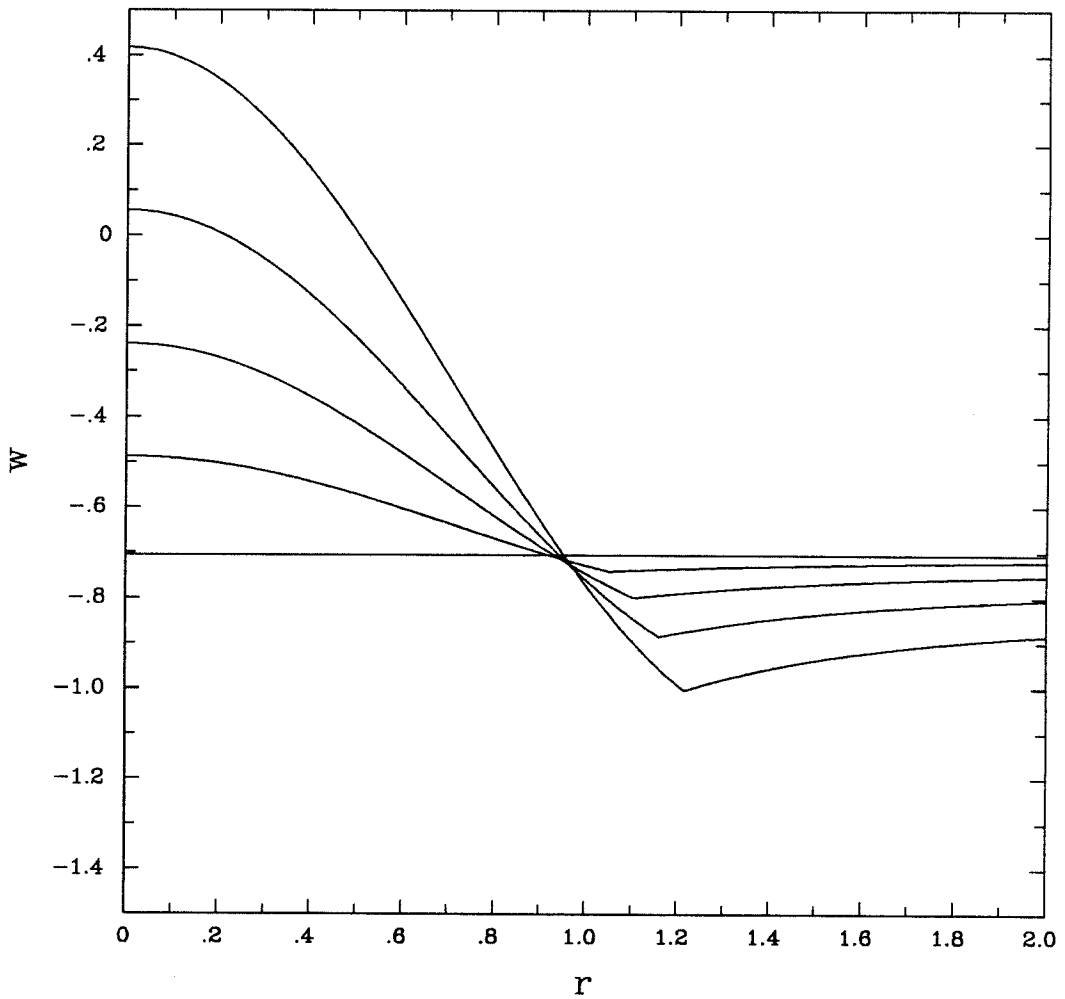

Fig. 5.4b Axial velocity as a function of the radial distance at $x = 0$ for $\varepsilon =$ 0, 0.05, 0.1, 0.15 and 0.2. Axial velocity increases at $r = 0$ with increasing ε. The corner in the profiles indicates the location of the core boundary.

dependence of H and Ω. As a side point we note that the dependence of H is linear inside the bubble as well. But this is inconsequential.

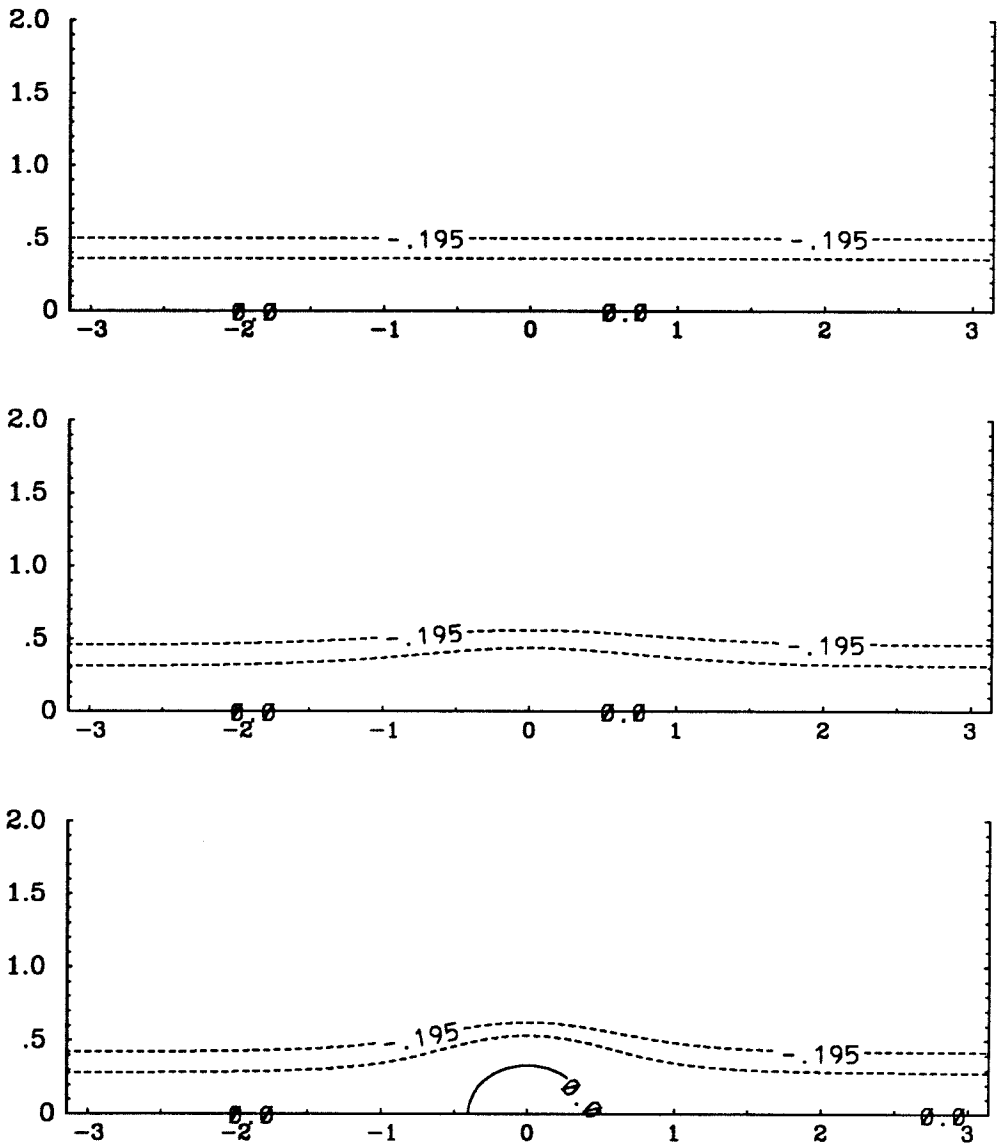

Fig. 5.5a Plot of streamlines for $\varepsilon = 0{,}0.05$ and 0.1 for a vortex with $a_{00} = 0.5$ and a total circulation of unity. The streamline with $\psi = -0.195$ coincides with the core boundary. Contour interval=0.1.

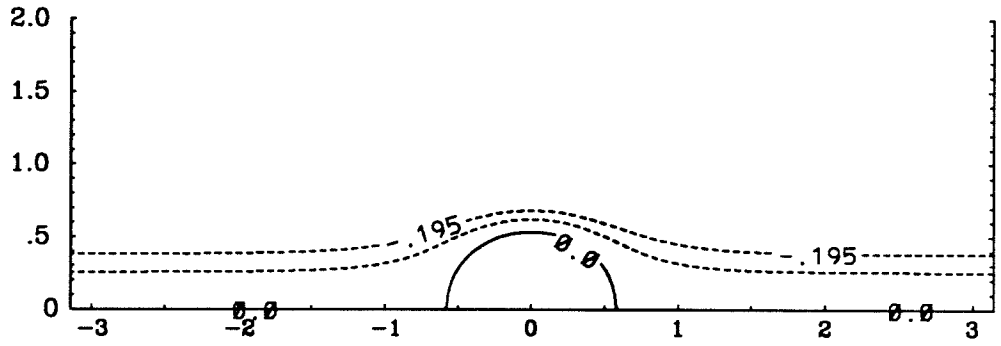

Fig. 5.5a continued. Plot of streamlines for $\varepsilon = 0.15$ for a vortex with $a_{00} = 0.5$ and a total circulation of unity. The outermost streamline with $\psi = -0.195$ coincides with the core boundary. Contour interval=0.1.

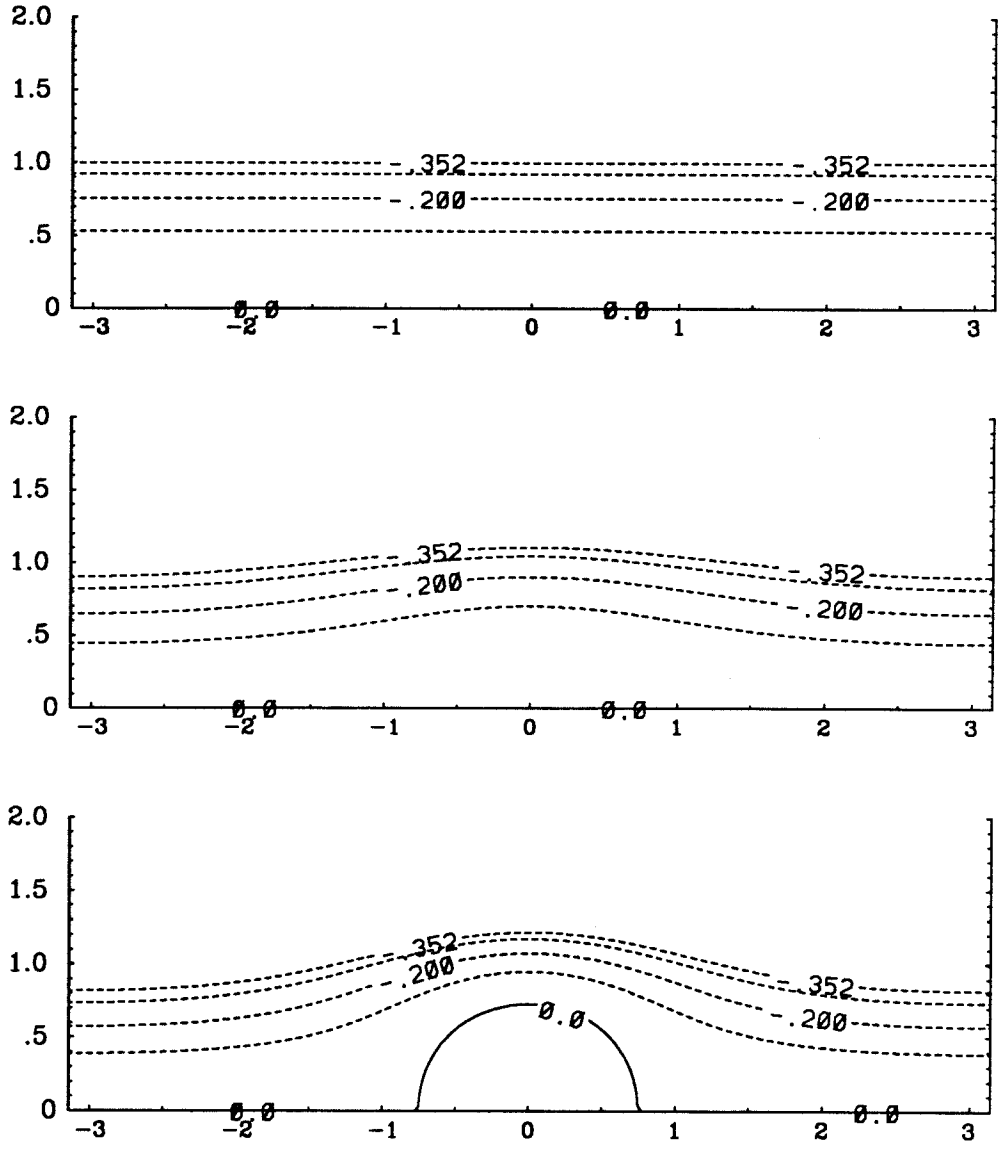

Fig. 5.5b Plot of streamlines for $\varepsilon = 0,0.1$ and 0.2 for a vortex with $a_{00} = 1.0$ and a total circulation of unity. The streamline with $\psi = -0.352$ coincides with the core boundary. Contour interval=0.1.

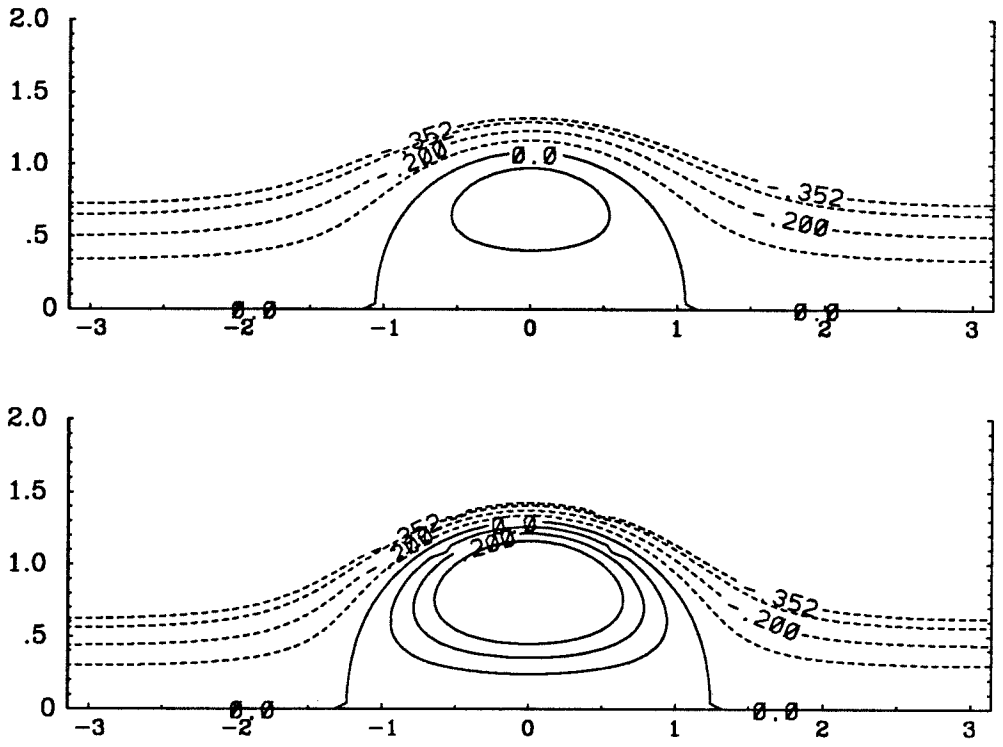

Fig. 5.5b continued. Plot of streamlines for $\varepsilon = 0.3$ for a vortex with $a_{00} = 1.0$ and a total circulation of unity. The outermost streamline with $\psi = -0.352$ coincides with the core boundary. Contour interval=0.1.

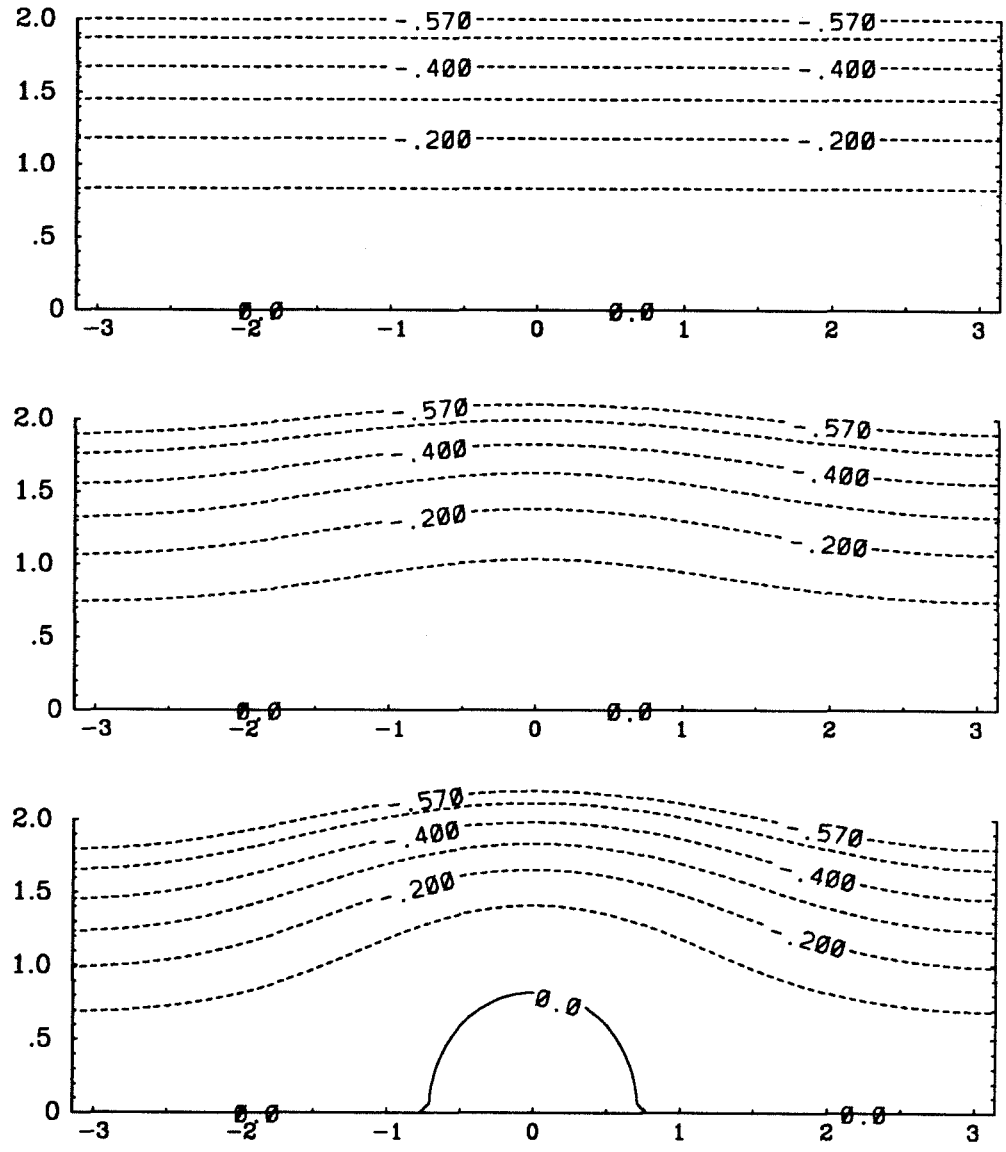

Fig. 5.5c Plot of streamlines for $\varepsilon = 0$,0.1 and 0.2 for a vortex with $a_{00} = 2$ and a total circulation of unity. The streamline with $\psi = -0.57$ coincides with the core boundary. Contour interval=0.1.

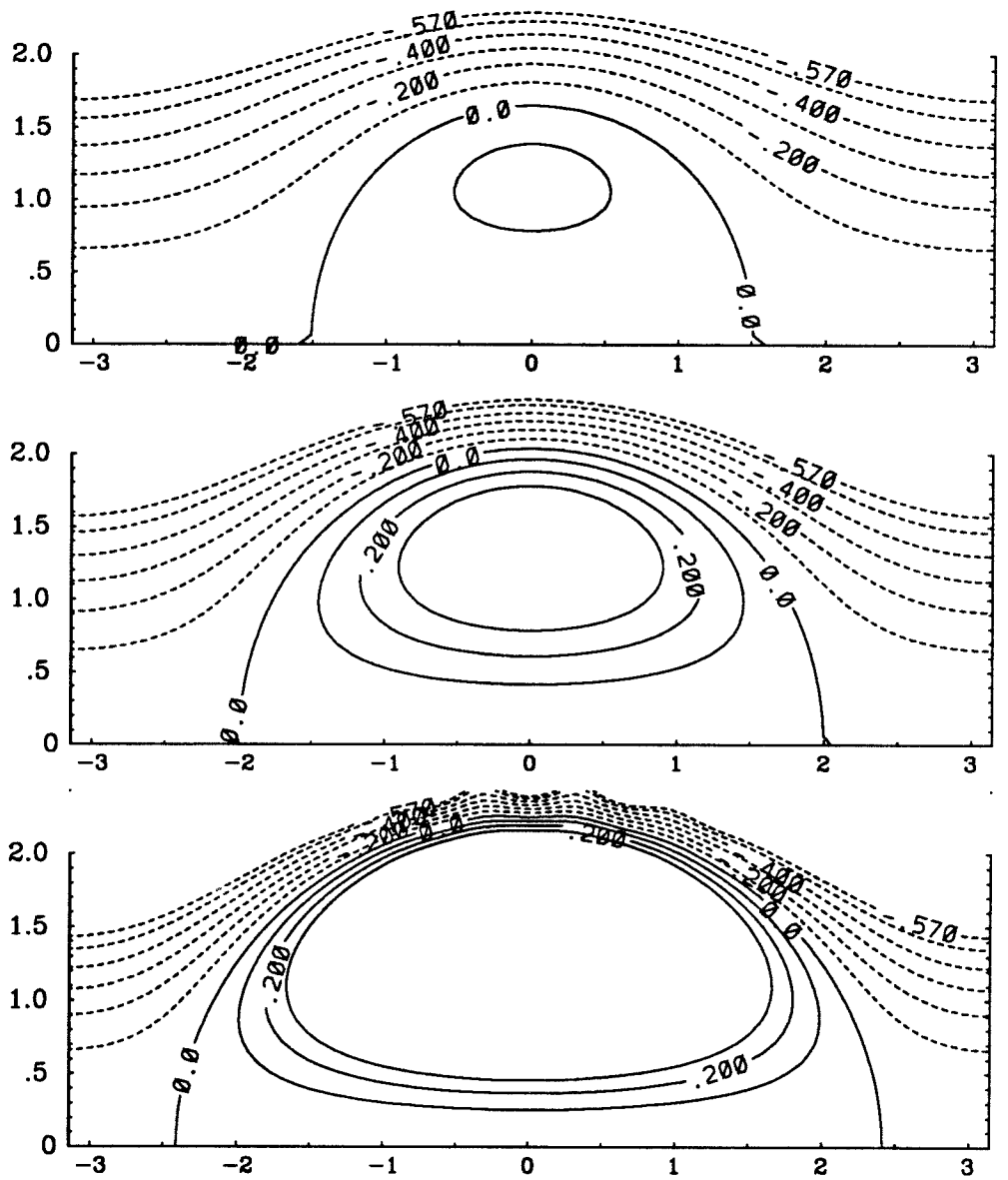

Fig. 5.5c continued. Plot of streamlines for $\varepsilon = 0.3$,0.4 and 0.5 for a vortex with $a_{00} = 2$ and a total circulation of unity. The outermost streamline with $\psi = -0.57$ coincides with the core boundary. Contour interval=0.1.

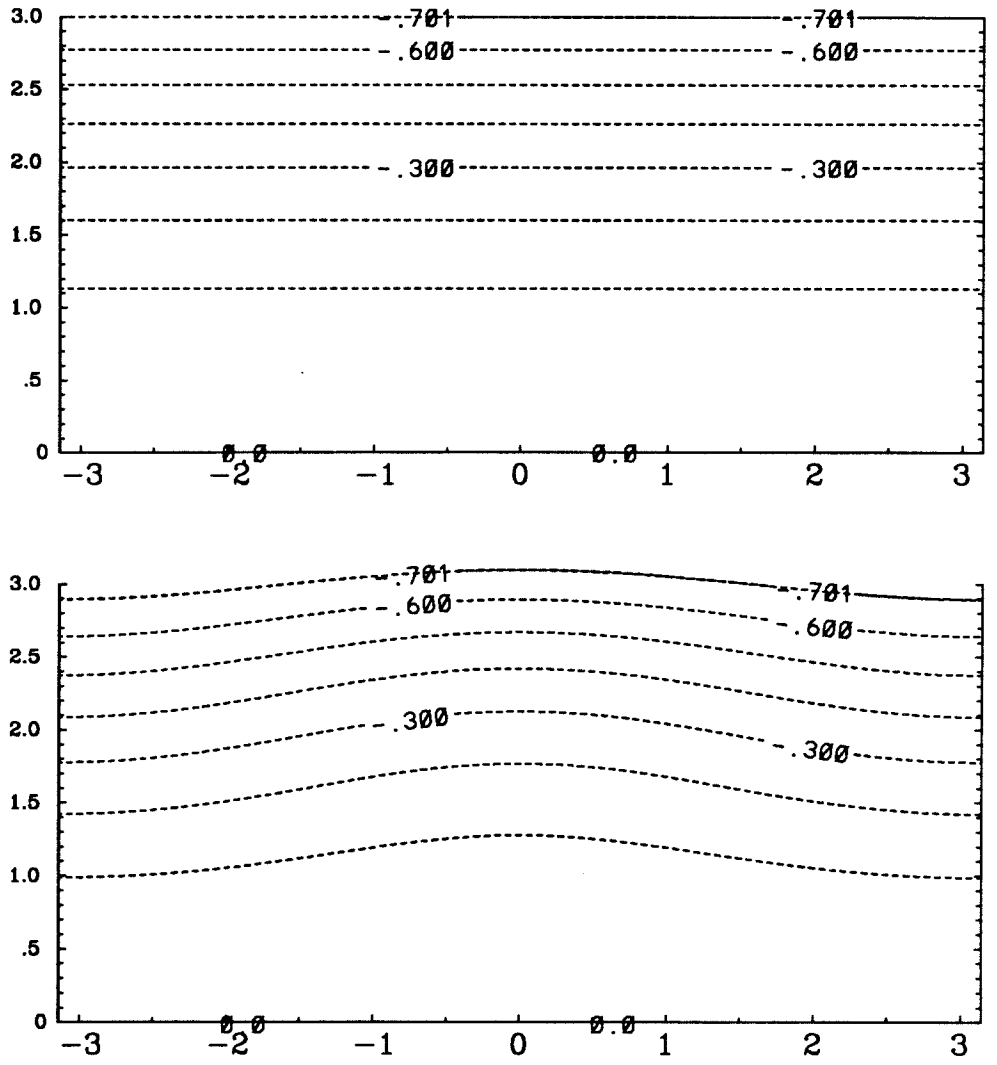

Fig. 5.5d Plot of streamlines for $\varepsilon = 0$ and 0.1 for a vortex with $a_{00} = 3$ and a total circulation of unity. The streamline with $\psi = -0.701$ coincides with the core boundary. Contour interval=0.1.

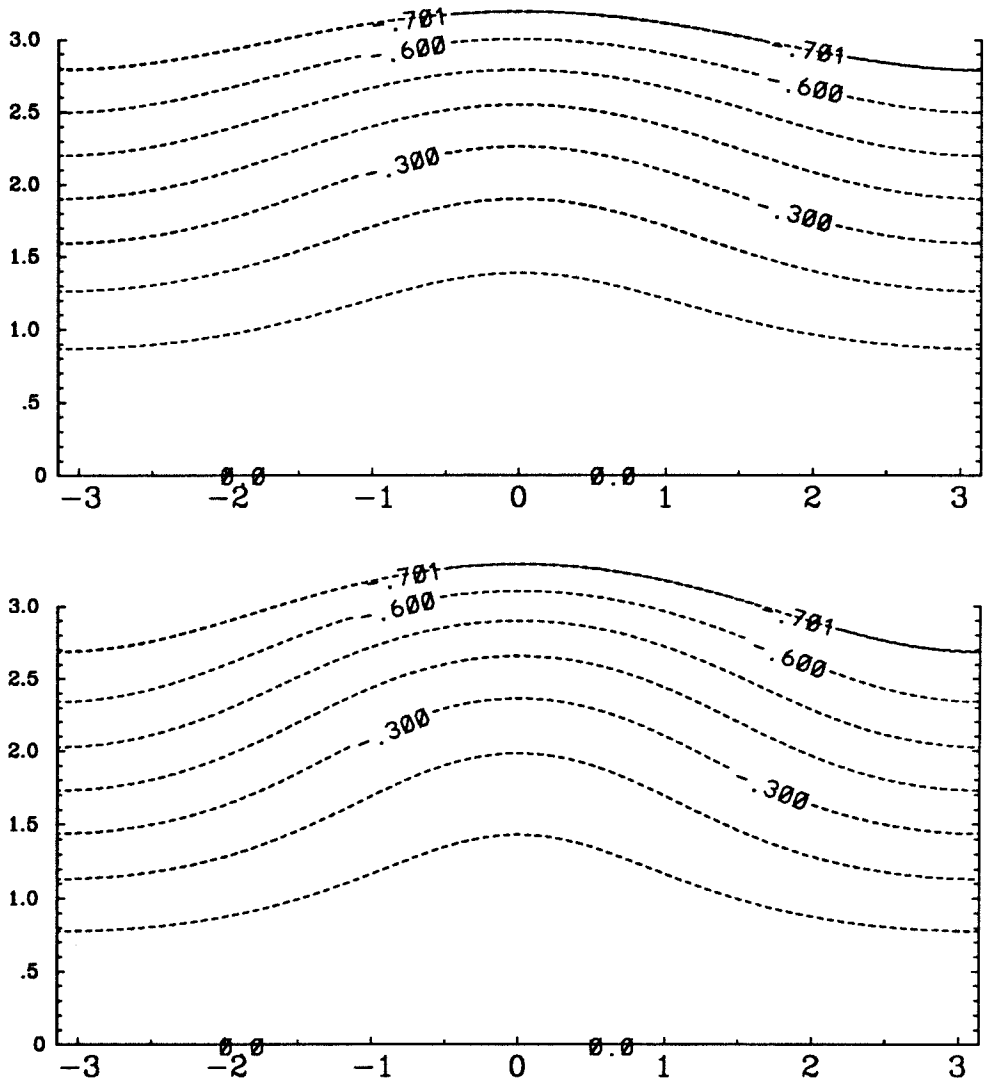

Fig. 5.5d continued. Plot of streamlines for $\varepsilon = 0.2$ and 0.3 for a vortex with $a_{00} = 3$ and a total circulation of unity. The streamline with $\psi = -0.701$ coincides with the core boundary. Contour interval=0.1.

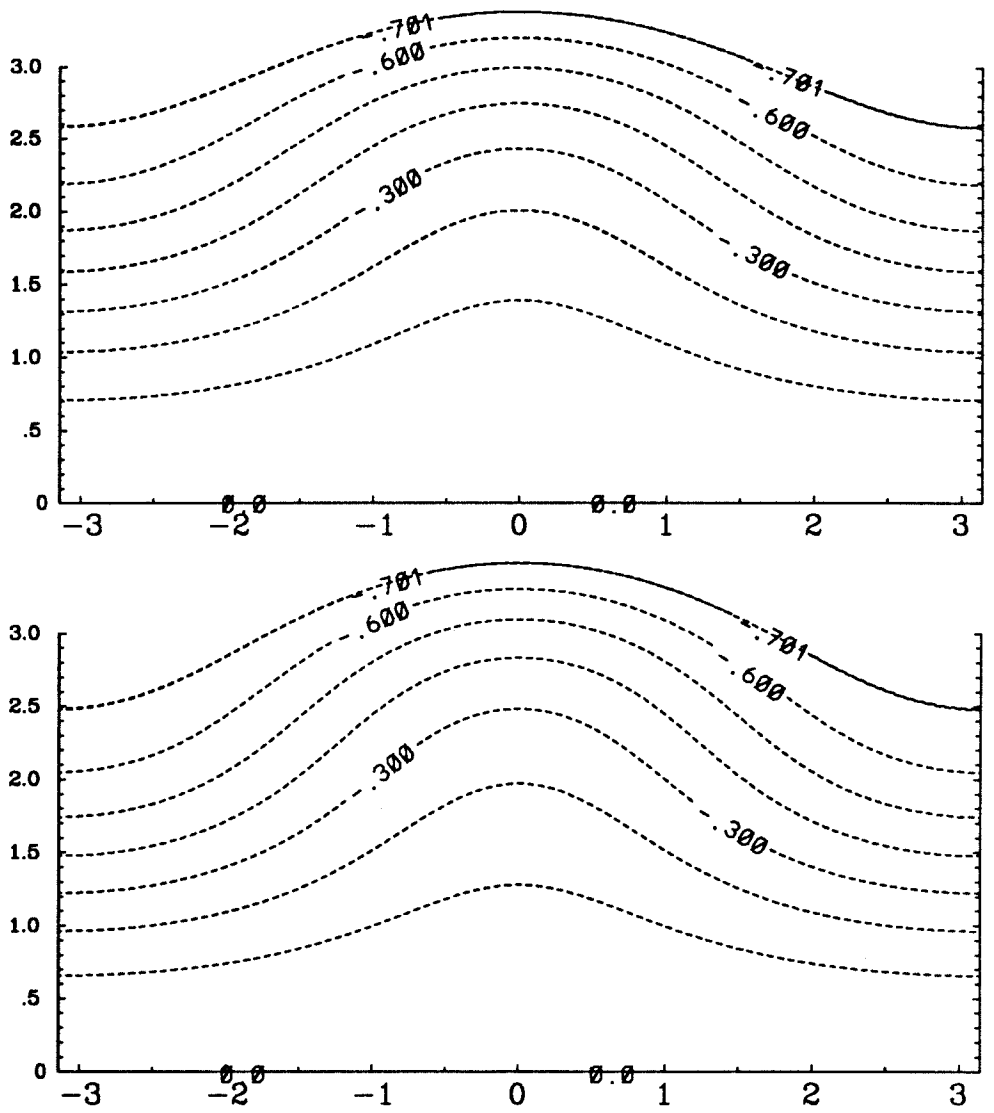

Fig. 5.5d continued. Plot of streamlines for $\varepsilon = 0.4$ and 0.5 for a vortex with $a_{00} = 3$ and a total circulation of unity. The streamline with $\psi = -0.701$ coincides with the core boundary. Contour interval=0.1.

CHAPTER 6

Kelvin Waves on Smooth Vorticity Distributions

6.1 Introduction

In this chapter we consider the numerical solution of the equations for nonlinear axisymmetric steady state internal waves. Our idea is to consider a base flow similar to Kelvin's columnar vortex but with continuously distributed axial vorticity. Linear stability of such a vortex reveals the existence of periodic waves moving at a constant speed in the axial direction. In an appropriate moving frame, the linear waves become steady. We obtain nonlinear solutions by continuing in the wave amplitude of linear steady waves. The speed of the moving frame is corrected to account for nonlinear effects. We compute the nonlinear solution by two different methods. In the first method, we construct a perturbation solution adopting a procedure similar to the nonlinear Kelvin waves described in Chapter 5. This establishes that the solution branch so found is unique. In a second method, we compute the solution using Newton's method. We verify that the solution found by these two methods is the same.

It was mentioned in the previous chapter that inviscid axisymmetric flows with swirl are characterized by two functions: the Bernoulli function H and the circulation function Ω. The only constraint on these functions is that they must be constant on a given streamline in a steady flow. They can vary from streamline to streamline in an arbitrary manner. However, a solution is fully determined once the dependence of H and Ω on the streamfunction ψ in a region of flow is specified. In the previous chapter, we found nonlinear solutions such that on the solution branch, the dependence of H and Ω on ψ was held fixed. It is not necessary that on a solution branch $H(\psi)$ and

$\Omega(\psi)$ have the same dependence. The dependence can vary from solution to solution in a specific way. Leibovich and Kribus (1990) found solutions by assuming that $\Omega(\psi) = \Lambda f(\psi)$ in which the functional form f was taken to be fixed but the value of Λ was varied from solution to solution. In this chapter we find solutions that have the same axial mean, the integral of the solution over one wave period, as that of the base flow. This constraint specifies some dependence of H and Ω on ψ that varies from solution to solution in general. The variation can be computed once the solution is found.

We solve the Euler equations numerically in a domain that is periodic in the axial direction and unbounded in the radial direction. We employ a spectral method in the axial direction and solve the resulting Galerkin equations using finite difference methods. The far field boundary conditions are derived by matching the solution to the potential flow.

6.2 Equations of motion

We consider the motion of an incompressible and inviscid fluid in cylindrical co-ordinates. Let r, ϕ and z denote the radial, the swirl and the axial co-ordinates, respectively. We take the fluid density to be unity. Let u, v and w denote velocity components along the r, ϕ and z axes, respectively. There is a streamfunction ψ and a circulation function Ω such that

$$u = -\frac{1}{r}\frac{\partial \psi}{\partial z}, \quad v = \frac{\Omega}{r} \quad w = \frac{1}{r}\frac{\partial \psi}{\partial r}. \tag{6.1}$$

Let ξ, χ and η denote the components of vorticity along r, ϕ and z co-ordinates, respectively. They are given by

$$\xi = -\frac{1}{r}\frac{\partial \Omega}{\partial z}, \quad \chi = -\frac{1}{r}\zeta, \quad \eta = \frac{1}{r}\frac{\partial \Omega}{\partial r}, \tag{6.2}$$

where

$$\zeta = D^2\psi, \tag{6.3}$$

and

$$D^2 = \frac{\partial^2}{\partial r^2} - \frac{1}{r}\frac{\partial}{\partial r} + \frac{\partial^2}{\partial z^2}. \tag{6.4}$$

The axisymmetric Euler equations governing the motion may be written (see Goldstein, 1965, article 39) as

$$\frac{\partial \zeta}{\partial t} + \frac{2\Omega}{r^2}\frac{\partial \Omega}{\partial z} + \frac{1}{r}\frac{\partial(\psi,\zeta)}{\partial(r,z)} + \frac{2}{r^2}\frac{\partial \psi}{\partial z}\zeta = 0, \tag{6.5}$$

$$\frac{\partial \Omega}{\partial t} + \frac{1}{r}\frac{\partial(\psi,\Omega)}{\partial(r,z)} = 0, \tag{6.6}$$

where the Jacobian is defined as

$$\frac{\partial(A,B)}{\partial(r,z)} = \frac{\partial A}{\partial r}\frac{\partial B}{\partial z} - \frac{\partial A}{\partial z}\frac{\partial B}{\partial r}. \tag{6.7}$$

Now we consider another frame (x, ϕ, r) moving along the z-axis at a constant speed. In particular we set

$$x = \kappa z - \alpha t. \tag{6.8}$$

so that this frame moves from left to right with speed α/κ if α is positive. Assuming the existence of steady solutions in this frame we have

$$\zeta = \frac{\partial^2 \psi}{\partial r^2} - \frac{1}{r}\frac{\partial \psi}{\partial r} + \kappa^2 \frac{\partial^2 \psi}{\partial x^2}, \tag{6.9}$$

$$-\alpha\frac{\partial \zeta}{\partial x} + \frac{2\kappa}{r^2}\Omega\frac{\partial \Omega}{\partial x} + \frac{\kappa}{r}\frac{\partial(\psi,\zeta)}{\partial(r,x)} + \frac{2\kappa}{r^2}\frac{\partial \psi}{\partial x}\zeta = 0, \tag{6.10}$$

$$-\alpha\frac{\partial \Omega}{\partial x} + \frac{\kappa}{r}\frac{\partial(\psi,\Omega)}{\partial(r,x)} = 0. \tag{6.11}$$

The phase speed α is treated as an unknown and is found as part of the solution.

6.3 Method of solution

Any pair of functions $\psi_{0,0}(r)$ and $\Omega_{0,0}(r)$ will form a solution to the Euler equations (6.10) and (6.11). The functions $\psi_{0,0}$ and $\Omega_{0,0}$ therefore specify a base flow that comprises a cylindrical vortex with an axial vorticity distribution controlled by $\Omega_{0,0}$. The axial velocity is found from $\psi_{0,0}$. The radial velocity for this base flow is zero. We discuss below different forms for the base flow used in our solutions. Next we consider linear waves and state their properties. The linear wave solution is used as a starting solution for both the perturbation method and Newton's method.

We assume that the steady nonlinear waves are periodic in x with period 2π. We restrict ourselves to solutions that are symmetric about $x = \pi$. We consider a Fourier decomposition of ψ and Ω and give the structure of the Galerkin equations to be solved. The boundary conditions to be satisfied are given together with the Galerkin equations. Next we consider the discretization of the equations satisfied by the Fourier modes of ψ and Ω. Newton's method and a perturbation method are discussed following a discussion of the discrete equations.

6.4 Base flow

We consider two different profiles for $\Omega_{0,0}$ that specify the distribution of axial vorticity. One of these gives an axial vorticity distribution that approaches the Kelvin's columnar vortex under a limiting condition. We refer to this as the Kelvin type vortex. The second distribution is referred to as the Burgers-Rott type vortex. This profile resembles the vorticity distribution in an experimental set up such as Harvey (1964). Leibovich and Kribus (1990) also used the Burgers-Rott type vorticity distribution in their solutions. In combination with swirl profile of either the Kelvin type or the Burgers-Rott type vortex, we may consider axial velocity in the vortex core. A simple Gaussian type of axial velocity profile is used. We give the form of these profiles below.

6.4.1 Kelvin type vortex

Given a distribution of an axial vorticity $\eta_{0,0}(r)$, we find the distribution of the circulation function $\Omega_{0,0}(r)$ by

$$\Omega_{0,0}(r) = \int_0^r \eta_{0,0}(\tilde{r})\,\tilde{r}\,d\tilde{r}. \tag{6.12}$$

We consider an axial vorticity distribution of the form

$$\eta_{0,0}(r) = \frac{\Omega_\infty}{a^2}\ \frac{1}{2}\left[1 - \tanh\frac{r-a}{\beta}\right] F(\beta, a), \tag{6.13}$$

where

$$\Omega_\infty = \lim_{r\to\infty} \Omega_{0,0}(r), \tag{6.14}$$

$$F(\beta, a) = a^2 \Big/ \left\{ \frac{a^2}{2} + \beta a \ln(2) + \frac{\beta^2 \pi^2}{24} + \beta a \ln\cosh(-a/\beta) - \beta^2 C_1 \right\}. \qquad (6.15)$$

Here, β is a parameter such that the axial vorticity distribution approaches that of Kelvin's columnar vortex with a core radius a as $\beta \to 0$. The profile of the circulation distribution and the axial vorticity for various values of β are shown in Figure 6.1. We will refer to the parameter a as the 'core' radius even though we do not have any identifiable core in the problem. The quantity Ω_∞ is the total circulation of the vortex filament. We compute the integral in (6.12) and obtain

$$\Omega_{0,0}(r) = \frac{\Omega_\infty F(\beta, a)}{a^2} \left\{ \frac{r^2}{2} - \beta a \ln\cosh(y) - \beta^2 I(y) + \beta a \ln\cosh(-a/\beta) - \beta^2 C_1 \right\}, \qquad (6.16)$$

where

$$y = \frac{r - a}{\beta}, \qquad (6.17)$$

and

$$I(y) = \int_0^y \tilde{y} \tanh(\tilde{y})\, d\tilde{y}, \qquad C_1 = -I(-a/\beta). \qquad (6.18)$$

The integral $I(y)$ is calculated numerically by expanding the tanh function into a series of exponentials and integrating term by term.

6.4.2 Burgers-Rott vortex

For this case we take the following form for the unperturbed swirl velocity,

$$v_{0,0}(r) = \frac{\Omega_\infty}{r} \left(1 - e^{-r^2/a^2} \right), \qquad (6.19)$$

where Ω_∞ is the total circulation of the vortex. Since the circulation $\Omega_{0,0} = r\ v_{0,0}$, we get

$$\Omega_{0,0}(r) = \Omega_\infty \left(1 - e^{-r^2/a^2} \right). \qquad (6.20)$$

The axial vorticity is of the form

$$\eta_{0,0}(r) = \frac{2\Omega_\infty}{a^2} e^{-r^2/a^2}. \qquad (6.21)$$

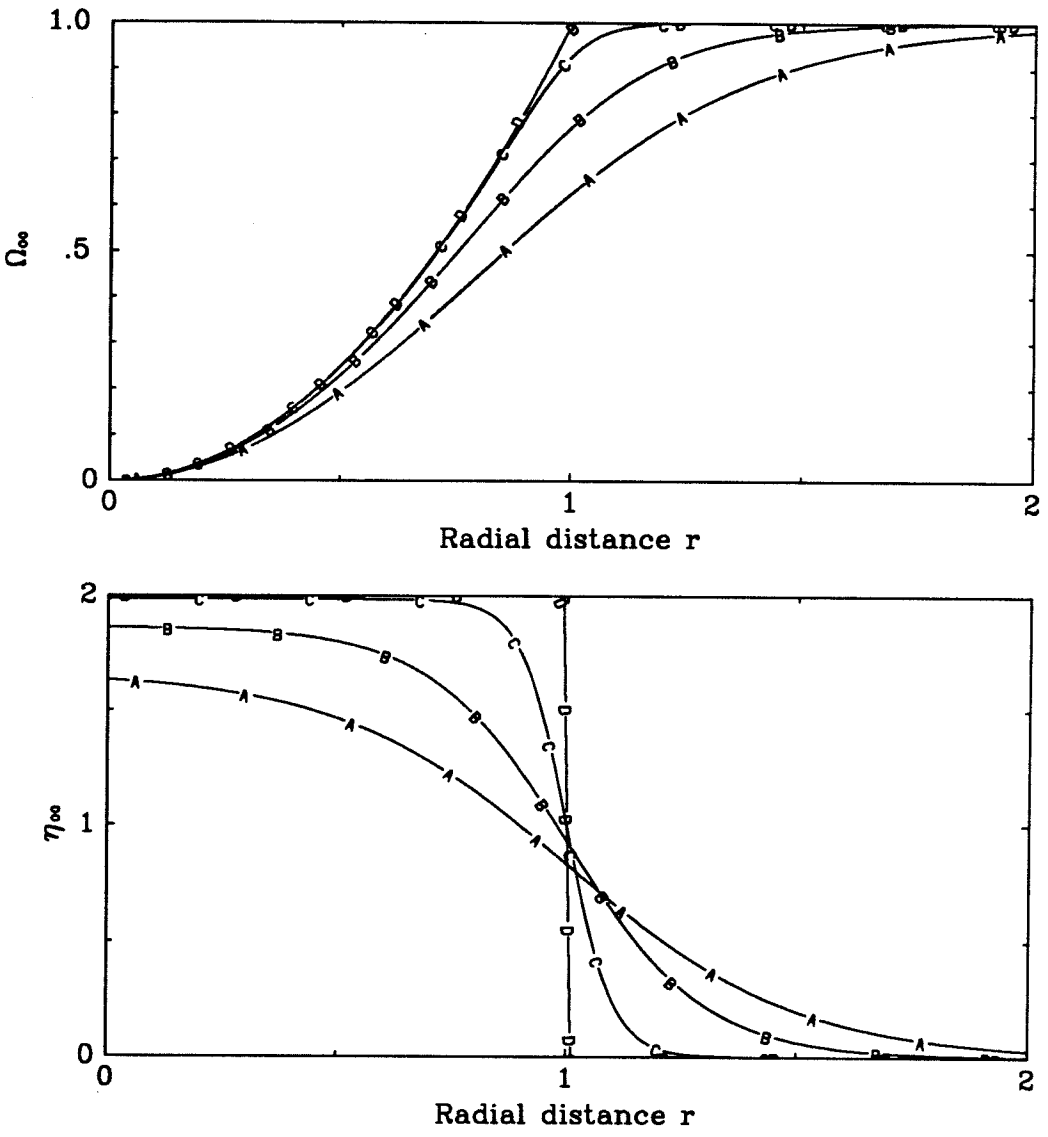

Fig. 6.1 Profiles of the circulation function $\Omega_{0,0}$ and the axial vorticity $\eta_{0,0}$ are shown here for A. $\beta = 0.5$, B. $\beta = 0.3$, C. $\beta = 0.1$, and D. $\beta \to 0$.

6.4.3 Axial velocity profile

For the axial velocity, we take

$$w_{0,0}(r) = W_m e^{-r^2/b^2}, \tag{6.22}$$

where b is a length scale which controls the decay rate of the axial velocity and W_m is the maximum axial velocity if it is positive and minimum when it is negative. The profiles of the unperturbed ψ and ζ are found to be of the form

$$\psi_{0,0}(r) = \frac{b^2 W_m}{2}\left(1 - e^{-r^2/b^2}\right), \quad \zeta_{0,0}(r) = -\frac{2W_m}{b^2} r^2 e^{-r^2/b^2}. \tag{6.23}$$

6.5 Properties of linear waves

A study of linear waves arising in the Euler equations not only gives us an idea of the expected structure of the subsequent nonlinear waves, but, as stated earlier, also provides us with a solution to start off the Newton continuation. The linear solution also forms the first order solution in the perturbation solution. We let, for some $\varepsilon \ll 1$,

$$\psi(r,x) = \psi_{0,0}(r) + \varepsilon\psi_{1,1}(r)\cos(x) + O(\varepsilon^2), \tag{6.24a}$$

$$\Omega(r,x) = \Omega_{0,0}(r) + \varepsilon\Omega_{1,1}(r)\cos(x) + O(\varepsilon^2), \tag{6.24b}$$

$$\alpha = \alpha_0. \tag{6.24c}$$

Substituting equation (6.24a) into (6.9) we get

$$\zeta(r,x) = \zeta_{0,0}(r) + \varepsilon\zeta_{1,1}(r)\cos(x) + O(\varepsilon^2), \tag{6.24d}$$

where

$$\zeta_{0,0} = \psi''_{0,0} - \frac{1}{r}\psi'_{0,0}, \quad \zeta_{1,1} = \psi''_{1,1} - \frac{1}{r}\psi'_{1,1} - \kappa^2\psi_{1,1}. \tag{6.25}$$

Here, primes denote derivatives with respect to r. For simplicity assume that the base flow has no axial flow. This requires that $\psi_{0,0} =$ constant. We take

$$\psi_{0,0} = 0. \tag{6.26}$$

We now substitute (6.24) into the Euler equations (6.10) and (6.11) and neglect all terms $O(\varepsilon^2)$ and higher. We get

$$\alpha_0 \zeta_{1,1} - \frac{2\kappa}{r^2}\,\Omega_{0,0}\Omega_{1,1} = 0, \tag{6.27a}$$

$$\alpha_0 \Omega_{1,1} + \frac{\kappa}{r}\,\Omega'_{0,0}\psi_{1,1} = 0. \tag{6.27b}$$

Eliminating $\Omega_{1,1}$ we can combine the above into the single equation

$$\alpha_0^2 \left(\psi''_{1,1} - \frac{1}{r}\,\psi'_{1,1} - \kappa^2 \psi_{1,1}\right) + \frac{2\kappa^2}{r^3}\,\Omega_{0,0}\,\Omega'_{0,0}\,\psi_{1,1} = 0. \tag{6.28}$$

Since for both the Kelvin type vortex and the Burgers-Rott type vortex, the vorticity of the base flow decays exponentially, the vorticity of the perturbed system (6.24) must also decay exponentially. In particular, we must have

$$\zeta_{1,1} \to 0, \quad \text{as} \quad r \to \infty. \tag{6.29}$$

From (6.25) we get

$$\psi_{1,1}(r) \sim K_1(\kappa\, r), \quad \text{as} \quad r \to \infty, \tag{6.30}$$

where K_1 is the Bessel function. Differentiating (6.30) once, we obtain the following far field boundary condition

$$\psi'_{1,1} + \kappa\,\frac{K_0(\kappa\, r)}{K_1(\kappa\, r)}\,\psi_{1,1} = 0, \quad \text{as} \quad r \to \infty. \tag{6.31}$$

As $r \to 0$, we assume that the flow approaches that of solid body rotation. From this we obtain the second boundary condition

$$\psi_{1,1}(0) = 0. \tag{6.32}$$

The linear equation (6.28) can be put into the form of a Sturm-Liouville eigenvalue problem with $1/\alpha_0^2$ as the eigenvalue. Therefore, there are an infinite number of eigenvalues and all of them are real. There are two branches of solutions to the linear system (6.28) with

$$\alpha = |\alpha_0|, \quad \text{or} \quad \alpha = -|\alpha_0|. \tag{6.33}$$

The positive branch corresponds to the right moving wave and the negative branch corresponds to the left moving wave. We can arrange the eigenvalues on the positive branch so that $\alpha_{0_p} > \alpha_{0_{p+1}}$, $p = 0, 1, \ldots, \infty$. The eigenfunction $\psi_{1,1_p}$ corresponding to the eigenvalue α_{0_p} has exactly p internal zeroes. We mainly consider linear solutions with $p = 0$. These solutions exhibit no internal zeroes. This property is highly desirable for numerical purposes.

If $\psi_{0,0}$ is not zero, then the linear system becomes

$$\mathcal{L}_1 \, \psi_{1,1} = 0, \tag{6.34}$$

where the linear operator is defined as

$$\begin{aligned} \mathcal{L}_1 = &\left(\alpha_0 - \frac{\kappa}{r}\psi'_{0,0}\right)^2 \left(\frac{\mathrm{d}^2}{\mathrm{d}r^2} - \frac{1}{r}\frac{\mathrm{d}}{\mathrm{d}r} - \kappa^2\right) \\ &+ \left(\alpha_0 - \frac{\kappa}{r}\psi'_{0,0}\right)\frac{1}{r}\zeta_{0,0} + \frac{2\kappa^2}{r^3}\Omega_{0,0}\Omega'_{0,0}. \end{aligned} \tag{6.35}$$

The boundary conditions remain unchanged. The observations made regarding the linear solution for base flow without axial flow still remain valid for the linear solution with axial flow. Special attention is needed if at some point $\alpha_0 = \kappa\psi'_{0,0}/r$. However, this situation was not encountered for all the cases considered. This appears to be similar to the result of Chandrasekhar (1961; section 78b) which states that for a vortex in a pipe if the swirl distribution is positive everywhere (which is true in the present case), then, the eigenvalue is real and is either less than the minimum axial velocity or greater than the maximum axial velocity. The eigenvalue in the case of pipe flow considered by Chandrasekhar can be identified with α_0/κ. The quantity $\psi'_{0,0}/r$ is the axial velocity.

6.6 Galerkin equations

We decompose ψ and Ω into a truncated cosine series

$$\psi(r, x) = \psi_0(r) + \sum_{k=1}^{m} \psi_k(r)\cos(kx), \tag{6.36a}$$

$$\Omega(r,x) = \Omega_0(r) + \sum_{k=1}^{m} \Omega_k(r)\cos(kx). \tag{6.36b}$$

Here m is some given integer that determines the modal resolution. The functions $\psi_0(r)$ and $\Omega_0(r)$ are held fixed and taken to equal the base flow. Therefore we have

$$\psi_0(r) = \psi_{0,0}(r), \quad \Omega_0(r) = \Omega_{0,0}(r). \tag{6.37}$$

Substituting (6.36a) into (6.9) we get

$$\zeta(r,x) = \zeta_0(r) + \sum_{k=1}^{m} \zeta_k(r)\cos(kx), \tag{6.38}$$

with

$$\zeta_k(r) = D_k^2\psi_k, \quad k = 0,\ldots,m, \tag{6.39}$$

where

$$D_k^2 = \frac{\mathrm{d}^2}{\mathrm{d}r^2} - \frac{1}{r}\frac{\mathrm{d}}{\mathrm{d}r} - \kappa^2 k^2. \tag{6.40}$$

In order to find the equations satisfied by the modes of ψ and Ω, we substitute the assumed forms into the Euler equations and collect the coefficients of like harmonics and equate them to zero. Then the solution to (6.9 – 6.11) is equivalent to satisfying

$$f_k(r) = 0, \quad g_k(r) = 0, \qquad k = 1,\ldots,m, \tag{6.41}$$

where

$$\begin{aligned} f_k(r) = &\left(\alpha - \frac{\kappa}{r}\psi_0'\right)\zeta_k + \frac{\kappa}{r}\zeta_0'\psi_k - \frac{2\kappa}{r^2}\Omega_0\Omega_k \\ &- \frac{\kappa}{kr}\left\{\frac{2}{r}N_k(\Omega,\Omega) + N_k(\psi',\zeta) - N_k(\zeta',\psi) + \frac{2}{r}N_k(\zeta,\psi)\right\}, \end{aligned} \tag{6.42}$$

$$g_k(r) = \left(\alpha - \frac{\kappa}{r}\psi_0'\right)\Omega_k + \frac{\kappa}{r}\Omega_0'\psi_k - \frac{\kappa}{kr}\left\{N_k(\psi',\Omega) - N_k(\Omega',\psi)\right\}. \tag{6.43}$$

Primes denote derivatives with respect to r. N_k is the contribution arising from nonlinear products. It is defined as follows. Suppose there are two functions $A(r,x)$ and $B(r,x)$ with representation

$$A(r,x) = A_0(r) + \sum_{k=1}^{m} A_k(r)\cos(kx), \quad B(r,x) = B_0(r) + \sum_{k=1}^{m} B_k(r)\cos(kx).$$

Then the product $A \cdot \partial B/\partial x$ is written

$$A \cdot \frac{\partial B}{\partial x} = -\sum_{k=1}^{m} [kA_0B_k + N_k(A,B)]\sin(kx),$$

where

$$N_k(A,B) = \frac{1}{2}\sum_{l=1}^{k-1}(k-l)A_lB_{k-l} - \frac{1}{2}\sum_{l=k+1}^{l\leq m}(l-k)A_lB_{l-k} + \frac{1}{2}\sum_{l=1}^{l+k\leq m}(l+k)A_lB_{l+k}. \tag{6.44}$$

We drop all the terms contributing to $(m+1)$ and higher harmonics with wavenumber greater than $(m+1)$. Next we discuss the boundary conditions to be satisfied by the Fourier modes of ψ and Ω.

6.6.1 Boundary conditions

The solution to (6.41) is found subject to the following boundary conditions. As $r \to 0$ we assume that the flow approaches that of solid body rotation. This implies that azimuthal and radial components of the vorticity must vanish and the axial component must tend to a constant. Equivalently, the radial and swirl components of velocity must vanish. From this we infer

$$\psi \sim r^2, \quad \Omega \sim r^2, \qquad \text{as} \quad r \to 0. \tag{6.45}$$

This gives us two choices for the inner boundary condition. We can either take

$$\psi_k'(0) = 0, \quad \Omega_k'(0) = 0, \qquad k = 1,\ldots,m, \tag{6.46}$$

or

$$\psi_k(0) = 0, \quad \Omega_k(0) = 0, \qquad k = 1,\ldots,m. \tag{6.47}$$

In either case we found the solution to be the same. We use the condition (6.47) in our calculations.

Since vorticity for the base flow decays exponentially as $r \to \infty$, the vorticity must also decay exponentially for the solution assumed in (6.36). This implies that

$$\frac{\partial \Omega}{\partial r} \to 0, \quad D^2\psi \to 0, \qquad \text{as} \quad r \to \infty. \tag{6.48}$$

Substituting the expansion (6.36) into (6.48) we get

$$\Omega_k' = 0, \quad k = 1, \ldots, m, \qquad \text{as} \quad r \to \infty, \tag{6.49}$$

and

$$\psi_k'' - \frac{1}{r}\psi_k' - \kappa^2 k^2 \psi_k = 0, \quad k = 1, \ldots, m, \qquad \text{as} \quad r \to \infty. \tag{6.50}$$

Since the Fourier modes ψ_k decay exponentially, the consistent solution to (6.50) is

$$\psi_k = a_k r K_1(\kappa k r),$$

where a_k is a constant and K_1 is the Bessel function. By differentiating this relation we can eliminate the constant a_k and get the following far field boundary condition

$$\psi_k' + \mu_k(r)\psi_k = 0, \quad \mu_k(r) = k\kappa \frac{K_0(k\kappa r)}{K_1(k\kappa r)}, \quad k = 1, \ldots, m, \qquad \text{as} \quad r \to \infty. \tag{6.51}$$

6.7 Discrete equations

The solution to the nonlinear set of equations represented by (6.41) subject to the above mentioned boundary conditions is found by two methods. In one approach we solve them directly by employing Newton's method. In a second approach a perturbation method is used which results in a set of linear boundary value problems. In both approaches, we compute the solution by replacing the continuous derivatives with discrete derivatives. We give the form of discretization used in either method.

Since the vorticity decays rapidly in the far field, the solution is also expected to decay fairly rapidly in the outer region of the flow. Therefore, we do not require a high grid resolution in order to accurately compute the solution. However, within the core of the vortex, the solution could develop steep gradients. If this happens, we need a high grid resolution. Hence the grid on which the entire solution is computed needs to be concentrated so that we have a denser set of points within the 'core' and less so in the outer region. To do this we consider the following 'grid function' transformation and its inverse

$$r = r(\rho) \qquad \rho = \rho(r). \tag{6.52}$$

Then we replace the derivatives in the equations above by

$$\frac{\mathrm{d}}{\mathrm{d}r} = \frac{\mathrm{d}\rho}{\mathrm{d}r}\frac{\mathrm{d}}{\mathrm{d}\rho},$$

and redefine

$$D_k^2 = P\frac{\mathrm{d}^2}{\mathrm{d}\rho^2} + Q\frac{\mathrm{d}}{\mathrm{d}\rho} - \kappa^2 k^2, \tag{6.53}$$

where

$$P = \left(\frac{\mathrm{d}\rho}{\mathrm{d}r}\right)^2, \quad Q = \frac{\mathrm{d}^2\rho}{\mathrm{d}r^2} - \frac{1}{r}\frac{\mathrm{d}\rho}{\mathrm{d}r}. \tag{6.54}$$

We now consider a uniform grid defined by the grid points

$$\rho_j = j\Delta\rho, \qquad j = 0,\ldots,J, \quad \Delta\rho = \rho(R)/J, \tag{6.55}$$

where R is a suitably chosen radial distance at which we apply the far field boundary conditions. The boundary condition on the streamfunction given by (6.50) takes into account the decay rate in the outer region. The circulation function decays far more rapidly than the streamfunction. Therefore, we can apply the conditions (6.49) and (6.50) at R which is typically three or four times the core radii for a reasonably accurate solution.

We evaluate (6.41) on the discrete grid using second order finite differences to approximate the derivatives. Thus we find a solution satisfying

$$f_{kj} = f_k(r_j) = 0, \quad g_{kj} = g_k(r_j) = 0, \quad k = 1,\ldots,m, \quad j = 0,\ldots,J. \tag{6.56}$$

For $j = 1,\ldots,J-1$, we have

$$\begin{aligned} f_{kj} = &\left(\alpha - \frac{\kappa}{r_j}\psi_{0j}'\right)\zeta_{kj} + \frac{\kappa}{r_j}\zeta_{0j}'\psi_{kj} - \frac{2\kappa}{r_j^2}\Omega_{0j}\Omega_{kj} \\ &- \frac{\kappa}{kr_j}\left\{\frac{2}{r_j}N_{kj}(\Omega,\Omega) + N_{kj}(\psi,\zeta) - N_{kj}(\zeta',\psi) + \frac{2}{r_j}N_{kj}(\zeta,\psi)\right\}, \end{aligned} \tag{6.57}$$

$$g_{kj} = \left(\alpha - \frac{\kappa}{r_j}\psi_{0j}'\right)\Omega_{kj} + \frac{\kappa}{r_j}\Omega_{0j}'\psi_{kj} - \frac{\kappa}{kr_j}\left\{N_{kj}(\psi',\Omega) - N_{kj}(\Omega',\psi)\right\}. \tag{6.58}$$

For $j = 0$ and $j = J$ we make use of the boundary conditions and define

$$f_{kj} = \psi_{kj}, \quad g_{kj} = \Omega_{kj}, \qquad \text{for} \quad j = 0, \tag{6.59}$$

and

$$f_{kj} = \psi'_{kj} + k\frac{K_0(k\kappa r_j)}{K_1(k\kappa r_j)}\psi_{kj}, \quad g_{kj} = \Omega'_{kj}, \qquad \text{for} \quad j = J. \tag{6.60}$$

The quantity N_{kj} is given by

$$N_{kj}(A,B) = \frac{1}{2}\sum_{l=1}^{k-1}(k-l)A_{lj}B_{k-l,j} - \frac{1}{2}\sum_{l=k+1}^{l\le m}(l-k)A_{lj}B_{l-k,j} + \frac{1}{2}\sum_{l=1}^{l+k\le m}(l+k)A_{lj}B_{l+k,j}. \tag{6.61}$$

For interior points, *i.e.*, for $j = 1, \ldots, J-1$, the derivatives are approximated by central differences. Letting $(\cdot)$ to denote various modes of ψ, Ω and ζ we have

$$\left(\frac{\mathrm{d}(\cdot)}{\mathrm{d}\rho}\right)_j = \frac{(\cdot)_{j+1} - (\cdot)_{j-1}}{2\Delta\rho}, \quad \left(\frac{\mathrm{d}^2(\cdot)}{\mathrm{d}\rho^2}\right)_j = \frac{(\cdot)_{j+1} - 2(\cdot)_j + (\cdot)_{j-1}}{\Delta\rho^2}. \tag{6.62}$$

At the outer boundary we need the derivative of ψ. For this purpose we use

$$\left(\frac{\mathrm{d}(\cdot)}{\mathrm{d}\rho}\right)_J = \frac{3(\cdot)_J - 4(\cdot)_{J-1} + (\cdot)_{J-2}}{2\Delta\rho} + O(\Delta\rho^2). \tag{6.63}$$

In the Newton's method, the solution can be found assuming ψ_k and Ω_k as our unknowns. We express ζ_k in terms of the streamfunction. Discretizing (6.39) we get

$$\zeta_{kj} = a_j\psi_{k,j-1} + \left(\gamma_j - k^2\kappa^2\right)\psi_{k,j} + b_j\psi_{k,j+1}, \qquad j = 1, \ldots, J-1, \tag{6.64}$$

where

$$a_j = \frac{P_j}{\Delta\rho^2} - \frac{Q_j}{2\Delta\rho}, \quad \gamma_j = -\frac{2P_j}{\Delta\rho^2}, \quad b_j = \frac{P_j}{\Delta\rho^2} + \frac{Q_j}{2\Delta\rho}. \tag{6.65}$$

Only the first derivative of ζ_k occurs. The discretization is given by

$$\left(\frac{\mathrm{d}\zeta_k}{\mathrm{d}\rho}\right)_j = \frac{1}{2\Delta\rho}\left(k^2\kappa^2\psi_{k,j-1} + a_{j+1}\psi_{k,j} + (\gamma_{j+1} - k^2\kappa^2)\psi_{k,j+1} + b_{j+1}\psi_{k,j+2}\right), \qquad \text{for} \quad j = 1, \tag{6.66a}$$

$$\left(\frac{\mathrm{d}\zeta_k}{\mathrm{d}\rho}\right)_j = \frac{1}{2\Delta\rho}\Big(-a_{j-1}\psi_{k,j-2} - (\gamma_{j-1} - k^2\kappa^2)\psi_{k,j-1} + (a_{j+1} - b_{j-1})\psi_{k,j} + (\gamma_{j+1} - k^2\kappa^2)\psi_{k,j+1} + b_{j+1}\psi_{k,j+2}\Big), \qquad \text{for} \quad j = 2, \ldots, J-2, \tag{6.66b}$$

and

$$\left(\frac{\mathrm{d}\zeta_k}{\mathrm{d}\rho}\right)_j = \frac{2}{3\Delta\rho}\Big(-a_{j-1}\psi_{k,j-2} + (a_j - \gamma_{j-1} + k^2\kappa^2)\psi_{k,j-1} + (\gamma_j - k^2\kappa^2 - b_{j-1})\psi_{k,j} + b_j\psi_{k,j+1}\Big), \qquad \text{for} \quad j = J-1. \tag{6.66c}$$

Next we consider the implementation of a perturbation method.

6.8 Perturbation solution

The approach adopted here is similar to the procedure described in Chapter 5. We showed in that chapter that two additional constraints other than the boundary conditions are necessary to compute a unique solution. The additional conditions were supplied by specifying the dependence of Bernoulli function H and the circulation function Ω on ψ. As noted, a variety of possibilities exist by which we can constrain the flow. Here we 'supply' the additional conditions by keeping the axial mean of ψ and Ω fixed. This selects a dependence of H and Ω on ψ which can be calculated from the known solution.

We solve the nonlinear equations (6.41) by expanding modes of ψ, Ω and ζ into a power series in a perturbation parameter ε. We assume the following form

$$\psi_k = \varepsilon^k\psi_{k,k} + \varepsilon^{k+2}\psi_{k,k+2} + \cdots, \tag{6.67a}$$

$$\Omega_k = \varepsilon^k\Omega_{k,k} + \varepsilon^{k+2}\Omega_{k,k+2} + \cdots. \tag{6.67b}$$

We also expand the phase speed α as

$$\alpha = \alpha_0 + \varepsilon^2\alpha_2 + \varepsilon^4\alpha_4 + \cdots. \tag{6.67c}$$

We define ε by

$$\langle \psi_1, \psi_{1,1} \rangle = \varepsilon \, \langle \psi_{1,1}, \psi_{1,1} \rangle, \tag{6.68}$$

where $\psi_{1,1}$ is the linear solution and

$$\langle u, v \rangle = \int_0^\infty u \, v \, \frac{1}{r} \, dr, \tag{6.69}$$

is an inner product defined on any pair of functions u and v. We substitute (6.67) into (6.41) and collect coefficients of like powers of ε. We next compute the contribution to the $O(\varepsilon^l)$ term from a typical product $A_p B_q$, where A_p and B_q represent Fourier modes of some functions A and B. Firstly, the number of terms that arise in such a product is given by

$$n = (l - p - q)/2 + 1, \quad \text{if} \quad (l - p - q) \bmod 2 = 0, \tag{6.70}$$

and $n = 0$ otherwise. If c_l denotes the coefficient of ε^l in the product $A_p B_q$, then

$$c_l = \sum_{s=1}^{n} A_{p,t} B_{q,u}, \quad t = p + 2(s-1), \quad u = l - t. \tag{6.71}$$

We employ these relations in (6.41) with an appropriate choice for A and B and after equating coefficients of various powers of ε we obtain a system of linear equations. Equating the coefficient of ε^l yields two equations in which the only unknowns would be $\psi_{k,l}$ and $\Omega_{k,l}$. The other terms would have already been determined. Retaining all the known terms on the right hand side, we can write the governing equations for $\psi_{k,l}$ and $\Omega_{k,l}$ as

$$\left(\alpha_0 - \frac{\kappa}{r} \psi'_{0,0}\right) \zeta_{k,l} + \frac{\kappa}{r} \zeta'_{0,0} \psi_{k,l} - \frac{2\kappa}{r^2} \Omega_{0,0} \Omega_{k,l} = p_{k,l}, \tag{6.72a}$$

$$\left(\alpha_0 - \frac{\kappa}{r} \psi'_{0,0}\right) \Omega_{k,l} + \frac{\kappa}{r} \Omega'_{0,0} \psi_{k,l} = q_{k,l}, \tag{6.72b}$$

where $p_{k,l}$ and $q_{k,l}$ are the known right hand sides and

$$\zeta_{k,l} = \psi''_{k,l} - \frac{1}{r} \psi'_{k,l} + \kappa^2 k^2 \psi_{k,l}. \tag{6.73}$$

Eliminating $\Omega_{k,l}$ in (6.72), we write

$$\mathcal{L}_k \, \psi_{k,l} = \left(\alpha_0 - \frac{\kappa}{r} \psi'_{0,0}\right) p_{k,l} + \frac{2\kappa}{r^2} \Omega_{0,0} q_{k,l}, \tag{6.74}$$

where

$$\mathcal{L}_k = \left(\alpha_0 - \frac{\kappa}{r}\psi'_{0,0}\right)^2 \left(\frac{\mathrm{d}^2}{\mathrm{d}r^2} - \frac{1}{r}\frac{\mathrm{d}}{\mathrm{d}r} - k^2\,\kappa^2\right) + \left(\alpha_0 - \frac{\kappa}{r}\psi'_{0,0}\right)\frac{1}{r}\zeta_{0,0} + \frac{2\kappa^2}{r^3}\Omega_{0,0}\Omega'_{0,0}. \tag{6.75}$$

These equations are readily solved by replacing the derivatives with central differences and inverting the tridiagonal matrices for various values of k and l. The solution proceeds from $l = 1$ to $l = m$ and k takes the values $l, l+2, l+4, \ldots$. When $k = 1$, the matrix to be inverted becomes singular and therefore cannot be inverted since the operator $\mathcal{L}_k$ coincides with the linear operator $\mathcal{L}_1$ defined in (6.34). For this case we proceed as follows. We re-write the right hand sides as

$$p_{1,l} = -\alpha_{l-1}\zeta_{1,1} + \tilde{p}_{1,l}, \quad q_{1,l} = -\alpha_{l-1}\zeta_{1,1} + \tilde{q}_{1,l}, \tag{6.76}$$

where the tilde terms include all the known quantities. The $O(\varepsilon^{l-1})$ co-efficient for the phase speed, α_{l-1}, is a constant yet to be determined. The equation satisfied by $\psi_{1,l}$ can be written

$$\mathcal{L}_1\psi_{1,l} = -\left[\left(\alpha_0 - \frac{\kappa}{r}\psi'_{0,0}\right)\zeta_{1,1} + \frac{2\kappa}{r^2}\Omega_{0,0}\Omega_{1,1}\right]\alpha_{l-1} + \left[\left(\alpha_0 - \frac{\kappa}{r}\psi'_{0,0}\right)\tilde{p}_{1,l} + \frac{2\kappa}{r^2}\Omega_{0,0}\tilde{q}_{1,l}\right]. \tag{6.77}$$

Using the Fredholm alternative condition, we readily establish that a solution to (6.77) exists if and only if

$$\alpha_{l-1} = \frac{\left\langle \left(\alpha_0 - \frac{\kappa}{r}\psi'_{0,0}\right)\tilde{p}_{1,l} + 2\kappa\Omega_{0,0}\tilde{q}_{1,l}/r^2 \quad , \quad \psi_{1,1} \right\rangle}{\left\langle \left(\alpha_0 - \frac{\kappa}{r}\psi'_{0,0}\right)\zeta_{1,1} + 2\kappa\Omega_{0,0}\Omega_{1,1}/r^2 \quad , \quad \psi_{1,1} \right\rangle}. \tag{6.78}$$

Once the value of α_{l-1} is found, the *particular* solution to the singular system (6.77) can be found uniquely. However, we are free to add an arbitrary amount of the linear solution since the linear solution satisfies the homogeneous equation. We restrict $\psi_{1,l}$ such that it is orthogonal to the linear solution. This is stated as

$$\left\langle \psi_{1,l}, \psi_{1,1} \right\rangle = 0, \quad l \neq 1. \tag{6.79}$$

In actual calculations, we solve the singular system (6.77) by augmenting it with the constraint (6.79) and solve simultaneously for $\psi_{1,l}$ and α_{l-1}. The value of α_{l-1} determined by this method was found to be in good agreement with (6.78).

The solution branch found by employing the perturbation method just described can be thought of as a path in the (ε, α) plane. Instead of constraining the solution by specifying the form of the Bernoulli function and the circulation function as done in the previous chapter, we have constrained the solutions so that on a given branch each of them have the same axial mean as the base flow. This is another way of finding a unique solution. If for every ε we find a unique value of the phase speed α then, the solution is unique. If there is more than one solution for some ε, then we will not be able to find unique values of the perturbation coefficients of the phase speed α. Using the method described above, a perturbation solution for a Kelvin type vortex without axial velocity was computed. The parameters defining the base flow were assumed to be $a = 1$, $\beta = 0.5$ and Ω_∞. A value of $R = 5$ was used for the length of the radial domain. The solution was generated up to 12^{th} order in ε. Table 6.1 shows the results for the expansion coefficients of the phase speed α. The convergence of the coefficients for various grid resolutions varying from $J = 20$ to $J = 640$ is shown. The results show good convergence. The last column of the table shows the rate of convergence. Since the discretization is second order accurate, the rate of convergence is expected to be 4. Since the expansion coefficients converge to unique values, the uniqueness of the solution branch defined by a path in (ε, α) space is established by this result.

6.9 Newton's method

We collect the equations for $f_{k,j}$ and $g_{k,j}$ (equations 6.57 and 6.58) into the vectors

$$\mathcal{F}_j = \{f_{1j}, f_{2j}, \ldots, f_{mj}\}, \quad \mathcal{G}_j = \{g_{1j}, g_{2j}, \ldots, g_{mj}\}. \tag{6.80}$$

Next we collect equations (6.80) for various values of j into the column vector

$$\mathcal{E} = \{\mathcal{F}_0, \mathcal{G}_0, \mathcal{F}_1, \mathcal{G}_1, \ldots, \mathcal{F}_J, \mathcal{G}_J\}^\top. \tag{6.81}$$

Table 6.1 Rates of convergence for the expansion coefficients of α. The results shown are for $a = 1$, $\beta = 0.5$, $\Omega_\infty = 1$, $\kappa = 1$ and $r \in [0, 5]$. l in the second column designates the expansion coefficient α_l of ε^l.

J	l	α_l	*difference*	*rate*
20	0	0.512901127		
40	0	0.513071120	$0.170019\,10^{-3}$	
80	0	0.513188303	$0.117145\,10^{-3}$	$0.1451\,10^{1}$
160	0	0.513223767	$0.354861\,10^{-4}$	$0.3301\,10^{1}$
320	0	0.513233125	$0.935770\,10^{-5}$	$0.3792\,10^{1}$
640	0	0.513235509	$0.237621\,10^{-5}$	$0.3938\,10^{1}$
20	2	0.976300418		
40	2	$0.103400004\,10^{1}$	$0.576996\,10^{-1}$	
80	2	$0.104940212\,10^{1}$	$0.154020\,10^{-1}$	$0.3746\,10^{1}$
160	2	$0.105326355\,10^{1}$	$0.386140\,10^{-2}$	$0.3989\,10^{1}$
320	2	$0.105422676\,10^{1}$	$0.963299\,10^{-3}$	$0.4009\,10^{1}$
640	2	$0.105446756\,10^{1}$	$0.240748\,10^{-3}$	$0.4001\,10^{1}$
20	4	$0.346679378\,10^{1}$		
40	4	$0.308515120\,10^{1}$	0.381643	
80	4	$0.296098423\,10^{1}$	0.124167	$0.3074\,10^{1}$
160	4	$0.292720342\,10^{1}$	$0.337808\,10^{-1}$	$0.3676\,10^{1}$
320	4	$0.291857219\,10^{1}$	$0.863107\,10^{-2}$	$0.3914\,10^{1}$
640	4	$0.291640353\,10^{1}$	$0.216868\,10^{-2}$	$0.3980\,10^{1}$
20	6	$0.510541611\,10^{2}$		
40	6	$0.275666389\,10^{2}$	$0.234875\,10^{2}$	
80	6	$0.189725723\,10^{2}$	$0.859407\,10^{1}$	$0.2733\,10^{1}$
160	6	$0.165713959\,10^{2}$	$0.240118\,10^{1}$	$0.3579\,10^{1}$
320	6	$0.159537954\,10^{2}$	0.617601	$0.3888\,10^{1}$
640	6	$0.157982941\,10^{2}$	0.155502	$0.3972\,10^{1}$
20	8	$0.111649573\,10^{4}$		
40	8	$-.179685001\,10^{2}$	$0.113446\,10^{4}$	
80	8	$-.494777740\,10^{3}$	$0.476809\,10^{3}$	$0.2379\,10^{1}$
160	8	$-.634998230\,10^{3}$	$0.140220\,10^{3}$	$0.3400\,10^{1}$
320	8	$-.671592102\,10^{3}$	$0.365939\,10^{2}$	$0.3832\,10^{1}$
640	8	$-.680841064\,10^{3}$	$0.924896\,10^{1}$	$0.3957\,10^{1}$
20	10	$0.309555664\,10^{5}$		
40	10	$-.202935566\,10^{5}$	$0.512491\,10^{5}$	
80	10	$-.458888438\,10^{5}$	$0.255953\,10^{5}$	$0.2002\,10^{1}$
160	10	$-.540509258\,10^{5}$	$0.816208\,10^{4}$	$0.3136\,10^{1}$
320	10	$-.562321250\,10^{5}$	$0.218120\,10^{4}$	$0.3742\,10^{1}$
640	10	$-.567868242\,10^{5}$	$0.554702\,10^{3}$	$0.3932\,10^{1}$
20	12	$0.998814375\,10^{6}$		
40	12	$-.127873575\,10^{7}$	$0.227755\,10^{7}$	
80	12	$-.269778500\,10^{7}$	$0.141905\,10^{7}$	$0.1605\,10^{1}$
160	12	$-.320765675\,10^{7}$	$0.509872\,10^{6}$	$0.2783\,10^{1}$
320	12	$-.334883475\,10^{7}$	$0.141178\,10^{6}$	$0.3612\,10^{1}$
640	12	$-.338507275\,10^{7}$	$0.362380\,10^{5}$	$0.3896\,10^{1}$

We define the vector of unknowns by

$$\mathcal{U} = \{\mathcal{P}_0, \mathcal{Q}_0, \mathcal{P}_1, \mathcal{Q}_1, \ldots, \mathcal{P}_J, \mathcal{Q}_J\}^{\mathsf{T}}, \tag{6.82}$$

where

$$\mathcal{P}_j = \{\psi_{1j}, \psi_{2j}, \ldots, \psi_{mj}\}, \quad \mathcal{Q}_j = \{\Omega_{1j}, \Omega_{2j}, \ldots, \Omega_{mj}\}. \tag{6.83}$$

An additional unknown not included in $\mathcal{U}$ is the phase speed α. To close the system, we supply an amplitude condition. This may be done in several different ways. We borrow the idea from the perturbation method. Thus, as before we define an inner product on any two functions $p(r)$ and $q(r)$

$$< p, q >= \int_0^\infty \frac{1}{r}\, p(r)\, q(r)\, dr. \tag{6.84}$$

We approximate the integral by using the trapezoidal rule. Thus the discrete inner product is denoted by

$$< p, q >_\Delta = \sum_{j=0}^{J} d_j \frac{p(r_j)q(r_j)}{r_j(\mathrm{d}\rho/\mathrm{d}r)_j}\, \Delta\rho, \tag{6.85a}$$

where

$$d_0 = 1/2, \qquad d_J = 1/2 \qquad d_j = 1, \quad \text{for} \quad j = 1, \ldots, J-1. \tag{6.85b}$$

The discrete version of (6.79) becomes

$$\varepsilon =< \psi_1, \psi_{1,1} >_\Delta / < \psi_{1,1}, \psi_{1,1} >_\Delta, \tag{6.86}$$

where ε is specified and serves as the continuation parameter, besides being a measure of the wave amplitude. We seek a solution $\mathcal{U}$ and α subject to the condition (6.86) so that $\mathcal{E} = 0$. The set (6.81) together with the condition (6.86) is closed and hence a unique solution can be found provided the Jacobian in the Newton iterates is non-singular. We now discuss two continuation procedures for finding a solution branch defined by (ε, α).

6.9.1 Simple continuation

Define a projection vector P such that

$$P^{\top}\mathcal{U} = \varepsilon. \tag{6.87}$$

The amplitude equation (6.86) may now be restated as

$$\mathcal{A} = P^{\top}\mathcal{U} - \varepsilon = 0. \tag{6.88}$$

The Newton iterates are simply given by

$$\begin{bmatrix} (\partial\mathcal{E}/\partial\mathcal{U})^i, & (\partial\mathcal{E}/\partial\alpha)^i \\ (\partial\mathcal{A}/\partial\mathcal{U})^i, & (\partial\mathcal{A}/\partial\alpha)^i \end{bmatrix} \begin{bmatrix} (\Delta\mathcal{U})^i \\ (\Delta\alpha)^i \end{bmatrix} = - \begin{bmatrix} \mathcal{E}^i \\ \mathcal{A}^i \end{bmatrix}, \quad i = 0, 1, \ldots. \tag{6.89}$$

The index i denotes the iterates at which all the entries are calculated. Starting with $i = 0$ we proceed by refining the solution till convergence is achieved. The improvements are given by

$$\mathcal{U}^{i+1} = \mathcal{U}^i + \Delta\mathcal{U}^i, \quad \alpha^{i+1} = \alpha^i + \Delta\alpha^i. \tag{6.90}$$

6.9.2 Pseudo-arc-length continuation

This continuation procedure is a generalization of the simple continuation method outlined above. It enables one to follow solution paths that may contain one or more folds. This was used in the place of simple continuation to determine if folds existed. The method described is a modified version of Keller's (1987) method.

Assume that $(\varepsilon^0, \alpha^0)$ is a known solution. In place of (6.88) we use instead

$$\mathcal{A}(\varepsilon, \alpha, \Delta s) = \dot{\varepsilon}^0(\varepsilon - \varepsilon^0) + \dot{\alpha}(\alpha - \alpha^0) - \Delta s = 0, \tag{6.91}$$

where $(\dot{\varepsilon}^0, \dot{\alpha}^0)$ is the tangent at the known solution and s is the arclength measured along the solution path. Using (6.87) we obtain

$$\begin{bmatrix} (\partial\mathcal{E}/\partial\mathcal{U})^i, & (\partial\mathcal{E}/\partial\alpha)^i \\ \dot{\varepsilon}^0 P^{\top}, & \dot{\alpha}^0 \end{bmatrix} \begin{bmatrix} (\Delta\mathcal{U})^i \\ (\Delta\alpha)^i \end{bmatrix} = - \begin{bmatrix} \mathcal{E}^i \\ \mathcal{A}^i \end{bmatrix}, \quad i = 0, 1, \ldots, \tag{6.92}$$

which replaces the iterates (6.89). Upon convergence, the new tangent is computed at the new point and the whole process is repeated.

6.9.3 Computation and structure of Jacobian

We now discuss the computation of the derivatives involved in the Jacobian and the structure of the matrices given in (6.89) and (6.92). All but $\partial\mathcal{E}/\partial\mathcal{U}$ are achieved easily. They are either row- or column-vectors as indicated. The derivative $\partial\mathcal{E}/\partial\mathcal{U}$ is a block penta-diagonal type square matrix with entries

$$\partial\mathcal{E}/\partial\mathcal{U} = \begin{bmatrix} \Lambda_{0,0} & & & & & \\ \Lambda_{1,0} & \Lambda_{1,1} & \Lambda_{1,2} & \Lambda_{1,3} & & \\ \Lambda_{2,0} & \Lambda_{2,1} & \Lambda_{2,2} & \Lambda_{2,3} & \Lambda_{2,4} & \\ \ddots & \ddots & \ddots & \ddots & \ddots & \\ & \Lambda_{J-2,J-4} & \Lambda_{J-2,J-3} & \Lambda_{J-2,J-2} & \Lambda_{J-2,J-1} & \Lambda_{J-2,J} \\ & & \Lambda_{J-1,J-3} & \Lambda_{J-1,J-2} & \Lambda_{J-1,J-1} & \Lambda_{J-1,J} \\ & & & \Lambda_{J,J-2} & \Lambda_{J,J-1} & \Lambda_{J,J} \end{bmatrix}, \tag{6.93}$$

where

$$\Lambda_{i,j} = \begin{bmatrix} \{\partial f_{k,i}/\partial\psi_{l,j}\} & \{\partial f_{k,i}/\partial\Omega_{l,j}\} \\ \{\partial g_{k,i}/\partial\psi_{l,j}\} & \{\partial g_{k,i}/\partial\Omega_{l,j}\} \end{bmatrix}, \tag{6.94}$$

is a block matrix with 4 sub-blocks. Each of the sub-blocks is of size $m \times m$. As an example, consider computation of the (k,l) element of upper-left sub-block in $\Lambda_{j,j}$. This is given by

$$\begin{aligned} \frac{\partial f_{k,j}}{\partial\psi_{l,j}} &= \left(\alpha - \frac{\kappa}{r_j}\psi'_{0,j}\right)\frac{\partial\zeta_{k,j}}{\partial\psi_{l,j}} + \frac{\kappa}{r_j}\zeta'_{0,j}\frac{\partial\psi_{k,j}}{\partial\psi_{l,j}} \\ &\quad - \frac{\kappa}{kr_j}\left[\frac{\partial N_{k,j}(\psi',\zeta)}{\partial\psi_{l,j}} - \frac{\partial N_{k,j}(\zeta',\psi)}{\partial\psi_{l,j}} + \frac{2}{r_j}\frac{\partial N_{k,j}(\zeta,\psi)}{\partial\psi_{l,j}}\right]. \end{aligned} \tag{6.95}$$

The various derivatives in (6.95) are defined below.

$$\frac{\partial\zeta_{k,j}}{\partial\psi_{l,j}} = (\gamma_j - k^2\kappa^2)\delta_{k,l},$$

$$\frac{\partial\psi_{k,j}}{\partial\psi_{l,j}} = \delta_{k,l},$$

where $\delta_{k,l}$ is the Kronecker delta. The derivative of nonlinear terms involves more work. For illustration, the derivative $\partial N_{k,j}(A,B)/\partial A_{l,j}$ is obtained by setting

$$\frac{\partial N_{k,j}(A,B)}{\partial A_{l,j}} = \frac{1}{2}\left(T_1 - T_2 + T_3\right),$$

where

$$T_1 = (k-l)B_{k-l,j}, \qquad \text{if} \quad l \leq k-1,$$

$$T_2 = (l-k)B_{l-k,j}, \qquad \text{if} \quad l \geq k+1,$$

$$T_3 = (k+l)B_{k+l,j}, \qquad \text{if} \quad l \leq m-k.$$

Similar expressions may be written down for other derivatives.

6.10 Computation of the pressure and the Bernoulli function

Since we have adopted an entirely different approach in fixing the solution branch, i.e., by keeping the base flow the same, we are naturally interested in knowing the form of the Bernoulli function H and the circulation function Ω. In particular, we are interested in the variation of $H(\psi)$ and $\Omega(\psi)$ with ε. We compute this variation by evaluating H and Ω on various streamlines for each ε. We describe the computation of H here.

In order to compute H, we need to compute the pressure. Since the pressure is assumed to be of the form

$$p(r,x) = \sum_{k=0}^{m} p_k \cos(kx), \tag{6.96}$$

we obtain from the axial momentum equation

$$p_k = \frac{\alpha}{\kappa} w_k + \frac{w_0'}{k\kappa} u_k + \frac{1}{k\kappa} \widetilde{N}_k^{oo}\left(u, w'\right) - w_0 w_k - \frac{1}{k} N_k^{ee}(w,w), \quad k \neq 0. \tag{6.97}$$

The equation for the constant mode of pressure is not obtainable. Instead from the radial momentum equation we obtain

$$p_0' = \frac{v_0^2}{r} - \kappa N_0^{eo}(w,u) + \frac{1}{r}\widetilde{N}_0^{eo}(v,v) - \widetilde{N}_0^{oe}(u,u'), \tag{6.98}$$

where, if $k \neq 0$, we have

$$\widetilde{N}_k^{ee}(A,B) = +\tilde{S}_1 + \tilde{S}_2 - \tilde{S}_3, \quad \widetilde{N}_k^{oo}(A,B) = +\tilde{S}_1 - \tilde{S}_2 + \tilde{S}_3, \tag{6.99a}$$

$$\widetilde{N}_k^{eo}(A,B) = +\tilde{S}_1 + \tilde{S}_2 + \tilde{S}_3, \quad \widetilde{N}_k^{oe}(A,B) = -\tilde{S}_1 + \tilde{S}_2 + \tilde{S}_3, \tag{6.99b}$$

and if $k = 0$, we have

$$\widetilde{N}_0^{eo}(A,B) = \frac{1}{2}\sum_{l=1}^{m} A_l B_l, \quad \widetilde{N}_0^{oe}(A,B) = \frac{1}{2}\sum_{l=1}^{m} A_l B_l, \tag{6.100}$$

with

$$\widetilde{S}_1 = \frac{1}{2}\sum_{l=1}^{k-1} A_l B_{k-l}, \quad \widetilde{S}_2 = \frac{1}{2}\sum_{l=k+1}^{l\le m} A_l B_{l-k}, \quad \widetilde{S}_3 = \frac{1}{2}\sum_{l=1}^{l+k\le m} A_l B_{l+k}, \tag{6.101}$$

$$S_1 = \frac{1}{2}\sum_{l=1}^{k-1}(k-l)A_l B_{k-l}, \quad S_2 = \frac{1}{2}\sum_{l=k+1}^{l\le m}(l-k)A_l B_{l-k},$$

and

$$S_3 = \frac{1}{2}\sum_{l=1}^{l+k\le m}(l+k)A_l B_{l+k}. \tag{6.102}$$

The functions N_k's are defined the same way as the $\widetilde{N}_k$'s except we use S_1, S_2 and S_3 in the place of $\widetilde{S}$. When $k = 0$ we take

$$N_0^{eo}(A,B) = \frac{1}{2}\sum_{l=1}^{m} l A_l B_l, \quad N_0^{oe}(A,B) = \frac{1}{2}\sum_{l=1}^{m} l A_l B_l. \tag{6.103}$$

In order to find p_0 we need to find the boundary conditions on the pressure both at $r = 0$ and as $r \to \infty$, so that equation (6.98) can be integrated. But since the pressure is arbitrary up to constant, and this is reflected in the constant mode, we simply take

$$p_0(0) = 0. \tag{6.104a}$$

Evaluating the radial momentum equation for large values of r we get our outer boundary condition to be

$$p_0'(r) = 0, \quad \text{as} \quad r \to \infty. \tag{6.104b}$$

Next we consider the computation of H. The Bernoulli function is defined only for a steady flow. The method we have adopted here is to compute the steady states via co-ordinate transformation and not via Galilean transformation. Since the flow can be made steady by adding an appropriate uniform axial velocity, we get

$$\begin{aligned} H &= p + \frac{1}{2}\left(u^2 + v^2 + (w - \alpha/\kappa)^2\right), \\ &= p + \frac{1}{2}\left(u^2 + v^2 + w^2\right) - \frac{\alpha}{\kappa} w + \frac{1}{2}\alpha^2/\kappa^2. \end{aligned} \tag{6.105}$$

Letting

$$H(r,x) = \sum_{k=0}^{m} H_k(r)\cos(kx), \tag{6.106}$$

we get upon substituting for the expansions of pressure and velocity components into (6.105)

$$H_k = p_k - \frac{\alpha}{\kappa} w_k + v_0 v_k + w_0 w_l + \frac{1}{2}\left[\widetilde{N}_k^{oe}(u,u) + \widetilde{N}_k^{eo}(v,v) + \widetilde{N}_k^{eo}(w,w)\right], \quad k = 1,\ldots,m, \tag{6.107a}$$

$$H_0 = p_0 - \frac{\alpha}{\kappa} w_0 + \frac{1}{2}\frac{\alpha^2}{\kappa^2} + \frac{1}{2}\left(v_0^2 + w_0^2\right) + \frac{1}{2}\left[\widetilde{N}_0^{oe}(u,u) + \widetilde{N}_0^{eo}(v,v) + \widetilde{N}_0^{eo}(w,w)\right], \tag{6.107b}$$

We compute a function $r(x)$ such that ψ is constant along it, and, therefore represents a streamline. Then we interpolate the values of H on to this streamline. As a check we must find that H is constant along any given streamline. The same procedure is adopted to verify the constancy of C on a given streamline. Table 6.2 shows the variation of H and C along a streamline. The results are given for a streamline near the 'core' boundary. The relative error stated in per cent is given by (max – min) · 100/average. of the quantity in question. As the results indicate, the constancy of both H and C is quite well maintained.

The variation of the functional form of $H(\psi)$ and $\Omega(\psi)$ is discussed with the results below.

6.11 Tests

We now establish the validity of the computed solutions and convergence via some tests. We consider convergence of linear eigenvalues as the parameter $\beta \to 0$ and as the grid size is reduced. We show the comparison of the full nonlinear solution and the perturbation solution. We also state here some tests performed for a vortex confined in a pipe. This case is considered to compare the results with those of Leibovich and Kribus (1990).

Table 6.2 Values of H and C on a streamline.

The results are for $\psi = -0.317$, $r \in [0, 5]$, $a = 1$, $J = 40$, $m = 10$ and $\beta = 0.3$.

ε	H avg	% error	C avg	% error
0.01	0.87889	0.13562	0.78577	0.16289
0.02	0.87958	0.23184	0.78522	0.27461
0.03	0.88125	0.29822	0.78484	0.34726
0.04	0.88391	0.32690	0.78467	0.37628
0.05	0.88757	0.32973	0.78469	0.38551
0.06	0.89225	0.33410	0.78492	0.38947
0.07	0.89795	0.32777	0.78539	0.39943
0.08	0.90477	0.34314	0.78619	0.42302
0.09	0.91194	0.35292	0.78649	0.44096
0.10	0.91990	0.36487	0.78679	0.45264
0.11	0.92885	0.44500	0.78734	0.51341
0.12	0.93860	0.53920	0.78796	0.63576
0.13	0.94933	0.53138	0.78893	0.63117
0.14	0.96103	0.58754	0.79047	0.74597

Table 6.3 Convergence of Linear Eigenvalues.

Convergence of linear eigenvalue as $\beta \to 0$. Relative error is given by (Numerical – Exact) · 100 / Exact. This case is for $a = 1$, $\Omega_\infty = 1$, $\kappa = 1$, $r \in [0, 10]$, $J = 640$.

β	α Exact	α Numerical	Relative Error(%)
0.10	0.7059052	0.692063	−1.961
0.05	0.7059052	0.702189	−0.526
0.02	0.7059052	0.705271	−0.090
0.01	0.7059052	0.705731	−0.025
0.005	0.7059052	0.705852	−0.007

As the parameter $\beta \to 0$, the flow tends to that of Kelvin's columnar vortex when the base flow considered is that of Kelvin-type. Under this limit the phase speed must approach that of Kelvin waves. The phase speeds for the Kelvin's vortex are tabulated in Table 5.1, Chapter 5. Table 6.3 summarizes the test for the largest eigenvalue with $\kappa = 1$. We conclude that the linear eigenvalue is indeed correct. The same trend was observed for other eigenvalues. A relatively large number of points in the radial directions were needed since the gradients were quite steep in the core region.

Since we have used central differences to approximate the derivatives, we expect the solution to be second order accurate in the radial spacing. Table 6.4 summarizes

Table 6.4 Rate of convergence of linear eigenvalues.

Results shown are for $a = 1$, $\kappa = 1$, $\Omega_\infty = 1$, $r \in [0, 10]$ and $\beta = 0.4$. 'Rate' is computed by dividing the successive differences. Only the convegence of the largest eigenvalue is shown.

J	α	*difference*	*Rate*
20	0.5617194		
40	0.5620591	$3.397\ 10^{-4}$	
80	0.5623861	$3.270\ 10^{-4}$	1.04
160	0.5624877	$1.016\ 10^{-4}$	3.22
320	0.5625146	$2.690\ 10^{-5}$	3.94
640	0.5625214	$6.800\ 10^{-6}$	3.96

these results and the last column, obtained by dividing the successive differences, shows the rate of convergence. The rate approaches 4 as expected since the grid spacing is halved successively. But the convergence appears to be rather "slow". A grid resolution of $J = 320$ points in a domain with $R = 10$ appears to be reasonable. The actual grid spacing within the core is smaller than $10/320$ for $J = 320$ and $R = 10$ due to grid stretching.

If the flow is constrained in a pipe of radius 'a', then the perturbation stream-function must vanish at $r = a$. Now consider the unperturbed fluid to be rotating at a uniform rate inside the pipe. The linear wave speed α/κ, where κ is the wavenumber of perturbation, can be obtained as

$$\alpha_n/\kappa = 2\Omega_a/a^2 \left(\kappa^2 + j_{1,n}^2\right)^{1/2}, \tag{6.108}$$

where, $j_{1,n}$ is the n^{th} zero of the Bessel function J_1 and Ω_a is the circulation of the vortex. Table 6.5 summarizes the comparisons of exact values of α_n with the numerically calculated values. The numbers stand in good agreement. The relative error tends to increase as n increases because the eigen functions associated with those eigenvalues become more oscillatory.

We also compared the linear eigenvalues for the flow configuration used by Leibovich and Kribus (LK). The base flow consists of a vortex in a pipe of radius one. The axial and swirl flow profiles are assumed to be of the form

$$w_{0,0} = 1, \quad v_{0,0} = \left(1 - e^{-r^2/a^2}\right)/r.$$

Table 6.5 Linear eigenvalues for a vortex in a pipe.

The table shows agreement between numerical and exact linear eigenvalues for a uniform vortex in a pipe. Results are for $a = 1$, $\Omega_a = 1$, $\kappa = 1$ and $J = 640$. Uniform grid was used in r.

n	α_n *(Exact)*	α_n *(Numer.)*	*Rel. Error(%)*
1	0.50505	0.505046	$-7.92\,10^{-4}$
2	0.282226	0.282229	−0.0011
3	0.195646	0.195650	−0.0018

Linear waves with period L are considered. For the case of $a = 1/\sqrt{2}$ and $L = 6$, we obtained the phase speed to be 1.4424 while the phase speed computed by LK is 1.4033 for the same grid resolution. The value found by LK is about 3% off from our case. Similar differences were found with various eigenvalues found in Table 1 of LK.

As noted earlier, the perturbation solution can be used to establish that the solution path followed by the Newton's method is unique. The only assumption built into the perturbation solution is that the base flow is not altered. Apart from this, the solution procedure is uniquely defined. If there were more than one solution at a given value of ε, this would be reflected in the computation of coefficients of the expansion of α. That is to say, the system defined by the equations (6.77) subject to the constraint (6.79) would result in a singular matrix. All the cases we looked at gave nonsingular matrices. Therefore we infer that the perturbation solution defines a unique solution. Figure 6.2 shows the plot of α as a function of perturbation parameter ε. The upper curve is for the full solution computed using Newton's method. The lower curve is the perturbation approximation given by $\alpha = \alpha_0 + \varepsilon^2\alpha_2$. As can be seen, even just one term gives a good approximation. Higher order approximations are nearly indistinguishable from the Newton's solution.

6.12 The limit of $\beta \to 0$

Under the limit of $\beta \to 0$, the base flow profile approaches that of Kelvin's columnar vortex. The natural question that arises is whether the nonlinear solution approaches the solution computed in Chapter 5. The nonlinear Kelvin wave solutions found in the previous chapter have the property that the velocity is continuous across

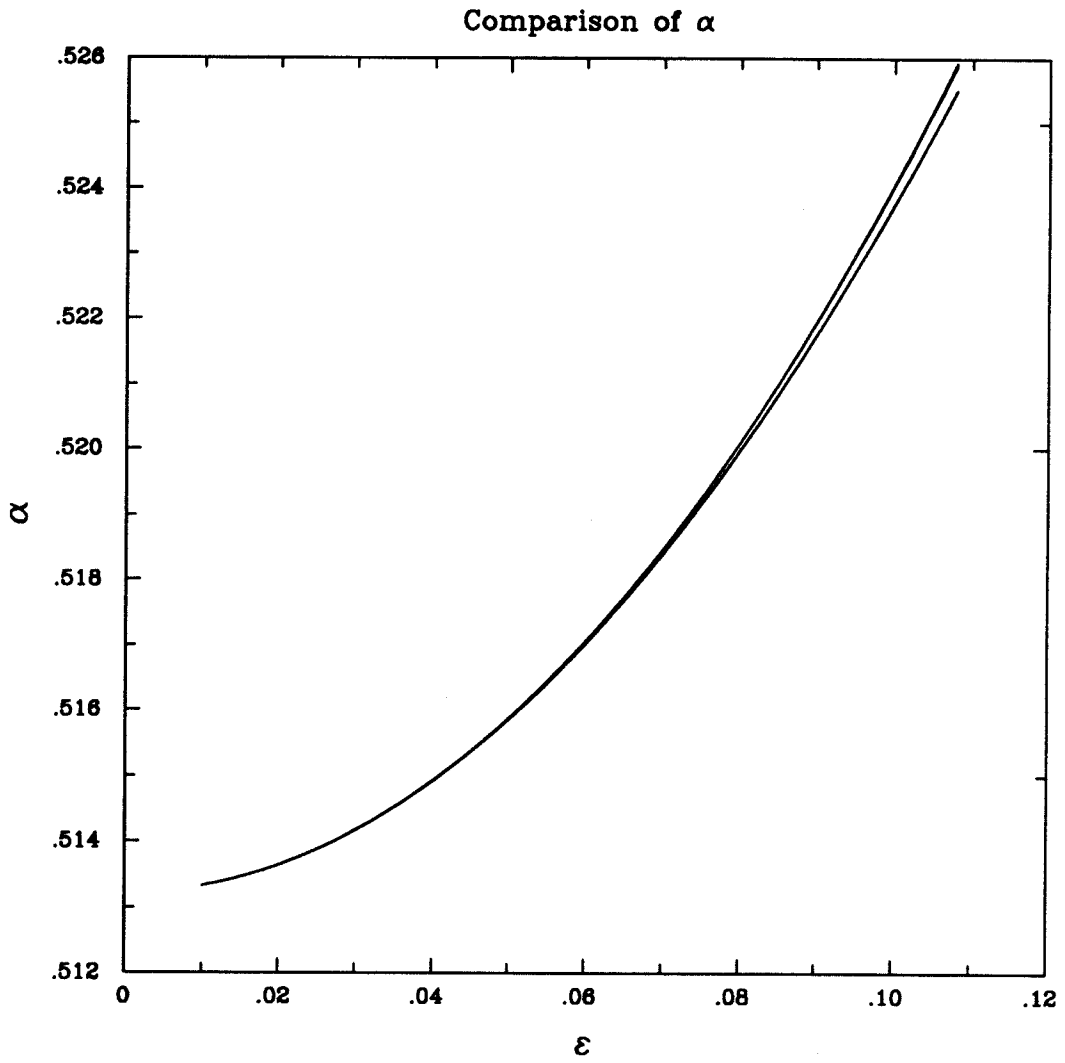

Fig. 6.2 Comparison of α for full solution with α for perturbation solution. The lower curve is the quadratic approximation $\alpha = \alpha_0 + \varepsilon^2\alpha_2$. Higher order approximation curves collapse on the the upper curve of Newton's solution. Here $a = 1$ and $J = 160$.

the core boundary. Thus the solutions are free of a vortex sheet at the core boundary. In order to maintain velocity continuity, the base flow must be corrected. But since the base flow remains unchanged in the present solutions, it is impossible to maintain velocity continuity at the "core boundary" as is clearly implied by equations (5.28) and (5.29). Thus a vortex sheet bound to the core boundary must exist at the second order. However, the linear solution is not affected by this. The shape of the "core boundary" is not computed explicitly when $\beta \neq 0$. Now we show that a vortex sheet does indeed arise in the limit $\beta \to 0$ by evaluating the normal and tangential velocities at the "core boundary." We make use of the perturbation solution to establish the result. Assume that as $\beta \to 0$, an interface (core boundary) begins to form and has the representation

$$\tilde{R}(x) = \tilde{a} + \varepsilon \tilde{a}_{11} \cos(x) + O(\varepsilon^2).$$

Clearly $\tilde{a} = a$, which is the radial distance at which the interface is located for the unperturbed flow. The normal (q_n) and the tangential (q_t) components of the fluid velocity at the interface are given by

$$q_n(r,x) = u - \kappa \frac{\mathrm{d}\tilde{R}}{\mathrm{d}x} w, \quad q_t(r,x) = \kappa \frac{\mathrm{d}\tilde{R}}{\mathrm{d}x} u + w, \quad \text{at} \quad r = \tilde{R}. \tag{6.109}$$

Assuming that the base flow is fixed, we obtain, upon using expansions for u and w,

$$\begin{aligned} q_n(\tilde{R}) = {} & \varepsilon \left[u_{11}(a) + a_{11}\kappa w_0(a)\right] \sin(x) \\ & + \varepsilon^2 \left[u_{22}(a) + \frac{a_{11}}{2} u_{11}'(a) + \kappa \frac{a_{11}}{2} w_{11}(a)\right] \sin(2x), \end{aligned} \tag{6.110a}$$

$$\begin{aligned} q_t(\tilde{R}) = {} & w_0(a) + \varepsilon w_{11}(a) \cos(x) + \varepsilon^2 \frac{a_{11}}{2} \left[w_{11}'(a) - \kappa u_{11}(a)\right] \\ & + \varepsilon^2 \left[\frac{a_{11}}{2} \kappa u_{11}(a) + w_{22}(a) + \frac{a_{11}}{2} w_{11}'\right] \cos(2x). \end{aligned} \tag{6.110b}$$

From Figure 6.3 we infer that the normal velocity must be continuous since all the terms are continuous at a. From Figure 6.4 we infer that the component of q_t contributing to $\varepsilon^2 \cos(2x)$ is continuous even though w_{11} and w_{22} jump at a. But since u_{11} is continuous and w_{11}' jumps at a, the tangential velocity jumps at a and is

independent of x but is $O(\varepsilon^2)$. Similar conclusions can be drawn about the swirl component of the velocity.

6.13 Results

Results of steady waves are presented in the Figures 6.5 through 6.9. We present here the contours of ψ, Ω and ζ and the swirl and axial velocity profile and the variation of the Bernoulli function and the circulation function. We wish to point out that ζ is a quantity related to azimuthal component of vorticity (cf. equation 6.2). We chose this quantity because it occurs as a natural variable in the given form of Euler equations. Since it is simply off by a factor of r in relation to true vorticity, it remains a useful diagnostic of the azimuthal vorticity field. The contours are shown in the $r - x$ plane.

Figures 6.5 shows the result for $a = 1/2$ and $\beta = 0.3$. As the amplitude of the wave increases, the streamlines around $x = 0$ show divergence away from the axis. This effect continues monotonically as ε, the wave amplitude is increased. A closed streamline containing reversed flow appears around $\varepsilon = 0.05$. Within the bubble, the circulation also reverses its sense as is shown by the contours of Ω. The ζ field shows a definite concentration near the vortex axis. The axial and the swirl velocity profiles reveal that the transition from the flow without closed streamlines to the flow with closed streamlines is reasonably smooth. In spite of this smoothness, we could not continue the solution forever. The Newton's method began to lose its quadratic convergence and when the arc-length continuation was employed with step size control, the solution seemed to simply wander within a very narrow region about the solution shown. The reason is far from evident. We believe it is a consequence of discretization. In some cases, the solution path in the (α, ε) space showed formation of a fold. On closer examination of the Fourier modes of ζ, grid oscillations were found. Therefore, these solutions perhaps need to be confirmed by employing the same constraints but a very different numerical approach.

The appearance of a bubble is of significance. Leibovich & Kribus (1990), Hafez

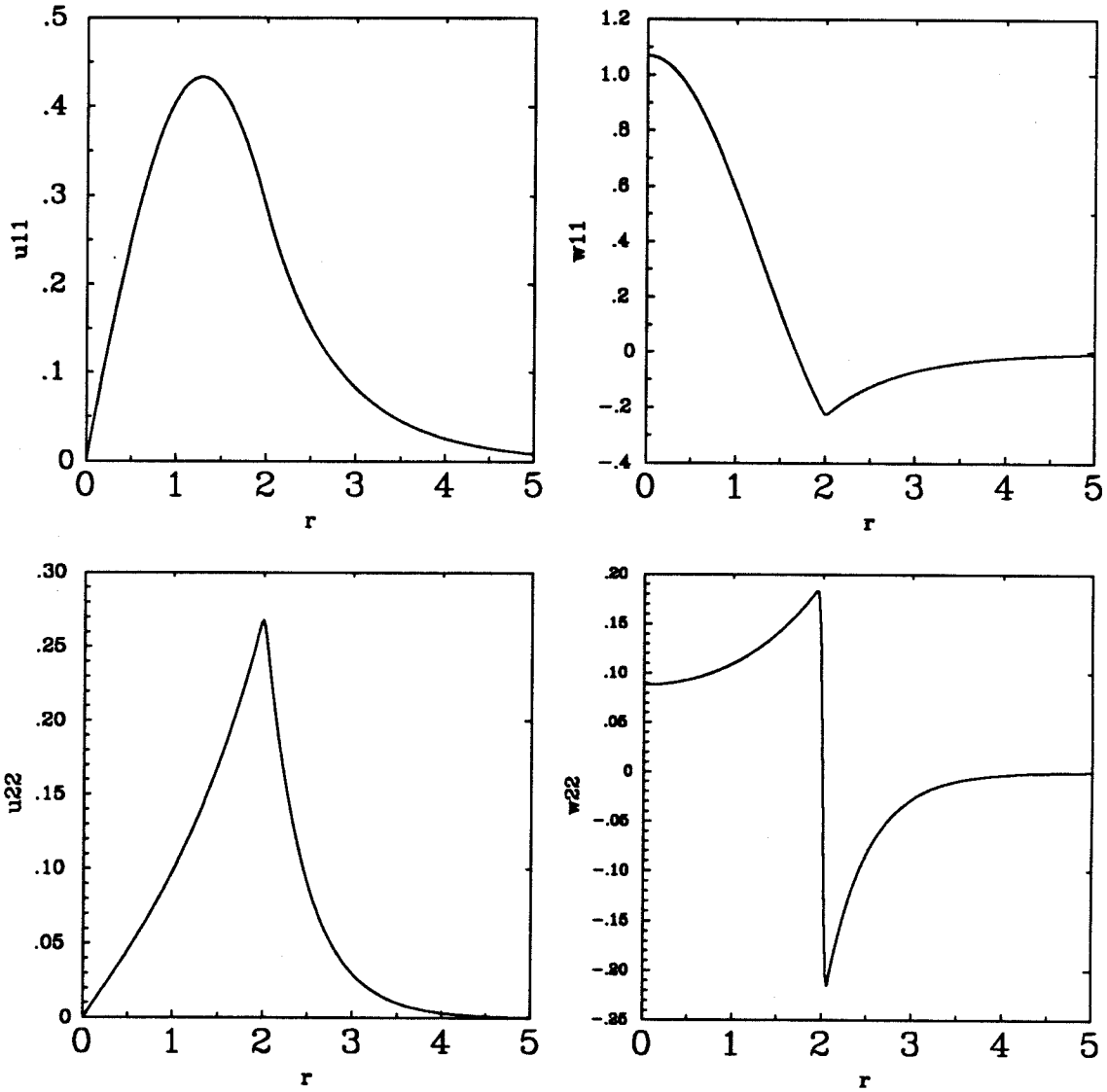

Fig. 6.3 Linear and second order components of u and w. Parameters used were $a = 2$, $\beta = 0.005$, $\Omega_\infty = 1$, $\kappa = 1$, $R = 5$, and $J = 160$.

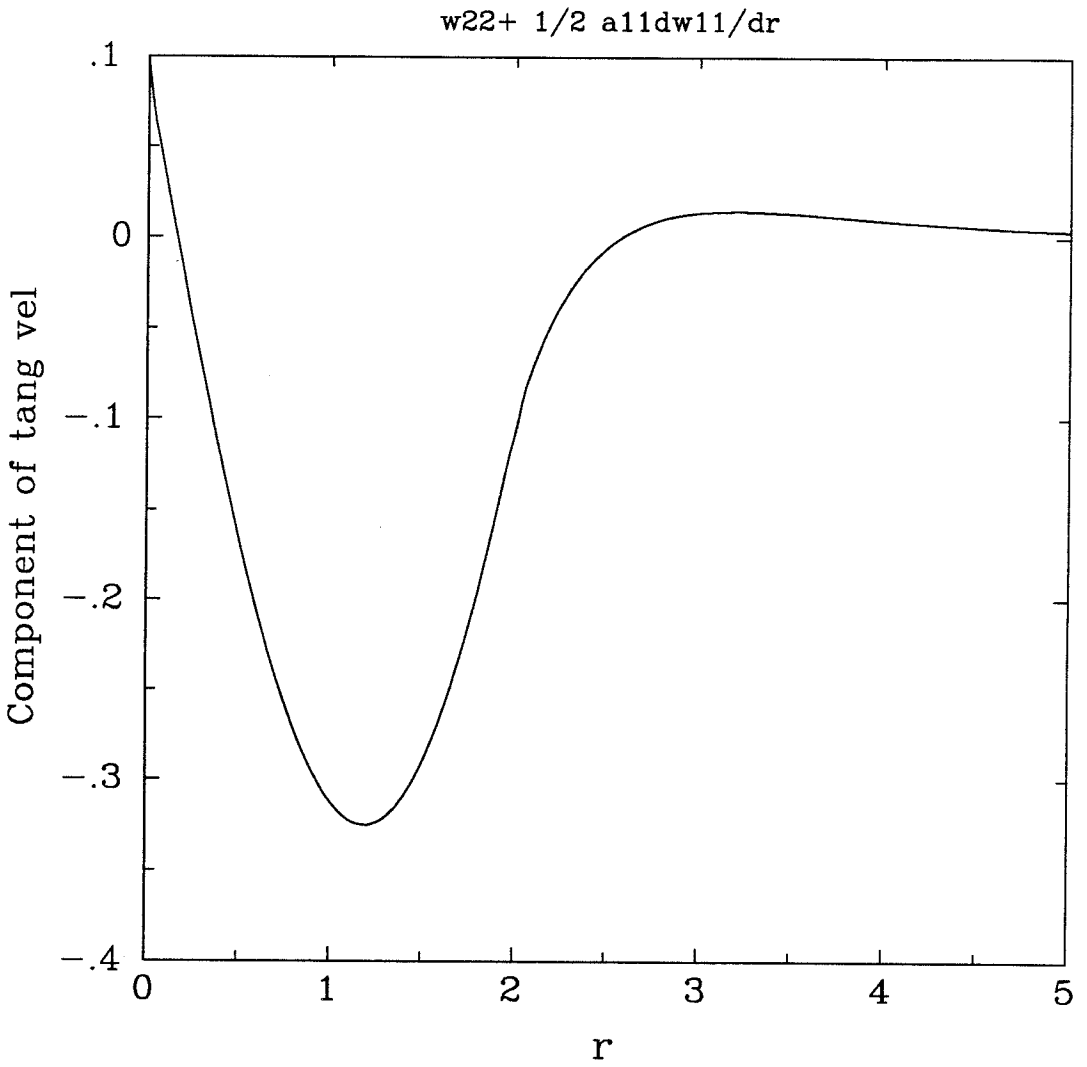

Fig. 6.4 Component of the tangential velocity contributing to the term $\varepsilon^2 \cos(2x)$. The term is continuous across the "interface" located at $a = 2$. Parameters are the same as in Figure 6.3.

et al. (1986) and others have also found reversed flow solutions but for a vortex in a pipe. Experiments of Harvey (1962) in a pipe and flow over highly swept wings show formation of bubbles. Appearance of reversed flow is generally accepted as an indication of a vortex breakdown. Benjamin (1962) also infers that a tendency towards stagnation on the axis is associated with the breakdown phenomenon.

An axial flow with $W_m = 0.5$ and $b = a$ was added to the vortex considered above. The results are shown in Figure 6.6. The addition of axial velocity reinforces the formation of the reversed flow region. The bubble is much wider in this case. The apparent corners are a result of contouring method used. The axial and the swirl velocity profiles again indicate a smooth transition as in the case above except that the axial profile is slightly wavy near the axis.

Figure 6.7 shows results for vortex with axial flow that is opposite to the case shown in Figure 6.6. That is, $W_m = -0.5$. Changing the direction of the axial flow suppresses the formation of the bubble. But the most interesting feature is the ζ field which develops a "circular patch."

Figure 6.8 shows the results for a Burgers-Rott type vortex with core size $a = 1/\sqrt{2}$. This is similar to the case considered by Leibovich and Kribus with the exception that the radial domain is unbounded. This also shows a bubble at finite amplitude, but the size appears to be smaller than in the previous case.

Figure 6.9 shows the result for $a = 1$, $\beta = 0.3$ and a zero axial flow. The same trend of bulging of streamlines and a concentration of ζ are seen. But for larger values of ε, the ζ field suffered numerical breakdown. For a smoother initial distribution, that is for larger value of β, the vorticity variable ζ still breaks down. This appears to be due to a lack of resolution. However, an increase in the number of points along x or r did not appear to improve the solution. We speculate that the number of points needed may be very large. In spite of this severe breakdown in ζ, the contours of ψ and Ω appear to be very smooth.

We have discussed at length the indeterminacy associated with axisymmetric flows

with swirl in the presence of closed streamlines as is the case when the bubble forms. It was quite clear in the sharp interface calculations that the dependence of H and C inside the bubble has the same character as the flow outside the bubble. In the solutions obtained here, the constraints are different. The numerical solution selects a form of dependence of H and C. The variations are shown for each case considered above. The functions $H(\psi)$ and $\Omega(\psi)$ extend continuously into the bubble region as shown in Figure 6.5.5b, 6.6.5b and 6.8.5b. The variation of $\Omega(\psi)$ with ε is seen to be small compared to the variation of the Bernoulli constant.

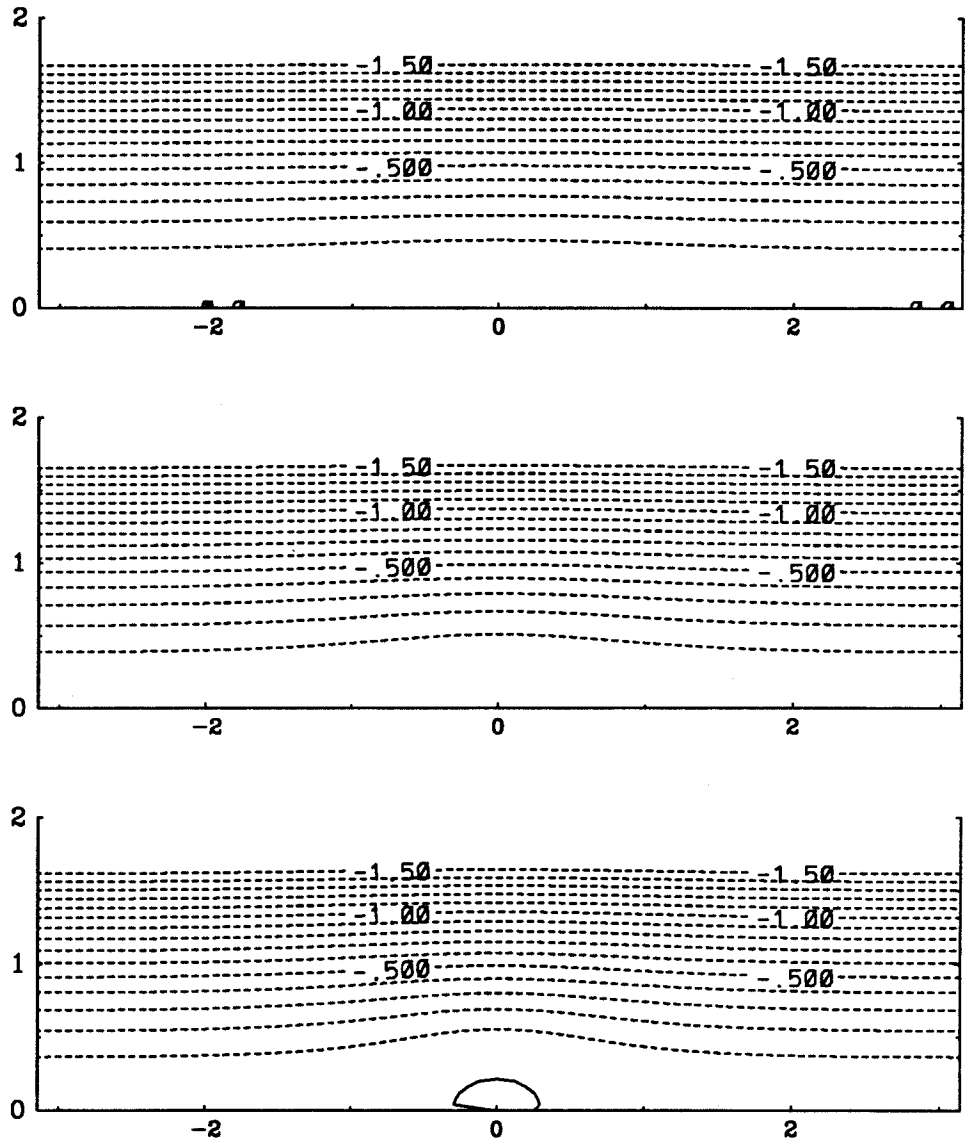

Fig. 6.5.1 Contours of ψ for $\varepsilon = 0.02,\ \ 0.04,\ \ 0.06$. Base flow is Kelvin type with $a = 1/2$, $\Omega_\infty = 1$ and $W_m = 0$. Contour interval = 0.1.

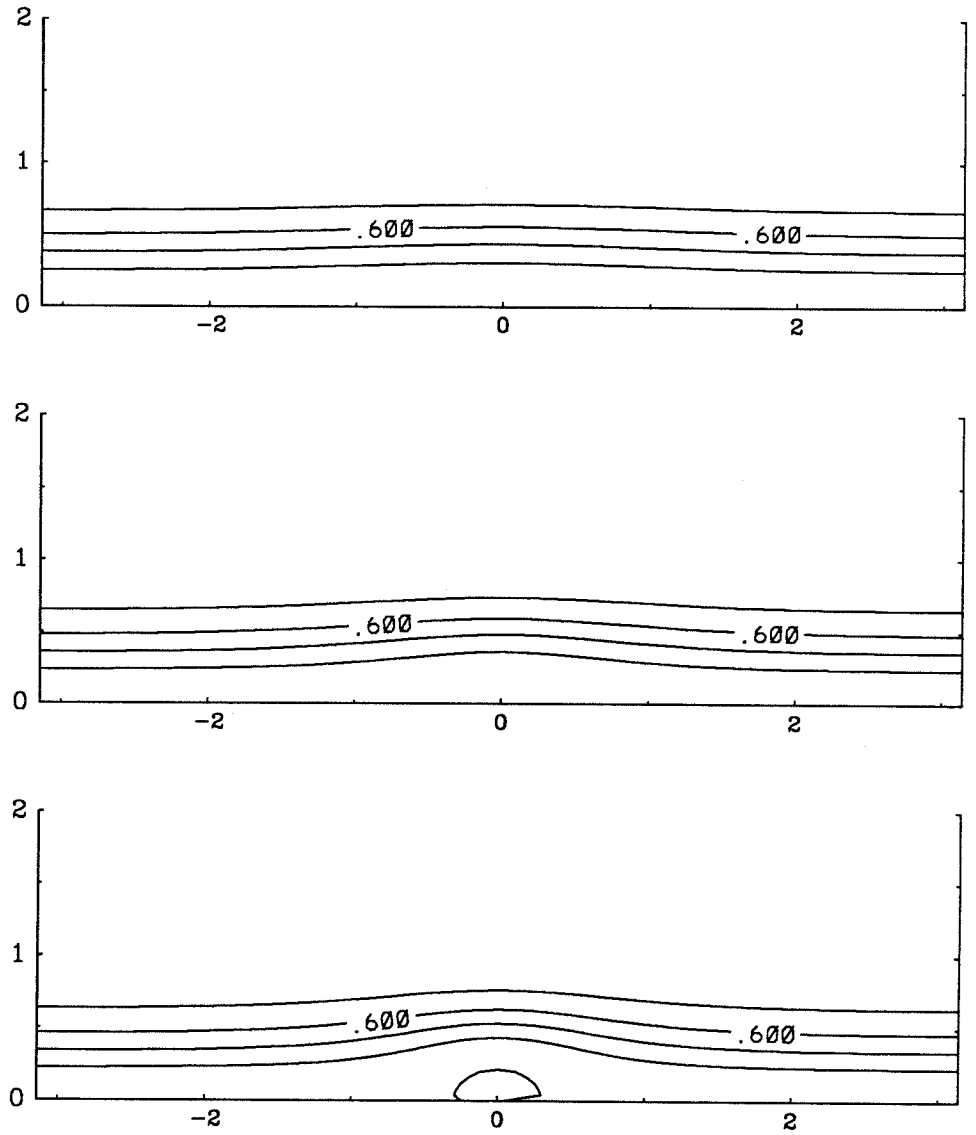

Fig. 6.5.2 Contours of Ω for $\varepsilon = 0.02,\ \ 0.04,\ \ 0.06$. Base flow is Kelvin type with $a = 1/2$, $\Omega_\infty = 1$ and $W_m = 0$. Contour interval = 0.2.

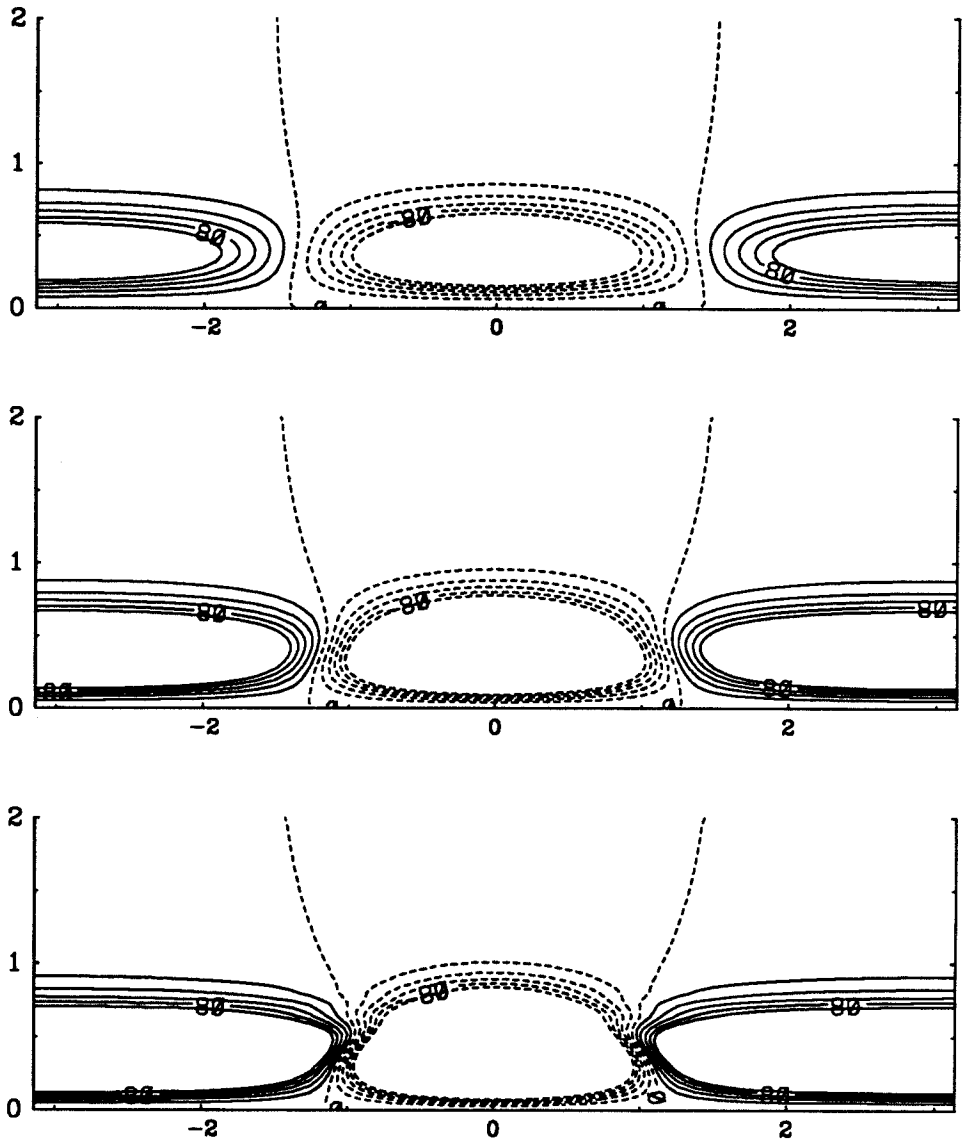

Fig. 6.5.3 Contours of ζ for $\varepsilon = 0.02,\ \ 0.04,\ \ 0.06$. Base flow is Kelvin type with $a = 1/2$, $\Omega_\infty = 1$ and $W_m = 0$. Contour interval = 0.02.

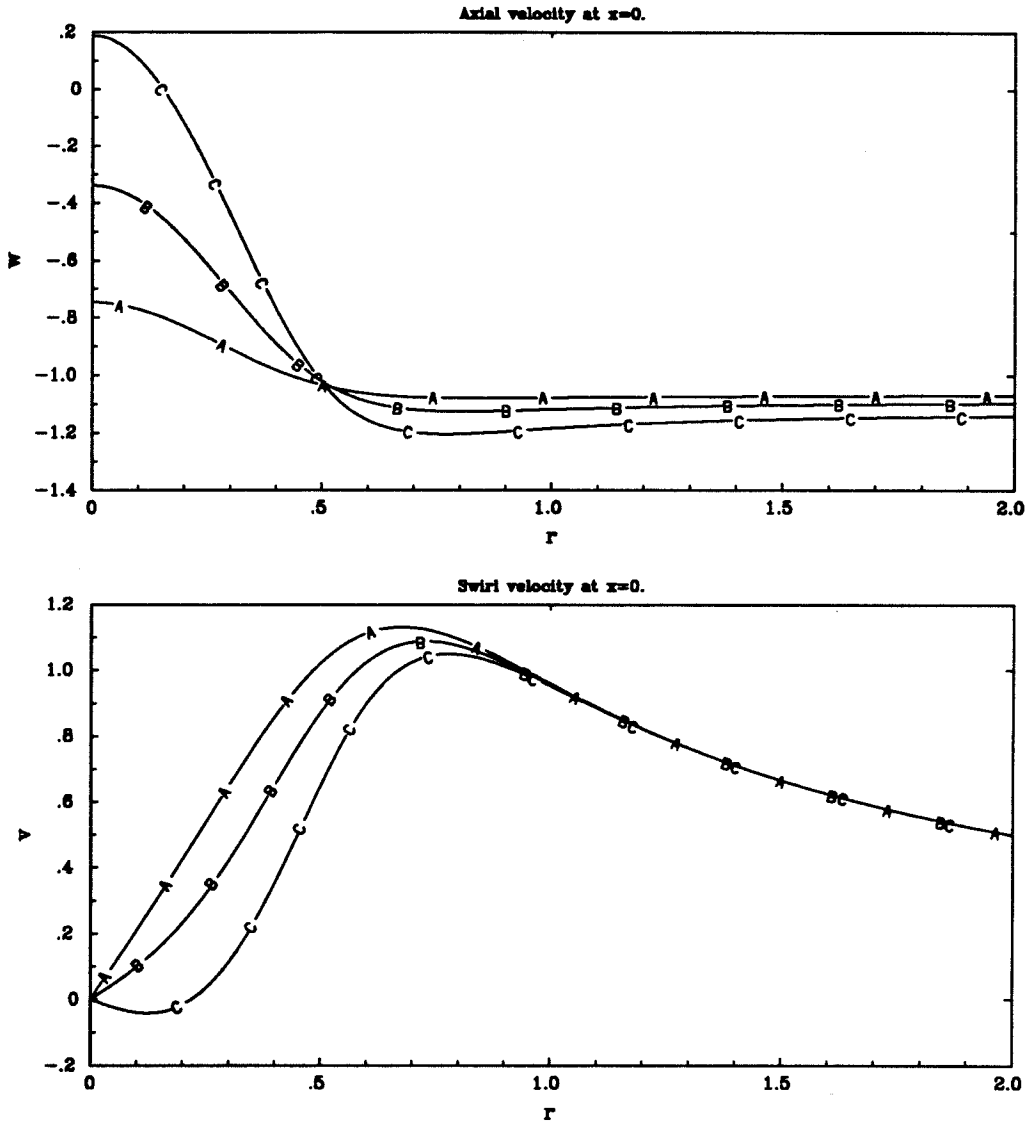

Fig. 6.5.4 Axial and swirl velocity at $x = 0$ for A. $\varepsilon = 0.02$, B. $\varepsilon = 0.04$, C. $\varepsilon = 0.06$. Base flow is Kelvin type with $a = 1/2$, $\Omega_\infty = 1$ and $W_m = 0$. Axial velocity increases at $r = 0$ with ε. The swirl decreases inside the core with increase in ε.

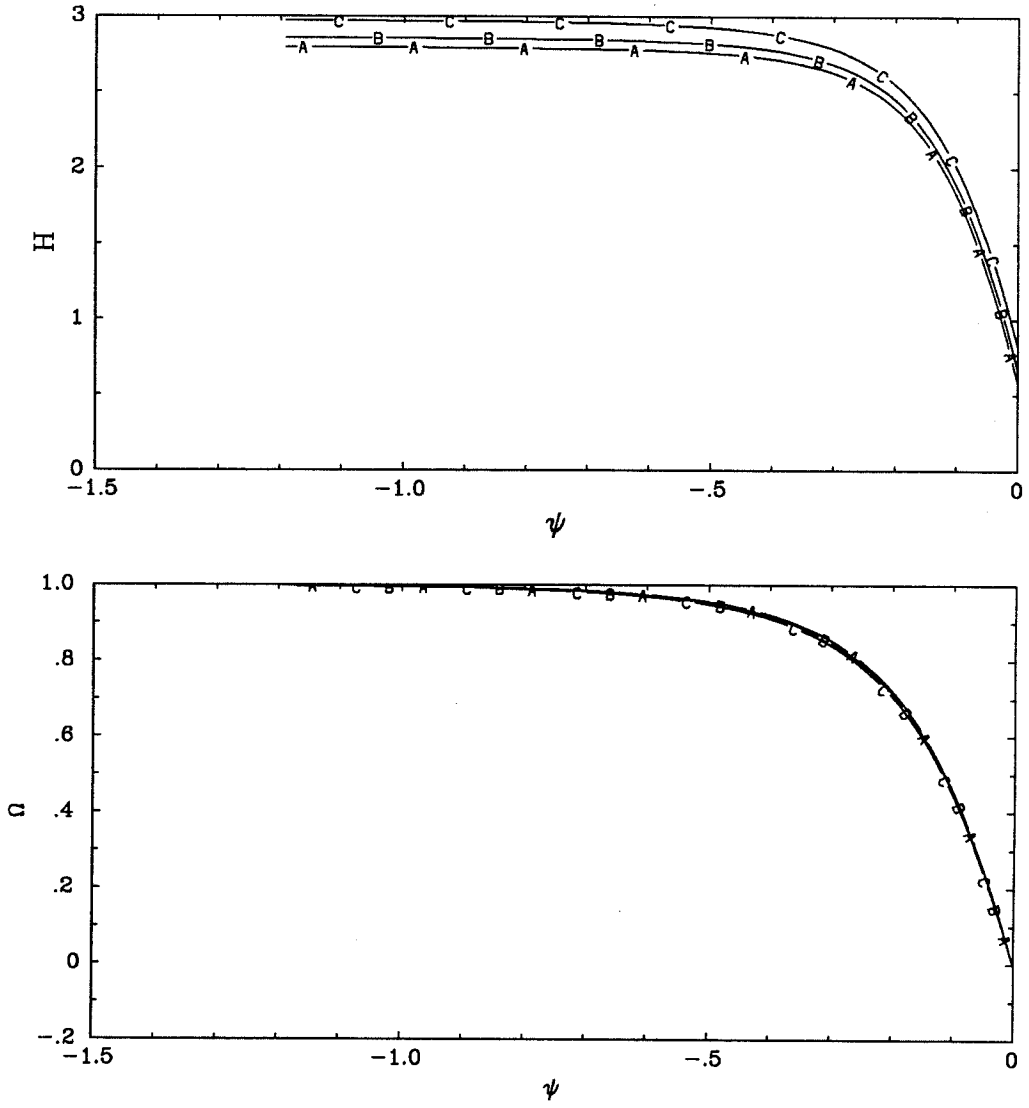

Fig. 6.5.5a Variation of $H(\psi)$ and $\Omega(\psi)$ for A. $\varepsilon = 0.02$, B. $\varepsilon = 0.04$, C. $\varepsilon = 0.06$. Base flow is Kelvin type with $a = 1/2$, $\Omega_\infty = 1$ and $W_m = 0$. $H(\psi)$ increases with ε. Variation in $\Omega(\psi)$ is small.

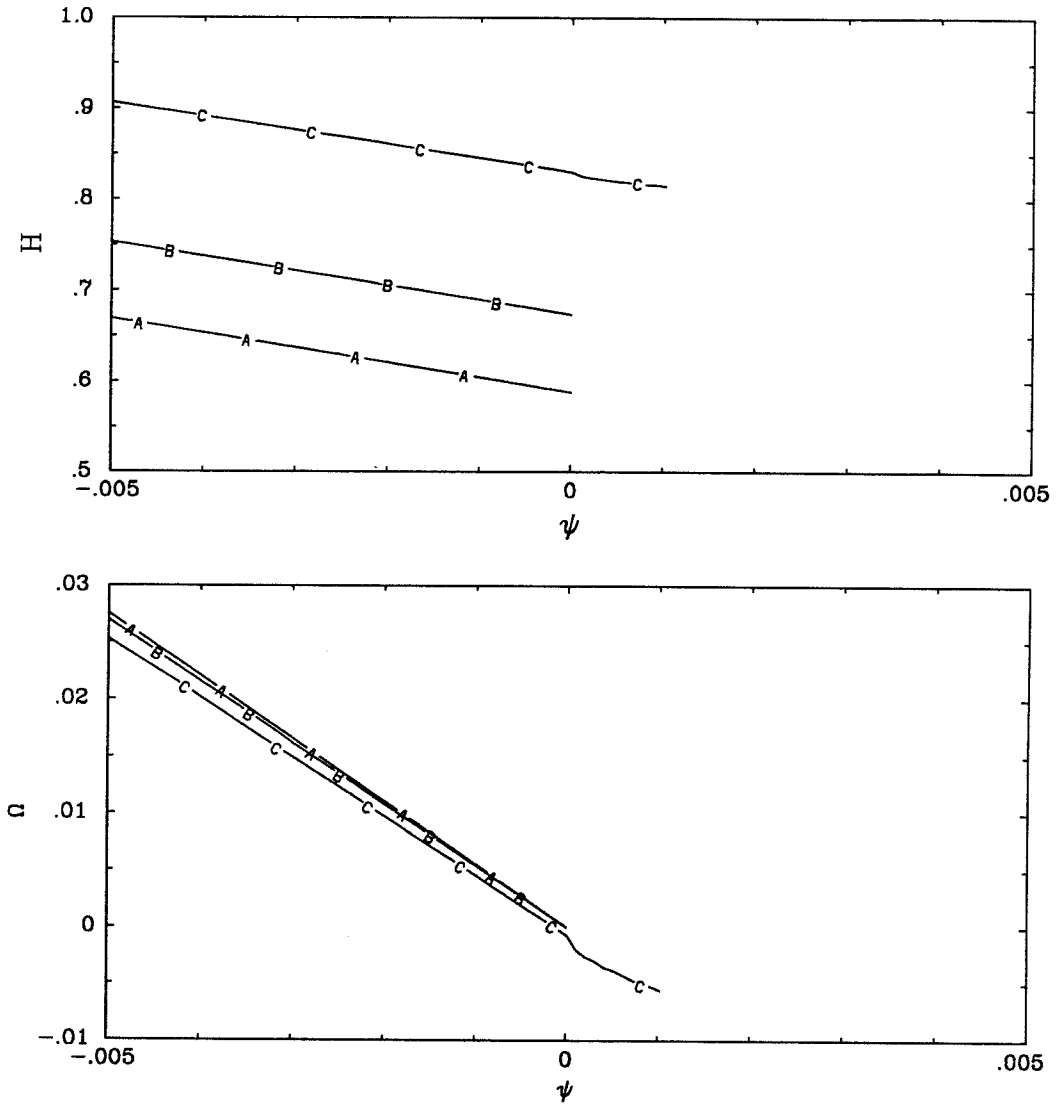

Fig. 6.5.5b Variation of $H(\psi)$ and $\Omega(\psi)$ inside the bubble for A. $\varepsilon = 0.02$, B. $\varepsilon = 0.04$, C. $\varepsilon = 0.06$. Base flow is Kelvin type with $a = 1/2$, $\Omega_\infty = 1$ and $W_m = 0$. $H(\psi)$ increases with ε. Variation in $\Omega(\psi)$ is small.

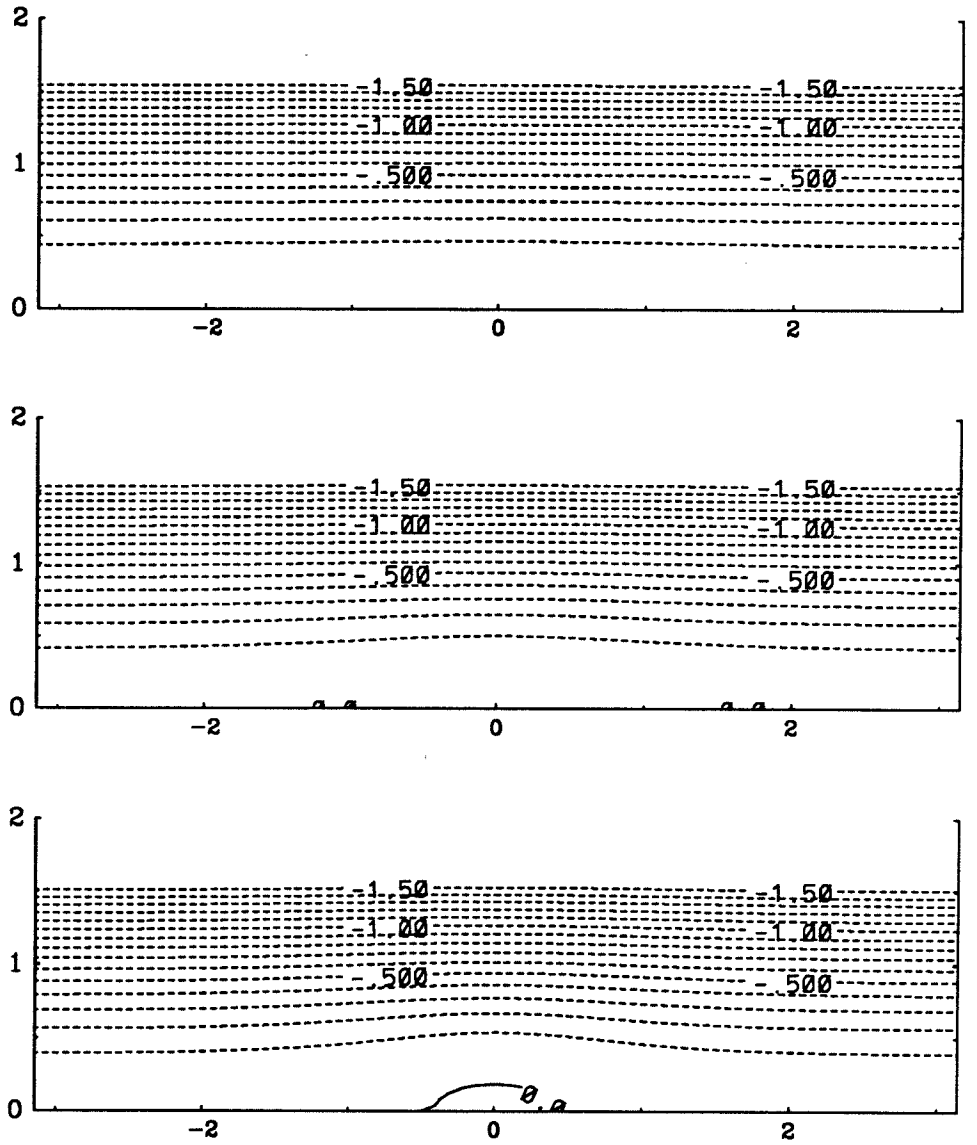

Fig. 6.6.1 Contours of ψ for $\varepsilon = 0.01,\ \ 0.03,\ \ 0.05$. Base flow is Kelvin type with $a = 1/2$, $\Omega_\infty = 1$ and $W_m = 0.5$. Contour interval = 0.1.

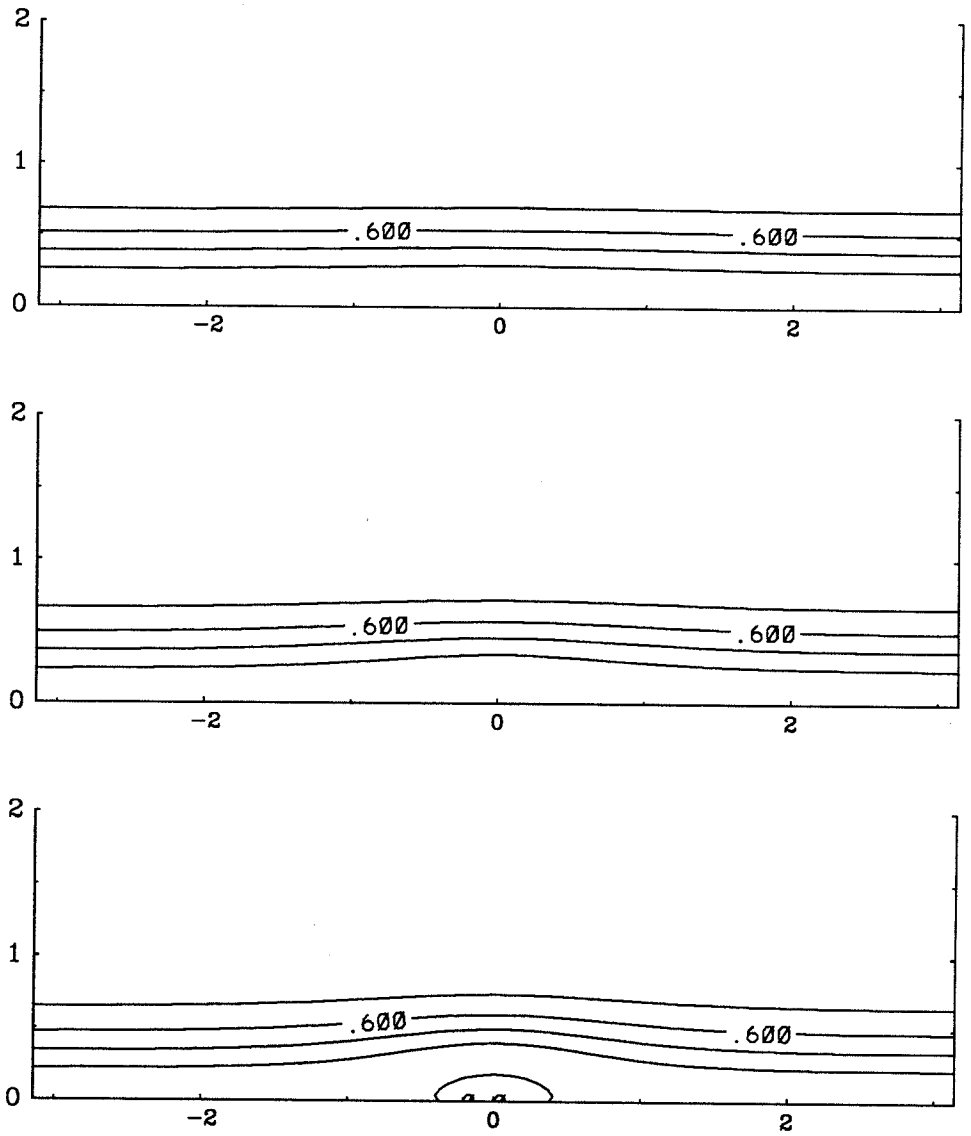

Fig. 6.6.2 Contours of Ω for $\varepsilon = 0.01,\ \ 0.03,\ \ 0.05$. Base flow is Kelvin type with $a = 1/2$, $\Omega_\infty = 1$ and $W_m = 0.5$. Contour interval $= 0.2$.

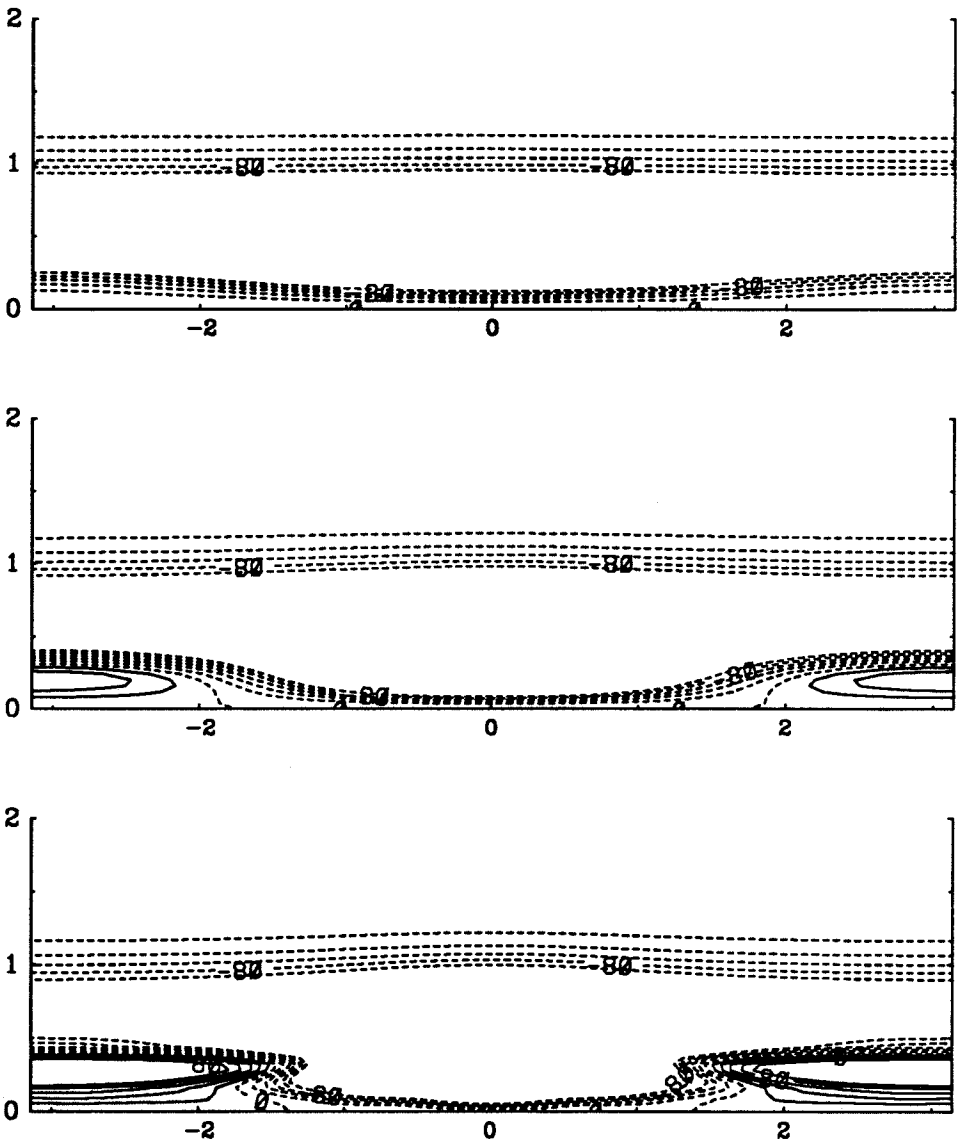

Fig. 6.6.3 Contours of ζ for $\varepsilon = 0.01,\ \ 0.03,\ \ 0.05$. Base flow is Kelvin type with $a = 1/2$, $\Omega_\infty = 1$ and $W_m = 0.5$. Maximum level=0.1, minimum level=-0.1 and contour interval = 0.02.

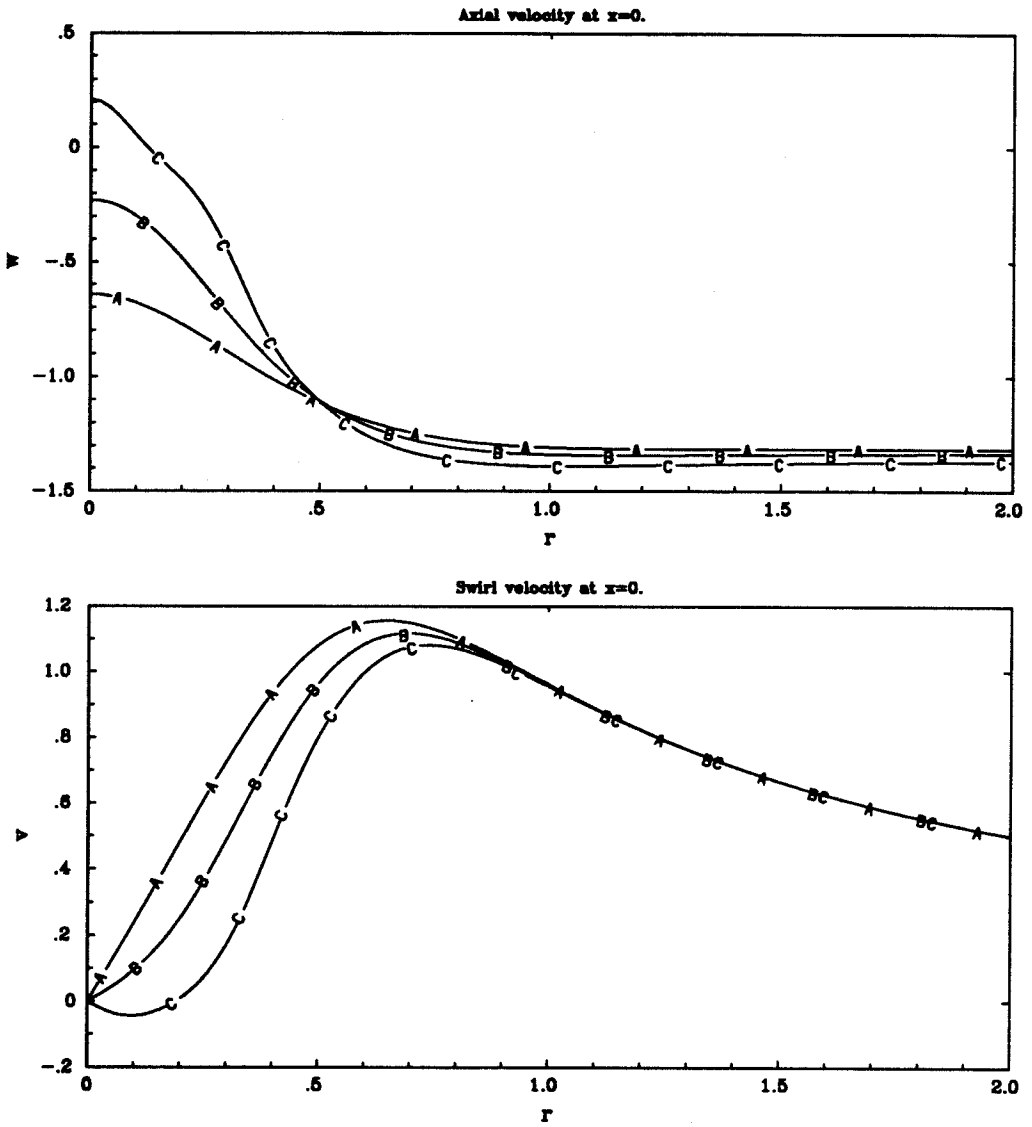

Fig. 6.6.4 Axial and swirl velocity at $x = 0$ for A. $\varepsilon = 0.01$, B. $\varepsilon = 0.03$, C. $\varepsilon = 0.05$. Base flow is Kelvin type with $a = 1/2$, $\Omega_\infty = 1$ and $W_m = 0.5$. Axial velocity increases at $r = 0$ with ε. The swirl decreases inside the core with increase in ε.

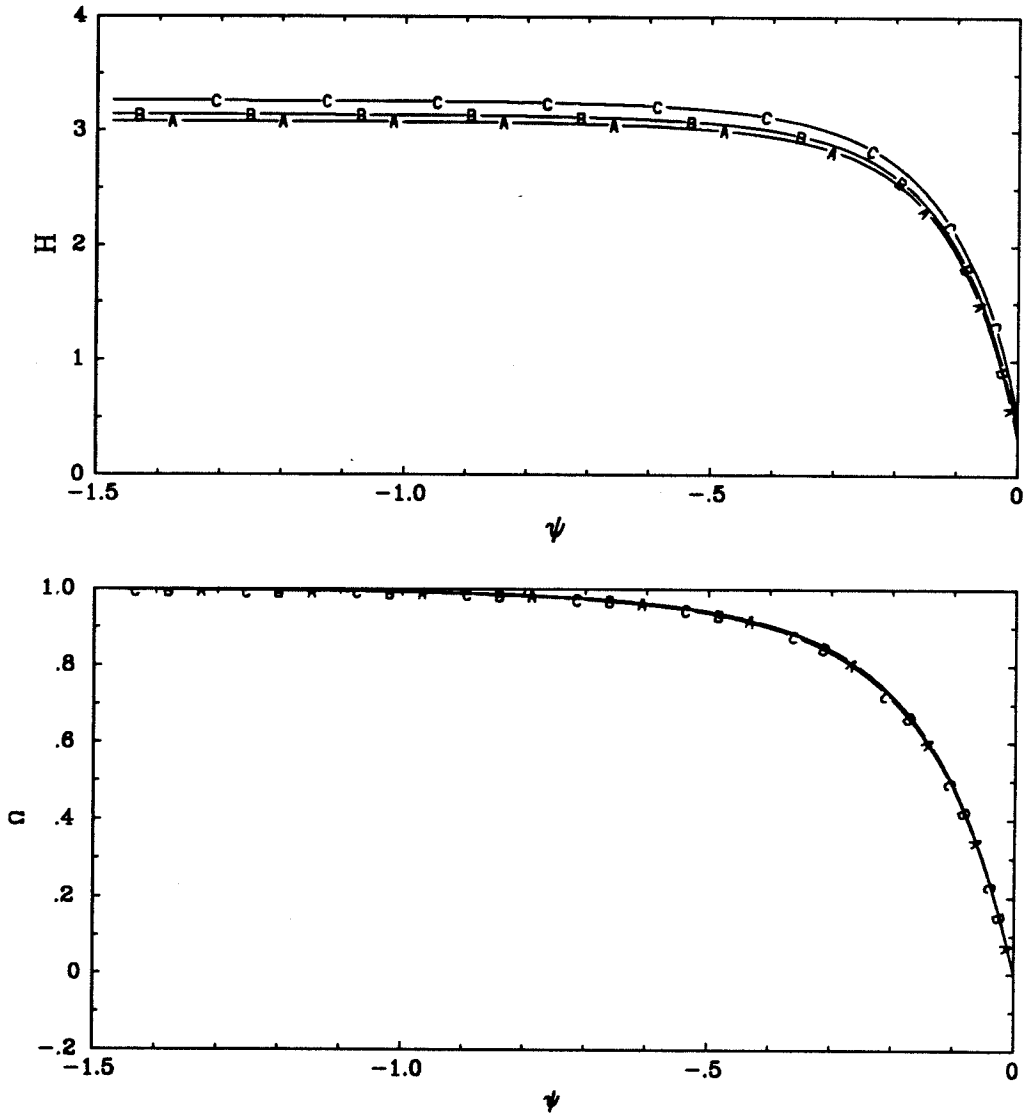

Fig. 6.6.5a Variation of $H(\psi)$ and $\Omega(\psi)$ for A. $\varepsilon = 0.01$, B. $\varepsilon = 0.03$, C. $\varepsilon = 0.05$. Base flow is Kelvin type with $a = 1/2$, $\Omega_\infty = 1$ and $W_m = 0.5$. $H(\psi)$ increases with ε. Variation in $\Omega(\psi)$ is small.

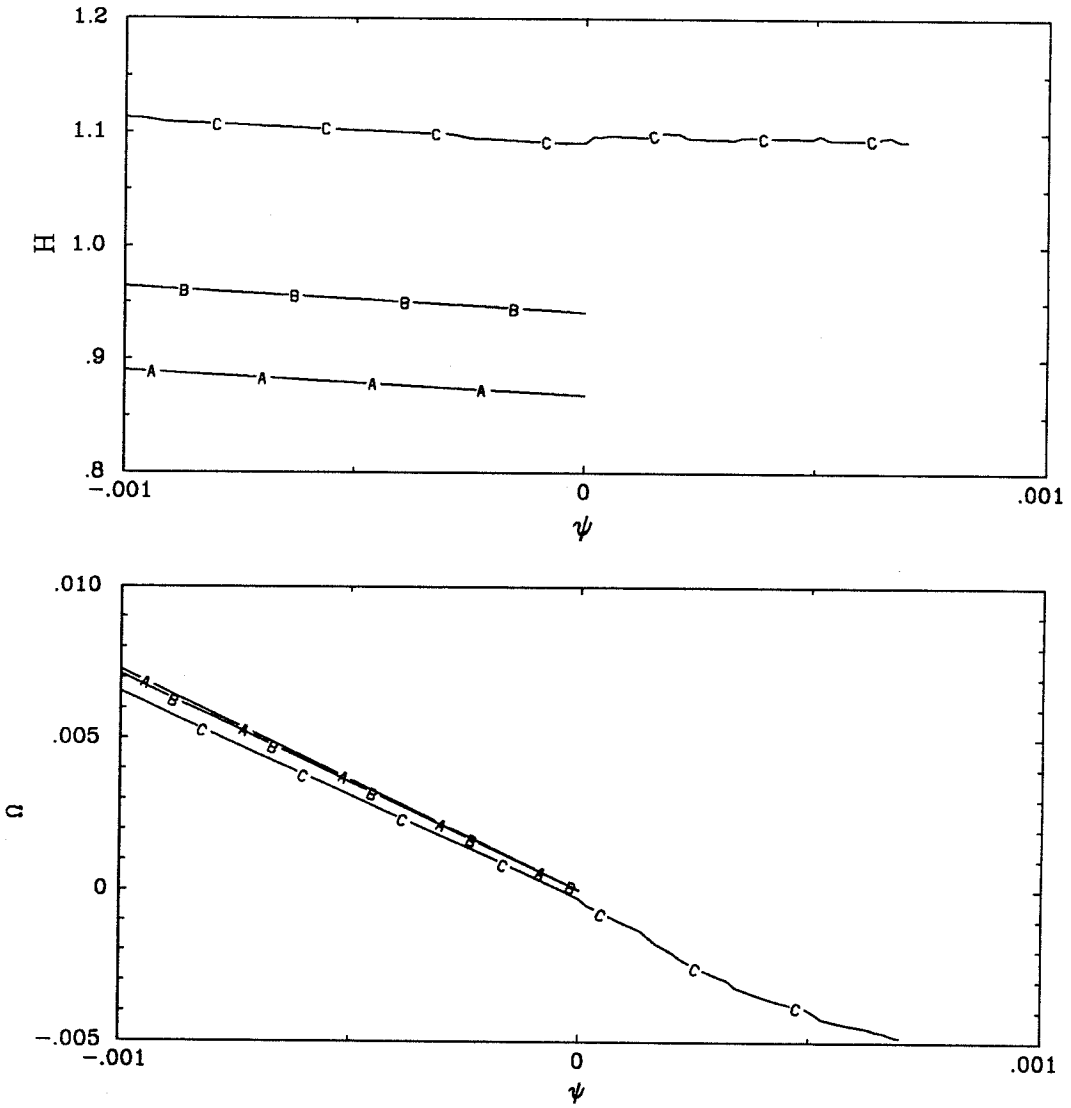

Fig. 6.6.5b Variation of $H(\psi)$ and $\Omega(\psi)$ inside the bubble for A. $\varepsilon = 0.01$, B. $\varepsilon = 0.03$, C. $\varepsilon = 0.05$. Base flow is Kelvin type with $a = 1/2$, $\Omega_\infty = 1$ and $W_m = 0.5$. $H(\psi)$ increases with ε. Variation in $\Omega(\psi)$ is small.

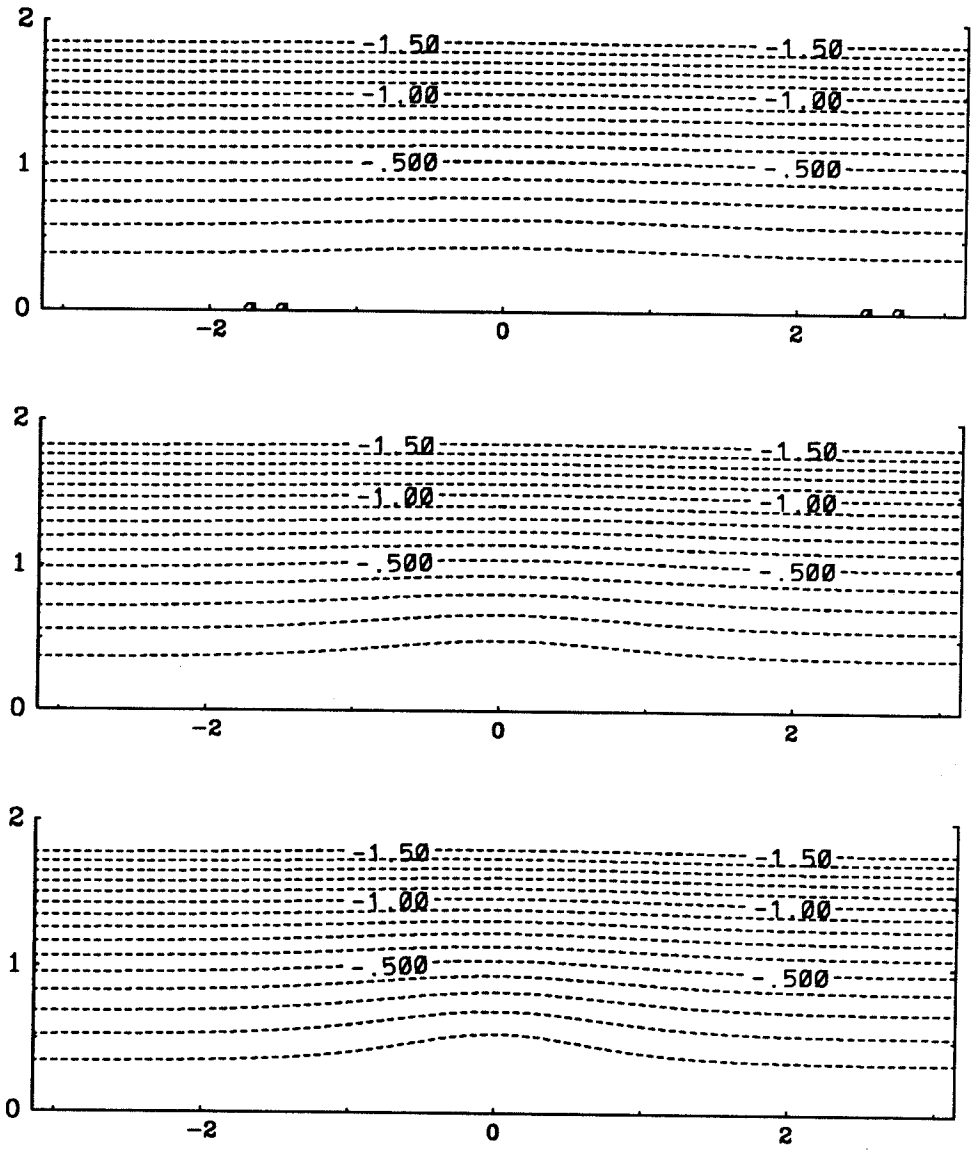

Fig. 6.7.1 Contours of ψ for $\varepsilon = 0.03,\ \ 0.05,\ \ 0.07$. Base flow is Kelvin type with $a = 1/2$, $\Omega_\infty = 1$ and $W_m = -0.5$. Contour interval $= 0.1$.

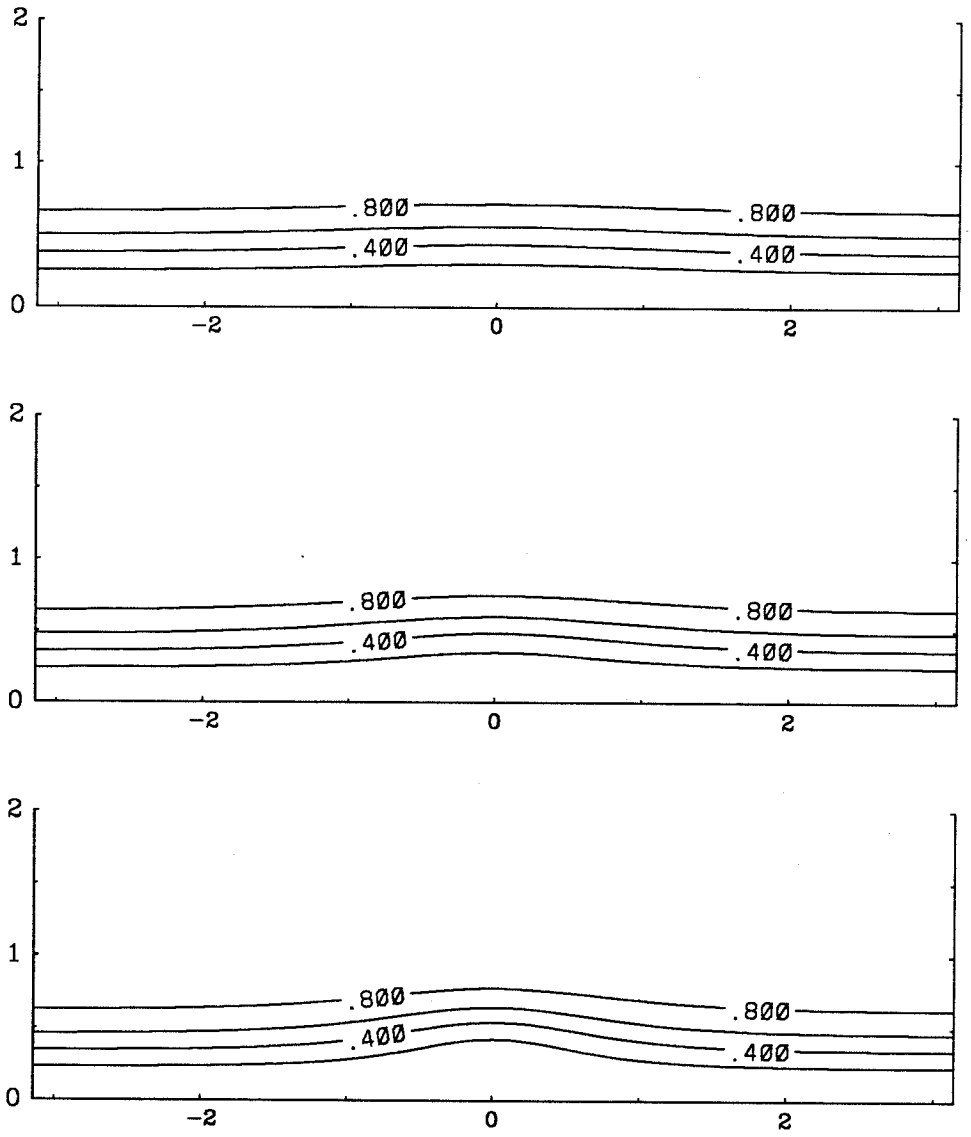

Fig. 6.7.2 Contours of Ω for $\varepsilon = 0.03,\quad 0.05,\quad 0.07$. Base flow is Kelvin type with $a = 1/2$, $\Omega_\infty = 1$ and $W_m = -0.5$. Contour interval = 0.2.

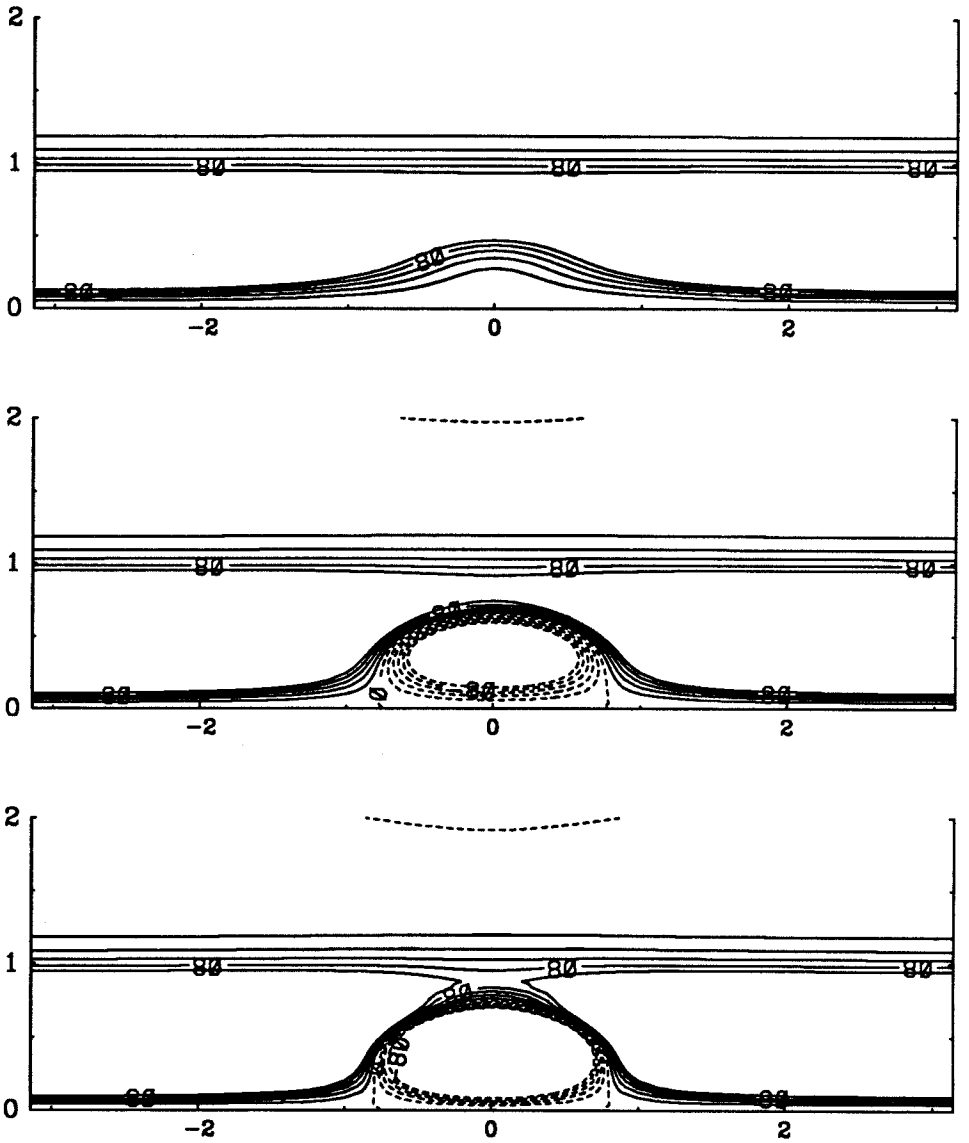

Fig. 6.7.3 Contours of ζ for $\varepsilon = 0.03,\ \ 0.05,\ \ 0.07$. Base flow is Kelvin type with $a = 1/2$, $\Omega_\infty = 1$ and $W_m = -0.5$. Contour interval = 0.02.

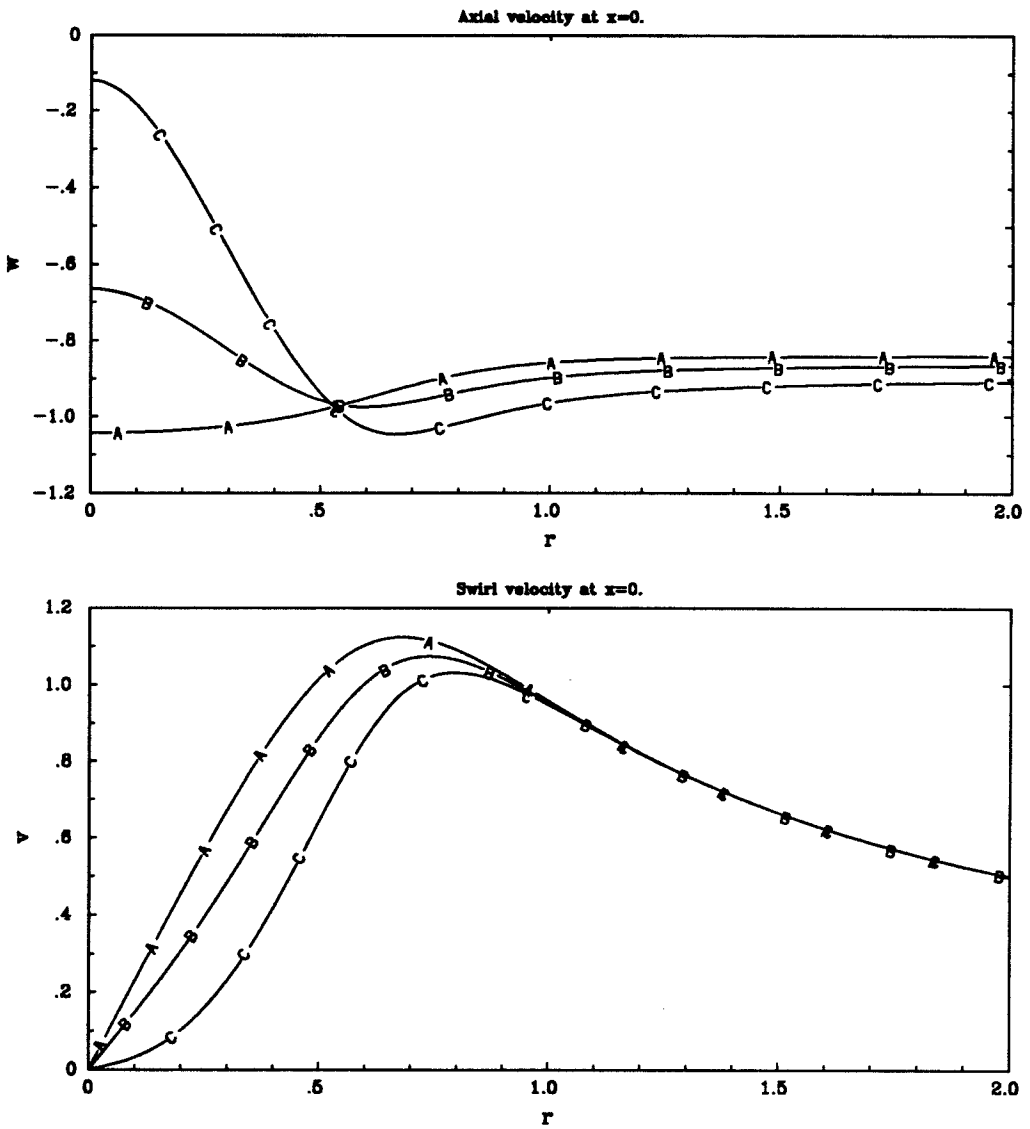

Fig. 6.7.4 Axial and swirl velocity at $x = 0$ for A. $\varepsilon = 0.03$, B. $\varepsilon = 0.05$, C. $\varepsilon = 0.07$. Base flow is Kelvin type with $a = 1/2$, $\Omega_\infty = 1$ and $W_m = -0.5$. Axial velocity increases at $r = 0$ with ε. The swirl decreases inside the core with increase in ε.

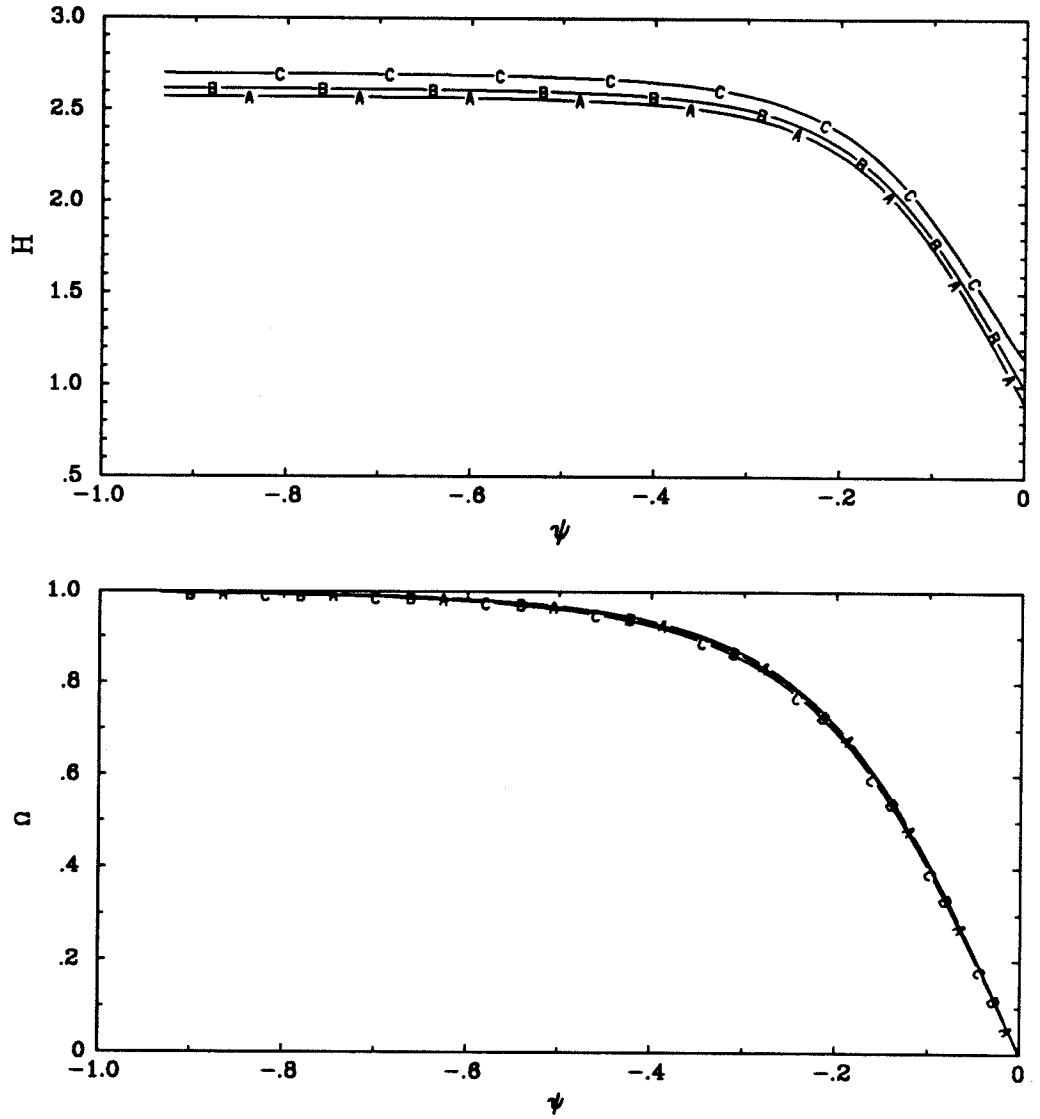

Fig. 6.7.5 Variation of $H(\psi)$ and $\Omega(\psi)$ for A. $\varepsilon = 0.03$, B. $\varepsilon = 0.05$, C. $\varepsilon = 0.07$. Base flow is Kelvin type with $a = 1/2$, $\Omega_\infty = 1$ and $W_m = -0.5$. $H(\psi)$ increases with ε. Variation in $\Omega(\psi)$ is small.

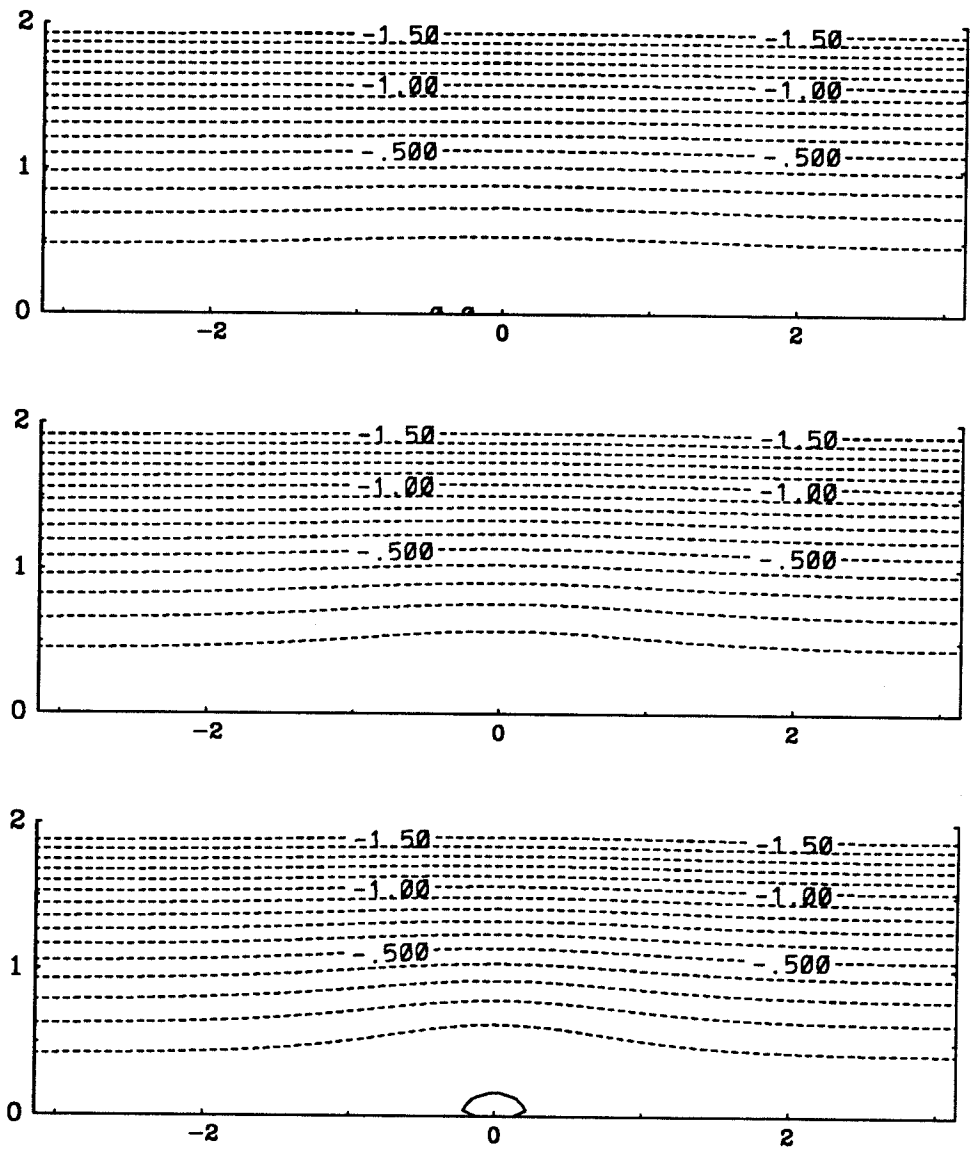

Fig. 6.8.1 Contours of ψ for $\varepsilon = 0.02,\ \ 0.04,\ \ 0.065$. Base flow is Burgers-Rott vortex with $a = 1/\sqrt{2}$, $\Omega_\infty = 1$ and $W_m = 0$. Contour interval = 0.1.

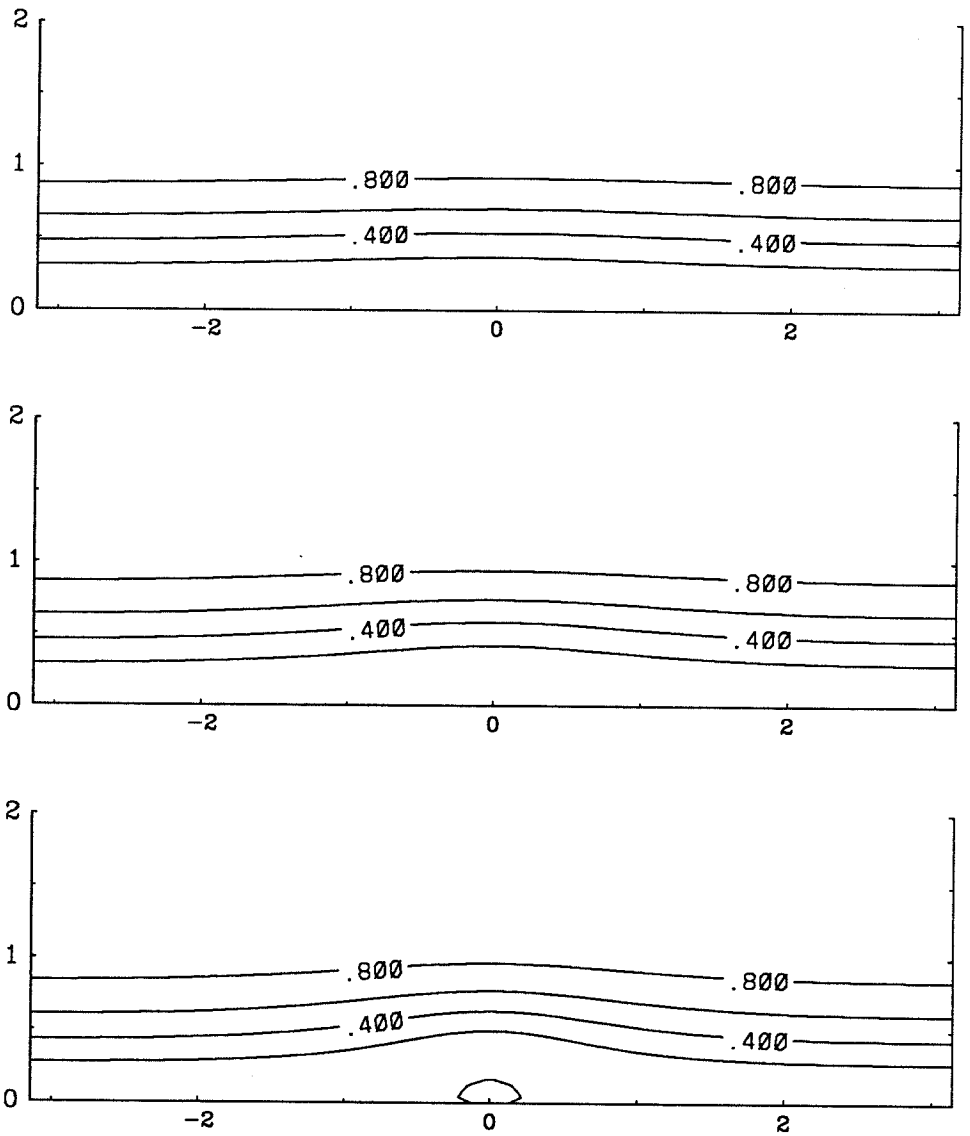

Fig. 6.8.2 Contours of Ω for $\varepsilon = 0.02,\ \ 0.04,\ \ 0.065$. Base flow is Burgers-Rott vortex with $a = 1/\sqrt{2}$, $\Omega_\infty = 1$ and $W_m = 0$. Contour interval = 0.2.

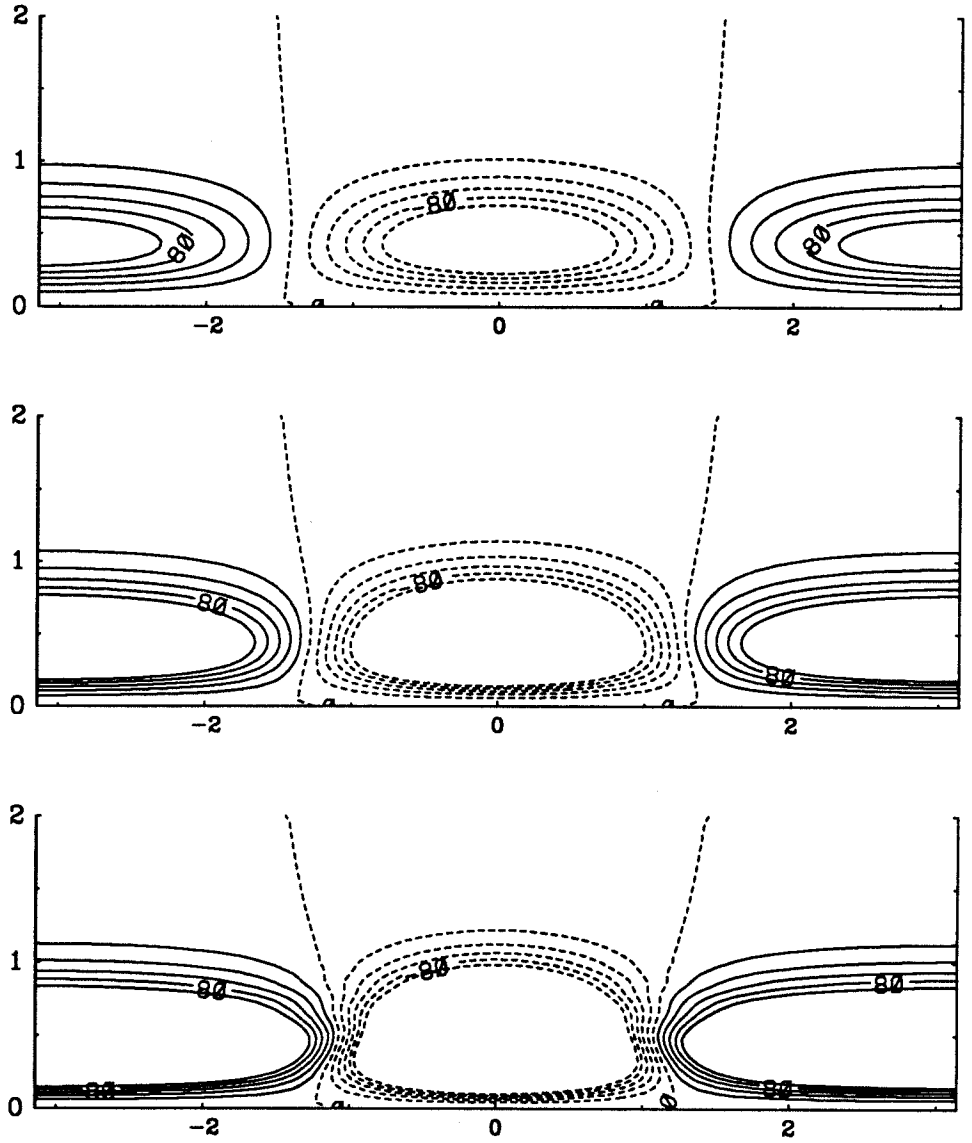

Fig. 6.8.3 Contours of ζ for $\varepsilon = 0.02,\ \ 0.04,\ \ 0.065$. Base flow is Burgers-Rott vortex with $a = 1/\sqrt{2}$, $\Omega_\infty = 1$ and $W_m = 0$. Contour interval = 0.02.

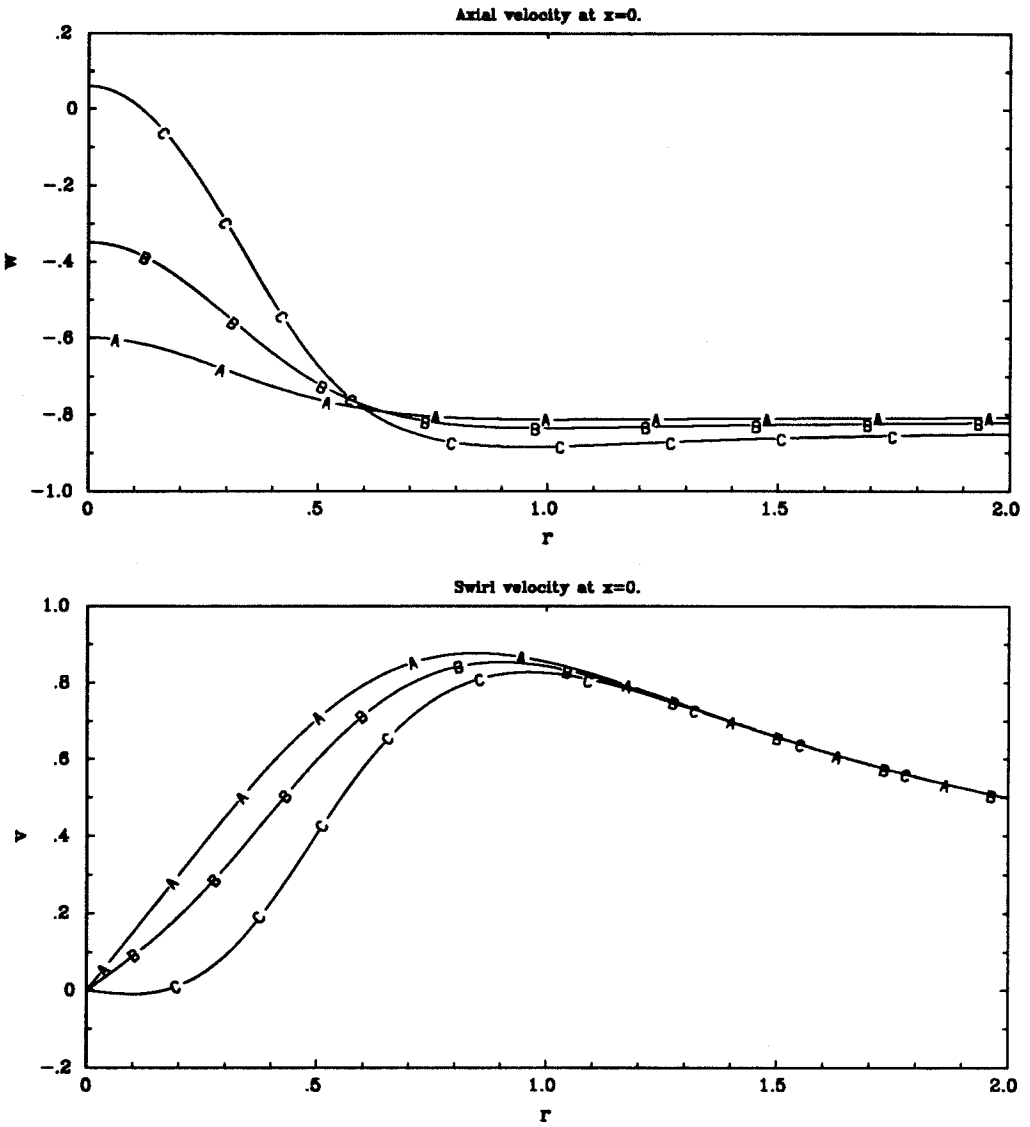

Fig. 6.8.4 Axial and swirl velocity at $x = 0$ for A. $\varepsilon = 0.02$, B. $\varepsilon = 0.04$, C. $\varepsilon = 0.065$. Base flow is Burgers-Rott vortex with $a = 1/\sqrt{2}$, $\Omega_\infty = 1$ and $W_m = 0$. Axial velocity increases at $r = 0$ with ε. The swirl decreases inside the core with increase in ε.

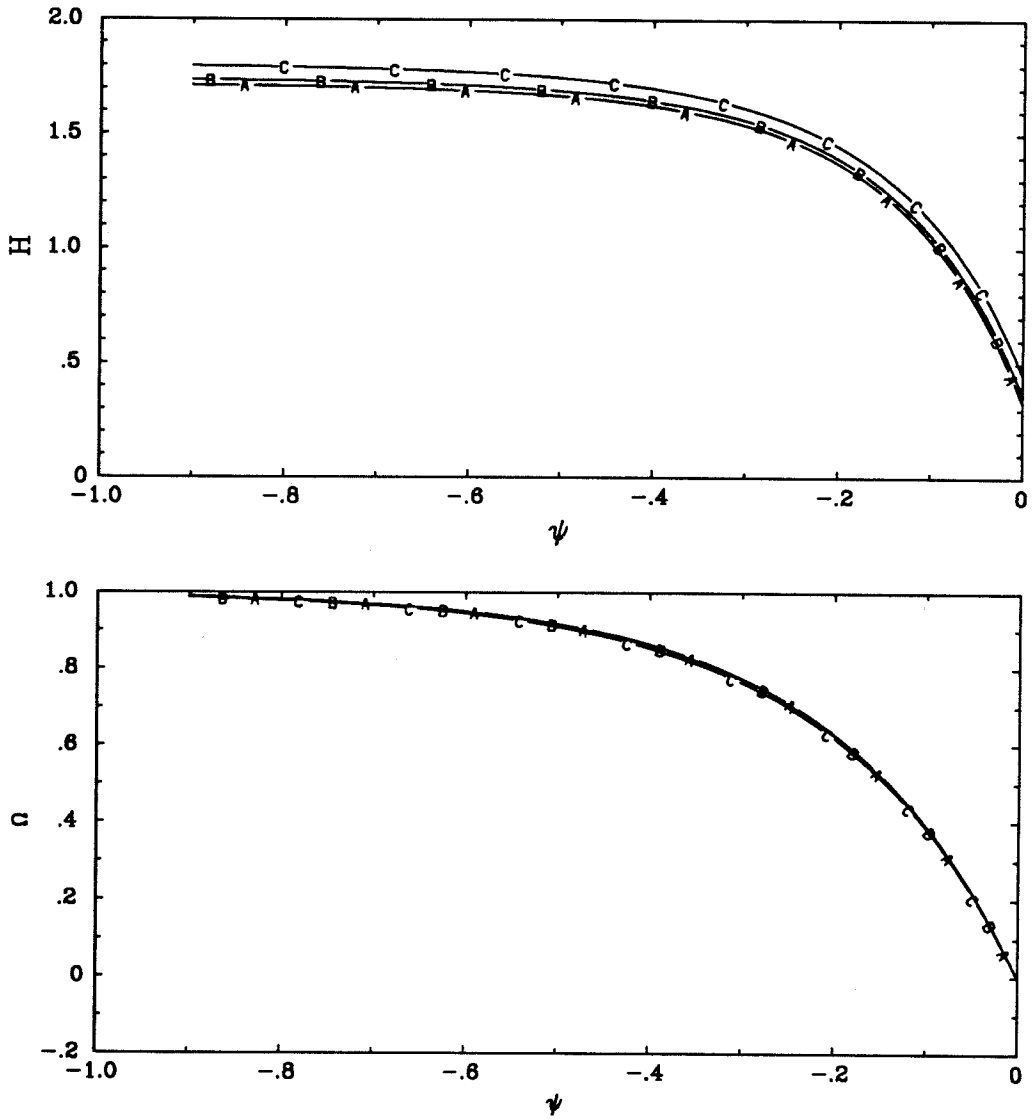

Fig. 6.8.5a Variation of $H(\psi)$ and $\Omega(\psi)$ for A. $\varepsilon = 0.02$, B. $\varepsilon = 0.04$, C. $\varepsilon = 0.065$. Base flow is Burgers-Rott vortex with $a = 1/\sqrt{2}$, $\Omega_\infty = 1$ and $W_m = 0$. $H(\psi)$ increases with ε. Variation in $\Omega(\psi)$ is small.

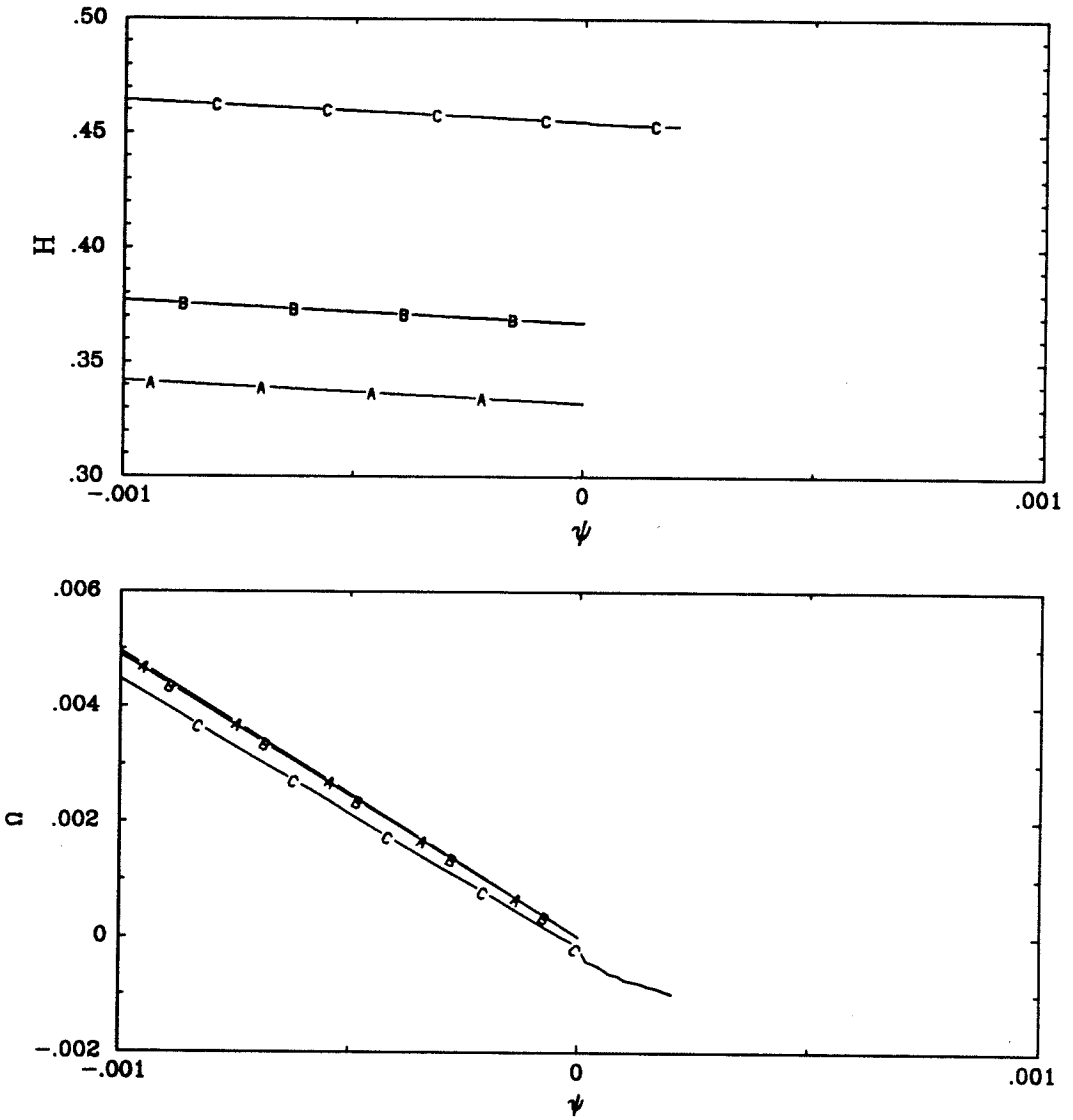

Fig. 6.8.5b Variation of $H(\psi)$ and $\Omega(\psi)$ inside the bubble for A. $\varepsilon = 0.02$, B. $\varepsilon = 0.04$, C. $\varepsilon = 0.065$. Base flow is Burgers-Rott vortex with $a = 1/\sqrt{2}$, $\Omega_\infty = 1$ and $W_m = 0$. $H(\psi)$ increases with ε. Variation in $\Omega(\psi)$ is small.

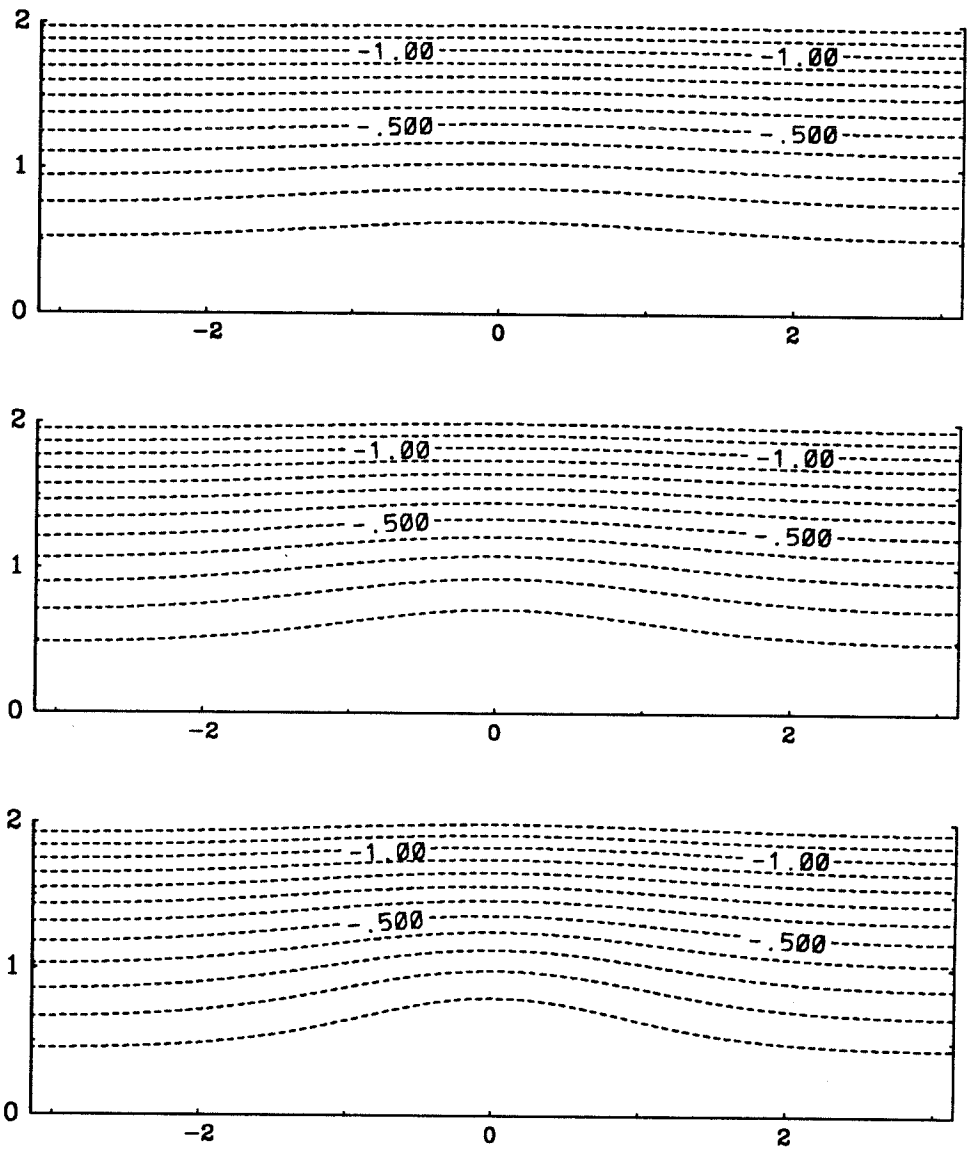

Fig. 6.9.1 Contours of ψ for $\varepsilon = 0.04,\ \ 0.08,\ \ 0.12$. Base flow is Kelvin type with $a = 1$, $\Omega_\infty = 1$ and $W_m = 0$. Contour interval = 0.1.

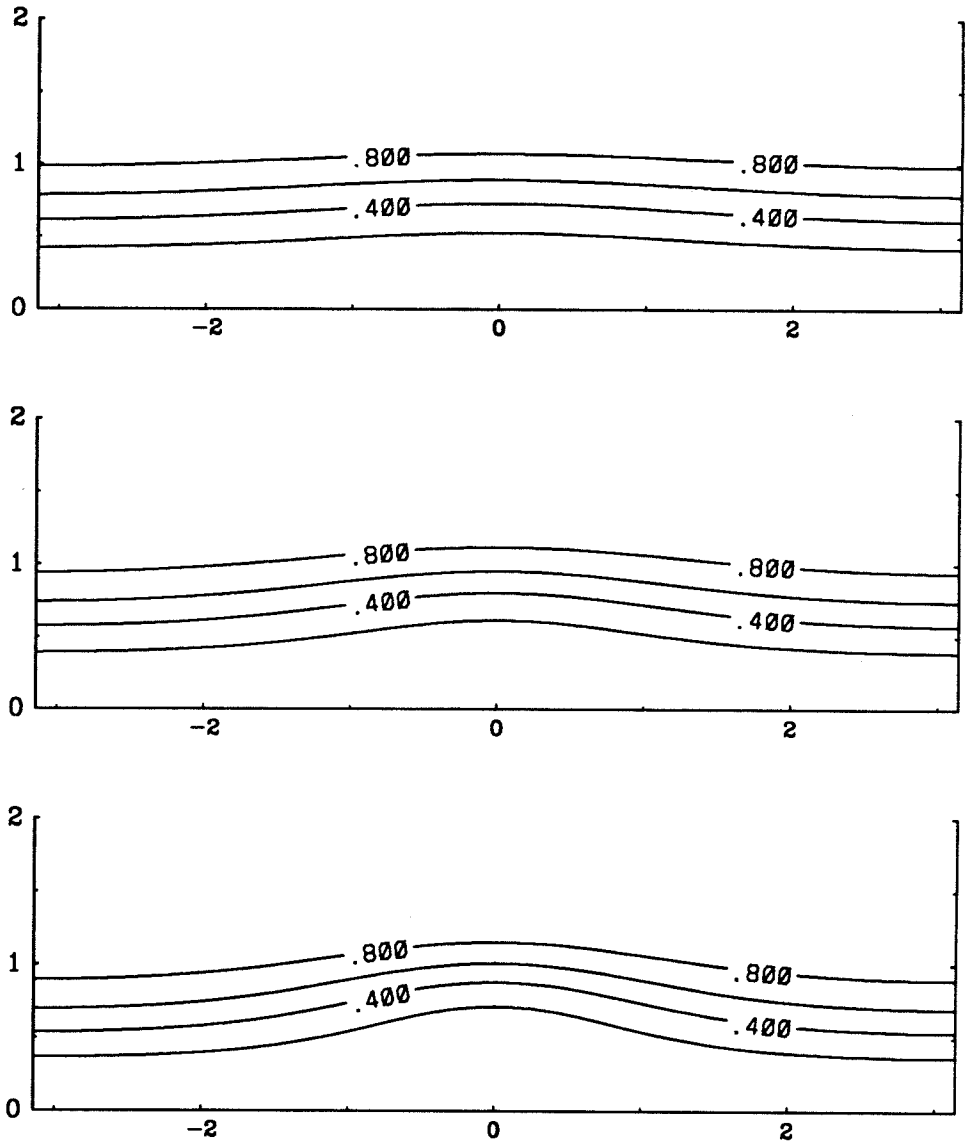

Fig. 6.9.2 Contours of Ω for $\varepsilon = 0.04,\ \ 0.08,\ \ 0.12$. Base flow is Kelvin type with $a = 1$, $\Omega_\infty = 1$ and $W_m = 0$. Contour interval = 0.2.

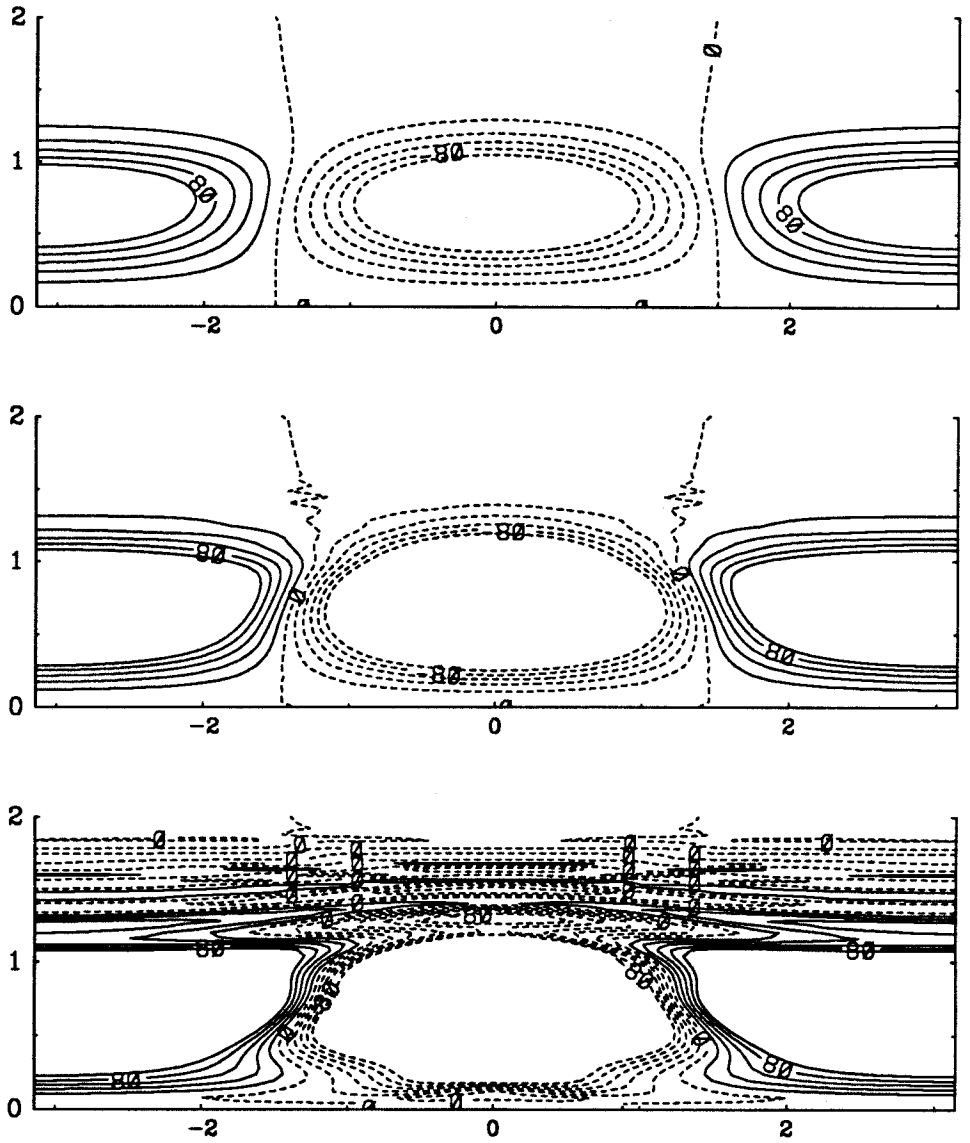

Fig. 6.9.3 Contours of ζ for $\varepsilon = 0.04,\ 0.08,\ 0.12$. Base flow is Kelvin type with $a = 1$, $\Omega_\infty = 1$ and $W_m = 0$. Contour interval = 0.02.

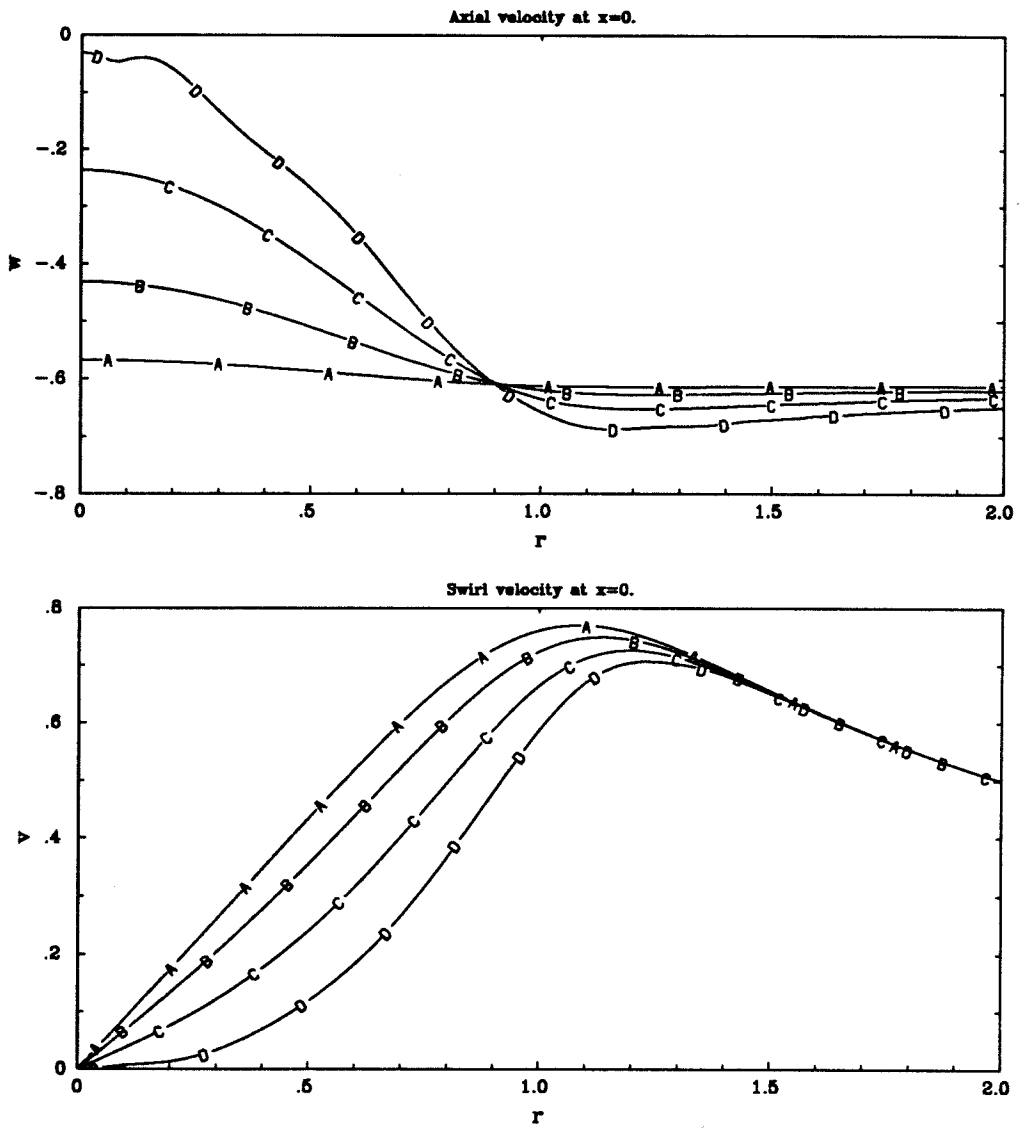

Fig. 6.9.4 Axial and swirl velocity at $x = 0$ for A. $\varepsilon = 0.01$, B. $\varepsilon = 0.04$, C. $\varepsilon = 0.08$, D. $\varepsilon = 0.12$. Base flow is Kelvin type with $a = 1$, $\Omega_\infty = 1$ and $W_m = 0$. Axial velocity increases at $r = 0$ with ε. The swirl decreases inside the core with increase in ε.

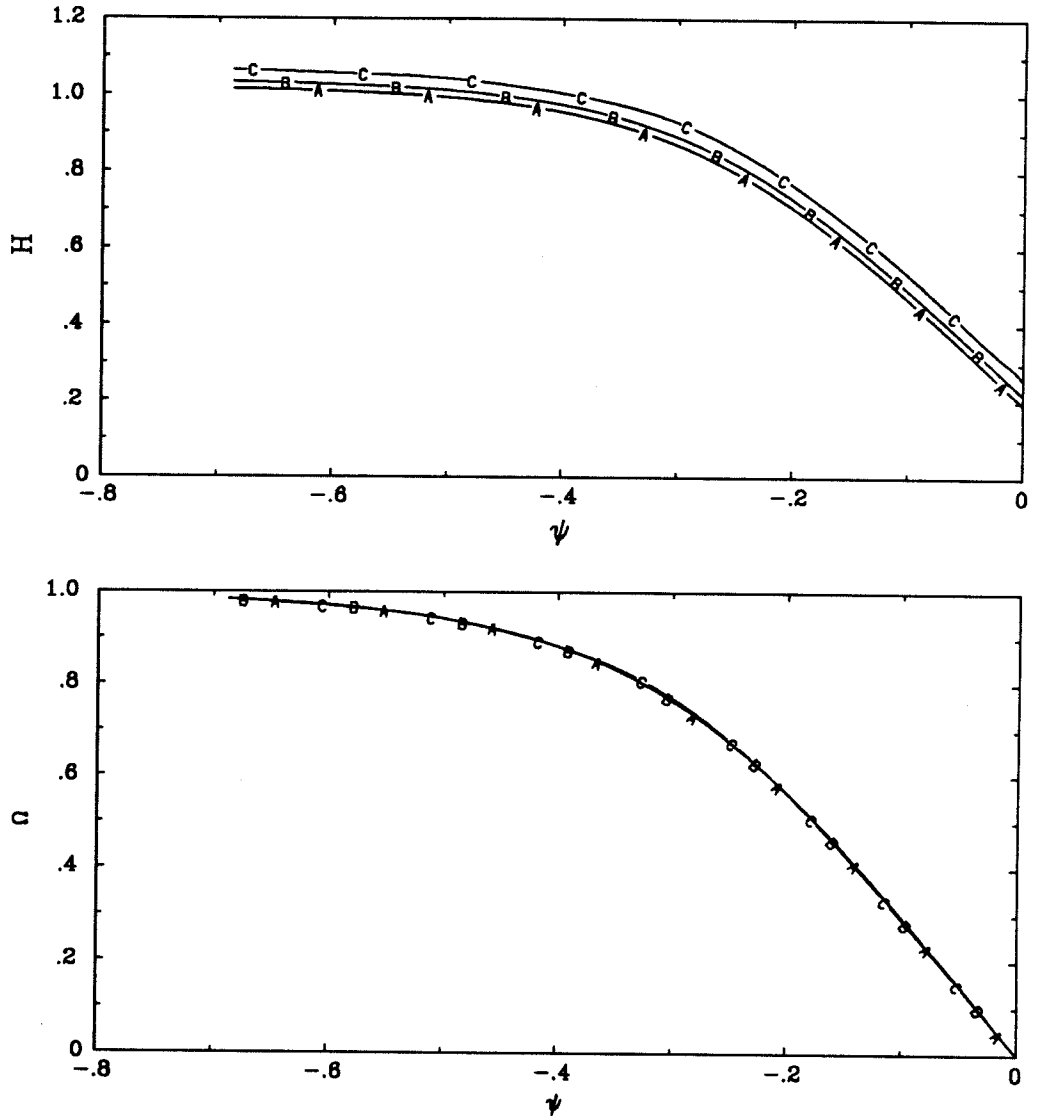

Fig. 6.9.5 Variation of $H(\psi)$ and $\Omega(\psi)$ for A. $\varepsilon = 0.01$, B. $\varepsilon = 0.04$, C. $\varepsilon = 0.08$, D. $\varepsilon = 0.12$. Base flow is Kelvin type with $a = 1$, $\Omega_\infty = 1$ and $W_m = 0$. $H(\psi)$ increases with ε. Variation in $\Omega(\psi)$ is small.

CHAPTER 7

Weakly Nonlinear Stability of a Columnar Vortex

7.1 Introduction

In this chapter we consider weakly-nonlinear stability of an axisymmetric columnar vortex with smooth vorticity distribution. The analysis is similar to the nonlinear stability of plane Poiseuille flow (Stewartson and Stuart, 1971). Using the same approach as Stewartson and Stuart, Leibovich (1972) has shown that the weakly nonlinear bending waves on vortex filaments are governed by a cubic nonlinear Schrödinger equation. The weakly-nonlinear analysis is usually based on the fact that there exists a critical parameter such as Reynold's number or wave number of perturbation at which the linear perturbation becomes unstable. In the case of an axisymmetric columnar vortex, the main difference as well as a great difficulty is the lack of a critical parameter. A similar difficulty arises in the case of plane Couette flow wherein one finds that the disturbances are stable for all Reynolds numbers. According to Stewartson and Stuart, the difficulty, in the absence of any critical value of Reynold's number, lies in the fact that no parameter seems to exist. Only in the presence of a parameter and when it is 'small' can one give meaning to the amplitude equation. The Reynolds number does not enter into our analysis since we consider inviscid fluid. Further, we have seen in the previous chapters that a columnar vortex sustains linear waves of permanent form. Therefore, linear stability does not yield a critical parameter. Hence we face a similar difficulty. As in the case of plane Couette flow, we can pursue the evolution of the amplitude of a linear wave if the amplitude which characterizes a "disturbance" is big enough. We implicitly assume that the "parameter" is the size of the disturbance and refer to it by ε. This parameter can be thought of

as the wave height.

Leibovich (1970) considered evolution of a long wave of small but finite amplitude on a vortex confined to a tube and showed that the amplitude satisfies the Korteweg-de Vries equation. This equation permits soliton solutions. The method used by Leibovich fails when the tube wall is moved to infinity. In contrast, we consider evolution of a wave of moderate wave length on a columnar vortex of the type described in Chapter 6. Further, the radial domain is unbounded. We find that the wave amplitude satisfies a cubic nonlinear Schrödinger equation which also permits solitary wave solutions.

7.2 Linear waves

We consider incompressible, inviscid fluid with unit density. The governing Euler equations are stated in Chapter 6 in terms of a stream function ψ and a circulation function Ω (equations 6.5 and 6.6). Any pair of functions $\psi_0(r)$ and $\Omega_0(r)$ form a solution to the Euler equations. Linear waves are of the form

$$\psi(r,z,t) = \psi_0(r) + \varepsilon\psi_1, \quad \Omega(r,z,t) = \Omega_0(r) + \varepsilon\Omega_1 \tag{7.1}$$

where ε is the approximate size of the disturbance. The disturbance is assumed to be of the form

$$\psi_1 = A_1\psi_{11}(r)E, \quad \Omega_1 = A_1\Omega_{11}(r)E, \tag{7.2}$$

where

$$E = e^{i(\kappa z - \alpha_0 t)} \tag{7.3}$$

and A_1 is some constant. We recall that for a given real value of κ, there are an infinite number of eigenvalues α_0 and corresponding eigenfunctions ψ_{11} and Ω_{11}.

7.3 Nonlinear stability

Now we wish to examine how the linear wave evolves if the perturbation is large enough to excite nonlinearity. We assume that the effect of nonlinearity is to modulate the given linear "carrier" wave both in space and in time. The amplitude of the carrier

wave is assumed to evolve 'slowly' in time and space. As a first trial, we consider the "amplitude" A_1 to depend on a slow time variable $\tau = \varepsilon t$ and a slow space variable $Z = \varepsilon z$. We find the equation satisfied by A_1 by considering the contribution to ε^2. We get

$$A_{1_\tau} + \alpha_1 A_{1_Z} = 0$$

suggesting that $A_1 \propto e^{i(Z-\alpha_1\tau)}$. The constant α_1 is determined from a consistency condition. This is an uninteresting case as it gives us a wave which gives rise to only a trivial modulation of the amplitude. Therefore we consider still higher order disturbances. We 'eliminate' the behavior exhibited at ε^2 by introducing the following set of slow variables,

$$Z = \varepsilon(z - \alpha_1 t), \quad \tau = \varepsilon^2 t. \tag{7.4}$$

The spatial and temporal derivatives are replaced by the following

$$\frac{\partial}{\partial t} \longrightarrow \frac{\partial}{\partial t} - \epsilon\,\alpha_1 \frac{\partial}{\partial Z} + \epsilon^2 \frac{\partial}{\partial \tau}, \tag{7.5}$$

$$\frac{\partial}{\partial z} \longrightarrow \frac{\partial}{\partial z} + \epsilon \frac{\partial}{\partial Z}, \tag{7.6}$$

$$\frac{\partial^2}{\partial z^2} \longrightarrow \frac{\partial^2}{\partial z^2} + 2\epsilon \frac{\partial^2}{\partial z \partial Z} + \epsilon^2 \frac{\partial^2}{\partial Z^2}. \tag{7.7}$$

For simplicity we take $\psi_0 = 0$ (which gives zero axial velocity) and decompose the solution as follows

$$\psi = 0 + \varepsilon\ \psi_1 + \varepsilon^2\ \psi_2 + \varepsilon^3\ \psi_3 + \cdots, \tag{7.8}$$

$$\Omega = \Omega_0 + \varepsilon\ \Omega_1 + \varepsilon^2\ \Omega_2 + \varepsilon^3\ \Omega_3 + \cdots, \tag{7.9}$$

where the perturbations are functions of r, z, t, τ and Z. The variable ζ that occurs in the Euler equations is defined as

$$\zeta = D^2\psi = \frac{\partial^2\psi}{\partial r^2} - \frac{1}{r}\frac{\partial\psi}{\partial r} + \frac{\partial^2\psi}{\partial z^2}. \tag{7.10}$$

We decompose ζ in the same manner and write

$$\zeta = 0 + \varepsilon\ \zeta_1 + \varepsilon^2\ \zeta_2 + \varepsilon^3\ \zeta_3 + \cdots. \tag{7.11}$$

After substituting for ψ and collecting coefficients of various powers of ε we get

$$\zeta_1 = D^2\psi_1, \tag{7.12a}$$

$$\zeta_2 = D^2\psi_2 + 2\psi_{1_{zZ}}, \tag{7.12b}$$

$$\zeta_3 = D^2\psi_3 + 2\psi_{2_{zZ}} + \psi_{1_{ZZ}}. \tag{7.12c}$$

Expressions for ζ_4, ζ_5 etc., are similar to (7.12c). We substitute the above expansions into the Euler equations. The equations obtained by equating coefficients of E are given by

$$\zeta_{1_t} + \frac{2}{r^2}\Omega_0\Omega_{1_z} = 0, \tag{7.13}$$

$$\Omega_{1_t} - \frac{1}{r}\Omega_0'\psi_{1_z} = 0. \tag{7.14}$$

Primes denote derivatives with respect to r from now on. The linear solution governed by (7.13) and (7.14) has the representation

$$\psi_1(r,t,\tau,z,Z) = A_1(\tau,Z)\ \psi_{11}(r)\ E + A_1^*\ \psi_{11}^*\ E^{-1}, \tag{7.15}$$

$$\Omega_1(r,t,\tau,z,Z) = A_1(\tau,Z)\ \Omega_{11}(r)\ E + A_1^*\ \Omega_{11}^*\ E^{-1}, \tag{7.16}$$

$$\zeta_1(r,t,\tau,z,Z) = A_1(\tau,Z)\ \zeta_{11}(r)\ E + A_1^*\ \zeta_{11}^*\ E^{-1}. \tag{7.17}$$

A superscript * denotes the complex conjugate and is added here so that the resulting solution is real. Back substitution into (7.13) and (7.14) yields

$$\zeta_{11} = \psi_{11}'' - \frac{1}{r}\psi_{11}' - \kappa^2\psi, \tag{7.18}$$

$$-\alpha_0\zeta_{11} + \frac{2\kappa}{r^2}\Omega_0\Omega_{11} = 0, \tag{7.19}$$

$$-\alpha_0\Omega_{11} - \frac{\kappa}{r}\Omega_0'\psi_{11} = 0. \tag{7.20}$$

Similar equations are obtained for the conjugate functions. The eigenfunctions ψ_{11} and Ω_{11} are determined along with the eigenvalue α_0. A discussion of the linear wave solution is given in Chapter 6. The equations obtained by equating powers of ε^2 are

given by

$$\left(D^2\psi_2\right)_t + \frac{2}{r^2}\,\Omega_0\Omega_{2z} = -2\,\psi_{1zZt} + \alpha_1\,\zeta_{1Z} - \frac{2}{r^2}\,\Omega_0\Omega_{1Z} - \left[\frac{2}{r^2}\,\Omega_1\Omega_{1z} + \frac{1}{r}\,\frac{\partial(\psi_1,\zeta_1)}{\partial(r,z)} + \frac{2}{r^2}\,\psi_{1z}\zeta_1\right], \quad (7.21)$$

$$\Omega_{2t} - \frac{1}{r}\,\Omega_0'\,\psi_{2z} = \alpha_1\,\Omega_{1Z} + \frac{1}{r}\,\Omega_0'\,\psi_{1Z} - \frac{1}{r}\,\frac{\partial(\psi_1,\Omega_1)}{\partial(r,z)}. \quad (7.22)$$

We substitute the linear solution on the right hand side and conclude that ψ_2 and Ω_2 must be of the form

$$\psi_2 = -i\,A_{1Z}\,\psi_{21}\,E + {A_1}^2\,\psi_{22}\,E^2 + \text{c.c.}, \quad (7.23)$$

$$\Omega_2 = -i\,A_{1Z}\,\Omega_{21}\,E + {A_1}^2\,\Omega_{22}\,E^2 + \text{c.c.}, \quad (7.24)$$

$$\zeta_2 = -i\,A_{1Z}\,\zeta_{21}\,E + i\,2\kappa\,A_{1Z}\,\psi_{11}\,E + {A_1}^2\,\zeta_{22}\,E^2 + \text{c.c.}. \quad (7.25)$$

Here, c.c. denotes the complex conjugate terms. We notice that the above form does not contain any terms proportional to E^0. This is because all terms contributing to E^0 cancel each other since the linear eigenfunctions are all real and the terms are symmetric in nature. We substitute (7.23) - (7.25) back into (7.21) and (7.22). After equating the coefficients of E we get

$$\zeta_{21} = \psi_{21}'' - \frac{1}{r}\,\psi_{21}' - \kappa^2\,\psi_{21}, \quad (7.26)$$

$$-\alpha_0\,\zeta_{21} + \frac{2\kappa}{r^2}\,\Omega_0\,\Omega_{21} = \alpha_1\,\zeta_{11} - \frac{2}{r^2}\,\Omega_0\,\Omega_{11} - 2\kappa\,\alpha_0\,\psi_{11}, \quad (7.27)$$

$$-\alpha_0\,\Omega_{21} - \frac{\kappa}{r}\,\Omega_0'\,\psi_{21} = \alpha_1\,\Omega_{11} + \frac{1}{r}\,\Omega_0'\,\psi_{11}. \quad (7.28)$$

Equating the coefficients of E^2 we get,

$$\zeta_{22} = \psi_{22}'' - \frac{1}{r}\,\psi_{22}' - (2\kappa)^2\,\psi_{22}, \quad (7.29)$$

$$-\alpha_0\,\zeta_{22} + \frac{2\kappa}{r^2}\,\Omega_0\,\Omega_{22} = -\frac{\kappa}{2}\left[\frac{2}{r^2}\,{\Omega_{11}}^2 + \frac{1}{r}\,(\psi_{11}'\zeta_{11} - \psi_{11}\zeta_{11}') + \frac{2}{r^2}\,\psi_{11}\zeta_{11}\right], \quad (7.30)$$

$$-\alpha_0\,\Omega_{22} - \frac{\kappa}{r}\,\Omega_0'\,\psi_{22} = -\frac{\kappa}{2r}\,(\psi_{11}'\Omega_{11} - \psi_{11}\Omega_{11}'). \quad (7.31)$$

A unique solution to (7.30) and (7.31) can be found because the linear operator on the left hand side is different from that arising in the linear solution. The differential

operator in (7.27) and (7.28) is the same as the linear operator given in (7.13) and (7.14). Therefore a nontrivial solution is not possible unless α_1 satisfies a solvability condition. It is found easily by employing the Fredholm alternative theorem. We state it in a separate section below. We notice that the functions with subscripts 21 and 22 are all real. Therefore, α_1, is also real.

Next we consider the equations obtained at ε^3. We get

$$\left(D^2\psi_3\right)_t + \frac{2}{r^2}\,\Omega_0\,\Omega_{3z} = P_3, \tag{7.32}$$

$$\Omega_{3t} - \frac{1}{r}\,\Omega_0'\,\psi_{3z} = Q_3, \tag{7.33}$$

where

$$\begin{aligned} P_3 = &-\zeta_{1\tau} - \psi_{1ZZt} - 2\,\psi_{2zZt} + \alpha_1\,\zeta_{2Z} - \frac{2}{r^2}\,\psi_{1Z}\,\zeta_1 \\ &- \frac{2}{r^2}\,(\Omega_0\,\Omega_{2Z} + \Omega_1\,\Omega_{1Z}) - \frac{1}{r}\,\frac{\partial(\psi_1,\zeta_1)}{\partial(r,Z)} \\ &- \left[\frac{1}{r}\,\frac{\partial(\psi_1,\zeta_2)}{\partial(r,z)} + \frac{1}{r}\,\frac{\partial(\psi_2,\zeta_1)}{\partial(r,z)} + \frac{2}{r^2}\,(\psi_{1z}\,\zeta_2 + \psi_{2z}\,\zeta_1)\right] \\ &- \frac{2}{r^2}\,(\Omega_1\,\Omega_{2z} + \Omega_2\,\Omega_{1z}), \end{aligned} \tag{7.34}$$

$$\begin{aligned} Q_3 = &-\Omega_{1\tau} + \alpha_1\,\Omega_{2Z} + \frac{1}{r}\,\Omega_0'\,\psi_{2Z} - \frac{1}{r}\,\frac{\partial(\psi_1,\Omega_1)}{\partial(r,Z)} \\ &- \frac{1}{r}\left[\frac{\partial(\psi_1,\Omega_2)}{\partial(r,z)} + \frac{\partial(\psi_2,\Omega_1)}{\partial(r,z)}\right]. \end{aligned} \tag{7.35}$$

After substituting for ψ_1, ψ_2 etc., the form of the right hand sides can be written as

$$P_3 = p_{31}\,E + p_{32}\,E^2 + \cdots + \text{c.c.}, \tag{7.36}$$

$$Q_3 = q_{31}\,E + q_{32}\,E^2 + \cdots + \text{c.c.}. \tag{7.37}$$

The functions p_{31} and q_{31} are the only ones of interest to us. Calculations show that

$$p_{31} = -\zeta_{11}A_{1\tau} + m_{p31}\;\; i\,A_{1ZZ} + n_{p31}\;\; i\,A_1\,|A_1|^2, \tag{7.38}$$

$$q_{31} = -\Omega_{11}A_{1\tau} + m_{q31}\;\; i\,A_{1ZZ} + n_{q31}\;\; i\,A_1\,|A_1|^2, \tag{7.39}$$

where

$$m_{p31} = \alpha_0\,\psi_{11} \;+\; 2\,\kappa\,\alpha_0\,\psi_{21} - \alpha_1\,\zeta_{21} + \frac{2}{r^2}\,\Omega_0\,\Omega_{21}, \tag{7.40}$$

$$\begin{aligned} n_{p31} = &-\frac{2\kappa}{r^2}\,\Omega_{11}^*\,\Omega_{22} - \frac{2\kappa}{r}\left(\psi_{11}^{*\,\prime}\,\zeta_{22} - \psi_{22}\,\zeta_{11}^{*\,\prime}\right) \\ &- \frac{\kappa}{r}\left(\psi_{11}^*\,\zeta_{22}' - \psi_{22}'\,\zeta_{11}^*\right) + \frac{2\kappa}{r^2}\left(\psi_{11}^*\,\zeta_{22} - 2\,\psi_{22}\,\zeta_{11}^*\right), \end{aligned} \tag{7.41}$$

$$m_{q31} = -\alpha_1\,\Omega_{21} - \frac{1}{r}\,\Omega_0'\,\psi_{21}, \tag{7.42}$$

and

$$n_{q31} = \frac{\kappa}{r}\left[-2\,\psi_{11}^{*\,\prime}\,\Omega_{22} - \psi_{11}^*\,\Omega_{22}' + \psi_{22}'\,\Omega_{11}^* + 2\,\psi_{22}\,\Omega_{11}^{*\,\prime}\right]. \tag{7.43}$$

There is no need to keep the superscript * on the above functions as they are all real. We have retained them simply to show the origin of the contributing terms. Once again we employ the Fredholm alternative theorem and obtain the following evolution equation for A_1,

$$i\,A_{1\tau} + c_1\,A_{1ZZ} + c_2\,A_1\,|A_1|^2 = 0, \tag{7.44}$$

where c_1 and c_2 are constants found in the following section.

7.4 Evaluation of constants

We define

$$r_{21} = \begin{pmatrix} p_{21} \\ q_{21} \end{pmatrix}, \qquad f_{11} = \begin{pmatrix} \psi_{11} \\ \Omega_{11} \end{pmatrix}, \qquad g_{11} = \begin{pmatrix} u_{11} \\ v_{11} \end{pmatrix}, \tag{7.45}$$

where p_{21} and q_{21} are the right hand sides of (7.27) and (7.28) respectively. f_{11} and g_{11} represent the linear and its adjoint solutions respectively.

If $\mathbf{L}$ denotes the linear operator and $\mathbf{L}^*$ its adjoint, we must have

$$\int_0^\infty g_{11}^{*\,\top}\,(\mathbf{L} f_{11})\,\frac{1}{r}\,dr = \int_0^\infty f_{11}^{\top}\,(\mathbf{L}^* g_{11}^*)\,\frac{1}{r}\,dr. \tag{7.46}$$

The operator $\mathbf{L}$ and its adjoint are given by

$$\mathbf{L} = \begin{pmatrix} -\alpha_0\left[\frac{\mathrm{d}^2}{\mathrm{d}r^2} - \frac{1}{r}\frac{\mathrm{d}}{\mathrm{d}r} - \kappa^2\right] & \frac{2\kappa}{r^2}\,\Omega_0 \\ -\frac{\kappa}{r}\,\Omega_0' & -\alpha_0 \end{pmatrix}, \quad \mathbf{L}^* = \mathbf{L}^{\top}. \tag{7.47}$$

We also find

$$u_{11} = \psi_{11}, \tag{7.48}$$

$$v_{11} = \frac{2\kappa}{r^2}\,\frac{\Omega_0}{\alpha_0}\,\psi_{11}. \tag{7.49}$$

Solution to (7.27) and (7.28) exists only if $\int_0^\infty r_{21}^{\top} g_{11}^{*}/r\ dr = 0$. This yields us the value of α_1 defined by

$$\alpha_1 \int_0^\infty (\zeta_{11}\, u_{11}^{*} + \Omega_{11}\, v_{11}^{*})\frac{1}{r}\ dr = \int_0^\infty \Big[\Big(\frac{2}{r^2}\,\Omega_0\,\Omega_{11} + 2\,\kappa\,\alpha_0\,\psi_{11}\Big)\, u_{11}^{*} - \frac{1}{r}\,\Omega_0'\,\psi_{11}\, v_{11}^{*}\Big]\ \frac{1}{r}\ dr. \tag{7.50}$$

Since the vector $(p_{31}, q_{31})^{\top}$ is required to be orthogonal to g_{11}, we get, after integrating and comparing with (7.44),

$$c_1 \int_0^\infty (\zeta_{11}\, u_{11}^{*} + \Omega_{11}\, v_{11}^{*})\ \frac{1}{r}\ dr = \int_0^\infty (m_{p31}\, u_{11}^{*} + m_{q31}\, v_{11}^{*})\ \frac{1}{r}\ dr, \tag{7.51}$$

$$c_2 \int_0^\infty (\zeta_{11}\, u_{11}^{*} + \Omega_{11}\, v_{11}^{*})\ \frac{1}{r}\ dr = \int_0^\infty (n_{p31}\, u_{11}^{*} + n_{q31}\, v_{11}^{*})\ \frac{1}{r}\ dr. \tag{7.52}$$

A check can be made at this point for the constant c_2. If we suppose that the amplitude A_1 depends only on τ then from equation (7.44) we must have

$$iA_{1_\tau} + c_2 A_1 |A_1|^2 = 0. \tag{7.53}$$

This has a solution

$$A_1 = Ae^{ic_2\tau}, \tag{7.54}$$

where A is some constant. From (7.8) we see that the solution takes the form

$$\psi = \varepsilon\psi_{11}(r)\tilde{E} + \varepsilon^2\psi_{22}(r)\tilde{E}^2 + \cdots + \text{c. c.}, \tag{7.55}$$

where

$$\tilde{E} = e^{i(\kappa z - \alpha t)}, \quad \alpha = \alpha_0 + \varepsilon^2\alpha_2 + \cdots, \quad c_2 = -\alpha_2. \tag{7.56}$$

The constant A has been absorbed into ε. The quantity $-c_2$ is thus the correction to the wave speed due to nonlinearity whose value was found using a perturbation method in Chapter 6. It is easily verified that equation (7.52) and equation (6.78)

Table 7.1 Values of constants.

The values of α_1, c_1 and c_2 are shown for various a and Ω_∞.

a	Ω_∞	α_1	c_1	c_2	c_1/c_2
0.50	0.50	0.46549267	$-0.99090\ 10^{-2}$	$-0.29281\ 10^{+3}$	$0.3384\ 10^{-4}$
0.50	1.00	0.93098534	$-0.19818\ 10^{-1}$	$-0.58562\ 10^{+3}$	$0.3384\ 10^{-4}$
0.50	2.00	1.86197067	$-0.39636\ 10^{-1}$	$-0.11712\ 10^{+4}$	$0.3384\ 10^{-4}$
0.75	0.50	0.32923588	$-0.97280\ 10^{-2}$	$-0.33504\ 10^{+2}$	$0.2904\ 10^{-3}$
0.75	1.00	0.65847177	$-0.19456\ 10^{-1}$	$-0.67007\ 10^{+2}$	$0.2904\ 10^{-3}$
0.75	2.00	1.31694353	$-0.38912\ 10^{-1}$	$-0.13401\ 10^{+3}$	$0.2904\ 10^{-3}$
1.00	0.50	0.23760486	$-0.92697\ 10^{-2}$	$-0.59974\ 10^{+1}$	$0.1546\ 10^{-2}$
1.00	1.00	0.47520971	$-0.18539\ 10^{-1}$	$-0.11995\ 10^{+2}$	$0.1546\ 10^{-2}$
1.00	2.00	0.95041943	$-0.37079\ 10^{-1}$	$-0.23990\ 10^{+2}$	$0.1546\ 10^{-2}$
1.50	0.50	0.13255434	$-0.80461\ 10^{-2}$	$-0.47670\ 10^{+0}$	$0.1688\ 10^{-1}$
1.50	1.00	0.26510869	$-0.16092\ 10^{-1}$	$-0.95340\ 10^{+0}$	$0.1688\ 10^{-1}$
1.50	2.00	0.53021738	$-0.32184\ 10^{-1}$	$-0.19068\ 10^{+1}$	$0.1688\ 10^{-1}$
2.00	0.50	0.07966699	$-0.67927\ 10^{-2}$	$-0.78509\ 10^{-1}$	$0.8652\ 10^{-1}$
2.00	1.00	0.15933397	$-0.13585\ 10^{-1}$	$-0.15702\ 10^{+0}$	$0.8652\ 10^{-1}$
2.00	2.00	0.31866795	$-0.27171\ 10^{-1}$	$-0.31404\ 10^{+0}$	$0.8652\ 10^{-1}$

with $\ell = 3$ determine the same constant except for sign. The constant c_2 must equal $-\alpha_2$ even when the amplitude depends on Z and τ since equation (7.52) is unaffected by this.

Constants α_1, c_1 and c_2 were computed for a columnar vortex with a Kelvin type vorticity distribution described in Chapter 6. The parameter β was fixed at 0.3. The results for various values of the core size a and the total circulation Ω_∞ are shown in Table 7.1. All the cases show that the constants c_1 and c_2 are negative. The stability is determined by the sign of product of c_1 and c_2. If the sign is positive, as in the present case, the linear wave train is unstable (see Whitham, 1974). By instability it is implied that the perturbations grow in time. It is only in this unstable case that solitary waves are possible. They can found by assuming that

$$A_1 = e^{i(\lambda Z - c_1 \theta \tau)} B_1(X), \quad X = Z - c_1 U \tau, \tag{7.57}$$

where

$$\lambda = \frac{U}{2}, \quad \theta = \frac{U^2}{4} - \gamma. \tag{7.58}$$

Here, U and γ are parameters. The quantity B_1 has the form

$$B_1 = \left(\frac{2\gamma c_1}{c_2} \right) \mathrm{sech}\gamma^{1/2} \left(Z - c_1 U \tau \right). \tag{7.59}$$

Thus, the amplitude of the solitary wave is proportional to the square root of c_1/c_2. From Table 7.1 it is evident that this ratio remains the same for a vortex with fixed core size but variable total circulation. It appears therefore, that the total circulation scales out of the equations. But, the change in core area has significant effect. The ratio increases significantly with increase in core size.

References

Batchelor, G. K. (1967), *An introduction to Fluid Dynamics.* Cambridge University Press, Cambridge.

Bender, C. M. & Orszag, S. A. (1978), *Advanced mathematical methods for scientists and engineers.* McGraw-Hill.

Benjamin, T. Brooke (1962), Theory of the vortex breakdown phenomenon. *J. Fluid Mech.* **14**, p. 593-629.

Benjamin, T. Brooke (1967), Some developments in the theory of vortex breakdown. *J. Fluid Mech.* **28**, p. 65-84.

Beran, P. S. (1989), *An investigation of the bursting of trailing vortices using numerical simulation.* Ph. D. Thesis, California Institute of Technology.

Broadbent, E. G. & Moore, D. W. (1985), Waves of extreme form on a layer of uniform vorticity. *Phys. Fluids* 28, pp. 1561–1563.

Brown, G. L. & Lopez, J. M. (1988), Axisymmetric vortex breakdown Part II: Physical Mechanisms. *Aero. Res. Lab. Aero. Report 174.*

Chandrasekhar, S. (1961), *Hydrodynamic and hydromagnetic stability.* Oxford University Press.

Crow, S. C. (1970), Stability theory for a pair of trailing vortices. *AIAA J.* **8**, p. 2172.

Elle, B. J. (1960), On the breakdown at high incidences of the leading E. V. on Delta Wings. *J. Roy. Aero. Soc.*, **64**, pp. 491.

Faler, J. H. (1976), Some experiments in swirling flows: Detailed velocity measusrements of a vortex breakdown using a laser doppler anemometer. *NASA CR - 135115*

Faler, J. H. & Leibovich, S. (1977), Disrupted states of vortex flow and vortex breakdown. *Phys. Fluids* **20** p. 1385.

Fukumoto, Y. & Miyazaki, T. (1991), Three-dimensional distortions of a vortex filament with axial velocity. *To be published.*

Garg, A. K. & Leibovich, S. (1979) Spectral characteristics of vortex breakdown flowfields. *Phys. Fluids* bf 22(11), p. 2053.

Goldstein, S. (1965), *Modern developments in fluid dynamics.* Dover Publications Inc.

Hafez, M., Kuruvila, G. & Salas, M. D. (1986), Numerical study of vortex breakdown. *Appl. Num. Math.* **2**, pp. 291–302.

Hall, M. G. (1972), Vortex breakdown. *Ann. Rev. of Fluid Mech.* **4**, p. 195.

Harvey, J. K. (1962), Some observations of the vortex breakdown phenomenon. *J. Fluid Mech.* **14**, pp. 585–592.

Hicks, W. M. (1884), On the steady motion and the small vibrations of a hollow vortex. *Phil. Trans. R. Soc. Lond.* **A 175**, p. 175.

Holyer, J. Y. (1979), Large amplitude progressive interfacial waves. *J. Fluid Mech.* **93**, pp. 433–448.

Keller, H. B. (1987), *Numerical methods in bifurcation problems.* Springer-Verlag.

Kelvin, Lord (1880), Vibrations of a columnar vortex. *Phil. Mag.* **10**, pp. 155-168.

Lambourne, N. C. & Bryer, D. W. (1961), The bursting of leading-edge vortices – Some observations and discussions of the phenomenon. *Aero. Res. Council* RM-3282.

Leibovich, S. (1970), Weakly non-linear waves in rotating fluids. *J. Fluid Mech.* **42**, pp. 803–822. Leibovich, S. (1971), Waves and bifurcations in vortex filaments. *Studies of vortex dominated flows.* Ed: Hussaini, M. Y. & Salas, M. D., Springer-Verlag, pp. 3–15.

Leibovich, S. (1978), The structure of vortex breakdown. *Ann. Rev. Fluid Mech.* **10**, pp. 221-246.

Leibovich, S. & Kribus, A. (1990), Large-amplitude wavetrains and solitary waves in vortices. *J. Fluid Mech.* **216**, pp. 459–504.

Leonard, A. (1985), Computing three-dimensional incompressible flows with vortex elements. *Ann. Rev. Fluid Mech.* **17**, pp. 523-559.

Lundgren, T. S. & Ashurst, W. T. (1989), Area-varying waves on curved vortex tubes with application to vortex breakdown. *J. Fluid Mech.* **200**, pp. 283–307.

Maxworthy, T., Mory, M. & Hopfinger, E. J. (1983), Waves on vortex cores and their relation to vortex breakdown. *Proc. AGARD conf. on Aerodynamics of vortical type flows in three dimensions.* CPP-342, pp. 29-1 – 29-13.

Moore, D. W. & Saffman, P. G. (1971), The motion of a vortex filament with axial flow. *Phil. Trans. Roy. Soc. Lond.* **A 272**, pp. 403–429.

Moore, D. W. & Saffman, P. G. (1973), Axial flow in laminar trailing vortices. *Proc. Roy. Soc. Lond.* **A 333**, p. 491-508

Peckham, D. H. & Atkinson, S. A. (1957), Preliminary results of low-speed wind tunnel tests on gothic wing of AR 1.0. *Aero. Res. Council* CP-508.

Pocklington, H. C. (1895) The complete system of the periods of a hollow vortex ring. *Phil. Trans. Roy. Soc. Lond.***A 186**, pp. 603-619.

Rosenhead, L. (1930) The spread of vorticity in the wake behind a cylinder. *Proc. Roy. Soc. Lond.* **A 127**, p. 590.

Saffman, P. G. (1991), *Vorticity*. To be published.

Salas, M. D. & Kuruvila, G. (1989), Vortex breakdown simulation: A circumspect study of the steady, laminar, axisymmetric model. *Computers and Fluids* **17**, pp. 247–262.

Sarpkaya, T. (1971), On stationary and travelling vortex breakdowns. *J. Fluid Mech.* **45**, p. 585.

Sarpkaya, T. (1974), Effect of the adverse pressure gradient on vortex breakdown. *AIAA Journal* **12**, p. 602.

Schwartz, L. W. (1974), Computer extension and analytic continuation of Stoke's expansion for gravity waves. *J. Fluid Mech.* bf 62, pp. 553–578.

Stewartson, K. & Stuart, J. T. (1971), A non-linear instability theory for a wave system in plane Poiseuille flow. *J. Fluid Mech.* bf 48, pp. 529–545.

Stuart, J. T. (1987), A critical review of vortex-breakdown theory. *Proceedings: Symposium on "Vortex control and breakdown behaviour,"* Baden, Switzerland.

Ting, L. (1971), Studies in the motion and decay of vortices. *Aircraft wake turbulence and its detection*, Plenum Press, pp. 11–39.

Whitham, G. B. (1974), *Linear and nonlinear waves.* Wiley-interscience publication.

Widnall, S. E., Bliss, D. & Zalay, A. (1971), Theoretical and experimental study of the stability of a vortex pair. *Aircraft wake turbulence and its detection*, Plenum Press, pp. 305–338.